Self-desiccation and its importance in concrete technology : proceedings of the third international research seminar in Lund, June 14-15, 2002

Persson, Bertil; Fagerlund, Göran

2002

LUND UNIVERSITY
LUND INSTITUTE OF TECHNOLOGY
Division of Building Materials TVBM - 3104

SELF-DESICCATION AND ITS IMPORTANCE IN CONCRETE TECHNOLOGY

B Persson and G Fagerlund, Editors

Proceedings of the Third International Research Seminar in Lund, June 14-15, 2002

ISRN LUTVDG/TVBM--02/3104--SE(1-250)
ISSN 0348-7911 TVBM
ISBN 91-631-1993-5

Lund Institute of Technology
Division of Building Materials
Box 118
SE-221 00 Lund, Sweden

Telephone: 46-46-2227415
Telefax: 46-46-2224427
www.byggnadsmaterial.lth.se

PREFACE

This is the third Research Seminar on *Self-Desiccation in Concrete* organised at our Department. The first seminar was held in 1997[1] and the second in 1999[2].

Self-desiccation, or internal drying, is a phenomenon caused by the chemical reaction of cement with water. The reaction leads to a net reduction in the total volume of water and solid. Consequently, an air-space is formed inside concrete that is protected from water ingress.

Self-desiccation occurs in all concrete irrespectively of the water-cement ratio. However, its effects are very different in different types of concrete. In normal concrete, with water-cement ratio above about 0.45 to 0.50, self-desiccation often occurs unnoticed. Therefore, the phenomenon was seldom noticed or considered until concrete with low w/c-ratio, e.g. high performance concrete became more frequently used during the last few decades. In such high-quality concrete self-desiccation is evident, affecting many properties. The main reason is that it causes a reduction in the internal relative humidity (RH) of the concrete. A reduced RH-level, and reduced saturation level, can be maintained for long time also when the concrete is stored in water. Thus, self-desiccation has both negative and positive effects; e.g., (i) the reduced RH gives rise to drying shrinkage which will add to normal drying shrinkage, but which takes place earlier than this, and which may give internal micro-cracking, (ii) the self-desiccation shrinkage adds to thermal shrinkage caused by hydration, thus increasing the risk of early (macro-) cracking, (iii) the reduced RH radically shortens the required drying time before concrete can be covered by moisture and alkali sensitive materials, (iv) the reduced saturation level increases the resistance to internal frost damage, especially when the concrete is young.

Mechanisms by which self-desiccation occurs, and by which self-desiccation affects different concrete properties, have been explored by researchers contributing their results to this Research Seminar. By understanding the mechanisms one may also find ways of reducing the negative effects of self-desiccation. Attempts in this direction are presented at the Seminar.

[1)] Persson, B., Fagerlund, G. (Eds.), Self-Desiccation and Its Importance in Concrete Technology, Report TVBM-3075, Div. of Building Materials, Lund Institute of Technology, Lund University, Lund, 255 pp. (1997).

[2)] Persson, B., Fagerlund, G. (Eds.), Self-Desiccation and Its Importance in Concrete Technology, Report TVBM-3085, Div. of Building Materials, Lund Institute of Technology, Lund University, Lund, 171 pp. (1999).

I want to thank all those who have contributed to this Research Seminar. I am particularly grateful to my colleague Dr. Bertil Persson who took the initiative for and organised the Seminar.

Lund, May 2002

Göran Fagerlund

TABLES OF CONTENTS PAGE

VERY EARLY AGE AUTOGENOUS SHRINKAGE: GOVERNED BY CHEMICAL SHRINKAGE OR SELF-DESICCATION?

Erika Holt
VTT Building and Transport
The Technical Research Centre of Finland, Espoo, Finland

Abstract
Autogenous shrinkage is often fully attributed to self-desiccation, or the lowering of internal relative humidity with age. Research at VTT has shown that autogenous shrinkage can still occur even if the humidity is at 100%, immediately after casting. Even before the setting time, measurements of autogenous deformation have been recorded. The presence of very early age autogenous shrinkage was also supported in the physical test arrangement by the development of internal capillary under-pressure. This paper aims at identifying the factors governing autogenous shrinkage during the very early hours.

The very early age autogenous shrinkage took place in three stages: liquid, setting, and stiffening. During the first *liquid stage* all of the volume change was in the vertical direction, or settlement. As the concrete is forming an internal skeleton (around the *setting* time) the volumetric autogenous shrinkage (both horizontal and vertical) was equal in magnitude to the amount of chemical shrinkage. This correlation during the setting stage resulted in the conclusion that cement properties, and thus chemical shrinkage, are highly responsible for the initial autogenous shrinkage. Early age autogenous shrinkage also increased with a decreasing water-to-cement (w/c) ratio, a lower volume of aggregate (which provides restraint), and the use of superplasticiser.

Approximately 4 hours after the final set time the concrete entered the third stage, where it had developed enough *stiffness* to resist shrinkage strains and the autogenous shrinkage was no longer equivalent to the chemical shrinkage. Beyond this time the additional autogenous shrinkage was governed by self-desiccation as traditionally described in literature.

1. Background

1.1 Early age concerns
Concrete shrinkage is of increasing concern when focusing on maintaining durable structures. Shrinkage takes place in two distinct *phases*: early and later ages. In this work early age is defined as the first day, while the concrete is setting and starting to harden. Early age shrinkage is a concern because it is during the early hours, immediately after casting, that concrete has the lowest strain capacity and is most sensitive to internal stresses. Early age shrinkage can result in cracks that form in the

same manner as at later ages. Even if the early resulting cracks are internal and microscopic, further shrinkage at later ages may merely open the existing cracks and cause problems. It is suggested by VTT and others that if the early age shrinkage magnitude exceeds 1 mm/m there is a high risk of cracking. [1, 2]

The most common solution to reduce early age volume changes is to avoid drying by proper handling of the concrete for the first few hours after placement. It is imperative that the concrete curing begins immediately and follows correct methods. [3]

1.2 Autogenous shrinkage

Under ideal curing conditions, the only remaining early age deformations are those attributed to autogenous reactions. Autogenous shrinkage is usually a concern in high strength or high performance concrete (> 40 MPa) where there is a low water-to-cement (w/c) ratio. In this work the factors governing autogenous shrinkage in the first hours were examined. Though autogenous shrinkage is typically attributed to self-desiccation, as the internal relative humidity is lowered, other factors were investigated in this work.

Few, if any, quantitative values of early age autogenous shrinkage (< 12 h) have been reported in literature. After the concrete has hardened, autogenous shrinkage can be measured using more standard long-term measuring practices. It was suspected in this work that during the early ages while the concrete is still liquid and without stiffness, the autogenous shrinkage is equivalent to chemical shrinkage.

It had been seen during work at VTT that during this liquid stage most volume changes are in the vertical (settlement) direction. The next stage is around the time of setting, where the development of capillary pressure is measured and indicates shrinkage stresses. This pressure mechanism works as the water, or meniscus, is moving between the pores. As the water is lost from subsequently smaller pores, the water meniscus will continue to be pulled into the capillary pores and will generate more stress on the capillary pore walls. This is similar to the phenomena described by Radocea [4] for drying shrinkage and it again causes a contraction in the cement paste. Once concrete has reached a hardened stage with aging (> 1+ day), the autogenous shrinkage result from self-desiccation [5, 6], which is the localized drying resulting from a decreasing relative humidity in the concrete's internal pores. The lower humidity is due to the cement requiring extra water for hydration.

In a high strength concrete with a low w/c ratio, the finer porosity causes the water meniscus to have a smaller radius of curvature. These menisci cause a large compressive stress on the pore walls, thus having a greater autogenous shrinkage as the paste is pulled inwards in both early age and long-term shrinkage.

1.3 Chemical shrinkage

The primary suspect for early age autogenous shrinkage was chemical shrinkage, which is an *internal* volume reduction while the autogenous shrinkage is an *external* volume change.

Chemical shrinkage is a result of the reactions resulting between cement and water, which lead to a volume reduction. The basic reactions of cement clinker are well understood and generally defined by four reactions of C_3S, C_2S, C_3A and C_4AF. Each of these reactions requires water for reaction, are exothermic and result in a decreased volume of the reaction products.

This volume reduction, or chemical shrinkage, begins immediately after mixing of water and cement and the rate is greatest during the first hours and days. The magnitude of chemical shrinkage can be estimated using the molecular weight and densities of the compounds as they change from the basic to reaction products. [1, 7, 8] A generalized way to estimate the chemical shrinkage is given by the equation (1):

$$V_{CS\text{-}TOTAL} = 0.0532\,[C_3S] + 0.0400\,[C_2S] + 0.1113\,[C_4AF] + 0.1785\,[C_3A] \quad (1)$$

The rate of chemical shrinkage is dependent on cement and concrete mixture parameters, such as the cement fineness and the efficiency of cement dispersion. Higher magnitudes of chemical shrinkage due to quicker cement reactions during the very early hours will lead to greater autogenous shrinkage.

Equation (1) has been modified by Holt [3] to account for the different phases (ettringite and monosulphate) within the C_3A reaction. The modification also accounts for rates of hydration, to allow estimation of the chemical shrinkage at various times. Full details of this modified Holt method of estimating chemical shrinkage can be found elsewhere [3].

2. Measuring methods

2.1 Equipment

Early age shrinkage measurements provide a challenge due to the difficulty in making accurate measurements of the concrete prior to demoulding. The shrinkage must be measured immediately after casting in a mould which permits constant readings without disturbing the concrete. The main difference between measurements of chemical and autogenous shrinkage is that in chemical shrinkage there is an external water source providing additional water to be absorbed by the paste. In autogenous shrinkage tests the concrete sample is sealed and there is no moisture transfer to the surrounding environment.

Chemical shrinkage of paste and mortar is measured by placing a sample in a container and measuring the amount of water the material uptakes. The excess space generated by the smaller volume of hydration products provides pores for the exterior water source

penetrate. Chemical shrinkage measurements can been done by either the dilatometry arrangement using a pipette and beaker or the reduced buoyancy arrangement with a flask underwater. Boivin [9] has established a strong correlation between the two methods.

Early age autogenous shrinkage can be measured by volumetric or linear measurements. Volumetric assessments are done by taking the weight of a paste or mortar sample sealed in a thin rubber membrane underwater. Linear measurements are done on a paste, mortar or concrete sample that is cast in a slab-mould. The linear measurements are a more realistic representation of actual field construction and the material behavior, since thermal dilation, bleeding, setting time and other factors are accounted for in the slab test. It is possible to convert the horizontal and vertical displacements measured on the slab test to a volumetric shrinkage. It is also possible to factor out the volume change resulting from thermal changes associated with cement hydration to get a measure of pure autogenous shrinkage.

There is no standardized method of measuring early age length change as there is for long term shrinkage (such as ASTM C157). The most practical measures of length change are done on a concrete slab simulating field situations such as floors or facades. These tests have been developed by work at VTT, the Technical Research Centre of Finland [10-13], as well as others in Scandinavia and Japan [4, 14-16]. The early age test arrangement can be used to measure drying shrinkage, autogenous shrinkage, or both.

In the slab tests both vertical (settlement) and horizontal shrinkage are measured, along with evaporation and capillary pressure. The slab holds 7.3 liters of concrete and the maximum aggregate size can be 32 mm. A temperature profile is also taken at least at 2 different depths, along with a simultaneous measure of setting time on a separate sample. Within the slab, a change in internal capillary pressure is the primary indicator of the start of autogenous shrinkage. The early age measurements begin immediately after concrete placing (approximately 30 minutes) and continue for 24+ hours. The horizontal shrinkage is measured by LVDTs over a length of 200 mm.

2.2 Data interpretation

The data from chemical shrinkage was evaluated using Archimedes principle that a volume reduction of a water-submerged sample registers as a weight increase. The amount of volume reduction due to chemical shrinkage is given as mm^3 per gram of cement in the mixture. The change of weight in the sample is divided by the density of water to be converted to a volume change.

When analysing early age slab test results, it was necessary to have a consistent referencing or “zeroing” point of the data. For uniformity when comparing the shrinkage measurements of various mixtures, it was assumed that any horizontal shrinkage occurring prior to the initial setting time was insignificant because of the fluid

nature of the concrete. Any horizontal shrinkage prior to initial set is an artifact of the test arrangement. An additional concern when choosing the referencing point was the presence of bleed water on the concrete surface. In autogenous conditions the bleed water is re-absorbed into the concrete and registers as an expansion with the displacement gauges. Therefore, if there was still bleed water on the surface of the concrete at the time of initial set, the reference point was not be taken until the bleed water was fully re-absorbed. Further discussions about the selection of the referencing point for the shrinkage data can be found in Holt's work [3].

Another factor that was accounted for in the autogenous shrinkage slab tests was the early age thermal dilation. Often coinciding with the time of bleed water re-absorption was the start of heat generation due to the cement hydration. The thermal volume change due to this cement hydration was removed to provide a measure of the true autogenous shrinkage without the thermal factors included.

A typical temperature profile comparison of paste, mortar, and concrete is shown in Figure 1. In this figure the paste and mortar have w/c = 0.35 and the concrete has w/c = 0.30 with 2% superplasticiser. The temperature changes result from the cement hydration which in-turn causes an expansion and contraction during the early ages. These initial thermal volume changes can be estimated from existing data of thermal dilation coefficients and can be factored out of the shrinkage measured in a slab test. For instance, Hedlund [17] had measured a thermal dilation value of approximately 25 με/°C for a concrete at the age of 10 hours. More details of this process of removing thermal dilation from slab test data can be found in other reports [3].

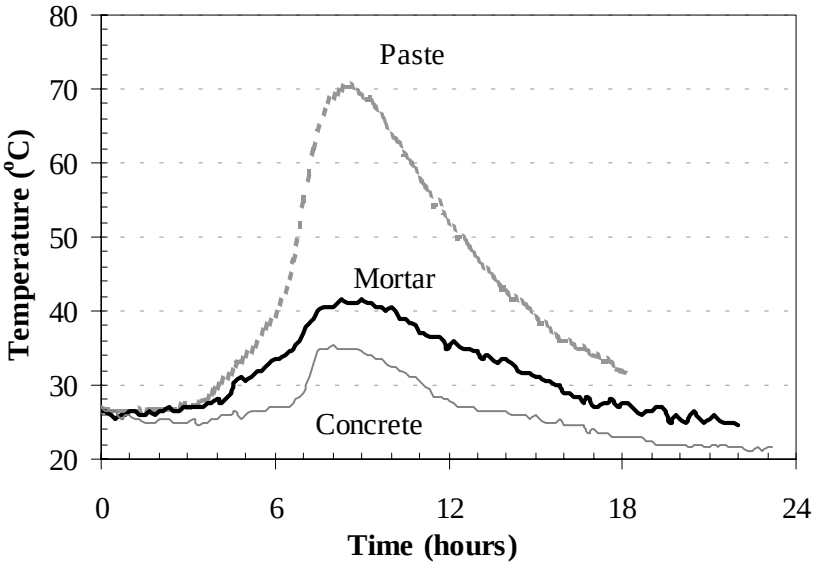

Figure 1 - Sample temperature development with time since concrete mixing.

3. Materials and mixture designs

Tests were done using cement paste or mortar, comprised of typical Finnish materials. Aggregate consisted of Finnish clean natural granite, with a density of 2670 kg/m^3. The fine aggregate was natural sand and the coarse aggregate had rounded particles. The maximum aggregate size was 2 mm in the mortar mixtures and 10 mm in the concrete mixtures.

Most tests used Finnish rapid hardening cement called “Rapid” which is a type CEM IIA (comparable to Type III cements in the USA). Rapid cement is commonly used for high strength and/or high performance products, such as in pre-cast facade manufacturing. In one test series 2 other cement types were used to study the effect the cement type on the autogenous shrinkage: “SR” and “White” cement. SR is a sulphate resistant cement and White cement is often used for architectural work such as facades. Table 1 shows the chemical composition and fineness for the 3 cements.

Table 1 - Composition of Finnish cements.

Compounds & Bogue	Cement Types and Composition (%)		
	Rapid	SR	White
$K_2O + Na_2O$	0.5	0.3	-
SO_3 (gypsum)	3.5	3.3	2.2
C_3S	68	75	67
C_2S	10	5	23
C_3A	8	1	4
C_4AF	8	14	1
Blaine (m^2/kg)	440	330	400

In some cases chemical admixtures were added to the concrete mixtures to improve the mixture characteristics. This mainly included the use of superplasticisers to aid workability of the mixtures. The primary superplasticiser (SP) used was ®Rheo-Build, which is naphthalene-based and sold by Masterbuilders. One test of concrete autogenous shrinkage used a naphthalene-based superplasticiser, ®Superparmix. No air entraining chemicals or mineral admixtures were used in any tests. In most cases the target fresh mixture properties were a slump of 50-100 mm and an air content of 3 %.

The mixture designs used when testing chemical and autogenous shrinkage of cement pastes, mortars and concretes are detailed in Table 2. Mixtures in bold denote ones that were used in both the chemical and autogenous shrinkage tests.

Table 2 - Mixture designs for autogenous and chemical shrinkage tests

Type	w/c	SP (%)	Cement type	Cement (kg/m^3)	Water (kg/m^3)	Aggregate / cement
Paste	**0.35**	-	Rapid	1440	505	0
Mortar	**0.30**	-	Rapid	915	275	1.17
Mortar	**0.35**	-	Rapid	780	275	1.51
Mortar	**0.40**	-	Rapid	685	275	1.85
Mortar	0.45	-	Rapid	610	275	2.18
Mortar	**0.30**	1	Rapid	915	275	1.17
Mortar	0.30	-	White	915	275	1.17
Mortar	0.30	-	SR	915	275	1.17
Concrete	0.30	5	Rapid	545	165	3.11
Concrete	0.35	2	Rapid	505	165	3.36

4. Results

4.1 Autogenous data interpretation

The early age chemical and autogenous shrinkages resulting from altering the mixture designs are presented in the next subsections. The main tests were done on mortars, since they allow comparison to the chemical shrinkage tests. Testing mortars had the secondary effect of complicating the data interpretation due to their greater thermal change during the early ages compared to concrete. The mixture parameters that were altered included aggregate content, the use of a superplasticiser admixture, water-to-cement ratio (w/c), and Finnish cement types. The tests are summarized in Table 3 along with their measured setting times and temperature histories. All mixtures had materials at 20°C at the start of mixing. The time when the bleed water was re-absorbed is also listed, but these times are based on estimates from the horizontal shrinkage data. Finally, the time when the capillary pressure started to develop is noted in Table 3 based on the test data. This development point was taken when the pressure reached a level of 3kPa, with a typical maximum of about 50 kPa.

4.2 Effect of aggregate restraint

To assess the contribution of aggregate restraint to autogenous shrinkage, tests were done on neat paste, mortar and concrete. The measurements on cement pastes are not very representative of the true behavior of concrete because of their large thermal changes. The high heat of hydration of the cement paste results in a large thermal expansion and thus the slab shrinkage measurements will include this change that must be factored out of the results. Figure 2 shows one of the few tests done on cement paste in the autogenous shrinkage test arrangement. The paste can be compared to a similar mortar at the same w/c ratio of 0.35 with no superplasticiser.

Table 3 - Summary of early age autogenous slab test mixtures. All mixtures are with Rapid cement unless otherwise noted on the left column.

Type	w/c	SP	Initial set (hr:min)	Bleeding done (hr:min)	Pressure start (hr:min)	Temperature peak (°C)	Temperature time (hr:min)
Paste	0.35	-	3:15	4:10	4:10	70.3	9:00
Mortar	0.30	-	1:30	-	2:15	44.0	7:50
Mortar	0.35	-	2:10	3:50	3:10	41.5	8:50
Mortar	0.40	-	2:25	4:30	4:10	37.8	11:50
Mortar	0.45	-	3:35	7:50	6:30	34.5	12:10
Mortar	0.30	1%	1:30	-	2:30	47.5	8:00
Mortar – White	0.30	-	1:55	3:10	3:20	39.5	7:20
Mortar – SR	0.30	-	2:35	4:10	-	36.5	10:00
Concrete	0.30	5%	0:35	-	3:00	35.5	8:00
Concrete	0.35	2%	2:35	-	2:25	34.0	9:00

The data was referenced at the time when all of the bleed water was reabsorbed to the mixture and thus there was an end of expansion prior to capillary pressure development. For the mortar and neat paste mixtures of Figure 2 this was at about 4 hours. If there had been no bleeding the reference point would have been taken at the time of initial set.

As expected, the neat paste had much greater shrinkage than the mortar due to the lack of aggregate providing restraint. The difference in the two mixtures showed the neat paste having about 1.7 times greater shrinkage compared to the mortar.

The paste mixture in Figure 2 also showed a slight expansion beyond 12 hours. This is probably not an accurate depiction resulting from too great of a calculated thermal contraction as the mixture cooled. A more accurate measure of the thermal dilation coefficient would be required to improve the paste's true autogenous shrinkage estimate in the first day.

Another two tests were done to compare the restraint provided by increasing the aggregate, both in size and volume. Both concrete and mortar mixtures were tested at a w/c ratio of 0.30 and including superplasticiser. The aggregate amount was 70% in the concrete compared to 47% in the mortar. The comparison of the autogenous shrinkage with the mixture types is given in Figure 3.

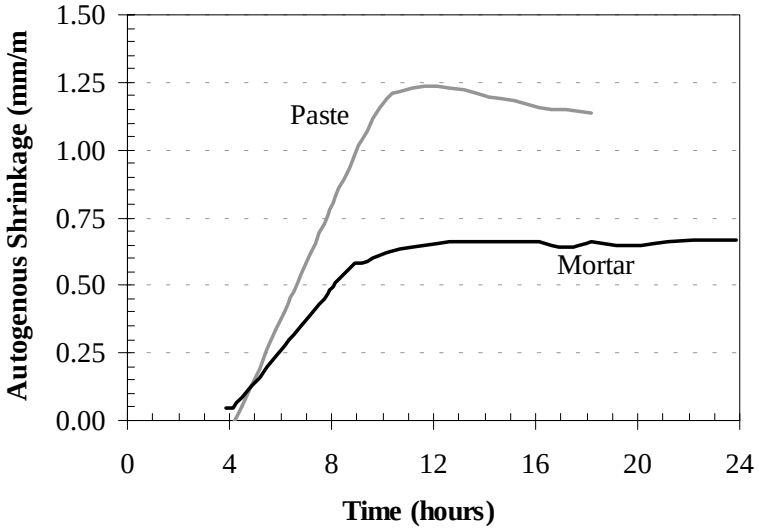

Figure 2 - Autogenous shrinkage resulting with addition of aggregate, from paste to mortar at w/c=0.35.

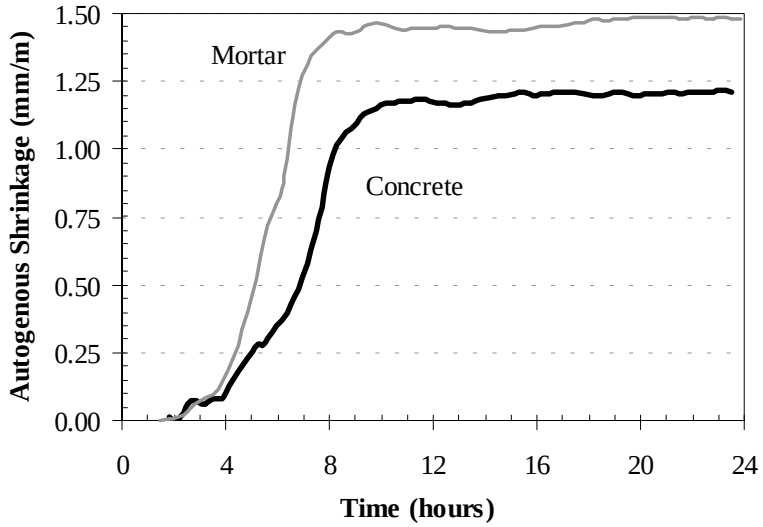

Figure 3 - Autogenous shrinkage resulting with addition of aggregate from mortar to concrete at w/c=0.30.

In the test of Figure 3 it was expected, based on the mortar and paste comparisons in Figure 2, that the concrete mixture would have less shrinkage than the mortar since the concrete has more aggregate restraining the shrinkable paste. The concrete mixture also had less cement (545 kg/m^3, as given in Table 1) compared to the mortar mixture (915 kg/m^3) so the amount of chemical shrinkage would be less in the concrete. Both of these theories held true, with the concrete shrinking less than the mortar, though there was still sufficient stresses to induce a high amount of shrinkage in the concrete.

Both the concrete and mortar mixtures in Figure 3 had shrinkage amounts greater than the paste and mortars shown in Figure 2. This is due to the lower w/c ratio and the presence of superplasticiser chemicals in the 0.30 w/c mixtures. The influences of these other two parameters are addressed in the next subsections.

4.3 Effect of superplasticiser

To test concrete mixtures having a low w/c ratio it is often necessary to add a superplasticiser, SP, to the mixture to improve the workability and allow for adequate placement. The effect on autogenous shrinkage when a was added to a mortar with w/c=0.30 is shown in Figure 4. Both mixtures had identical proportioning except for the addition of the chemical. Therefore, their workabilities were different but both mixtures still had little, if any bleed water. The non-superplasticised mixture is the same as the mortar with a w/c of 0.30 in Figure 6.

In both mixtures there was little bleeding and no signs of expansion due to bleed water re-absorption, thus the data curves start at the time of initial set (90 minutes). In these two mortars the setting time was not delayed with the addition of the superplasticiser, as is often expected.

The temperature peak of the two mixtures was at about the same time of 8 hours, though the superplasticised mortar had a slightly greater temperature rise. The early age autogenous shrinkage ended at about the time of maximum thermal expansion. The results showed that the superplasticized mixture had shrinkage 50% greater than the reference mixture. The greater autogenous shrinkage with superplasticiser was a result of the improved cement dispersion and faster rate of hydration reactions generating shrinkage.

The same trend of greater early age shrinkage with the use of superplasticiser also held true in the chemical shrinkage tests. The chemical shrinkage results for neat paste with the addition of 1% superplasticiser is given in Figure 5. Similar to Figure 4, the mixtures in Figure 5 also were made from Finnish rapid cement and had a w/c = 0.30, but no aggregate. Again the chemical addition aided the dispersion of the cement and reaction speed during the early hours.

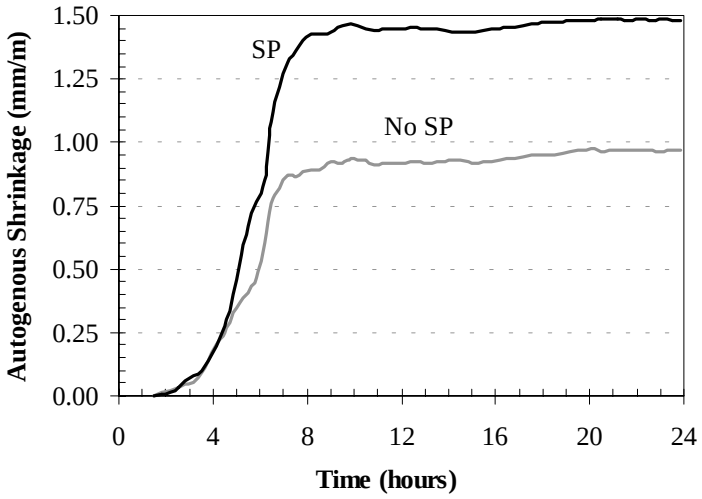

Figure 4 - Autogenous shrinkage resulting with superplasticiser addition to mortar, w/c=0.30.

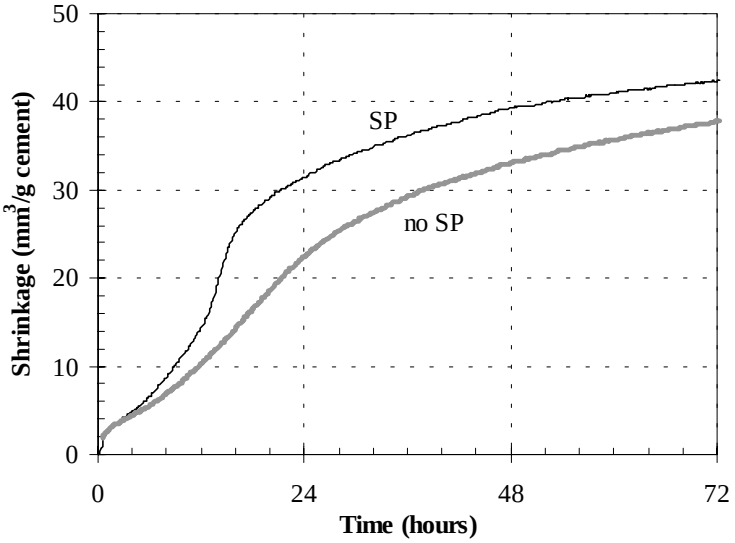

Figure 5 - Chemical shrinkage resulting with superplasticiser addition to paste, w/c=0.30.

4.4 Effect of w/c ratio

The next set of tests investigated the changes in autogenous shrinkage magnitude due to the variation in w/c ratio of mortars. The w/c ratio was changed from 0.30 to 0.45 while the water amount was held constant at 275 kg/m^3. This corresponds to an increasing cement content and paste content while the aggregate amount remained constant. No superplasticisers were added to the mortars so the workability varied with the four mixtures. The results of altering the w/c ratio are shown in Figure 6.

The data was referenced at the time when the bleed water absorption was completed. For the mixture with a w/c of 0.30 there was no bleeding so the referencing was done at 90 minutes, the time of initial set. All the mortar mixtures of this test set had increasing workability and also increasing bleeding amounts as the w/c increased, and thus the referencing point was later with succeeding w/c ratios. The autogenous shrinkage ended at about the time of maximum heat generation due to cement hydration. The temperature peaks were lower and slightly later as the w/c ratio increased.

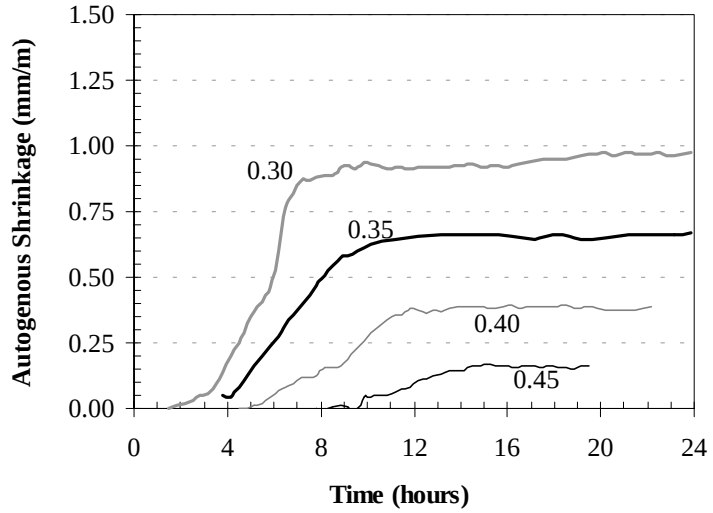

Figure 6 - Autogenous shrinkage resulting with changing w/c ratio and equivalent water amount.

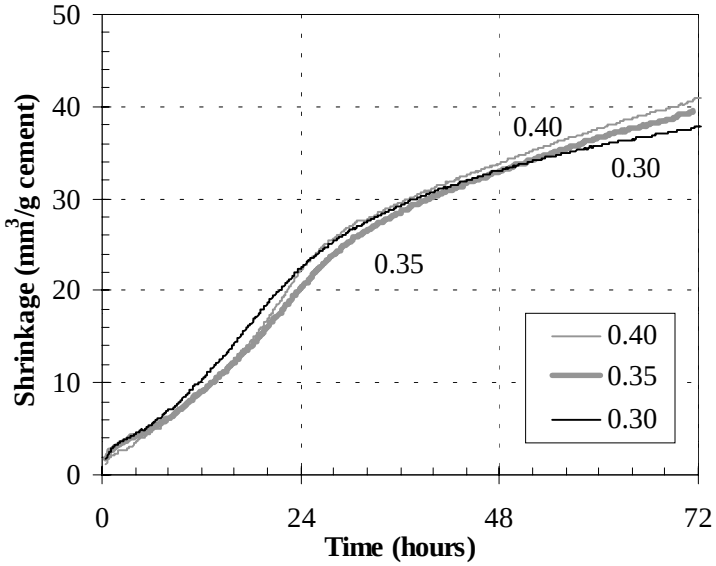

Figure 7 - Chemical shrinkage resulting with changing w/c ratio and equivalent water amount.

As expected, the mortar with the lowest w/c ratio had the greatest amount of autogenous shrinkage. This is because the mixtures have higher cement contents at the lower w/c ratios. The greater amount of cement results in larger autogenous shrinkage due to the contribution of chemical shrinkage. The trend is in agreement with those seen in the chemical shrinkage test, shown in Figure 7. Figure 7 shows that with sufficient external water to aid hydration, chemical shrinkage is independent of the w/c ratio. The chemical shrinkage results are presented "per gram of cement" so for equivalent cement contents the shrinkage is constant.

Figure 8 shows the pressure build-up corresponding to the shrinkages of Figure 6. As expected, as the w/c ratio of the mortar mixtures was lowered the capillary pressure started earlier. This is due to the finer pores in the microstructure and lower amount of water in the mixtures at low w/c ratios. The 0.30 w/c mixture had an initial setting time of 1 hour and 30 minutes (Table 2), no bleeding, and the pressure began rising at about 2 hours. Near the same time the shrinkage began. The other mixtures had later setting times and a delayed onset of pressure, as well as a delayed start of horizontal shrinking. Since the mortars with w/c ratios of 0.40 and 0.45 had much later bleed water absorption times (4:30 and 7:50, in Table 2) the early development of capillary pressure did not induce shrinkage.

Similar to the mortar tests, additional tests were done when increasing the w/c ratio of concrete mixtures. Two tests were done with concrete at w/c ratios of 0.30 and 0.35, 2 and 5% superplasticiser and an equal amount of 165 kg/m^3 of water in each mixture. Neither mixture had any bleeding and therefore the testing results began at the time of initial setting. The results showed higher autogenous shrinkage in the concrete with a lower w/c ratio. This mixture also had a greater temperature peak at an earlier time, as well as an earlier setting time.

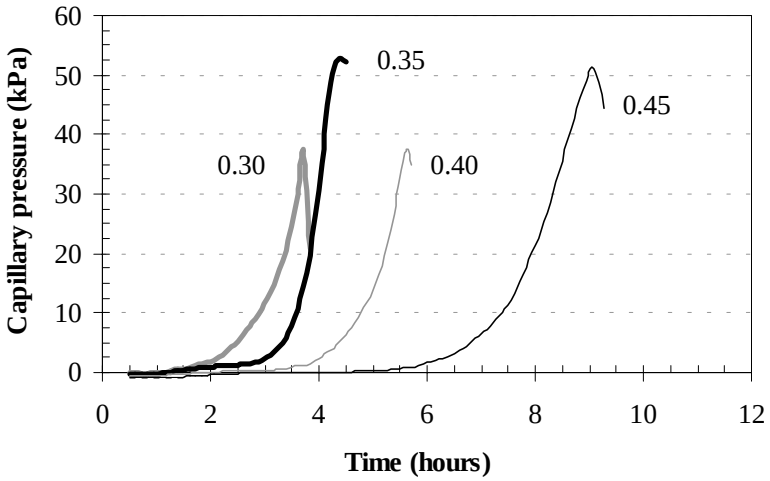

Figure 8 - Capillary pressure resulting with changing w/c ratio, corresponding to autogenous shrinkage test of Figure 6.

4.5 Effect of cement type

The final set of tests investigated how altering the cement type influences the magnitude of autogenous shrinkage. The mortar mixtures had identical mixture designs with a w/c ratio of 0.30. The workability varied a lot because of the different fineness of the 3 cements. This in-turn affected the bleeding and the expected amount of autogenous deformation. The results of altering the cement type are shown in Figure 9.

The mixture made from Rapid cement had no bleeding and thus the autogenous shrinkage began immediately after placement. The Rapid cement mortar mix had 40% greater shrinkage than the White cement mix and about 140% greater shrinkage than the SR cement mixture.

These autogenous shrinkage results are in agreement with the chemical shrinkage tests, which are presented in Figure 10 for the same mixtures. These values can be compared to the expected chemical shrinkage as calculated by existing models as described in Section 1.3. The values predicted by the Holt method [3] as well as Equation 1 [7] are given in Table 4. As both the Holt calculations and physical measurement show, the Rapid cement mixture had greater chemical shrinkage than both the White and SR cement mixtures. The Holt method overestimated the chemical shrinkage at 72 hours compared to the actual chemical shrinkage test, while Equation 1 falsely predicted that the SR cement mixture would have greater shrinkage than the White cement mixture.

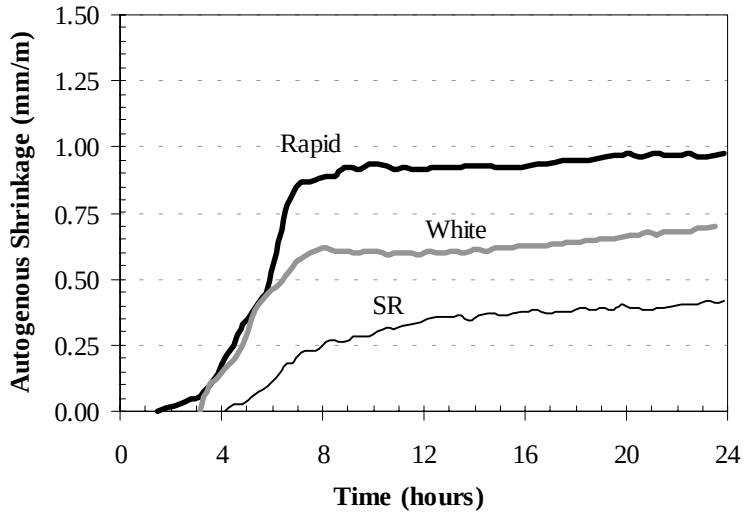

Figure 9 - Autogenous shrinkage resulting with changing cement types.

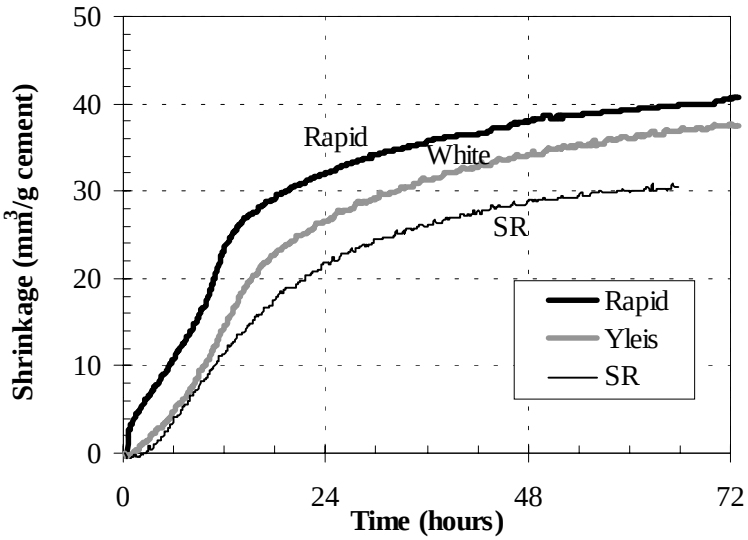

Figure 10 - Chemical shrinkage resulting with changing cement types.

Table 4 - Predicted early age chemical shrinkage based on Modified Holt model [3] accounting for degree of hydration at various times and Equation 1 [7].

Cement Type	Estimated Chemical Shrinkage (mm^3/g) Modified Holt [3] 72 hours	Modified Holt [3] Ultimate	Equation 1 [7] Ultimate
Rapid	35	54	63
White	29	52	53
SR	28	49	59

4.6 Contribution of chemical shrinkage to autogenous shrinkage

Chemical shrinkage tests were done for all of the pastes and mortars presented in the previous section. The volumetric measurement of chemical shrinkage was converted to a linear measurement in order to make a comparison to the autogenous shrinkage measured in the slab tests [3]. Figure 11 shows a comparison of the horizontal, vertical and chemical shrinkage for the Rapid cement mortar mixture at the 0.30 w/c ratio. During the first hours it is seen that all of the autogenous shrinkage is attributed to vertical movement, or settlement. Later there is an increase in both the horizontal and vertical shrinkage once the pressure started to rise and reached about 10 kPa.

Further analysis of Figure 11 was done by converting the data to a volumetric measurement of shrinkage (see further details about transformation in [3]). Figure 12 shows the comparison of chemical and autogenous shrinkage during the first hours. Prior to setting all autogenous movement is attributed to settlement. Once a skeleton had formed at about the time of setting the chemical and autogenous shrinkage diverge since there is some strength. The mortar has stiffened enough to resist some of the chemical shrinkage. At about 4 hours the autogenous shrinkage again increases as a result of the capillary pressure. By about 7 hours, or 4 hours after the final setting time, the mortar was again stiff enough due to hardening to resist most of the shrinkage due to both chemical changes and pressure. Any subsequent autogenous deformation would be the result of self-desiccation.

This example has supported the theory that both chemical shrinkage and capillary pressure drive autogenous shrinkage during the early ages.

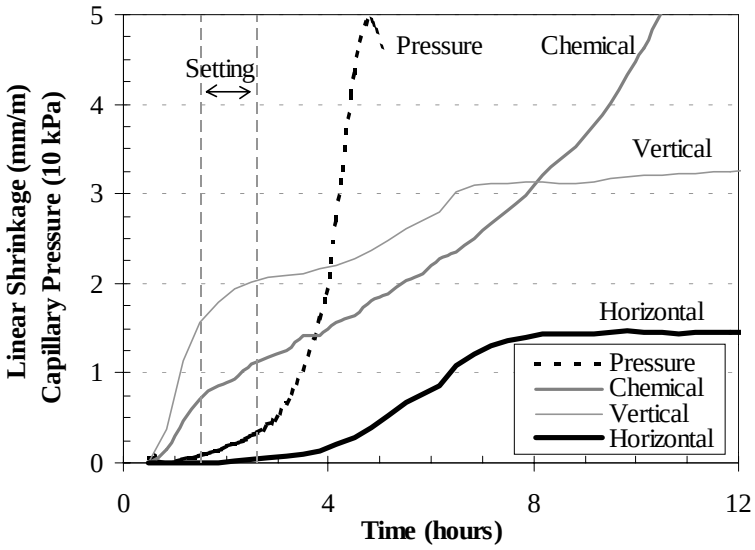

Figure 11 - Linearized chemical, horizontal and vertical shrinkage of mortar (Rapid mortar with w/c = 0.30 and superplasticiser).

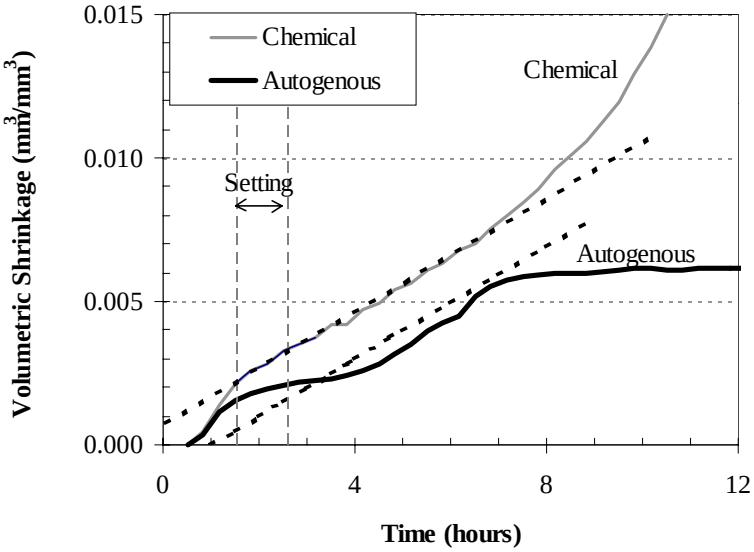

Figure 12 - Volumetric chemical and autogenous shrinkage of the mortar from Figure 11 with w/c = 0.30.

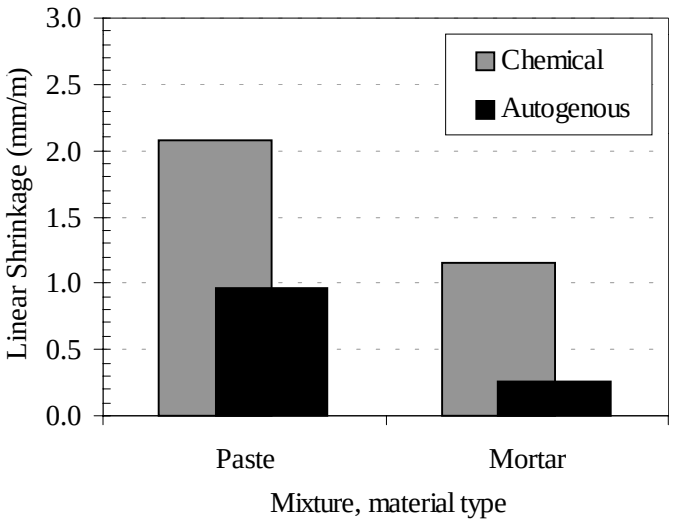

(a)

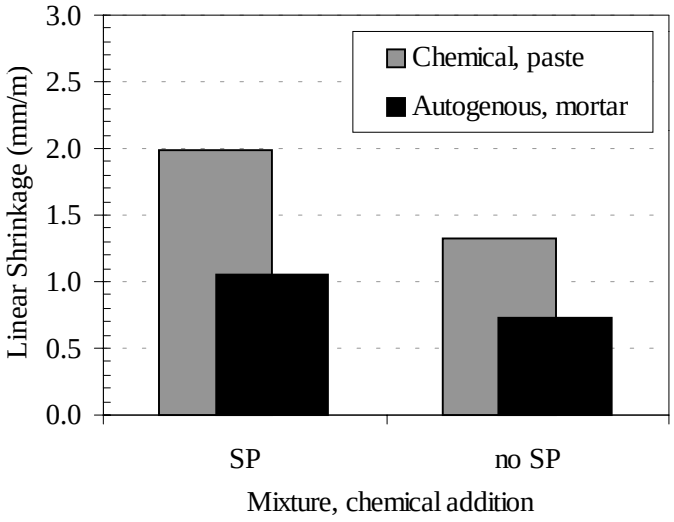

(b)

Figure 13 - Comparison of chemical to autogenous shrinkage from start of tests (initial set or end of bleeding) until 4 hours beyond final set time. Note that cement amounts can vary, as given in Table 1. (continued on next page)

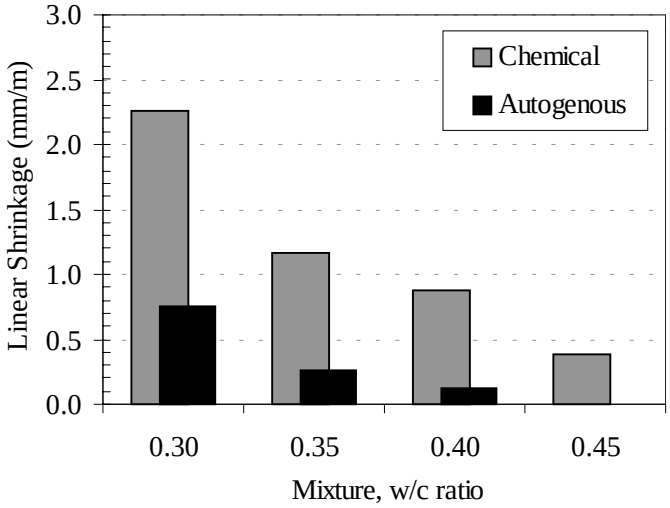

(c)

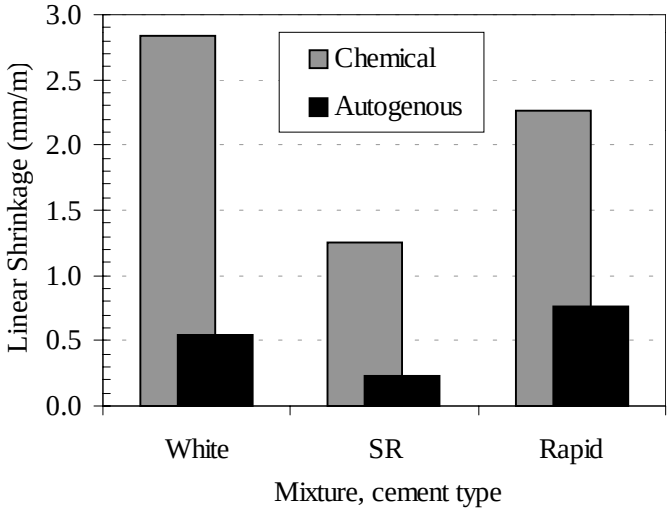

(d)

Figure 13 – continued from previous page.

Figure 13 shows the contribution of chemical to autogenous shrinkage for the mixture presented earlier. In Figure 13a the paste mixture had greater autogenous and chemical shrinkage due to the higher amount of cement and less aggregate restraint. In Figure 13b the addition of superplasticiser improved cement dispersion and thus shrinkage. In

Figure 13c the increasing w/c ratio mixtures had less shrinkage due to the lower cement content, coarser pore structure, and greater aggregate content. In Figure 13d the Rapid cement mixture had greater autogenous shrinkage than the White and SR cement mixtures due to the chemical composition of the cement. Specifically, the Rapid cement had the highest amount of C_3A (8%) and the highest fineness which contributed to less bleeding and earlier autogenous deformations.

Note that in Figure 7 the chemical shrinkage had been equivalent for all mixtures with varying w/c ratios, but this was presented with the shrinkage normalized per gram of cement. In Figure 6 and 13c the amount of cement was altered in each mortar mixture so the chemical shrinkage result is varying per cubic meter of mortar.

4.7 Controlling autogenous shrinkage

Figure 14 depicts the correlation between autogenous shrinkage and chemical shrinkage during the early ages. In the first phase the concrete is very fluid and all volume change is attributed to settlement (vertical deformation). The test arrangement used in this work could not always accurately quantify the horizontal autogenous shrinkage magnitude during this phase. This is not a concern for modeling field concrete practice, since during the liquid stage the concrete with high plasticity is not effected by stress. Even though chemical shrinkage is progressing there is no resulting harmful autogenous stress in the slab test due to the concrete's fluidity.

In the next phase the concrete begins to stiffen and form a skeleton, while the continuing chemical shrinkage stresses induce a stain in the concrete as autogenous shrinkage. In modeling, ideally the autogenous shrinkage curve would be parallel to the chemical shrinkage as long as there is insufficient concrete stiffness to resist the forces. This means autogenous shrinkage is nearly equal to chemical shrinkage for a short period during setting and the few hours afterwards. Eventually the concrete has hardened enough to resist further stresses and the measurement changes to one of long-term deformations which are driven by self-desiccation.

Overall, the early age autogenous and chemical shrinkages are not equivalent during the first 24 hours due to many factors. There are differences in the two types of shrinkages such as bleed water, thermal dilation, strength development (setting) and restraint provided by aggregates. Figure 15 shows these main parameters effecting the magnitude of early age autogenous shrinkage. Chemical shrinkage provides the potential for greater autogenous shrinkage. The bleeding and hardening are material parameters that affect the autogenous shrinkage in reality. All three of these factors interrelated. Yet the sum autogenous shrinkage accounting for all three factors simultaneously cannot be predicted by numeric model because of their mixture-dependent nature.

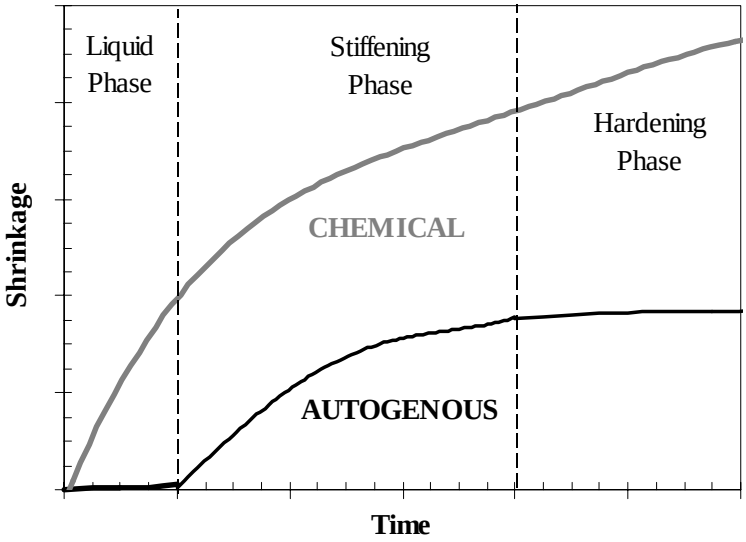

Figure 14. Stages of autogenous and chemical shrinkage during the very early ages.

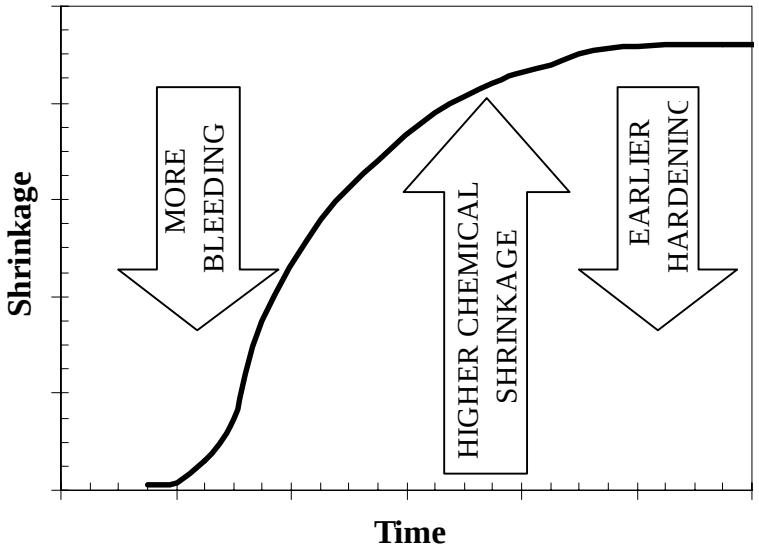

Figure 15. Direction of shift in early age autogenous shrinkage when influenced by other material factors.

In practice, some of the measures that can be taken to reduce the risk of early age autogenous shrinkage are to:

- lower the chemical shrinkage by selecting cements with a low C_3A and high C_2S content,
- lower the rate of chemical shrinkage by selecting coarser ground or slow reacting cements,
- limit the chemical shrinkage by using the minimum amount (or no) superplasticiser, since these chemicals improve cement dispersion and accelerate chemical shrinkage,
- encourage a coarser pore structure (i.e. high w/c ratio, limited or no silica fume, etc.) to minimize the amount of early age capillary pressure,
- accelerate the setting time so the concrete is stiff enough to resist shrink stresses,
- accept some bleed water, since it acts as a self-curing blanket and prevents autogenous shrinkage,
- use higher amounts of coarse aggregate to provide restraint to shrinking paste.

5. Discussion

Autogenous shrinkage is a concern in high strength and/or high performance concrete mixtures. It occurs when there are ideal curing conditions, with no moisture transferred to the surrounding environment. Typically it has been addressed as a long-term durability problem that can lead to cracking if not properly designed for with the mixture proportioning. Risky autogenous shrinkage has been linked to lower w/c ratios when there is not enough water for cement hydration at later ages, thus the concrete exhibits self-desiccation. This work has shown that autogenous shrinkage is also a concern during the very early ages, immediately after concrete mixing and placing. The tests described here were performed on field-simulated slab tests to assess the effects of material parameters on the magnitude of early age autogenous shrinkage.

Autogenous shrinkage during the first hours occurs in the liquid, skeleton formation and hardening stages. In the first stage the autogenous deformation parallels the chemical shrinkage, until the point when there is some stiffening and a skeleton formation. With further stiffening the concrete can resist the autogenous shrinkage stresses and the driving force changes to self-desiccation.

In this work autogenous shrinkage at early ages was accurately measured by linear displacement of field-simulated slabs. The best correlation of the amount of chemical to autogenous shrinkage was found at the time of four hours after the final setting time. It was possible to account for test arrangement artifacts, such as thermal dilation, to get a measure of pure autogenous shrinkage. Many other material parameters effected the magnitude of autogenous shrinkage in secondary ways. These factors, such as amount of bleed water and time of setting, were accounted for in the slab measurements by means of the shrinkage data referencing point. Precautions were recommended to reduce the likelihood of cracking due to early age chemical and autogenous shrinkage.

Even with any of these precautions it is still crucial to remember that autogenous shrinkage may be insignificant if drying forces are present. The best way to ensure high-quality, crack-free concrete is to provide adequate curing immediately after mixing and placing. [12] After proper construction techniques are established, minimizing the autogenous shrinkage can be addressed by clarifying "just how strong or fast does one really need the concrete to be?".

6. Summary

In the hours immediately after casting, autogenous shrinkage is primarily attributed to chemical shrinkage rather than self-desiccation. The only way to minimise this shrinkage is by mixture design, such as cement type and amount, w/c ratio, aggregate amount, and use of admixtures. In this work these parameters were evaluated to gain a better understanding of early age autogenous shrinkage.

Acknowledgement

This material is based on the dissertation *Early Age Autogenous Shrinkage of Concrete* [18], published at the University of Washington in June 2001 and by VTT [3]. The material is also based upon work supported by the National Science Foundation under Grant No. 9978607.

References

[1] Uno P., Plastic shrinkage cracking and evaporation formulas. ACI Mat. Jour. 95(4):365-367 (1998)

[2] ACI 209-92. Prediction of creep, shrinkage, and temperature effects in concrete structures. Farmington Hills: American Concrete Institute (1997)

[3] Holt, E., Early age autogenous shrinkage of concrete, VTT Publications 446, ISBN 951-38-5870-7, Espoo, Finland, 184 p. (2001)

[4] Radocea, A., A Study on the Mechanisms of Plastic Shrinkage of Cement-Based Materials, Report P-92:9, Ph.D. thesis. ISBN 91-7032-760-2, Göteborg, Chalmers University of Technical (1992)

[5] Baroghel-Bouny, V., Texture and moisture properties of ordinary and high-performance cementitious materials. In: Proceedings of Seminaire RILEM 'Benton: du Materiau a la Structure'. Arles France (1996)

[6] Tazawa, E., Miyazawa, S., Influences of cement and admixtures on autogenous shrinkage of cement paste. Cem Concr Res 25(2)281 – 287 (1995)

[7] Paulini, P., A weighing method for cement hydration. In: 9th International Congress on the Chemistry of Cement. New Delhi, pp. 248-254 (1992)

[8] Justnes, H., Sellevold, E,J., Reyniers, B., Van Loo, D., Van Gemert, A., Verboven, F., Van Gemert, D., The influence of cement characteristics on chemical shrinkage. In: Tazawa, E., editor. Autogenous Shrinkage of Concrete, London: E&FN Spon, p. 71-80 (1999)

[9] Boivin, S., Acker, P., Rigaud, S., Clavaud, B., Experimental assessment of chemical shrinkage of hydrating cement paste. In: Tazawa, E., editor. Autogenous Shrinkage of Concrete, London: E&FN Spon, p. 81-92 (1999)
[10] Kronlöf, A., Leivo, M., Sipari, P., Experimental study on the basic phenomena of shrinkage and cracking of fresh mortar. Cem Concr Res 25(8):1747-1754 (1995)
[11] Leivo, M., Holt, E., Autogenous volume changes at early ages. In: Persson, B., Fagerlund, G.. editors. Self-Desiccation and Its Importance in Concrete, Lund: Lund University, p. 88-98 (1997)
[12] Holt, E., Where did these cracks come from? Conc Int 22(9):57-60 (2000)
[13] Leivo, M., Holt, E., Concrete shrinkage, VTT Research Notes No. 2076, Espoo: VTT (2001)
[14] Bjøntegaard, Ø., Thermal Dilation and Autogenous Deformation as Driving Forces to Self-Induced Stresses in High Performance Concrete. Ph.D. thesis. ISBN 82-7984-002-8, Trondheim, Norwegian University of Science and Technology (1999)
[15] Mak, S.L., Ritchie, D., Taylor, A., Diggins, R., Temperature effects of early age autogenous shrinkage in high performance concrete. In: Tazawa, E., editor. Autogenous Shrinkage of Concrete, London: E&FN Spon, p. 155-156 (1999)
[16] Hammer, T.A., Test methods for linear measurement of autogenous shrinkage before setting. In: Tazawa, E., editor. Autogenous Shrinkage of Concrete, London: E&FN Spon, p. 143-154 (1999)
[17] Hedlund, H., Stresses in High Performance Concrete Due to Temperature and Moisture Variations at Early Ages. Ph.D. thesis. Report 2000:25, ISBN 91-89580-00-01, Luleå, Luleå University of Technology, 394 pp. (2000)
[18] Holt, E., Early Age Autogenous Shrinkage of Concrete, Ph.D. thesis, Seattle, University of Washington, UMI Publishing: Bell & Howard Company (2001)

IS THERE A RELATIONSHIP BETWEEN PORE WATER PRESSURE AND AUTOGENOUS SHRINKAGE BEFORE AND DURING SETTING?

Tor Arne Hammer
SINTEF Civil and Environmental Engineering
Cement and Concrete, Trondheim, Norway

Abstract

In hardened concrete, the capillary tension of pore water is commonly regarded as the driving force for autogenous shrinkage. According to the observations presented, this is not true in the time before and during setting. A simple model is suggested and used to explain it: The structure of early age cement paste consists of a water filled permeable grid of unhydrated cement particles bridged by hydration products. The grid expands by hydration and the water volume decreases (chemical shrinkage). Surface water may penetrate the grid and compensate for some of the chemical shrinkage. Then, the external deformation. i.e. the autogenous deformation, may be swelling. The swelling may continue as long as there is water available at the surface and the permeability of the grid is high enough to allow sufficient water transport. When the water transport becomes less than that corresponding to the sum of chemical shrinkage and grid swelling, the pore water pressure turns into tension. Thus, the PWP may be in tension both when the autogenous deformation is shrinkage and when it is swelling.

1. Introduction

In hardened concrete, the capillary tension of pore water is commonly regarded as the driving force for autogenous shrinkage (AS). When there is insufficient transport of water from external the hydration uses water in the pores. This self-drying causes continuously reduced radii of the water menisci in the pores, and thus, increased capillary tension. The capillary tension (ΔP) in this state is difficult to measure because of the very fine pores and the discontinuity of the pore water. However, the capillary tension it is a function of the relative humidity (RH) in the pores, according to Kelvin-Laplace shown below, which is less complicated to measure at least when values are lower than 97-98 %.

$$\Delta P = 2\sigma^{lg} / r = (RT/v^{l}) \cdot \ln(RH)$$

where σ^{lg} = surface tension of water (liquid-gas)
r = meniscus radius
R = gas constant
T = temperature
v^{l} = molar volume of water

The AS is of course influenced by resistance of the concrete to shrink, i.e. the E-modulus of the concrete. As the E-modulus and of hardened concrete changes relatively little by time, a good correlation between AS and RH is expected for a given concrete and temperature. This has been demonstrated by several authors, e.g. Persson [1].

Both AS and pore water tension have been measured on concrete before and during setting, also, but the relationship between the two is not consistent. One particular apparent inconsistency is related to autogenous swelling seen in linear measurements, but not in volumetric measurements, and not reflected in pore water pressure. The paper gives an introduction to the problem and discusses a possible model which may be used to explain it.

2. Testing techniques

2.1 Overview

In the work at SINTEF and the Norwegian University of Science and Technology (NTNU) the following techniques have been used:

- Chemical shrinkage of pastes using pychnometer
- Volumetric autogenous deformation of pastes using the buoyancy principle ("Condom Method")
- Linear autogenous deformation measuring the vertical component (settlement) and the horizontal component (shrinkage) of pastes, mortars and concretes
- Pore water pressure in pastes, mortars and concretes

2.2 Chemical shrinkage

The chemical shrinkage is found as follows: A small amount of paste is filled in a glass tube (Erlenmeyer flask). The rest of the volume is filled with water. The volume change is recorded as the reduction of the water level in the system [2]. The flasks are placed in a water bath for temperature control. The method has proven to be reliable, and it may be started at a short time after mixing (less than 15 minutes). The method is based on the assumption that the self-desiccation pores continuously fill with water. This is true in most cases because the thickness of the paste samples is small (maximum 10 mm), at least in the first days of age.

2.3 Volumetric autogenous deformation

The autogenous shrinkage was measured according to the buoyancy principle, using a rubber balloon (a condom) filled with paste of which the weight in water is recorded continuously or at fixed intervals [2]. The method may allow bleeding water to lay on the surface. If so, the subsequent absorption will be observed as an extra contraction. In order to avoid the bleeding, the filled condom is usually placed in a tube and placed on rolls to be rotated. The effect of rotation is discussed by Justnes et al [2]. The procedure has proven to give good correlation with the chemical shrinkage method [2]. Temperature control is taken care of by the continuos immersion in water.

2.4 Shrinkage and settlement

The shrinkage and settlement was measured on beams in a steel mould, see Figure 1. For pastes the length/thickness/height is 280/50/50 mm and for concretes 280/100/100 mm. A double layer of plastic sheets with talc powder in between were used inside the mould in order to keep the friction between the concrete and the mould as low as possible. The shrinkage was measured as the horizontal movement of two "nails" placed centric in both ends of the specimen. The nails were made of 3 mm thick steel rods with a 15 x 15 mm steel plate soldered to the end, placed 30 mm in the concrete. The other end was wedged and screwed into inductive displacement transducers through a hole in the ends of the mould. The transducers were fixed to the mould. The measurements have shown acceptable reproducibility.

The settlement was measured as the vertical movement of two circular plastic meshes with diameter of 50 mm, placed with its centre approximately 70 mm from the ends of the mould. In order to prevent any external load from the inductive displacement transducer, the movable part of it resting on the mesh was very light. The meshes penetrate any bleed water. The top surface was covered immediately after finishing with plastic sheet.

All data (settlement, shrinkage and pore water pressure) were recorded every second minute by the use of an electronic data logger. The rig is placed on a balance so that the water loss may be recorded in tests with external drying.

2.5 Pore water pressure

The pore water pressure was measured according to a procedure developed by Radocea [3], see Figure 2. A pressure transducer was connected to a water filled tube with inner diameter of 3 mm. The tube was placed vertically with the end at different depths below the top surface of the paste or concrete.

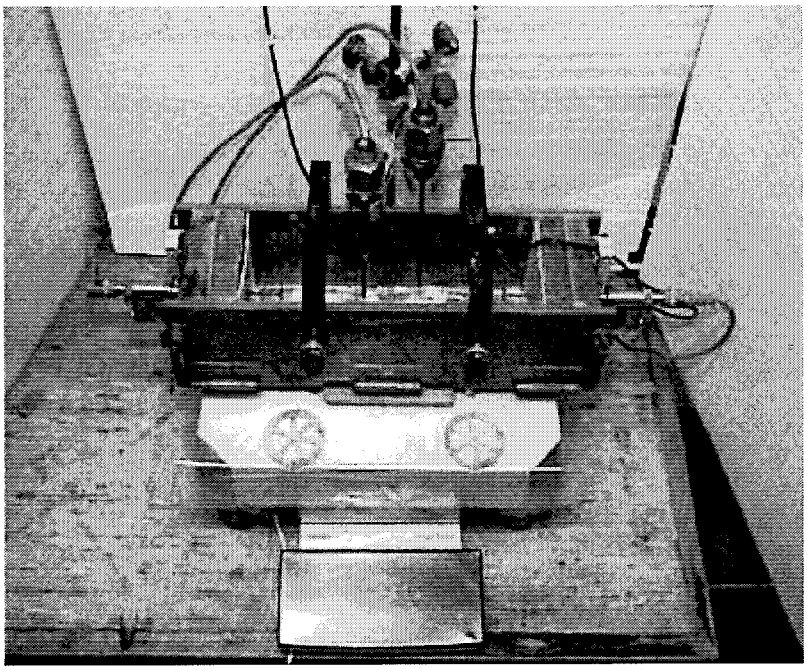

Figure 1. Picture of the rig with devices used to measure settlement, shrinkage, pore water pressure and weight loss in concrete before and during setting.

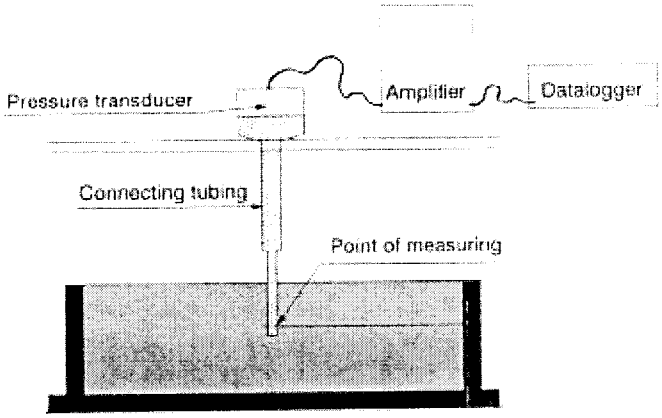

Figure 2. Principle sketch of set up for measurement of pore water pressure [3]

3. Observations

Autogenous deformation (AD) may be defined as all external volume change taking place without any mass change. Mostly, AD is shrinkage (AS), but any re-absorption of bleed water and/or absorbed water in the aggregates as well as early chemical reactions may give autogenous swelling as well [4].

The chemical shrinkage is the origin of AD and in the first few hours after mixing, when the paste-mortar-concrete behaves as a liquid, AD equals chemical shrinkage, see Figure 3 [5]. This time period may be called the "liquid phase". After a certain time the chemical shrinkage, growth on the cement particles and any bleeding have caused an inter-action of particles, and thus, a body that is stiff enough to withstand the chemical shrinkage. Consequently, as the chemical shrinkage continues regardless of the stiffness, empty pores are being created in the paste and the rate of external volume change, AD, decreases rapidly until it reaches a rather constant rate, see Figure 3, which occurs approximately around final setting. This time period may be called the "semi-liquid phase".

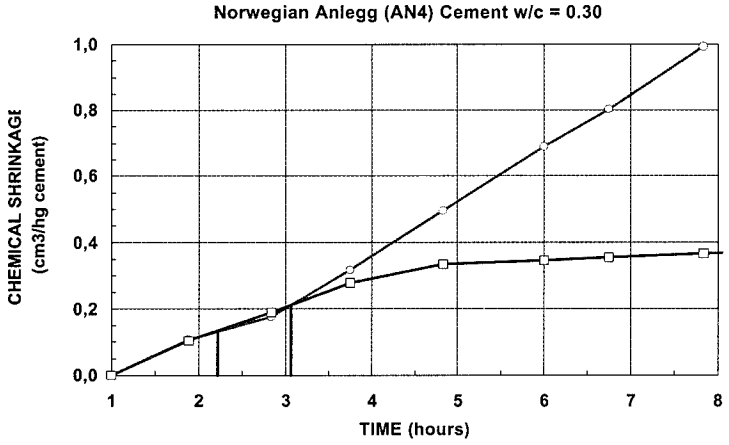

Figure 3. Chemical shrinkage (red) and autogenous shrinkage (blue) of a cement paste with w/c = 0.30 [5]

An important question is how and when empty pores arise? If we assume a cement paste in an air tight box with stiff walls, and where all space between the cement particles is filled with water that contains no air, the air space must origin from vacuum (cavitation). It means that the point where AS deviates from CS should correspond to a pore water pressure corresponding to the vapor pressure of water at the given temperature (here approximately 22 °C), i.e. approximately 20 Torr (approximately 2 700 mm water pile (wp)). Our observations show that this is not the case:

An example from testing of a paste with w/c = 0.30 is given in Figure. 3. It shows that the point where AS (volumetric measurements) start to deviate from CH is approximately 3 hours of age, indicating that empty pores arises at this time. Initial and final set measured according to the Vicat-tests on the same pastes [5], is 2,3 and 3,1 hours, respectively. Barcelo et al. [6] have done similar measurements, but with a set up that probably allows a more accurate recording of the AS. They found the AS and CS of a w/c = 0.28 paste start to diverge approximately 40 minutes after casting, already, which coincides with the point where a "mineral skeleton" is formed according to an ultrasonic test, referred to in [6]. However, the AS rate does not deviate much from the CS rate until approximately 3 hours of age, implying that the skeleton is very soft until then.

The linear measurements (50 x 50 x 280 mm beam) do no comply with the volumetric ones in the time before final setting: Figure 4 shows that the settlement levels out at approximately 1,5 hours already and rather abrupt. This indicates that empty pores arises at this point of time already. The time of 1.5 hours coincides fairly well with the point when the PWP becomes zero (i.e. equals the hydrostatic pressure of water), see Figure. 5. However, the PWP remains at a low PW tension until approximately 4 hours.

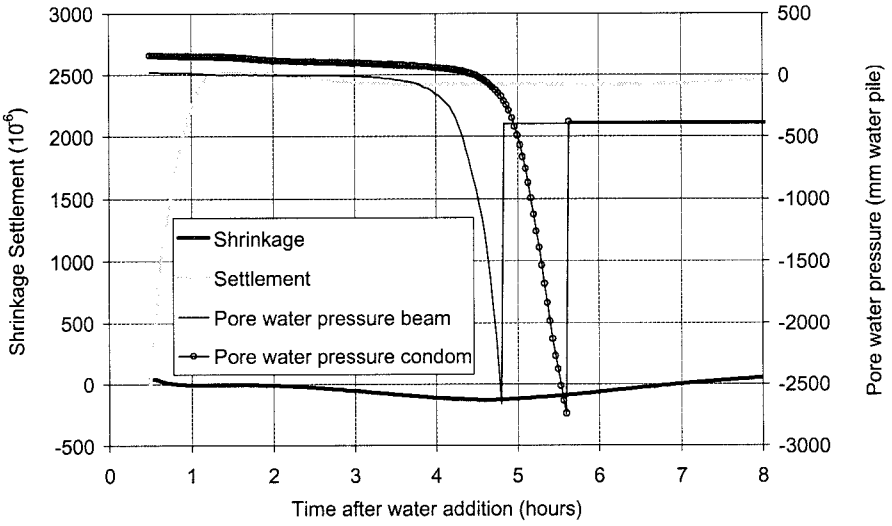

Figure 4. Autogenous settlement and shrinkage and pore water pressure of a cement paste with w/c = 0.30

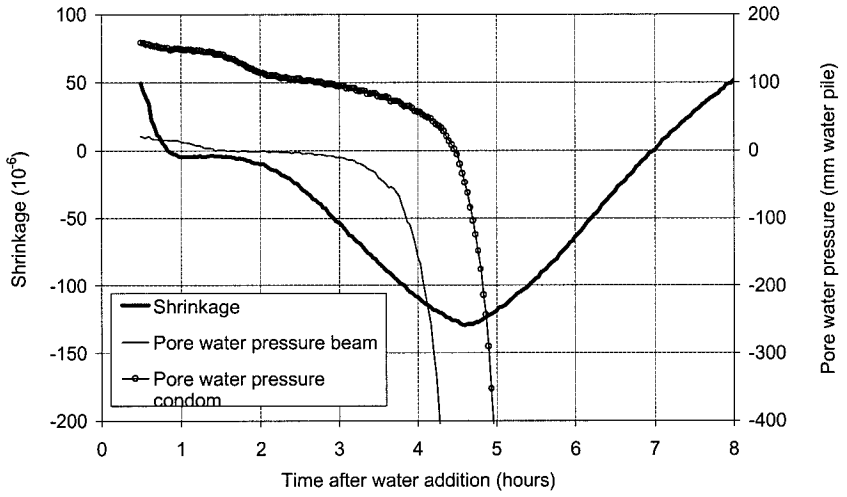

Figure. 5 Autogenous shrinkage and pore water pressure of a cement paste with w/c = 0.30

At the point of time when AS deviates from CS, the PWP is still close to zero, see Figures 3, 4 and 5. The PWP in the condom (when under water) was measured also. The results show that the PWP progresses a bit different from the PWP in the beam in that the initial pressure is higher (caused by the stretching of the condom) and a later "knee-point", see Figure 5. The latter may be related to difference in temperature and thus rate of hydration: The temperature in the condom was approximately 20 °C (submerged in water), while it in the beam increased from 23 to 24.5 °C at 4 hours of age.

Nevertheless, the results indicate that air space arises at a very low pore water tension, i.e. which is less than the tension at cavitation.

Another apparent contradiction is that we measure swelling (both in settlement and shrinkage) and simultaneous pore water tension, see Figures 4 and 5. Reabsorption of bleed water has been suggested to be one source of this expansion [4]. Figure. 6 shows that the time and magnitude of the swelling if pastes increases with decreasing w/c and with addition of silica fume, both leading to reduced bleeding. Bjontegaard [7] has demonstrated that increasing amount of water have the same effect on concrete, see Figure 7. Other results show that the expansion continues until far beyond the time of setting when the surface is kept wet, but the PWP still progresses in to tension rather irrespective of this and develops rapidly thereafter see Figure 8. The results demonstrate that the contradiction between volumetric and linear measurements as to the swelling observation, is apparently not reflected in the PWP measurements.

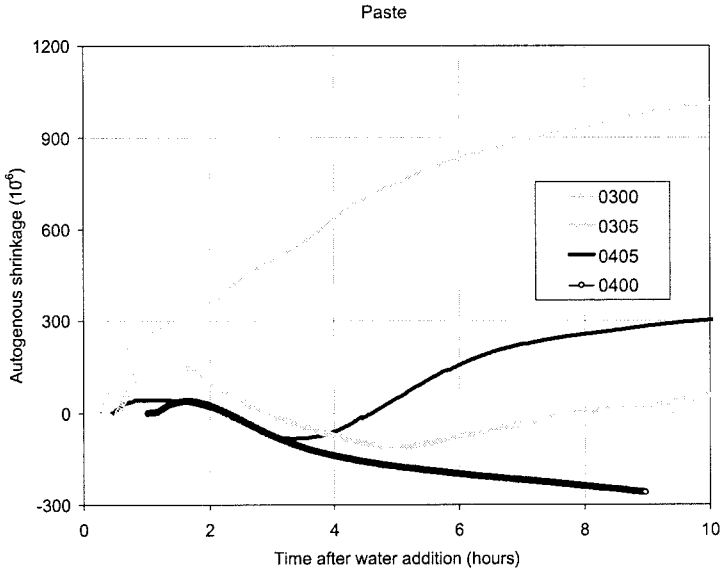

Figure 6. Autogenous shrinkage of cement pastes with w/b = 0.30 and 0.40 both with and without 5 % silica fume

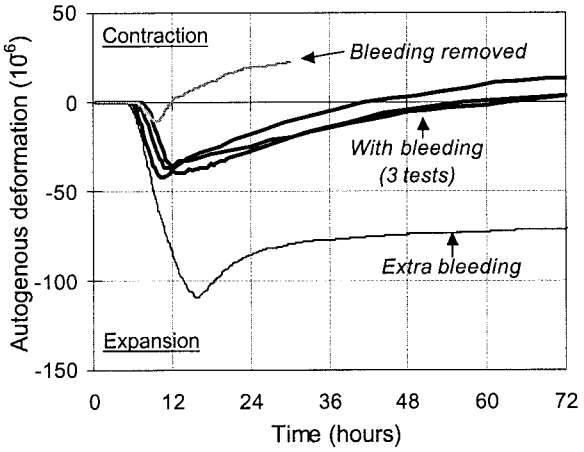

Figure 7. Autogenous shrinkage of a concrete with w/b = 0.40 with 5 % silica fume and with "Bleeding" ("natural bleeding"), "Bleeding removed" (sucked up externally), and with "Extra bleeding" (extra water added on top) [7]

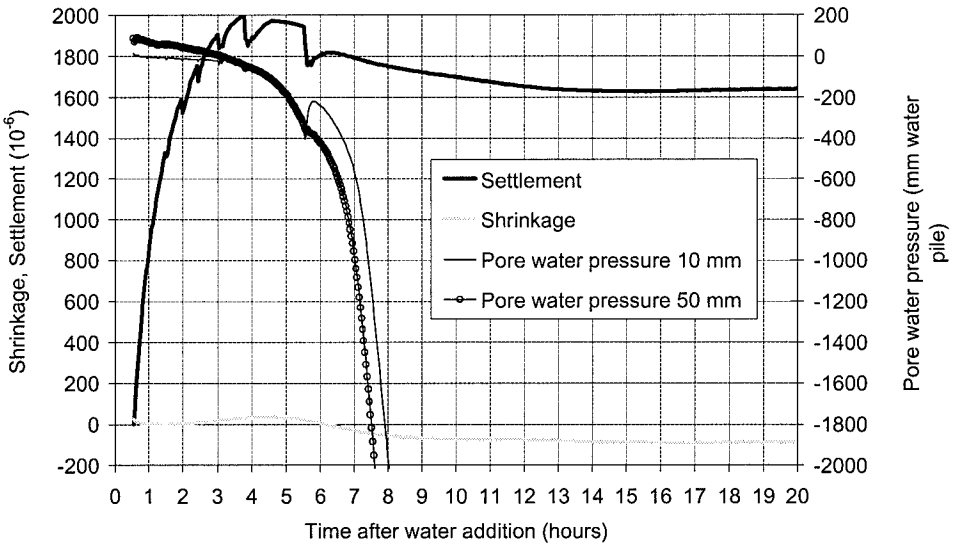

Figure 8. Settlement, shrinkage and pore water pressure (at 10 and 50 mm depths) of a concrete with w/b = 0.40 with 5 % silica fume, where the surface has been covered with water until approximately 12 hours of age.

A third observation which seems as an apparent contradiction is that concrete with high air content, by the use of air entraining admixture (AEA), gives faster PWP decrease in the semi-liquid period than seen in the equivalent concrete without AEA. Also, the AS is significant in the concrete with high air content, see Figure 9. One should expect that the air bubbles would act as buffers when the water amount decreases, i.e. that they grow. The growing should be accompanied by a pressure decrease, and thus, a PWP pressure increase and not a decrease as observed.

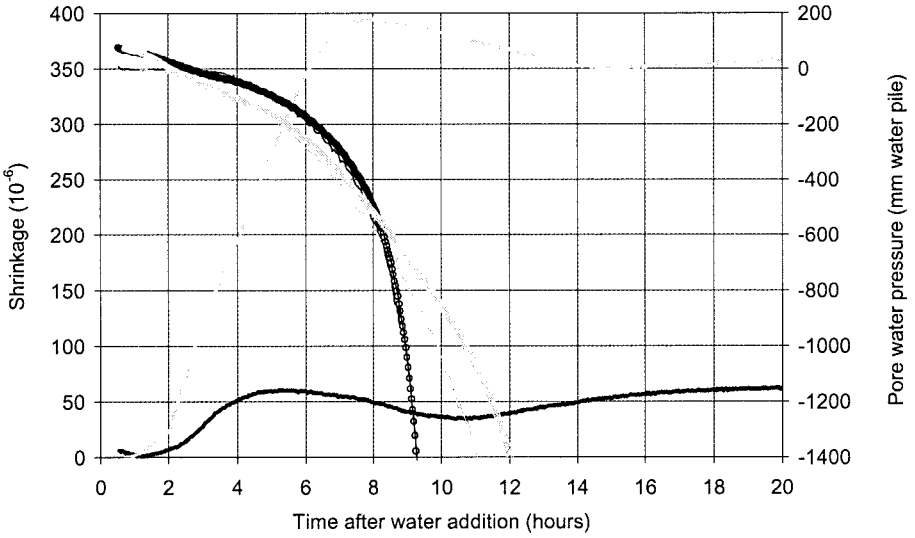

Figure 9. Autogenous shrinkage and pore water pressure (at 5 and 50 mm depths) of concretes with w/b = 0.40 with 5 % silica fume – one without air entraining + admixture (giving an air content of approx. 2 %), black curves, and one with (giving an air content of approx. 8 %), grey curves

4. Possible explanation

These contradictions are not yet fully understood. A possible model that may be used to explain it is suggested in the following: From the time of self-support and on the cement paste structure may be seen as a bearing structure consisting of unhydrated cement grains bridged with hydration products and with water in between which may flow through the bridges. Furthermore, the evolution of the structure may be seen as an expansion of the bearing structure due to the growing of the hydration products (the "bridges"), a decreasing permeability of the bridges, and a decreasing volume of water due to the chemical shrinkage. Barcelo et al. have surveyed expansion mechanisms and found that crystallization pressure of growing ettringite or portlandite, or even C-S-H formation have been suggested as causes for the expansion [6]. According to the suggested model, there is always an expansion going on.

At the point of self support, the structure is still soft (few contact points and "slender"), but withstand a part of the chemical shrinkage (seen as a leveling out of AD), i.e. empty

space is being generated. The PWP at this point is at a very low tension and far away from cavitation point, see section 3, so the question is how does the space arise?

One approach to explain it is to compare the model box which is air tight and has stiff walls, with the condition at testing: The most apparent difference is that the walls in the tests are not stiff, but made of thin plastic or rubber membranes. It means that the pore water is in contact with the atmosphere, and thus, that the PWP equals the atmospheric pressure (plus the hydrostatic pressure as a function of depth), as long as the water may flow at a sufficient rate. Thus, water may flow inwards from at the surface, e.g. bleed water, and thus, replace the water loss due chemical shrinkage. When the bleed water has been consumed or there is no bleeding, the surface water (i.e. between particles) may be sucked in. The plastic or rubber used to seal the paste samples have thickness less than 0,05 mm which is in the same magnitude as the average cement particle size, and thus, the center spacing of the particles. Following, the plastic or rubber may deform between the grains. This may continue as long as there is sufficient water transport from the surface. Then, the PWP progresses until cavitation occurs. Another possible water source is absorbed water in aggregates, in lightweight aggregates in particular (not yet explored).

This may also explain why expansion is observed in linear measurements, but not in the volumetric ones (condom method). The emptying of the surface pores will not be recorded in linear measurement, while in the volumetric test, the deformation of the condom will be recorded as a reduced buoyancy, and thus, a shrinkage.

Air bubbles made with AEA (i.e. fine and well distributed) are known to increase the stability of the concrete, and thus, reduce bleeding. The lack of bleeding may be the reason why the PWP decreases more rapidly in the semi-liquid period in the concrete with AEA, as seen in Figure 9. This is however not verified by bleeding measurements. Later, the opposite effect can be seen, which fits the buffer theory saying that air bubbles grow, and thus, releases the PWP. Accordingly, the period of swelling should be more pronounced in the concrete with AEA, as seen in Figure 9.

In addition to CS, swelling, stiffness and permeability of the grid are important parameters in the model. CS is relatively easy to measure (or calculate). The stiffness evolution may be deduced from e.g. ultrasonic techniques, but the swelling and permeability evolution seems to be difficult tasks to find separately. At the time we have not made attempts to find these parameters, and it is therefore not discussed further here.

5. Conclusion

According to the observations presented, there is no unique relationship between pore water pressure and autogenous deformation in paste-mortar-concrete before and during setting. A simple model is suggested and used to explain it:

The structure of early age cement paste consists of a water filled permeable grid of unhydrated cement particles bridged by hydration products. The grid expands becomes less permeable by hydration and the water volume decreases (chemical shrinkage). Surface water may penetrate the grid and compensate for some of the chemical shrinkage. Then, the external deformation. i.e. the autogenous deformation (AD), may be swelling. The swelling may continue as long as there is water available at the surface and the permeability of the grid allows sufficient water transport. When the water transport becomes less than that corresponding to the sum of chemical shrinkage and grid swelling, the pore water pressure (PWP) turns into tension. Thus, the PWP may be in tension both when the autogenous deformation is shrinkage and when it is swelling.

References

[1] Persson, B, "Quasi-instantaneous and Long-term deformations of High Performance Concrete". Doctor theses from Lund University, Sweden (1998).

[2] Justnes, H., Reyniers, B. and Sellevold, E.J., "An evaluation of methods for measuring chemical shrinkage of cementitious pastes". Nordic Concrete Research, publication no. 14. 1/94, Norwegian Concrete Association, Oslo (1994) pp. 44 – 61.

[3] Radocea, A., "A Study on the Mechanism of Plastic Shrinkage of Cement-based Materials". Thesis for the degree of Doctor of Engineering from Chalmers Technical University, Gothenburg, Sweden (1992).

[4] Hammer, T.A., "Test Method for Linear Measurements of Autogenous Shrinkage before setting", Autogenous Shrinkage of Concrete, (ed. E. Tazawa) E & FN Spon, London, pp. 143-154 (1999).

[5] Clemmens, F and Depuydt, P, "Early Hydration of Portland Cements". Diploma work at Katoholieke Universiteit Leuven and Norwegian University of Science and Technology (1999).

[6] Barcelo, L., Boivin, S., Acker, P., Toupin, J. and Clavaud, B. "Early Age Shrinkage of Concrete: Back to Physical Mechanisms". Accepted for publication in Concrete Science and Engineering (2001).

[7] Bjøntegaard, Ø., "Thermal Dilation and Autogenous Deformation as Driving Forces to Self.Induced Stresses in High Performance Concrete". Doctor theses from the Norwegian Institute of Science and Technology, Trondheim, Norway (2000).

Acknowledgement

The present work is a part of the Norwegian projects NOR-IPACS and NOR-CRACK supported by the Norwegian Research Council, Selmer ASA, Elkem ASA Materials, Fesil ASA, Norcem A/S, the Directorate of Roads and the Norwegian University of Science and Technology.

COMPARATIVE STUDY OF THE EFFECTS OF WATER/BINDER RATIO AND SILICA FUME ON THE VOLUME INSTABILITY OF HYDRATING CEMENT PASTES AT EARLY-AGE

J.-P. Charron, J. Marchand, B. Bissonnette, M. Pigeon and B. Zuber
CRIB - Université Laval, Canada

Abstract
The early-age volume instability of hydrating cement paste mixtures was investigated by chemical and external shrinkage measurements. Test variables included type of binders (CSA Type 10 and CSA Type 10 + 8 % silica fume) and water/binder ratio (0.27, 0.35 and 0.45). All volume change measurements were performed in a temperature-controlled bath kept at 20°C. Complementary determinations of the degree of hydration were carried out on companion samples after 8, 24, 48 and 144 hours of hydration. Test results confirm the significant influence of water/binder ratio on the volume instability of neat cement pastes at early-age. Data also show that the addition of silica fume contributes to increase external shrinkage after setting. Correlations between chemical and external shrinkage test results and degree of hydration are discussed.

1. Introduction

High-performance concretes (HPC) are now commonly used for the construction of various types of structures such as bridge decks, pavements, piers and commercial buildings. The low water/binder ratio of these mixtures, combined with the frequent use of supplementary cementing materials (e.g. silica fume, …), often contribute to enhance their long-term durability to aggressive environments. Unfortunately, previous experiences indicate that the significant reduction of the water added to these systems often reduces the volume stability of HPC during the first days of hydration and makes them more susceptible to early-age cracking [1-3]. Although thermal stresses are often at the origin of the premature cracking of HPC structures, many recent investigations clearly indicate that autogeneous shrinkage has a strong influence on the behavior of these systems.

A comprehensive research project on the early-age cracking of HPC was recently launched at Laval University. The main objective of this four-year program, conducted with different partners, is to develop practical ways to reduce the susceptibility of HPC mixtures to early-age cracking. The first phase of this program was devoted to the appraisal of various experimental techniques for the investigation of the early-age behavior of hydrating cement systems [1,4]. This paper summarizes the results of the second phase, which was focused on the study of the volume instability of neat cement paste mixtures. Test variables considered in this second part of the project included water/binder ratio and the addition of silica fume.

2. Experimental program

2.1 Materials and mixture preparation

Two different binders were tested as part of this investigation. A first series of neat cement pastes was prepared with an ordinary Portland cement (OPC) (CSA Type 10) while a blended silica fume binder (8% silica fume per total mass of binder) was used for the production of a second series of mixtures. Information on the composition of the cement is given in table 1. A (naphthalene-based) superplasticizer was also added to all mixtures.

OPC mixtures were prepared at three different water/binder ratios (0.27, 0.35 and 0.45). Two different water/binder ratios, 0.27 and 0.45, were tested for the silica fume pastes. Each mixture was produced and tested three times in order to investigate the reproducibility of the measurements. Information on the mixtures characteristics is given in table 2.

Prior to mixing, all constituents were stored at 20 ± 2 °C. The mixtures were prepared in a 5-L mixer using a 5-min batching sequence (based on ASTM 305-82 and ASTM C 109-88) under vacuum in order to minimize the formation of air bubbles.

Table 1 - Chemical and mineralogical compositions of cements

Chemical composition	Type 10
SiO_2 (%)	20,4
Al_2O_3 (%)	5,5
Fe_2O_3 (%)	2,3
CaO (%)	63,3
MgO (%)	2,7
SO_3 (%)	3,7
Alkalis (%)	0,3
Loss on ignition (%)	4,5

Mineralogical composition	Type 10
C_3S (%)	52,0
C_2S (%)	20,0
C_3A (%)	11,0
C_4AF (%)	7,0

Physical property	Type 10
Specific surface (m^2/kg)	382

Table 2 - Mixture characteristics

Components	P27	P27FS	P35	P35FS	P45	P45FS
Cement (kg/m³)	1670	1490	1490	1334	1301	1169
Silica fume (kg/m³)	-	130	-	116	-	102
Water (kg/m³)	451	437	522	508	586	572
Superpl (ml/kg liant)	39	39	13	13	3	3
Density (kg/m³)	2154	2090	2021	1967	1889	1844

2.2 Experimental methods

2.2.1 Chemical shrinkage

Chemical shrinkage measurements were carried out using the dilatometric method initially developed by Le Chatelier [5]. This method consists in immersing a given mass of cement paste in an Erlenmeyer flask filled with water and surmounted by a graduated capillary tube (Fig. 1a). Afterwards, the volume of water gradually consumed by the hydration reaction is measured at regular intervals. The apparatus is placed in a thermo-regulated bath kept at 20 °C. This technique allows measuring the total volume change of the hydrating material (i.e. the sum of the external shrinkage and the internal gas volume created by self-desiccation during the hydration process).

2.2.2 External shrinkage

The external deformation of the paste mixtures was measured using the immersion technique developed by Justnes et al. [6]. The external shrinkage test consists in filling a (impervious) plastic membrane with paste. The sealed membrane is then immersed in water and its change of mass is regularly measured. By applying Archimedes's principle, the apparent (or external) volume reduction of the hydrating mixture can be derived from its change of mass (as measured in water). During this test, the temperature of water is maintained at 20 °C (Figure 1b).

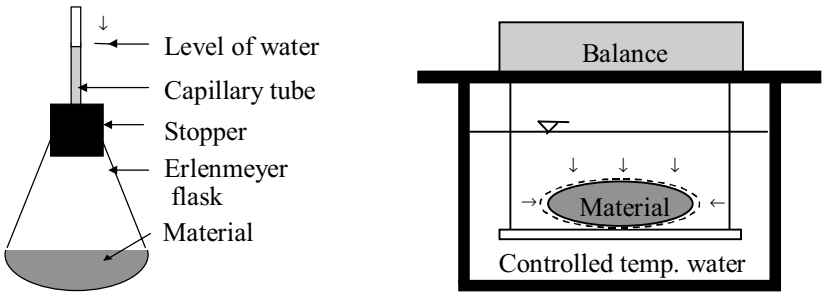

Figure 1 - Schematic illustrations of the two volumetric shrinkage tests
a) Chemical shrinkage, b) External shrinkage.

2.2.3 Degree of hydration

The assessment of the degree of hydration of the OPC mixtures was done by measuring the non-evaporable water content of the mixtures after 8, 24, 48 and 144 hours of hydration. The non-evaporable water content was assumed to correspond to the loss of mass of a powdered sample between 110 °C and 1000 °C. Samples from both chemical and external shrinkage specimens were tested. For each mixture, the ultimate non-evaporable water content (corresponding to full hydration of the sample) was estimated from the mineralogical composition of cement using Molina's equation [7].

3. Results

As previously emphasized, three samples of each mixture were tested for both chemical shrinkage and external deformation. For a given set of samples, the reproducibility of the results was estimated using the Student law [8] for a level of reliance of 90 % (Equation 1). The limits of the variability depend on the average ($\overline{X}$) and the variance ($\hat{\sigma}$) of the test results, the number of replicate samples per test series (n) and a probabilistic argument. This last argument is based on the level of reliance chosen (C_α).

$$\text{Limits} = \overline{X} \pm \frac{C_\alpha \cdot \hat{\sigma}}{\sqrt{n}} \qquad [1]$$

In order to facilitate the reader's task, each series of shrinkage test results is represented by its average curve and a set of bars, which corresponds to the variability of each data point. Shrinkage test results are also expressed both as a variation of the initial volume of the sample ($\Delta V/V_{init}$) and in ml/100g_{binder}.

Shrinkage test results obtained for the different OPC mixtures are presented in Figure 2 and Figure 3. The evolution of the degree of hydration of the OPC mixtures is presented in Figure 4. For the samples subjected to the chemical shrinkage test, degree of hydration values measured before 48 hours were found to be unreliable and are not therefore presented.

The relationship between the degree of hydration and the shrinkage test results is given in Figure 5. The straight line appearing in the first graph correspond to theoretical calculations of chemical shrinkage carried out on the basis of the equations proposed by Justness et al. [4]. More information on the subject is given in the following section.

Test results obtained for the OPC and silica fume mixtures of 0.27 water/binder ratio are given in Figure 6 and Figure 7. Those measured for the 0.45 water/binder ratio mixtures are presented in Figure 8 and Figure 9.

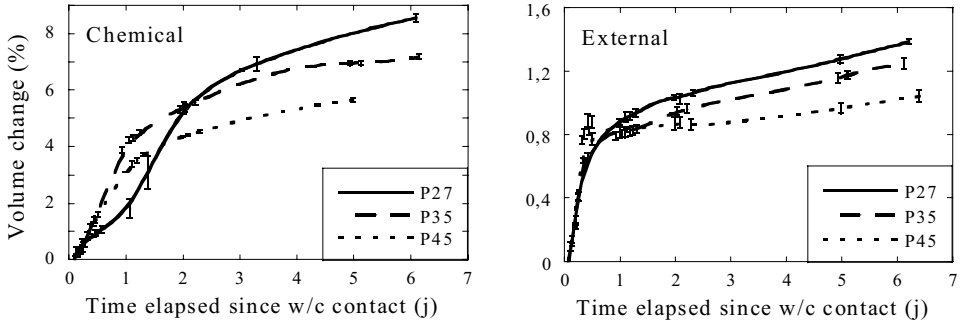

Figure 2 - Influence of water/binder ratio on OPC mixtures ($\Delta V/V_{init.}$- %),
a) Chemical shrinkage, b) External shrinkage.

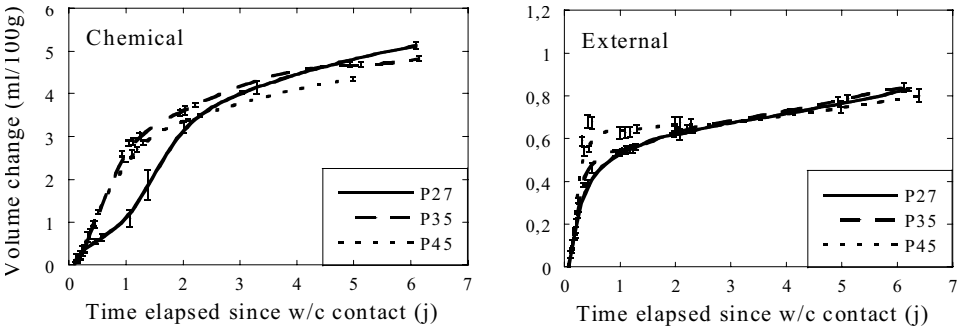

Figure 3 - Influence of water/binder ratio on OPC mixtures ($ml/100g_{binder}$),
a) Chemical shrinkage, b) External shrinkage.

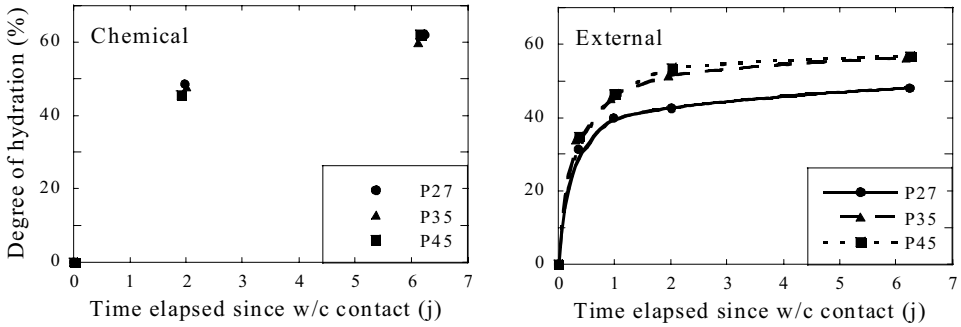

Figure 4 - Variation of the degree of hydration for OPC mixtures,
a) Chemical shrinkage samples, b) External shrinkage samples.

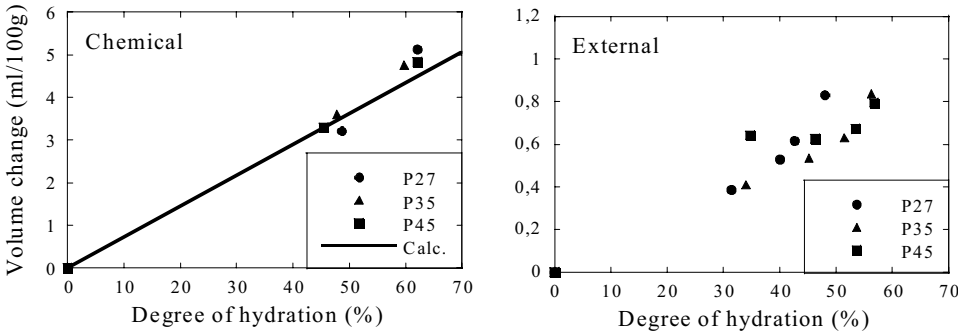

Figure 5 - Relationship between shrinkage and degree of hydration in OPC systems, a) Chemical shrinkage, b) External shrinkage.

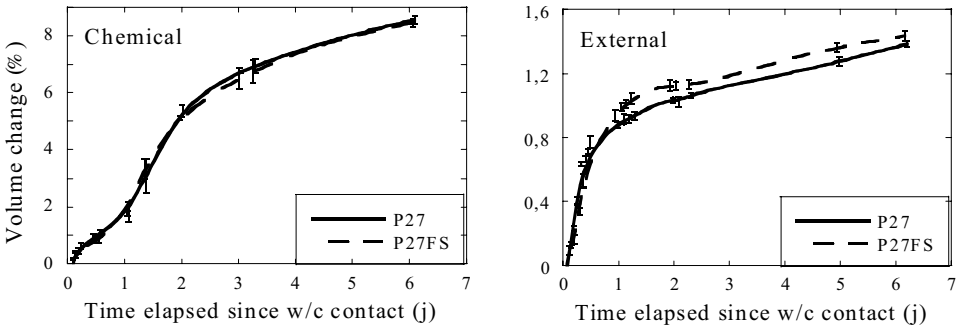

Figure 6 - Influence of 8 % of silica fume for 0.27 w/b systems ($\Delta V/V_{init.}$ - %), a) Chemical shrinkage, b) External shrinkage.

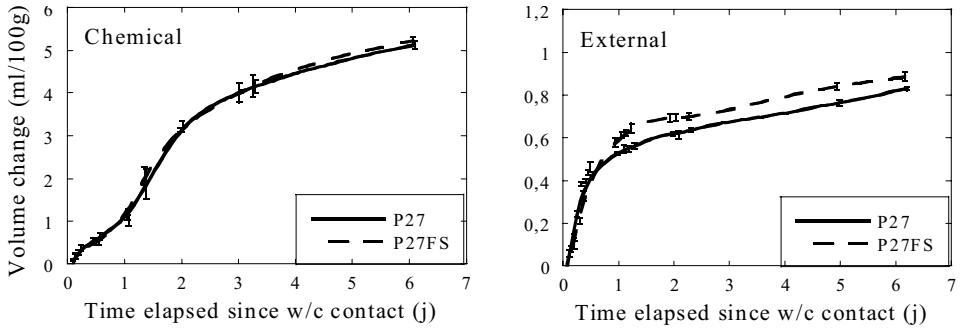

Figure 7 - Influence of 8 % of silica fume for 0.27 w/b systems (ml/100g_{binder}), a) Chemical shrinkage, b) External shrinkage.

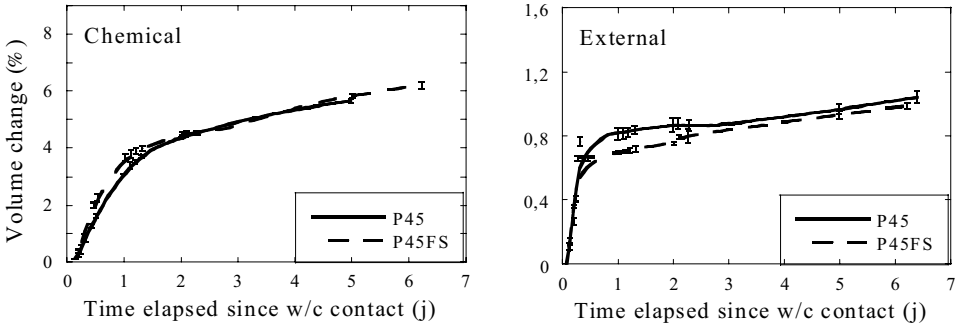

Figure 8 - Influence of 8 % of silica fume for 0.45 w/b systems ($\Delta V/V_{init}$ - %), a) Chemical shrinkage, b) External shrinkage.

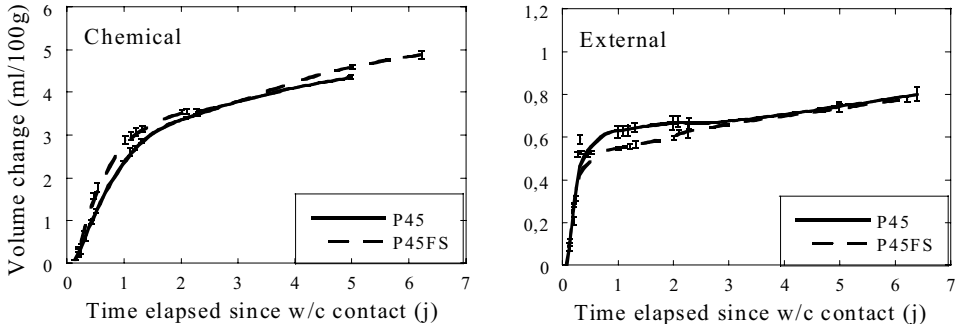

Figure 9 - Influence of 8 % of silica fume for 0.45 w/b systems (ml/100g_{binder}), a) Chemical shrinkage, b) External shrinkage.

It is important to note that the kinetics and magnitude of deformations measured in this study are similar to those reported by Justnes et al. [6, 9,10] and Boivin [11].

4. Discussion

4.1 Water/binder ratio

Test results show in Figure 2 and Figure 3 clearly confirm that the kinetics of both types of shrinkage is quite important during the first few hours of hydration. This period is approximately 48-hour long for the chemical shrinkage and 8-hour long for the external shrinkage. As previously emphasized by many authors, the knick point appearing in the external shrinkage curve corresponds to the formation of a self-supporting skeleton [11, 12]. As can be seen in the figures, a lower rate of chemical and external shrinkage is observed for the 0.27 water/cement ratio mixture during the first hours of hydration. This

phenomenon can be associated to the high dosage in superplasticizer of the mixture (see Table 2). Similar observations were made by Bissonnette et al. [13].

As can be seen in Figure 2, in which deformations are expressed as a reduction of the initial volume ($\Delta V/V_{init.}$), a reduction of the water/binder ratio contributes to significantly increase both types of shrinkage. This trend was observed by Justnes et al. [9] and Aouad [14]. It is also consistent with external shrinkage results estimated from 1-D measurements, which demonstrated higher shrinkage for low water/binder ratio [1, 2].

The marked effect of a reduction of the water/cement ratio on the external shrinkage curves is associated to the gradual densification of the paste that contributes to refine the material's pore structure. During the hydration process, self-desiccation effects favor the formation of menisci within the porous system. According to Kelvin and Laplace laws [15], the presence of menisci in the porosity places water under tension and the hydrating solid structure under compression. The net effect is a contraction of the material. In low water/binder ratio systems, self-desiccation takes place in smaller pores and then induces greater external deformation.

In the chemical shrinkage experiments, the formation of menisci is impeded by the penetration of water into the hydrating material. The significant influence of water/cement ratio on chemical shrinkage cannot be explained by the development of significant internal stresses within the material during the test. However, the effect of reduction of the water/cement ratio can be explained by considering the amount of cement that has hydrated after a given period. As can be seen in Figure 4a, non-evaporable water content determinations indicate that degree of hydration values are not affected by water/cement ratio. Since low water/cement pastes contain more cement per volume (see Table 2), the net amount of hydrated cement tends to increase with a reduction of the water/cement ratio.

The chemical and external shrinkage test results are expressed in terms of a reduction of volume per gram of cement in Figure 3. As can be seen in the figure, both types of shrinkage appear to be related to the amount of binder contained in the samples. The phenomenon was also reported by Boivin [7] and Justnes et al. [9].

4.2 Degree of hydration

Degree of hydration values measured for both chemical and external shrinkage samples are presented in Figure 4. As can be seen, two different trends can be distinguished. On the one hand, degree of hydration values do not seem to be significantly affected by the water/cement ratio of the pastes submitted to chemical shrinkage experiment. This phenomenon can be explained by the fact that samples contained in the Erlenmeyer flasks are continuously maintained in saturated conditions during the test.

On the other hand, results in Figure 4 tend to indicate that a reduction of the water/cement ratio results in a decrease of the degree of hydration for the external

shrinkage samples. This is particularly clear for the 0.27 water/cement ratio paste. In an external shrinkage sample, hydration happens in unsaturated conditions and is consequently delayed by the reduction of moisture in the materials [16]. This phenomenon is particularly significant for low water/binder ratio mixtures for which self-desiccation is important [1-2].

The comparison of volume change test results to degree of hydration values leads to interesting observations (Figure 5). For instance, it seems that chemical shrinkage data measured experimentally correlate well with theoretical values calculated with Justnes et al.'s coefficients [17]. Both series of results clearly confirm that chemical shrinkage is directly proportional to the hydration of cement [18].

As can be seen, Figure 5 does not reveal any clear relationship between external shrinkage results and degree of hydration values. Supplementary measurements of the level of hydration reached by the mixtures at very early ages would have been required.

4.3 Silica fume

The replacement of a proportion of cement by silica fume has mainly two consequences on the deformational behavior of cement pastes. On the one hand, the hydration reaction of silica fume with hydrated lime produces hydrates and increases chemical shrinkage [19]. This supplementary deformation should be added to the deformation caused by the hydration of cement. For this study, the chemical shrinkage of the cement CSA Type I was estimated to 7.3 ml/100g_{binder}. The chemical deformation associated to the reaction of silica fume has previously been estimated to be around 8.8 ml/100g_{binder} [16]. Thus, the additional chemical shrinkage of the binder with silica fume should be very small. On the other hand, the presence of silica fume induces a refinement of the capillary porosity. As previously mentioned, the effect of self-desiccation in a denser material generates higher tensile stresses in the liquid phase and consequently increases external shrinkage.

The chemical shrinkage test results for cement pastes of all water/binder ratio did not show any influence of the replacement of 8 % of cement by silica fume in the two types of analysis (Figure 6a to Figure 9a). The small difference of chemical shrinkage of the two binders probably explains this result. Justnes et al. [10] also reported a mitigated effect of a replacement of 10 % of cement by silica fume on chemical shrinkage. Their results depend largely on the type of cement used. The results of Aouad [14] for a proportion of 16 % of silica fume in the binder have demonstrated a reduction of the chemical deformation. As per the author, the experimental device used in his study was not really adapted to the determination of chemical shrinkage of low permeability materials and could have underestimated the deformation. Finally, it is important to note that the enhancing effect of self-desiccation cannot be observed in the chemical shrinkage results of this study, because the samples are kept in saturated conditions during the test.

The enhancing effect of silica fume can be seen in Figure 6b to Figure 9b. In fact, external shrinkage of the paste with silica fume of water/binder ratio equals to 0.27 seems to increase after setting compared to its counterpart without silica fume. The effect of self-desiccation appears more clearly when the material has reached setting. No extraneous deformation can really be observed for the mixtures of high water/binder ratio (0.45). This trend could be explained by the fact that the self-desiccation effects are negligible for material of coarse porous network. The results of Aouad [14] and Justnes et al. [10] support the observations of this study as regards to the enlargement of the external shrinkage caused by the utilization of silica fume.

5. Conclusion

Test results presented in this paper are in good agreement with the data found in the literature. They confirm that a reduction of the water/binder ratio leads to an increase of chemical and external deformations when data are expressed in terms of a reduction of volume on the initial volume of paste ($\Delta V/V_{init.}$). The analysis of the results considering the binder content ($ml/100g_{binder}$) tends to confirm that both chemical and external deformation are related to the amount of binder included in materials.

Degree of hydration measurements emphasize the significant importance of the hygrothermal conditions applied to the samples upon testing. In saturated conditions, the hydration occurs without any retarding effects associated with the lack of moisture. The development of hydration is independent of the water/binder ratio. In unsaturated conditions, the degree of hydration reached at any given time is lower for low water/binder ratio systems.

Test data also confirm that chemical shrinkage is directly proportional to the degree of hydration of cement.

Finally, the utilization of silica fume in replacement of 8 % of cement contributes to increase self-desiccation effects in low water/binder ratio mixtures (w/b = 0.27). This trend could not be observed for the 0.45 water/binder ratio mixtures.

6. Acknowledgments

This project was financially supported by the Natural Sciences and Engineering Research Council of Canada (NSERC) and the Fonds Québécois de la Recherche sur la Nature et les Technologies (FQRNT).

7. References

[1] Toma, G., Comportement des bétons au jeune âge, Ph.D. thesis of Université Laval, Québec, 2000.

[2] Bonjtegaard, O., Thermal dilation and autogenous deformation as driving forces to self-induced stresses in high performance concrete, Ph.D. thesis of NTNU, Trondheim, 1999.

[3] Krauss, P. D. and Rogalla, E. A., Transverse cracking in newly constructed bridge decks, National Academy Press, National Cooperative Highway Research Program Report 380, Washington, 1996.

[4] Charron, J.-P., Marchand, J., Bissonnette, B., Early-age deformations of hydrating cement systems, systematic comparison of linear and volumetric shrinkage measurements, Concrete Science and Engineering, **3** (2001) 168-173.

[5] LeChatelier, H., Recherches expérimentales sur la constitution des mortiers hydrauliques, Dunod, Paris, 1904.

[6] Justnes, H., Reyniers, B. and Sellevold, E.J., An evaluation of methods for measuring chemical shrinkage of cementitious pastes, Nordic Concrete Research, **25** (2) (1994) 45-61.

[7] Molina, L., On predicting the influence of curing conditions on the degree of hydration, CBI Report, 5: 92, Swedish Cement and Concrete Research Institute, Stockolm,1992.

[8] Alalouf, S., Labelle, D., Ménard, J, Introduction à la statique appliquée, Éditions Addison-Wesley, Montréal, 1983.

[9] Justnes, H., Van Gemert, A., Verboven, F. and Sellevold, E.J., Total and external chemical shrinkage of low w/c ratio cement pastes, Advances in cement Research, **8**, (31) (1996) 121-126.

[10] Justnes, H., Sellevold, E.J., Reyniers, B., Van Loo, D., Van Gemert, A., Verboven, F. and Van Gemert, D., Chemical shrinkage of cementitious pastes with mineral additives, Proceedings of the Second International Research Seminar on Self-desiccation and its Importance in Concrete Technology, Lund (1999) 73-84.

[11] Boivin, S., Retrait au jeune âge du béton - Développement d'une méthode expérimentale et contribution à l'analyse physique du retrait endogène, Doctoral thesis of École Nationale des Ponts et Chaussées, Paris, 1999.

[12] Justnes, H., Clemmens, F., Depuydt, P., Van Gemert, D. and Sellevold, E.J., Correlating the deviation point between external and total chemical shrinkage with setting time and other characteristics of hydrating cement paste, Proceedings of the International RILEM Workshop Shrinkage 2000, Toulouse (2000).

[13] Bissonnette, B., Marchand, J., Martel, C., Pigeon, P., Influence of superplasticizer on the volume stability of hydrating cement pastes at early age, Concrete: Material Science to Application, A Tribute to Professor Surendra, P. Shah Edited by Balaguru, P., Namaan, A., Weiss, J., ACI special Publication, To be published in 2002.

[14] Aouad, I., Étude de l'influence du rapport eau/liant, de la fumée de silice et d'un agent réducteur de retrait sur le retrait endogène de pâtes de ciment, Master thesis of Université de Sherbrooke, Sherbrooke (1999).

[15] Hua, C., Acker, P., Ehrlacher, A., Retrait d'autodessiccation du ciment, Bulletin de liaison Laboratoires des Ponts et Chaussée, (196) (1995) 79-89.

[16] Powers, T.C., Brownyards, T.L., Studies of the physical properties of hardened cement paste, Research Laboratories of the Portland Cement Association, Bulletin 22, Chicago (1947).

[17] Justnes, H., Sellevold, E.J., Reyniers, B., Van Loo, D., Van Gemert, A., Verboven, F., Van Gemert, D., The influence of cement charactheristics on chemical shrinkage, Proceedings of the International workshop on autogenous shrinkage of concrete, Hiroshima (1998) 67-76.

[18] Barcelo, L., Boivin, S., Acker, P., Toupin, J., Clavaud, B., Early age shrinkage of concrete : back to physical mechanisms, Concrete Science and Engineering, **3** (10) (2001) 85-91.

[19] Sellevold, E.J., Justnes, H., High strength concrete binders, Part B : Non evaporable water, self-desiccation and porosity of cement pastes with and whithout condenced silica fume, Proceedings of the Fourth Canmet/ACI international conference on fly ash, silica fume, slag and natural pozzolans in concrete, Istanbul, Turkey (1992) 891-902.

A NEW APPROACH FOR EVALUATION OF AUTOGENOUS SHRINKAGE OF HIGH STRENGTH CONCRETE UNDER HEAT OF HYDRATION

Yang Yang and Ryoichi Sato
Department of Civil and Environmental Engineering, Hiroshima University, Japan

Abstract

A new method is proposed to evaluate autogenous shrinkage of high strength concrete under hydration heat of cementicious materials in this study. Thermal expansion coefficients of HSC were obtained to which temperature change was given in low temperature region from -1 to 5 ℃ to control the hydration as far as possible. Using the newly obtained thermal expansion coefficients autogenous shrinkage strain and thermal strain were separated and temperature-dependence of autogenous shrinkage strain was also evaluated by curing specimens under 20 ℃ and semi-adiabatic conditions.

Thermal expansion coefficients of high strength concrete evaluated by the new method decreased rapidly with time after setting and then reached a minimum value at about 1 day and, thereafter, increased gradually depending on self-desiccating. Comparison of the autogenous shrinkage under 20 ℃ with that under semi-adiabatic condition showed that the maturity concept was not applicable for evaluating temperature-dependent autogenous shrinkage of high strength concrete containing silica fume based on the newly obtained thermal expansion coefficient.

1. Introduction

Temperature deformation and autogenous shrinkage (AS) arise simultaneously at an early age due to the hydration of cementitious materials in high strength concrete (HSC) unlike normal strength concrete. It is indispensable for controlling cracking to predict accurately strains produced by temperature change and AS. For this purpose, an exact thermal expansion coefficient (TEC) is needed. A constant TEC has been applied to compensate thermal strain up to now as is seen in previous studies [1,2]. However, it has not necessarily been made clear whether the constant coefficient gives thermal strain or not at early ages with acceptable accuracy.

As concrete is a porous multiphase composite material, macroscopic thermal expansion coefficient is made up of two movements, that is, the true kinetic thermal coefficient and swelling pressure [3]. The former relates to heat vibration of solid and the latter to the capillary tension change due to temperature change and moisture movement between internal pores of multiphase structure. Since the development of internal structure due to the hydration at an early age is rapid especially in the case of HSC, TEC of HSC in hardening process should not be constant but vary with time.

Therefore, a few studies were carried out on the separation of thermal and AS strains [4-6], while it was unclear how much the separation was achieved.

From the above-mentioned situation, a new method is proposed to evaluate autogenous shrinkage of HSC under hydration heat of cementicious materials in this study. Thermal expansion coefficients of HSC were obtained to which temperature change was given in low temperature region from -1 to 5℃ to control the hydration as far as possible. Using the newly obtained thermal expansion coefficients autogenous shrinkage strain and thermal strain of HSC containing silica fume were separated and temperature-dependence of autogenous shrinkage strain was also evaluated by curing specimens under 20℃ and semi-adiabatic conditions.

2. Experimental program

2.1 Materials and mix proportions

The materials and mix proportions of HSC containing silica fume used in this study are shown in Table 1 and Table 2.

Table 1-Materials

Material	Properties
Cement (C)	Ordinary portland cement; Specific gravity: 3.14; Blaine: 3220 cm^2/g
Silica fume (SF)	Specific gravity: 2.20; Blaine: 200000cm^2/g
Fine aggregate (S)	Sagami River sand; F.M.: 2.97; Specific gravity: 2.63
Coarse aggregate (G)	Oume crushed stone; F.M.: 6.73; Specific gravity: 2.66
Superplasticizer (SP)	Polycarbonate-type superplasticizer

Table 2-Mixture proportions

No.	W/B (%)	SF/B (%)	s/a (%)	Unit content (kg/m^3)					
				W	C	SF	S	G	SP
25-SF	25	10	41	160	576	64	677	985	11.52
35-SF	35	10	44	165	424	47	785	1019	8.478

B=C+SF; s/a: Percentage of fine aggregate volume

2.2 Thermal expansion coefficient

Thermal expansion coefficient (TEC) and temperature-dependence of AS are obtained in accordance with the procedure indicated in Figure 1. Considering that hydration of cementitious materials results in the development of AS of concrete, TEC excluding AS as far as possible could be obtained, if temperature change is given to concrete in very low temperature region. It is desirable to give temperature change to specimen in a lower temperature region up to -10 ℃, because the hydration reaction of cement stops at -10 ℃ [7]. However, fresh concrete is frozen at about -3 ℃ [7]. Therefore, in order to avoid the freezing-induced damage of concrete at early age and obtain TEC as exactly as

possible, temperature change was given to specimens in low temperature region from -1 to 5 ℃ in this study.

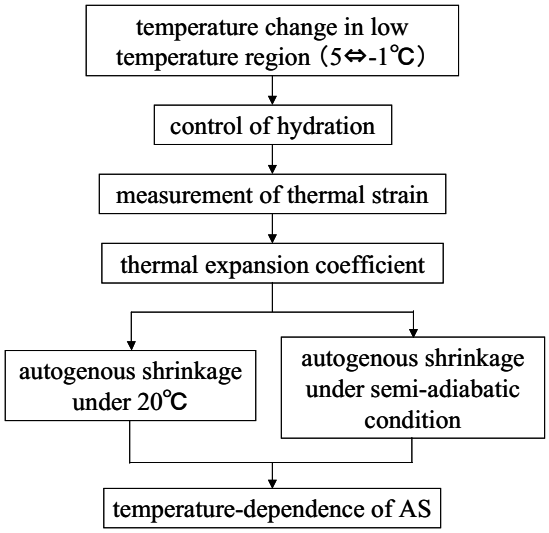

Figure 1-Evaluation of autogenous shrinkage under heat of hydration

2.2.1 Measurement equipment

Length change of the specimen with size of 100×100×400 mm for evaluating TEC was measured by displacement transducer with the sensitivity of 1000×10^{-6}/mm and the capacity of 10 mm. Thermocouples were placed at the center and the surface of cross section to catch the temperature distribution.

The device to control the temperature in low temperature region is shown in Figure 2. The device is composed of a heat insulating box of 800×800×750 mm, a cooler, a heater, a temperature controller and a recorder. Antifreeze solution was used as a heat transmission medium, and circulating pump was used to maintain uniform temperature of the solution. The rates of temperature rise and temperature drop were about 6 ℃/hour, and the temperature difference between the center and surface was about 0.3 ℃.

Before measuring, the specimen was demoulded and sealed with polyethylene films to prevent penetration of the antifreeze solution. The specimen was set on a stand, and the spindle of displacement transducer fixed on stand was attached to a chip on the surface of specimen. Then the specimen was set on the stand and placed into the heat of insulating box.

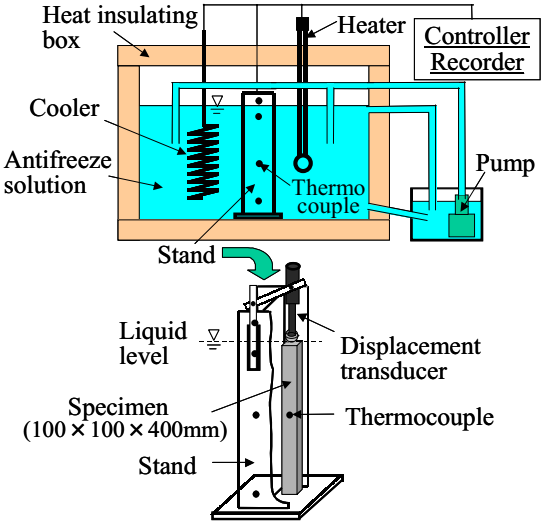

Figure 2-Experimental set up for thermal expansion coefficient

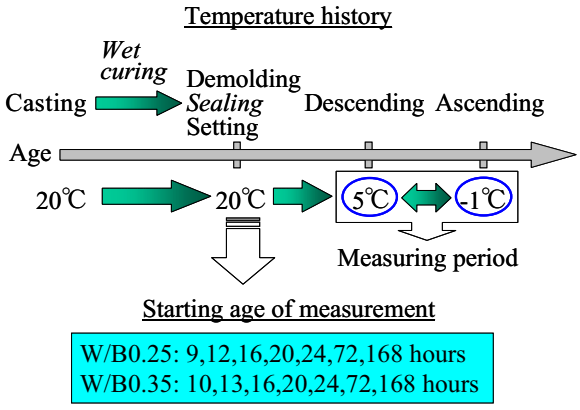

Figure 3-Temperature history and starting age of measurement

2.2.2 Temperature history and starting ages of measurement

The flow of test for TEC is shown in Figure 3, in which ages at starting the measurement of elongation and contraction are also exhibited. The specimens were cured under temperature of 20 ℃ and wet condition until measuring. Then they were cooled from 5 ℃ to -1 ℃ and then heated from -1 ℃ to 5 ℃. As shown Figure 3, in order to obtain TEC exactly at early ages, the shorter time interval of measurement was set before the age of 24 hours.

2.3 Autogenous shrinkage

As shown in Figure 4, prisms made in horizontal formwork were used for AS tests. These prisms had a cross section of 100×100 mm and length of 400 mm.

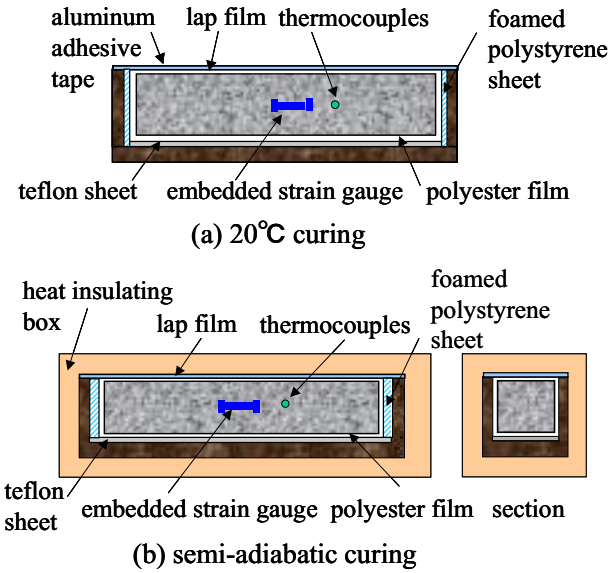

Figure 4-Curing method of specimens for temperature-dependence of AS

In order to decrease the friction between the concrete and the steel formwork, teflon sheets of 1 mm in thickness were placed inside the formwork before placing concrete.

Additionally, foamed polystyrene sheets of 2 mm in thickness were placed between the polyester film and the formwork to allow concrete expansion due to heat of hydration and from restraint at both ends. For the test to investigate the effect of heat of hydration on AS, concrete was cast in the formwork placed in the heat of insulating box.

After casting, all of the specimens in the mould were covered with polyethylene films and wet fabrics, and then stored in a room at the temperature of 20 ℃.

Specimens cured under 20 ℃ were demoulded and sealed with aluminum adhesive tape at the age of 1day in order to prevent water from evaporation or absorption.

Shrinkage strain was measured by means of strain gauges embedded in concrete along with thermocouples.

2.4 Bound water content

In order to investigate the effectiveness of low temperature for controlling the hydration rate of the binder, specimens of the binder paste were made to measure bound water content, which is closely related to hydration. Half of the specimens were cured under constant temperature of 20 ℃ and wet condition, and the other under the same conditions as the specimens for evaluating TEC.

Specimens were crushed into powder at the start and finish of measuring thermal strain. The samples obtained from the powder were vacuum-dried for 7 days after stopping the hydration with acetone. The ignition loss was, thereafter, measured by the method of ignition loss determination in 1000 ℃ for 12 hours. Ratio of ignition loss to binder mass is defined as bound water content. The difference of water bound content in specimens cured at 20 ℃ and 5 ℃～-1 ℃ is applied to evaluating the effect of low temperature on controlling the hydration.

3. Results and discussions

3.1 Effect of disturbing hydration

As an example, increment rates of bound water content during measuring thermal strain are shown in Figure 5, in which the paste with water-binder ratio 0.25, containing silica fume with SF/B of 10%, was used. The dotted line indicates the result from the specimens cured under 20 ℃ and the solid line shows result under 5 ℃～-1 ℃, respectively. Compared with the incremental rate of bound water content under 20 ℃ curing, those under 5 ℃～-1 ℃ curing is quite small. The latter is about half of the former at the age of 10 hours and one third at 15 hours, which shows the effectiveness of low temperature in controlling the hydration of binder.

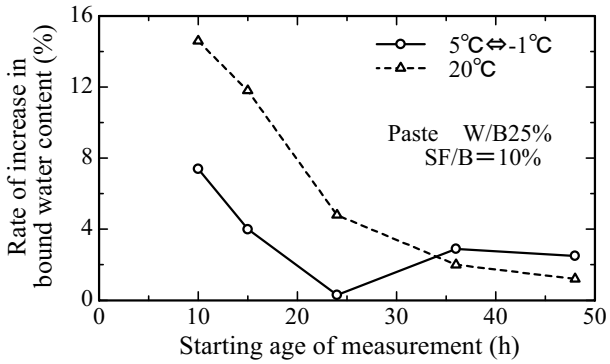

Figure 5-Influence of temperature on hydration

3.2 Thermal expansion coefficient

3.2.1 Relationship between strain and change of temperature

The relationships between strain and change of temperature for the specimen 25-SF measured at the age of 9 hours and for 35-SF at 10 hours are shown in Figure 6 and Figure 7, respectively. The temperature is an average value of temperatures at the center of the cross section and at the surface of the specimen. As shown in these figures, a good

linear relationship can be observed between the strain and change of temperature, and the ascending line coincided approximately with the descending line. As Nasu [8] pointed out, the difference between the gradient of ascending line i.e. apparent TEC and that of descending line could be due to the influence of AS. Therefore, it could be considered reasonable that influence of AS was reduced to being neglected, and thermal strain was obtained exactly by the new method proposed in this study.

A near linear relationship between thermal strain and temperature change was observed also at other measuring ages.

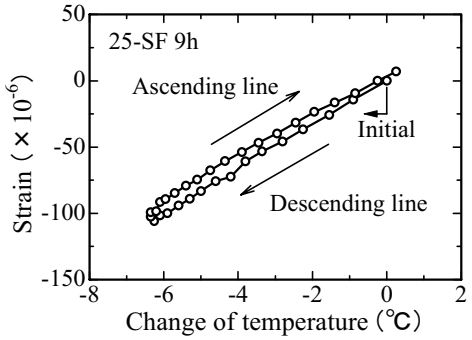

Figure 6-Relationship between thermal strain and change of temperature

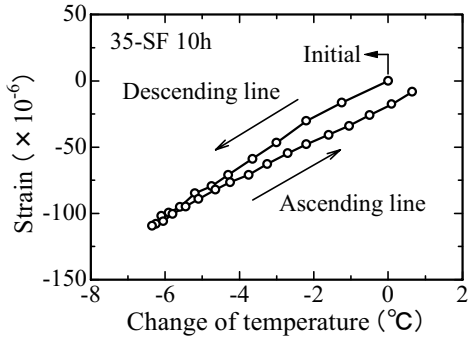

Figure 7-Relationship between thermal strain and change of temperature

3.2.2 Thermal Expansion Coefficient

Based on the experimental results, the variation of TEC with age was obtained. The coefficients are shown in Figure 8, in which the curves of TEC with age obtained by regression analysis are also shown. When considering the influence of temperature on the hydration, temperature-adjusted age defined in accordance with the Arrhenius's hypothesis is used instead of age. According to this figure, TEC of HSC evaluated by the new method decreased rapidly after setting, reached a minimum value at about 1 day and, thereafter, increased gradually with time up to the age of 7 days depending on the development of self-desiccation. This could be due to the fact that the amount of liquid phase decreased and solid phase increased rapidly with the progress of hydration. Structure change plays an important action on decreasing TEC at earlier ages. With the forming and developing of skeleton of concrete, the influence of humidity change due to self-desiccation on TEC could become gradually dominant. According to Meyers's research [9], TEC depends strongly on ambient relative humidity, reaching its maximum value at about 70% RH.

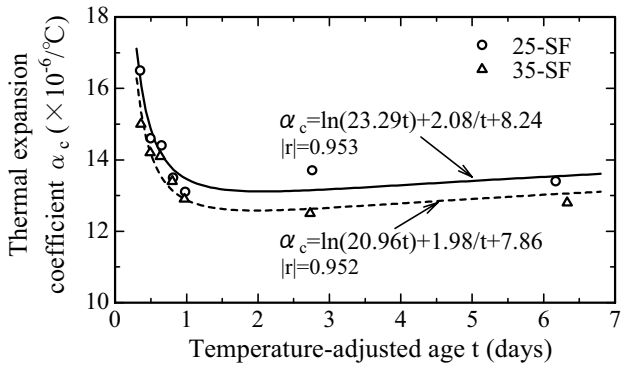

Figure 8-Time dependence of thermal expansion coefficient

In the case of water-binder ratio 0.35 TEC is smaller than that in the case of water-binder ratio 0.25. This difference between both water-binder ratios could be explained by the fact that the volume of paste is more in the case of water-binder ratio 0.25. Besides

self-desiccation, TEC of HSC is larger than that of normal strength concrete, in which 10 $\times 10^{-6}$/℃ is usually adopted, because the former contains a larger amount of paste than the latter.

Conveniently, based on regression analysis, the time-dependence of TEC up to the age of 7 days could be described by the equation shown in Figure 8, in which the natural logarithmic function and the power function represent the influences of humidity and structure change respectively.

3.3 Evaluation of AS based on conventional TEC

Time-dependence of AS strains under 20 ℃ curing and under semi-adiabatic temperature curing obtained using TEC of 10×10^{-6}/℃ are shown in Figure 9 and Figure 10 respectively. Here, AS strain was defined as the strain increment after initial setting.

In the case of 20 ℃ curing, the AS strain developed rapidly at early ages, but slowly at later ages. The lower the water-binder ratio is, the faster the development of the AS strain as well as the larger the AS strain at the age of 28 days is.

In the case of semi-adiabatic curing, a tendency similar to the case of 20 ℃ curing was shown in Figure 10. The development of AS strains under semi-adiabatic curing is faster

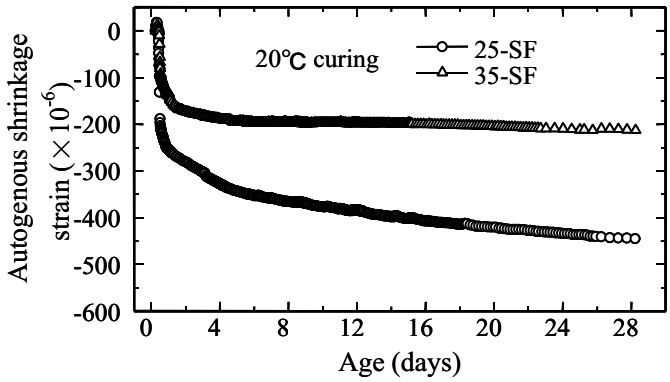

Figure 9- Time dependence of autogenous shrinkage strain

than under 20 ℃ curing, but becomes slow at later ages, especially for 25-SF. The AS strain of 25-SF under semi-adiabatic curing was about 40×10^{-6} smaller than that under 20 ℃ curing at the age of 28 days.

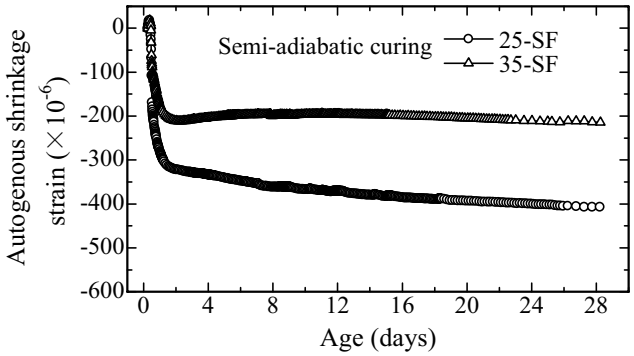

Figure 10-Time dependence of autogenous shrinkage strain

3.4 Evaluation of AS based on new TEC

AS strains at early age under 20 ℃ curing and semi-adiabatic curing are shown in Figure 11 and Figure 12, in which the new TEC was used. The AS strains obtained with the TEC of 10×10^{-6}/℃ and temperatures of concrete specimens are also shown in these figures.

As shown in these figures, in the case of 20 ℃ curing the differences of AS strains due to the different TEC are so small as to be negligible because the change of temperature is small.

However, in the case of semi-adiabatic curing, AS strain obtained with the new value of TEC considering its time-dependence was larger than that with the TEC of 10×10^{-6}/℃. Although the temperature rises of specimens measured in this study were about 10~17 ℃ because of the small section, the maximum differences of AS strains are about 56×10^{-6} for 25-SF, 35×10^{-6} for 35-SF. It is shown that AS strain could be

underestimated with the constant TEC of $10\times10^{-6}/℃$ if the time-dependence of TEC at the early ages is neglected. Therefore, in order to estimate thermal strain and AS strain accurately, it is necessary to consider the time-dependence of TEC of HSC because of high temperature rise.

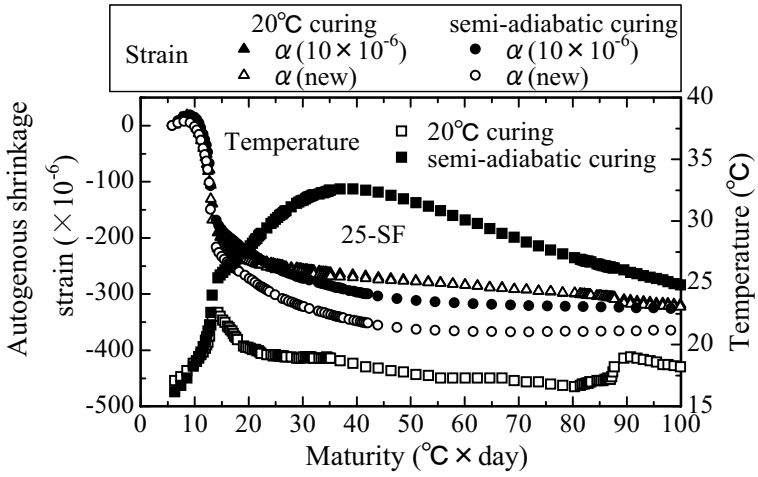

Figure 11-Temperature-dependence of autogenous shrinkage (25-SF)

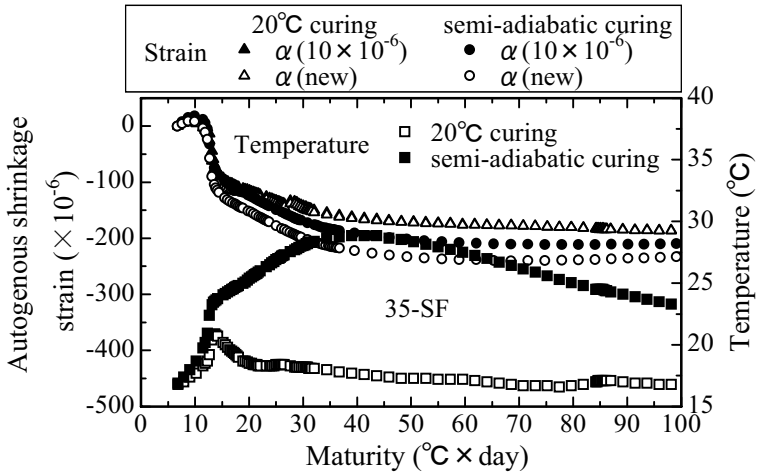

Figure 12-Temperature-dependence of autogenous shrinkage (35-SF)

3.5 Temperature dependence of AS

It has been reported that AS of concrete containing silica fume under various temperatures could be estimated by maturity concept [1]. On the other hand, it has been also pointed out that this maturity concept is not valid for some concrete containing blast furnace slag or fly ash admixture [2]. In these studies a constant TEC was used.

In order to evaluate the temperature dependence of AS properly, the influence of TEC was discussed. When TEC of $10\times10^{-6}/℃$ was adopted, as shown in Figure 11 and Figure 12, the difference of AS between different curing temperature was small. This result coincided with the results of reference [1]. When the time dependence of TEC is considered, maturity concept is not valid for evaluating temperature dependence of AS. There are distinct differences in different curing temperatures at the same maturity. The maximum difference was about 90×10^{-6} for 25-SF, 60×10^{-6} for 35-SF.

4. Conclusions

The following conclusions are drawn from the present study.

(1) Linear relationship between measured strain and temperature change was observed by the proposed method. This fact must mean that thermal strain and autogenous strain can be separated with sufficient accuracy by the new method.

(2) Thermal expansion coefficient of high strength concrete evaluated by the new method decreased rapidly after setting and then reached a minimum value at about 1 day and, thereafter, increased gradually with time depending on self-desiccating.

(3) Autogenous shrinkage strains were underestimated by 15% for SF-25 and 8% for SF-35 when the conventional thermal expansion coefficient of $10\times10^{-6}/℃$ was applied, compared with when the time-dependence of thermal expansion coefficient was applied.

(4) Maturity concept was not applicable for evaluating temperature-dependence of autogenous shrinkage of high strength concrete containing silica fume based on the newly obtained thermal expansion coefficient.

References

[1] Tazawa, E., Matsuoka, Y., Miyazawa, S. and Okamoto, S., Effect of Autogenous Shrinkage on Self Stress in Hardening Concrete, *Thermal Cracking in Concrete at Early Ages*, (ed. R. Springenschmid), E & FN SPON, London, pp.221-228. (1994)

[2] Matsunaga, A., Yoneda, S., Takeda, N. and Sogo, S., Thermal Cracking Resistance of Concrete Used Admixtures with Different Autogenous Shrinkage Properties (in Japanese), *Proceedings of the Japan Concrete Institute*, Vol.18, No.1, pp1287-1292. (1996)

[3] Neville. A. M, *Properties of Concrete* (second ed), Pitman Publishing, London, pp.432-438. (1977)

[4] Yamakawa, H., Nakauchi, H., Kita, T. and Ohnuma, H., Experimental Study of Thermal Expansive Properties of Concrete (in Japanese), *Proceedings of the Japan Concrete Institute*, Vol.8, pp313-316. (1986)

[5] Koyama, T. and Matsufuji, Y. Time Dependence of Coefficient of Thermal Expansion from Fresh to Green Mortar (in Japanese), *Proceedings of the Japan Concrete Institute*, Vol.16, No.1, pp687-692. (1994)

[6] Bjøntegaard, Ø. and Sellevold, E. J., Thermal Dilation-Autogenous Shrinkage : How to Separate, *Autogenous Shrinakge of Concrete*, (ed. Ei-ichi Tazawa), E & FN SPON, London, pp.245-256. (1999)

[7] Murata. J., Nagataki. S. and Kikukawa. H., *Concrete* (in Japanese), (second ed), Kyoritsu, Tokyo, pp.96-103. (1993)

[8] Nasu, S., Thermal Crack Characteristics of low-heat Concrete (in Japanese), *Honshi-giho*, Vol.18, No.69, pp.5-7～5-18. (1994)

[9] Meyers, S. L., How Temperature and Moisture Changes may Effect the Durability of Concrete, *Rock Products*, Chicago, Aug. 1951, pp.153-57. (1951)

COEFFICIENT OF THERMAL EXPANSION OF CONCRETE: EFFECTS OF MOISTURE

E.J. Sellevold and Ø. Bjøntegaard
The Norwegian University of Science and Technology (NTNU)
Department of Structural Engineering, Richard Birkelands vei 1a,
7491 Trondheim, Norway

Abstract
Crack sensitivity calculations for young concrete are strongly influenced by coefficient of thermal expansion (CTE) values for the concrete. This paper demonstrates the strong effect of moisture content on CTE, and discusses the mechanism(s) behind. From a practical point of view crack sensitivities may be reduced by keeping the concrete as wet as possible during the early phase. This minimizes CTE and will largely eliminate autogenous shrinkage.

1. Introduction
The current worldwide interest in early age cracking problems in structures with High Performance Concrete (HPC) has led to intensive work on autogenous deformations. This concentration has resulted in neglect of the, normally even more important, thermally induced deformations. CTE is often just given a constant default value in calculation programs, while we know that it varies strongly both with concrete mix constituents (particularly aggregate type) and time (degree of self-desiccation). Fig. 1 [1, 2] shows typical behavior from early times for a pure cement paste (a) and a concrete (b) with the same paste as binder (about 28 vol%). Both curves are for sealed hydration up to the time when the specimens are immersed in water. Before setting both cement paste and concrete have very high CTE values since no solid framework exists and the continuous water phase controls. CTE reduces as solids form, reaching a minimum value around the final set, which points are shown in Fig. 1. From then on CTE increases as self-desiccation proceeds. The increase for paste is about from 10 μs/°C to 22 μs/°C, and the reduction after water immersion back to 13 μs/°C. For concrete the equivalent numbers are about from 7 μs/°C to 11 μs/°C, and back to 7 μs/°C. These numbers demonstrate clearly the dominant influence of the water content on CTE;

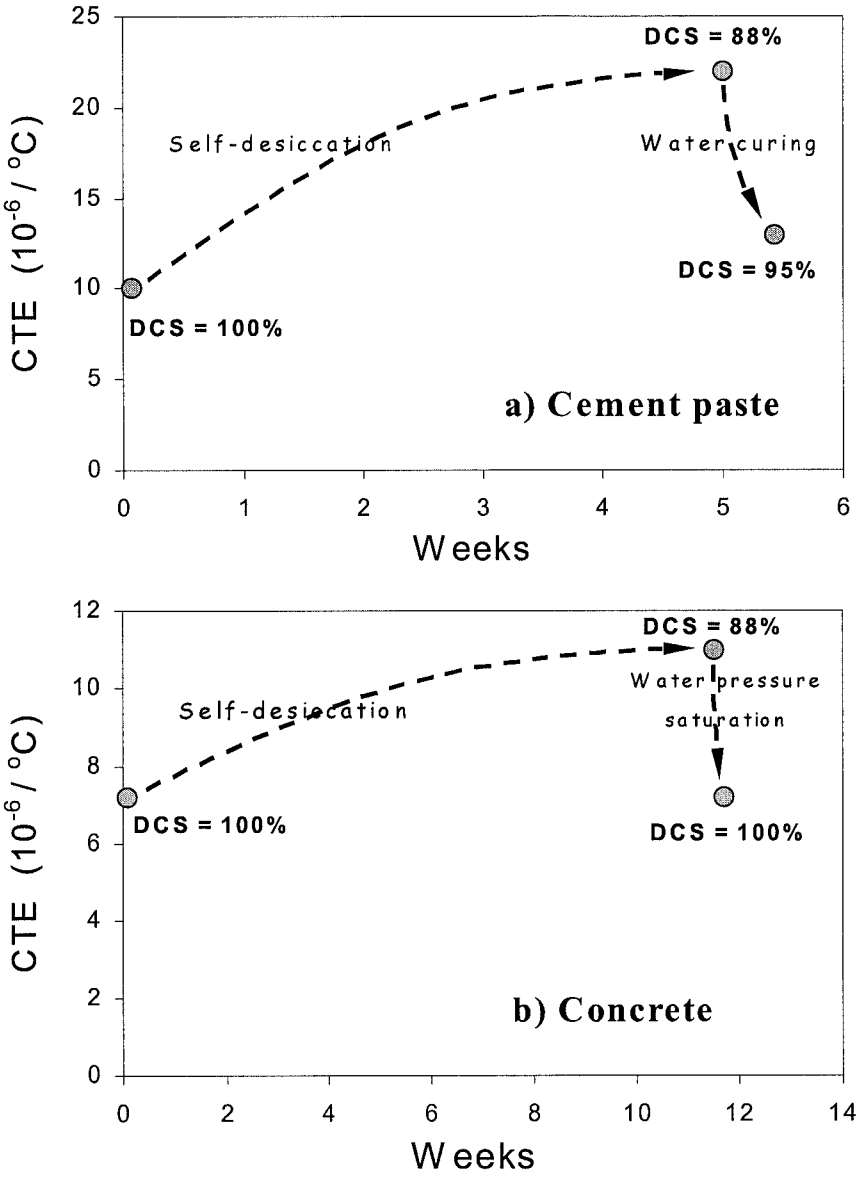

Fig.1 Effect of the degree of capillary saturation (DCS) on the Coefficient of Thermal Expansion (CTE) of: a) cement paste (w/b = 0.40 and 5% silica fume) and b) concrete with the same paste as binder (28 vol%). Bjøntegaard [1]

for the concrete CTE returns to the exact same value it had on setting after full saturation at an age of 11 weeks, i.e. the hydration has no net effect on the CTE in saturated state (!). The moisture effect is clearly very important from a practical point of view, and simple in the sense that the CTE value of a given concrete can be controlled by controlling the moisture content. Minimum CTE is obtained in a wet state, i.e. by supplying an internal water source during curing two important benefits are obtained: the autogenous deformation is reduced or eliminated and CTE is minimized.

This dramatic effect of moisture content on CTE has been demonstrated repeatedly for mature cement pastes since the classic work by Meyers, 1951 [3]. Helmuth, 1960 [4], Dettling, 1964 [5] and Bazant, 1970 [6] have made significant contributions to our, yet incomplete, understanding of the underlying mechanisms. This brief paper gives the authors' current view of the mechanisms as a basis for discussions.

CTE cannot be uniquely defined for concrete, since an imposed temperature change produces time dependent deformations. It is therefore a choice what is called immediate deformations (ID) and counted as CTE, and what is considered delayed deformation (DD) and, thus, not included in the CTE.

In practice thermal equilibrium in a test sample is reached much faster than deformation equilibrium, but still ½ - 1 hour is needed in most experimental setups before the temperature gradient is small enough to allow ID to be defined. Often in the literature CTE is found from dynamic experiments, i.e. deformations are recorded during heat-cool cycles. If there is no hysteresis then CTE is uniquely defined as the slope of the curve in a T vs. deformation plot; however, in practice there is hysteresis that depends both on the rate of temperature change and the magnitude of DD, producing a CTE value that may depend strongly on all the experimental conditions.

For hardening concrete, an important point in this context is that when deducing autogenous deformation from tests performed under realistic temperature developments (heating followed by cooling) it will contain "true" autogenous deformation as well as DD. This probably contributes to the unsystematic influence of temperature on autogenous deformation found during such tests [1, 2, 7].

2. Mechanisms

There appears to be general agreement in the literature that both the strong dependence of CTE on moisture content and the existence of DD are related to temperature-induced redistribution of moisture in the pore system. We share this view and will discuss the mechanisms in three categories, roughly (but not entirely) corresponding to those proposed by Bazant [6].

1) Pure thermal dilation
2) Thermal shrinkage or swelling
3) Relative humidity change

1) Pure thermal dilation

Each constituent material (solid particles, adsorbed water, pore water etc.) has a CTE value. CTE of water is much higher than CTE of solids and water in small pores probably has higher CTE than bulk water. Thus, a very fast temperature increase followed by an isothermal period will lead to fast expansion (ID), followed by a time dependent contraction (DD) as the induced excess pressure in filled pores is dissipated by flow to the outside or to partly empty pores. Scherer [8] and Ai et al. [9] have used this phenomenon to measure water permeability in saturated cement pastes. Depending on the permeability of the paste and the distance to available "sinks", the pressure relief may be fast or slow, i.e. it may appear as ID and hence be counted in CTE, or as DD. The literature shows that DD is much more prevalent in saturated samples than in partly dried. Thus, for concrete in practice where the normal moisture state is "natural self-dessicated condition" little DD is found, and any pressure relief mechanism is presumably very fast and counted as ID and part of CTE.

2) Thermal shrinkage and swelling

Pore water can roughly be divided into two types. Gel water, a collective term for water which is strongly influenced by its proximity to solid surfaces; i.e. interlayer water, adsorbed water and water in very small pores (gel pores). Capillary water is water in larger pores (smallest dimension over a few nm), and it is commonly treated as bulk water under the influence of capillary tension when the sample is not fully saturated, i.e. when curved water- air menisci exist. At saturation there is no capillary tension, but the water in these "larger" pores is still commonly referred to as capillary water, and the pores as capillary pores.

Equilibrium requires that the chemical potential (molar Gibbs free energy) of the two coexisting water phases is equal both before and after a temperature change. The rate of change of the chemical potential of a water phase with respect to increasing temperature is the negative of the entropy. The entropy of gel water is lower than that of capillary water as shown in Fig. 2, Radjy and Sellevold [10]. Thus, a sudden increase in temperature leads to a higher chemical potential in gel water than in capillary water, setting up a driving force for an internal redistribution of water from gel to capillary pores. This is expected to lead to shrinkage, i.e. sudden heating of cement paste sample is expected to produce a sudden expansion followed by a time dependent contraction. On cooling the opposite effect is expected; a sudden contraction followed by a time dependent expansion as water moves from capillary pores to the gel. It is perhaps difficult to visualize how water can redistribute in a saturated sample, i.e. when there is no available space. The theory is that, for example, cooling will force water to the gel pores in an amount necessary to increase the local pressure (disjoining pressure) enough to establish equilibrium in chemical potential with the water in capillary pores. This pressure in the gel water will produce expansion.

In partly saturated samples the situation is that the gel pores are full, but the capillary pores partly empty and with the water under capillary tension. The redistribution takes

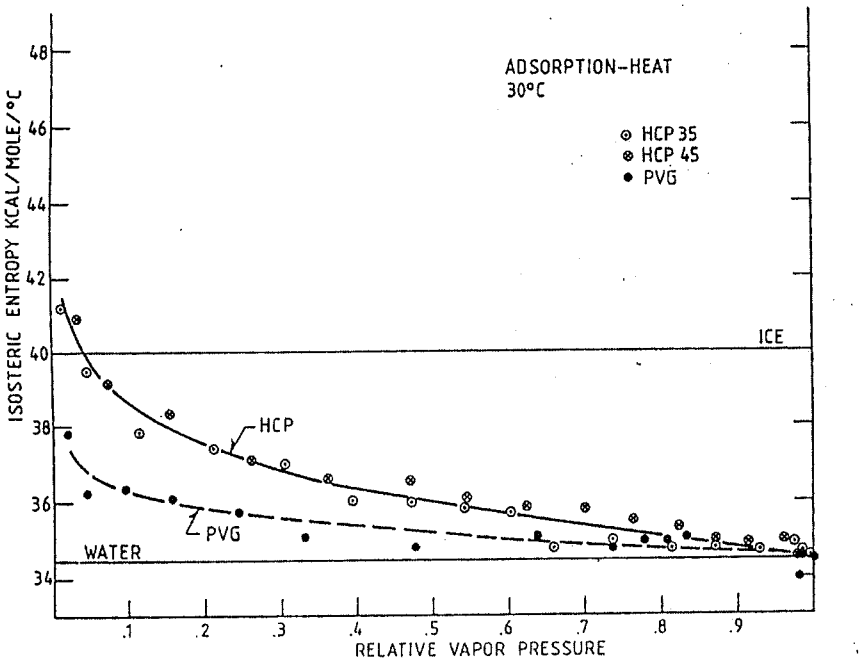

Fig.2 Entropy of adsorbed water (relative to saturated vapor). HCP = Hardened Cement Paste, PVG = Porous Vycor Glass. Low relative vapor pressure is associated with gel water, higher values with capillary water. Note that large ordinate values means large change from vapor state, i.e. low absolute entropy - as also demonstrated by the ref. water and ice lines. Radjy and Sellevold [10].

place as for saturated samples, in theory, implying the possibility of a situation after cooling when the gel water is under pressure (disjoining) while the capillary water is under tension. This situation produces chemical potential equilibrium, but the physical reality of the situation is perhaps questionable. It should be added that it is impossible to calculate the magnitude of any of the redistribution effects with any reasonable certainty. The thermodynamic arguments tells us in which direction water moves, but quantification requires much more basic data than we have presently.

Helmuth [4] explains his DD results only in terms of this gel-capillary redistribution mechanism. We consider that this mechanism is slow so that it mainly results in DD, and cannot explain the very large effect of moisture content on CTE shown in Fig.1. Note that Helmuth did consider the mechanism responsible for the moisture effect on CTE, in

the sense that at 82% degree of capillary saturation (DCS) there was "...not enough capillary water to allow redistribution" - i.e. it is the absence of redistribution that is responsible for high CTE at DCS = 82%. We do not share this view, but we recognize that the fact that there is very little DD in the DCS = 82% sample is difficult to reconcile with the gel-capillary redistribution mechanism being primary responsible for the large DD in saturated samples.

3) Relative humidity change

The raw data in the project to obtain enthalpy and entropy of pore water [10] was vapor pressure vs. temperature for a given cement paste at different moisture contents. Fig. 3 shows such data in a principle sketch. A characteristic of the results is that the curves are nearly straight lines, and that the slopes increase as the moisture contents are reduced, i.e. that the enthalpy of the pore water decreases with decreasing moisture content, see Fig. 4, as is true for all adsorbent/adsorbate systems. Fig. 3 illustrates clearly a very important aspect: If the lines were parallel then the RH would be independent of temperature (easy to prove mathematically, remembering that at any given temperature, RH equals the vapor pressure exerted at a certain moisture content divided by the saturation vapor pressure).

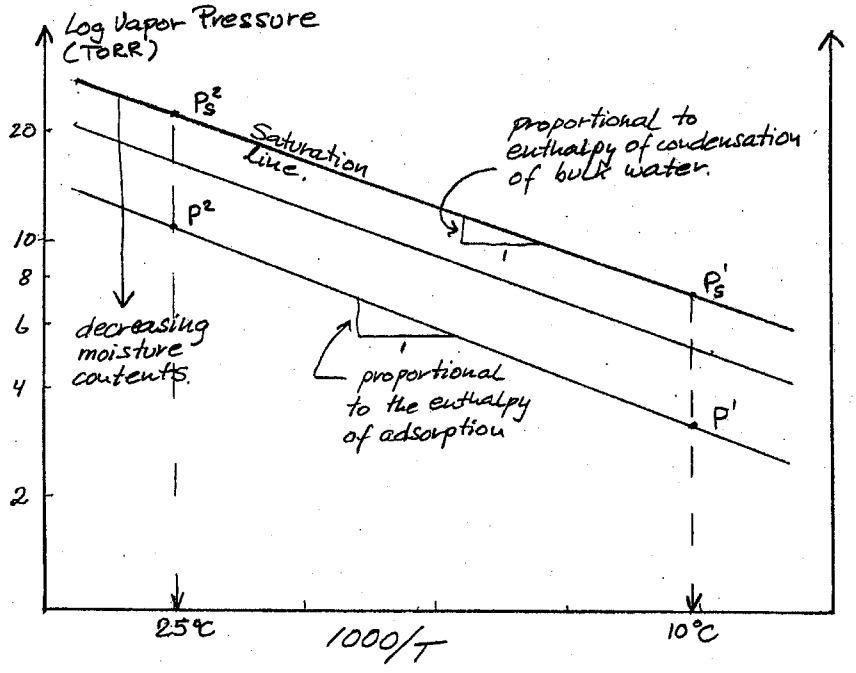

Fig. 3 Vapor pressure exerted by pore water in hardened cement paste vs. inverse of temperature for different constant water contents. Principle sketch.

When the lines are not parallel as in Fig. 3 the result of heating from T_1 to T_2 is that RH increases, since:

$$\frac{p^2}{p_s^2} > \frac{p^1}{p_s^1} \qquad \text{hence } RH_2 > RH_1$$

This effect has been measured by several researchers [6, 10, 11, 12], and has important consequences for CTE. The magnitude of the effect was found to be around 0.2% RH per degC [10]. This increase in RH leads to expansion, the magnitude of which may be estimated from existing isothermal shrinkage - RH data, for example [13]. The slope for a mature w/c = 0.40 paste at 80% RH is 60 μs per % RH, or per degC about 12 μs assuming the RH change to be 0.2% per degC (variation between 0.1 (w/c = 0.7) and 0.3% per degC (w/c = 0.4) is found in [11] and [12]). Fig. 1 showed CTE to be 22 μs/°C for the paste with DCS = 88%, of which maybe then 12 μs/°C are caused by the RH-effect. An argument based on changes in capillary tension because of the RH-increase gives a very similar result. Thus, the RH-mechanism alone is able to explain the whole moisture content effect on CTE. It is of course implied that the RH-effect is fast and the resulting deformation is ID - and hence recorded as part of the CTE.

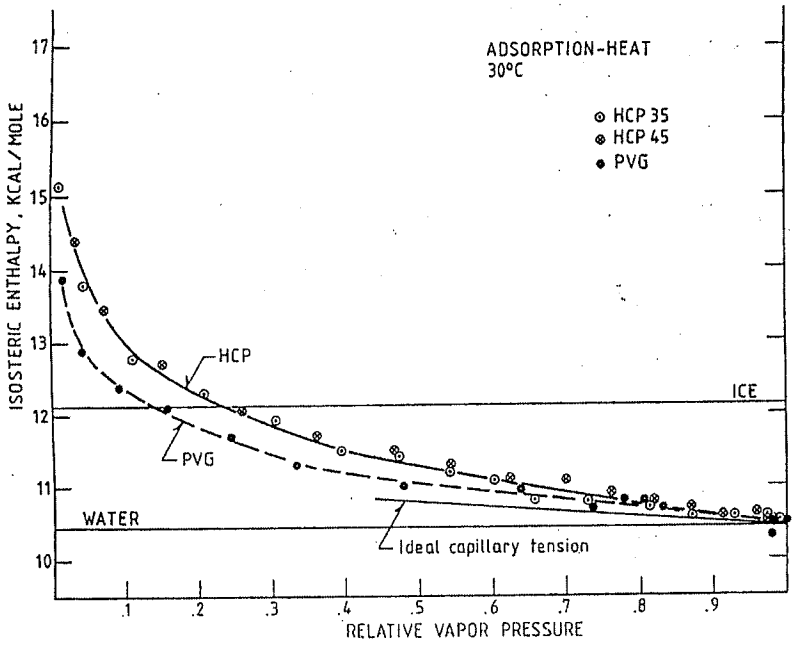

Fig. 4 Enthalpy of adsorbed water (relative to saturated vapor). HCP = Hardened Cement Paste, PVG = Porous Vycor Glass. Radjy and Sellevold [10]

3. Conclusions

Crack sensitivity calculations for young concrete are strongly influenced by CTE values for the concrete. This paper demonstrates the strong effect of moisture content on CTE, and discusses the mechanism(s) behind. From a practical point of view crack sensitivities may be reduced by keeping the concrete as wet as possible during the early phase. This minimizes CTE and will largely eliminate autogenous shrinkage.

From a fundamental point of view the situation is less clear. It is satisfactory that the RH-mechanism apparently alone is able to explain the effects of moisture content on CTE. However, the role of the different mechanisms at various moisture contents, and in particular their relationship to DD, cannot be coherently explained today in our view.

4. Acknowledgements

This paper is a product of the Norwegian NOR-CRACK project. The financial contribution of the Norwegian Research Council is gratefully acknowledged. The partners in the project are the Norwegian Public Roads Administration, Selmer-Skanska ASA, Norcem A.S., Elkem ASA and Fesil A.S., and NTNU-Department of Structural Engineering (project leader).

5. References

[1] Bjøntegaard, Ø., Thermal Dilation and Autogenous Deformation as Driving Forces to Self-Induced Stresses in HPC, Doctoral thesis, NTNU, Dec. 1999.

[2] Bjøntegaard Ø. and Sellevold E.J., Interaction between Thermal Dilation and Autogenous Deformation in HPC, Matr. and Str., Vol.34, June 2001, pp 266-272

[3] Meyers S.L., How Temperature and Moisture Changes May Affect the Durability of Concrete, Rock Products, August 1951, pp. 153-178

[4] Helmuth R.A., Dimensional Changes of Hardened Portland Cement Pastes Caused by Temperature Changes, Highway Research Board, 40, 1960, pp. 315-336

[5] Dettling H., "Die Wärmedehnung des Zementstaines, der Gesteine und der Betone" (thermal dilation of cement paste, aggregate and concrete), Deutscher Ausschuss für Stahlbeton, Heft 164, Berlin 1964 (in German)

[6] Bazant Z.P., Delayed Thermal Dilatations of Cement Paste and Concrete due to Mass Transport, Nuclear Eng. and Design, 1970, pp. 308-318

[7] Bjøntegaard Ø. and Sellevold E.J., Thermal Dilation and Autogenous Deformation, Proc. of the RILEM Int. Conf. on Early Age Cracking in Cementitious Systems, Ed. by K.Kovler and A.Bentur, Haifa, Israel, March 12 - 14, 2001, pp.63-70

[8] Scherer G.W., Measuring Permeability of Rigid Materials by a Beam-Bending Method: I, Theory, J. Am. Ceram. Soc., 83, 9, 2000, pp 2231-2239

[9] Ai H., Young J.F. and Scherer G.W., Thermal Expansion Kinetics: Methods to Measure Permeability of Cementitious Materials: II, Application to Hardened Cement Pastes, J. Am. Ceram. Soc., 84, 2, 2001, pp. 385-391

[10] Radjy F. and Sellevold E.J., Work performed at DTH, Lyngby, Denmark, 1970-77. Will be available from the second author during 2002.
[11] Nilsson L.O., Temperature Effects in RH Measurements on Concrete - Some Preliminary Studies. The Moisture Group. Report 1987:1, BFR. 1987, pp. 84
[12] Persson B., Compatibility Between Flooring Material on Concrete and Moisture, Volatile Organic Compound, and Adhesion, Working Report, Division of Building Materials, Lund Institute of Technology, Lund 2001, pp. 29 (in Swedish)
[13] Hansen W., Drying Shrinkage Mechanisms in Portland Cement Paste, J. Am. Ceram. Soc., 70, 5, 1987, pp. 323-328

DEFORMATION COMPOSED OF AUTOGENOUS SHRINKAGE AND THERMAL EXPANSION DUE TO HYDRATION OF HIGH-STRENGTH CONCRETE AND STRESS IN REINFORCED STRUCTURES

Hiroshi Hashida & Nobuyuki Yamazaki
Institute of Technology,
Shimizu Corporation, Tokyo, Japan

Abstract

Reinforced concrete members made of high-strength concrete are subjected to stress due to coupled strain resulting from autogenous shrinkage and thermal expansion/contraction, which may cause severe cracking at early age. In the paper, the coupled strain of concrete specimens under semi-adiabatic curing was measured and estimated both components, autogenous shrinkage and thermal expansion. Actual strain and shrinkage stress in full-scale model columns were then investigated by comparing the estimated values with the experimental measurements. The concrete with water to binder ratio between 0.20 and 0.40, ordinary Portland cement or belite-rich Portland cement, silica fume or blast furnace slag as mineral admixture, was used for the experiment. By taking account of the increase of thermal expansion coefficient with age, it was possible to estimate the coupled strain of high-strength concrete subjected to a high temperature history and the actual strain and stress in the reinforced structures. While autogenous shrinkage of concrete with usual Portland cement subjected to a high temperature history was considered to be smaller than that of 20˚C-curing, autogenous shrinkage of concrete with admixtures was considered to be larger when the admixture content was high.

1. Background and objective

The number of reinforced concrete structures made of high-strength concrete with a design strength of more than 60 N/mm^2 has been increasing in Japan. Though members made of such concrete basically exhibit high strength and high durability, they are vulnerable to early cracking. The high cement content causes a large temperature rise during early hydration, while autogenous shrinkage is at the same time also a matter of concern. For this reason, the reinforced concrete members are subjected to stress due to deformation composed of autogenous shrinkage and thermal expansion/ contraction, leading to cracking. However, few studies have dealt with the coupled deformation and stress of high-strength concrete members at early ages [1-4].

Accordingly, the authors measured the coupled strain of high-strength concrete specimens under semi-adiabatic curing and estimated both components, autogenous shrinkage and thermal expansion. Actual strain and the shrinkage stress in full-scale model columns were then investigated by comparing the estimated values with the experimental measurements.

2. Experimental procedure

2.1 Laboratory test

The materials of high-strength concrete are given in Table 1 and proportioned as shown in Table 2. Four types of cement or binder were used: ordinary Portland cement (OPC), belite-rich Portland cement (BPC), BPC with 5% replaced by mass with silica fume (BSC) and blast furnace slag cement (OPC with about 42% replaced by mass with slag, OBC). Eight types of concrete were prepared, with OPC or BPC having a water-cement ratio (W/C) of 0.40, 0.27, and 0.20, BSC having a water-binder ratio (W/B) of 0.20 and OBC having a W/C of 0.27. The belite (C_2S) content of BPC was 46% in terms of mineral composition. Table 2 also shows the averages of the 28-day compressive strength, f_{cs} of standard-cured specimens.

The changes in the autogenous shrinkage strain and pore humidity at a constant temperature of 20˚C and the total strain under semi-adiabatic curing, i.e. the strain composed of autogenous

Table 1 - Materials of concrete.

Materials	Desig-nations	Kind / Characteristics
Cement	OPC	Ordinary Portland cement Density=3.16 g/cm^3 , Blaine=0.327 m^2/g
	BPC	Belite-rich Portland cement (C_2S=46%) Density=3.20 g/cm^3 , Blaine=0.411 m^2/g
	OBC	Blastfurnace slag cement B type Density=3.04 g/cm^3 , Blaine=0.370 m^2/g (OPC replaced about 42 wt% by slag)
Silica fume	SF	Density=2.20 g/cm^3 , Blaine=20 m^2/g
Fine aggregate	S	Land sand / Density=2.59, Absorption=1.63%, F. M.=2.80
Coarse aggregate	G	Crushed sand stone / Max. size=20mm Density=2.65, Absorption=0.60%
Chemical admixture	SP	Air entraining and high-rage water reducing agents

Table 2 - Mix proportions.

Mix	W/B	W	C	SF	S	G	f_{cs}
	(%)	kg/m^3					(N/mm^2)
BPC40	40	168	420	—	785	975	76.8
BPC27	27	165	611	—	697	940	101
BPC20	20	165	825	—	581	896	119
BSC20	20	165	784	41	606	856	123
OPC40	40	168	420	—	780	975	68.2
OPC27	27	165	611	—	692	940	97.4
OPC20	20	165	825	—	573	896	109
OBC27	27	165	611	—	751	859	109

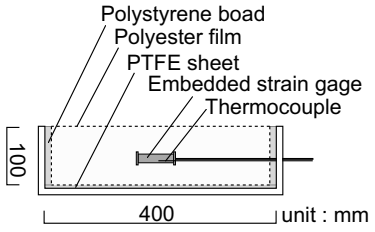

Figure 1 - Test specimen for measurement of autogenous shrinkage cured at 20˚C.

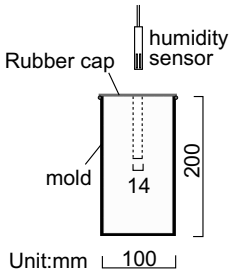

Figure 2 - Test specimen for measurement of pore humidity cured at 20˚C.

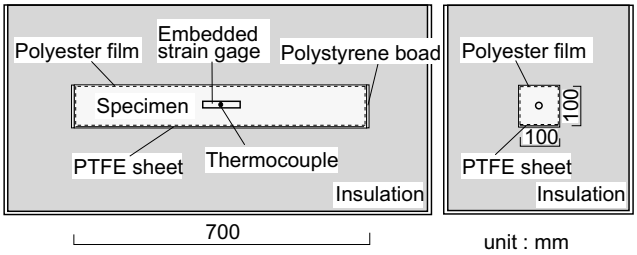

Figure 3 - Test specimen for semi-adiabatic curing.

shrinkage and thermal expansion, were measured. The autogenous shrinkage and pore humidity test at 20˚C were conducted using beam specimens 100×100×400 mm and cylinders ϕ100×200 mm in size as shown in Figure 1 and 2. For the semi-adiabatic curing test, beam specimens 100× 100×700 mm in size were fabricated using molds made of insulation as shown in Figure 3. They were adiabatic-cured from immediately after placing to undergo a temperature history similar to the actual members. The strains and temperatures of beam specimens were measured with embedded strain gauges and thermocouples.

2.2 Experiments on full-scale members

Two types of ready-mixed concrete, OPC-Rm and BPC-Rm with materials and mix proportions (Table 3) similar to OPC27 and BPC27 in the laboratory test, were used for an experiment on full-scale members. For the experiment, unreinforced and reinforced concrete model columns (U-column and R-column) 550 x 600 mm in cross section and 1500 mm in height were prepared as shown in Figure 4. Whereas the U-column was used for measuring the total strain composed of autogenous shrinkage, thermal expansion and internally restricted strain, the R-column was used for measuring the actual strain of the main reinforcing bar and concrete under restraint of the reinforcing bar. To minimize the effect of drying, the exposed surfaces of the wooden formwork were covered with curing sheets. The placing surface of OPC-Rm, however, was exposed to the air by mistake, while

Table 3 - Mix proportions of RMC.

Mix	W/C (%)	W	C	S	G	f_{cs} (N/mm^2)
		kg/m^3				
BPC-Rm	27	170	630	741	854	92.7
OPC-Rm	28	165	589	719	922	96.1

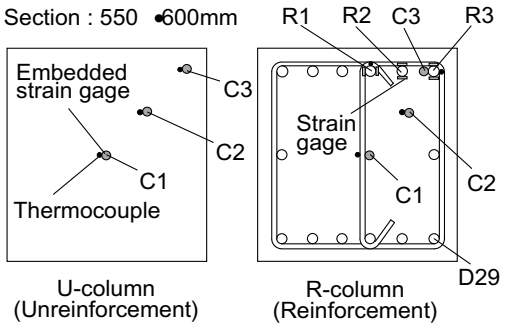

Figure 4 - Full-scale model columns.

that of BPC-Rm was covered with curing sheets from immediately after placing. The strains of concrete and the reinforcing bar were measured with embedded strain gauges and foil strain gauges (the 4 gauge method), respectively. The measuring points for strain and temperature are shown in the cross sectional view in Figure 4. Measurements were made at 3 heights, but this paper deals with only the central measuring point readings.

3. Results

3.1 Autogenous shrinkage at 20˚C

The autogenous shrinkage strains of specimens cured at 20˚C are shown in Figure 5. In this paper, the datum strain of the autogenous shrinkage is the value at the time of final setting because final setting nearly corresponds to the practical revelation of elasticity and stress of concrete. The autogenous shrinkage developed to 50% of the 28-day value by an equivalent age of 1 day and gradually converged. When comparing specimens with the same water-cement ratio, the autogenous shrinkage strain of BPC specimens was much lower than OPC specimens, presumably due to the C_3A content of belite-rich cement as low as approximately 3% [2].

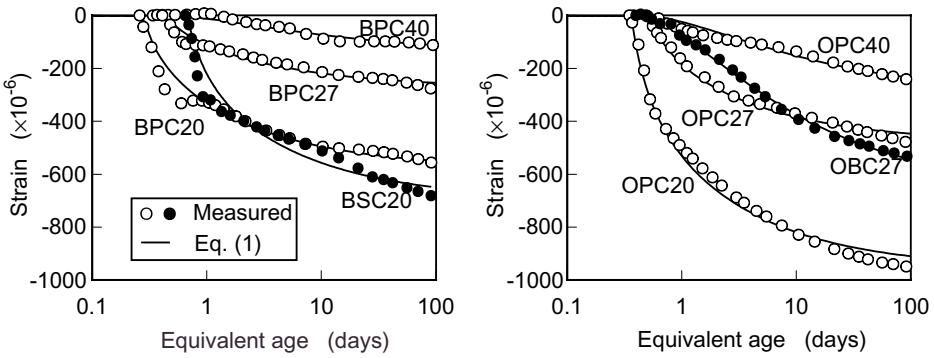

Figure 5 - Autogenous shrinkage strains of specimens at 20˚C.

Table 4 - ε_{ass} and s_ε regressed by euation(1).

Mix	BPC40	BPC27	BPC20	BSC20	OPC40	OPC27	OPC20	OBC27
$\varepsilon_{ass}(\times 10^{-6})$	98	236	512	610	193	420	900	473
s_ε	0.37	0.13	0.09	0.13	0.37	0.13	0.09	0.32

The autogenous shrinkage strain can be approximated by the model curve of equation (1).

$$\varepsilon_{as}(t) = \varepsilon_{ass} \cdot \exp\left\{ s_\varepsilon \left[1 - \left(\frac{28 - t_{fs}}{t - t_{fs}} \right)^{0.5} \right] \right\} \quad (1)$$

where $\varepsilon_{as}(t)$= autogenous shrinkage strain at t days, t = equivalent age (days), ε_{ass}= autogenous shrinkage strain at 28 days, s_ε= factor for rate of autogenous shrinkage development and t_{fs}= final setting time (days). The equivalent age used in the paper is specified in CEB-FIP Model Code 90 [5] and expressed by equation (2).

$$t_T = \sum_{i=1}^{n} \Delta t_i \cdot \exp\left[13.65 - \frac{4000}{273 + T(\Delta t_i)} \right] \quad (2)$$

where t_T= equivalent age (days), $T(\Delta t_i)$= temperature in period Δt_i(˚C) and Δt_i= duration of temperature T (days). The solid lines in Figure 5 are the autogenous shrinkage strain curves at 20˚C approximated by Equation (1). The values of ε_{ass} and s_ε regressed for each concrete are listed in Table 4. These parameters are significantly dependent on the water-cement ratio.

Figure 6 shows the changes in the pore humidity of concrete in an environment at 20˚C. The humidity of all concretes progressively decreased over time. Those of BPC20, BSC20, OPC20, and OBC27 particularly decreased to around 75%RH at 3 months, clearly exhibiting self-desiccation due to hydration. Figure 7 shows the relationship between the pore humidity and autogenous shrinkage, exhibiting correlation, though some types show certain scatter. It is therefore considered that autogenous shrinkage of high strength concrete significantly depends on the self-desiccation.

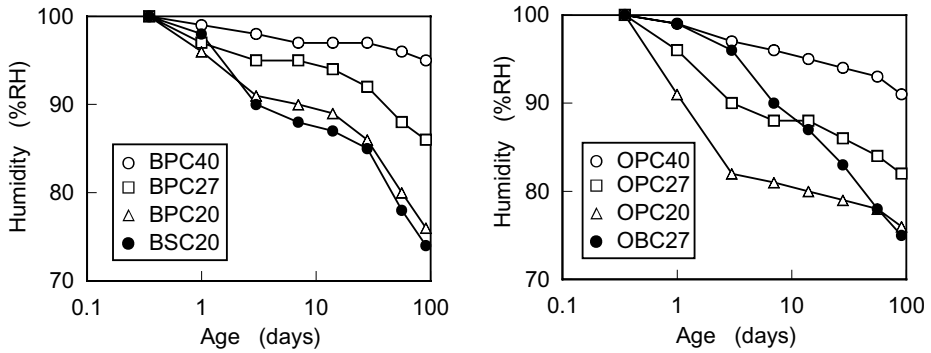

Figure 6 - Pore humidity changes of specimens at 20˚C.

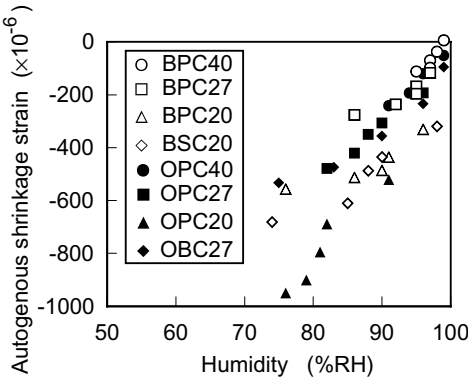

Figure 7 - Pore humidity versus autogrnous shrinkage.

3.2 Coupled strain under semi-adiabatic curing

Figure 8 shows the changes in the total strain of the specimens under semi-adiabatic curing, i.e. the coupled strain from autogenous shrinkage and thermal expansion/contraction. Temperature histories of the specimens are shown in Figure 9. These temperature histories are very similar to those of the full-scale model columns shown in Figure 10.

The datum strain for plotting the coupled strain was also the value at the time of final setting. The solid lines in Figure 8 show the changes in the strain due to autogenous shrinkage at 20˚C (ε_{as20}) superposed on the thermal expansion (ε_{therm}). Thermal expansion coefficients were measured by subjecting post-test specimens to temperature changes at an age of 3 months, when the autogenous shrinkage had almost converged. They widely varied from one concrete to another, ranging from 8.0 to 13.3×10^{-6}/˚C (see Figure 14). In the case of BPC40, BPC27 and BSC20, there were small differences between the superposed strain and the measurement. In the case of BPC20, OPC40 and OPC27, the differences were moderate, whereas in the case of OPC20 and OBC27, the differences were great. These may result from the differences in autogenous shrinkage development and thermal expansion coefficients through semi-adiabatic curing.

3.3 Actual strain in full-scale model columns

Temperature histories of the full-scale model members, U-columns which had much the same histories as R-columns, are shown in Figure 10. Figure 11 shows the actual strain changes of concrete measured in U-columns and those of reinforcing bars measured in R-columns. Accordance of the strain changes from the center (C1) to the corner (C3) demonstrates that the plane section of the column remains plane under the temperature histories. The difference in actual strain between the concrete in U-columns and the reinforcing bars in R-columns was considered to cause the shrinkage stress of concrete in R-columns. Some shrinkage cracks tended to relax the strain of R1 bar in R-columns with OPC-Rm.

4. Discussion

4.1 Coupled strain from autogenous shrinkage and thermal expansion

As shown in Figure 8, the actual changes in the strain of high-strength concrete subjected to high temperatures differ from the superposed strain consisting of the autogenous shrinkage at 20˚C and

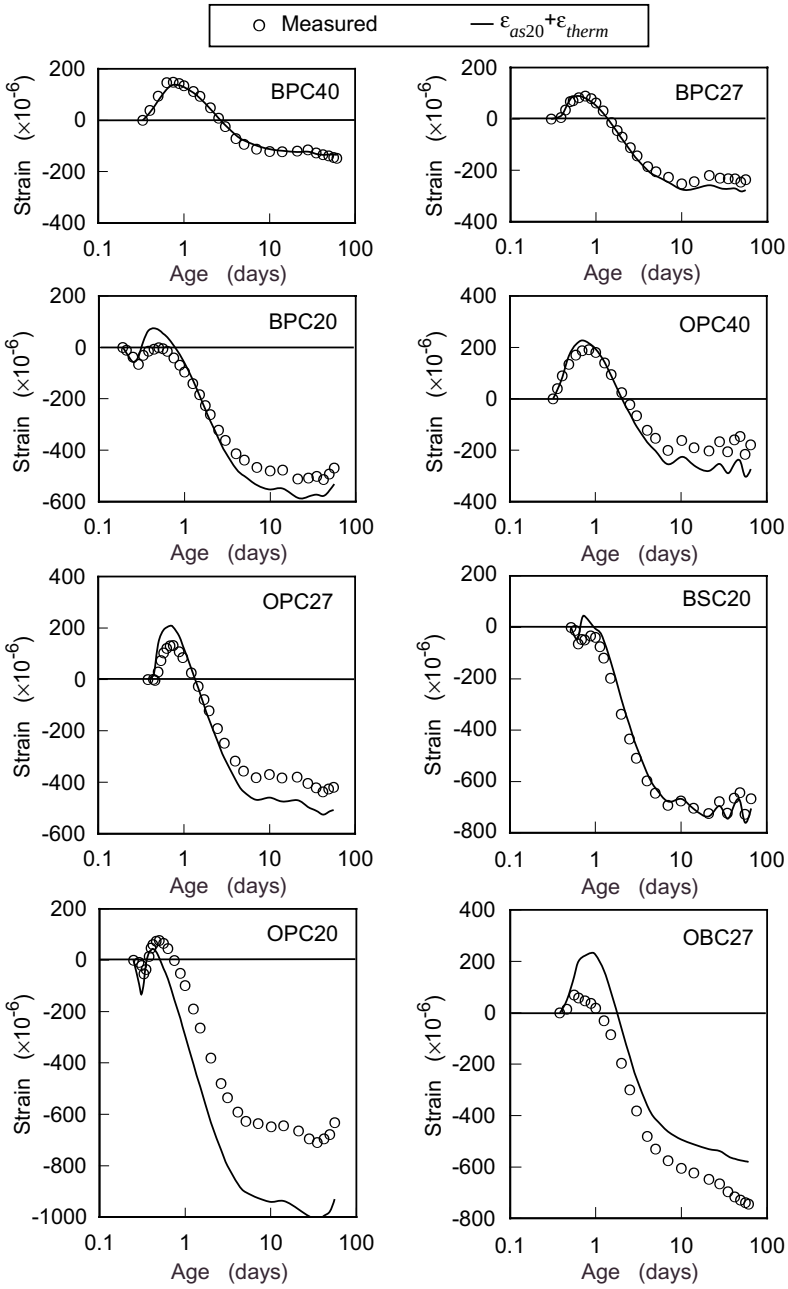

Figure 8 - Coupled strains under semi-adiabatic curing.

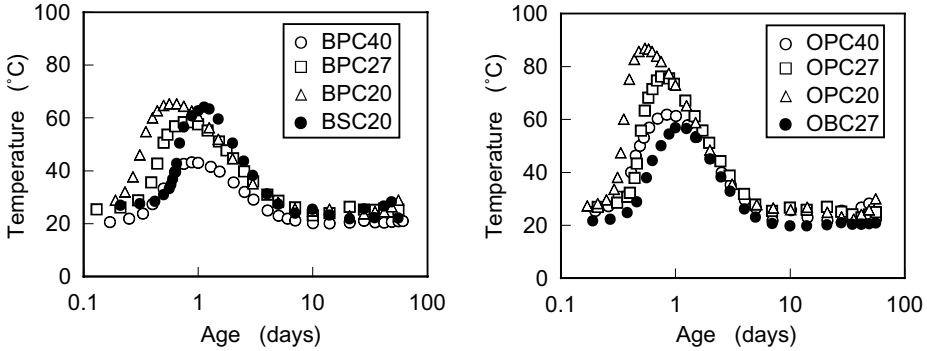

Figure 9 - Temperature histories under semi-adiabatic curing.

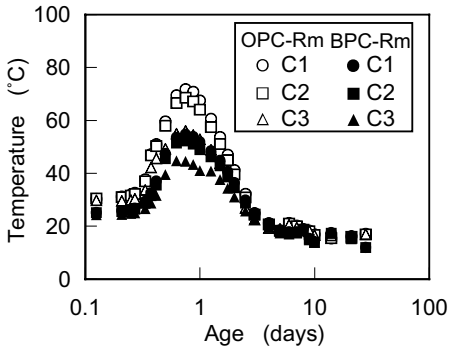

Figure 10 - Temperature histories of model columns.

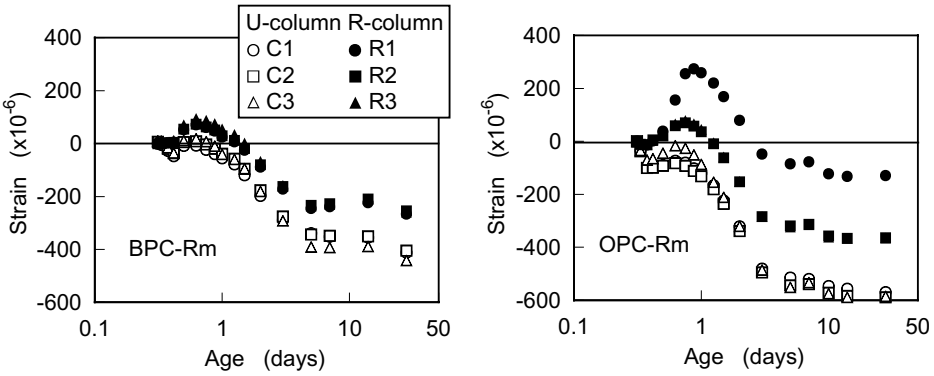

Figure 11 - Actual strains of full-scale model columns.

the thermal expansion. One reason for the difference may be that the actual thermal expansion coefficient is not constant throughout the ages. However, the thermal expansion coefficient of high-strength concrete at early ages has scarcely been measured, as the simultaneous autogenous shrinkage strain makes it difficult to identify. Nevertheless, it is reported that the thermal expansion coefficient of cement paste increases with age [6] and is highest when the relative humidity is around 70% [7]. It is therefore expected that the thermal expansion coefficient of high-strength concrete with a large autogenous shrinkage, i.e. large self-desiccation, increases with age as shown in Figure 12, referring to the results of measurement by [3]. It was considered that the thermal expansion coefficient of concrete is great before the final setting, as the thermal expansion coefficient of water is large and the fabric of the microstructures has not been fully formulated. The thermal expansion coefficient is considered minimized near the final setting, when the fabric has been formed and the concrete is still in a wet condition. Also, it is judged rational to assume the thermal expansion coefficient at the final setting to be 7.0×10^{-6}/°C, since the pore humidity correlates with the thermal expansion coefficient regardless of concrete types as evidently shown in Figure 13. Accordingly, as a case study hereafter, the coefficient of thermal expansion, α, was assumed to be 7.0×10^{-6}/°C at the final setting and increases in proportion to the logarithm of the age up to an age of 3 months as shown in Figure 14 and expressed by equation (3).

$$\alpha(t) = a_1 \ln(t / t_{fs}) + b_1 \tag{3}$$

where $\alpha(t)$= coefficient of thermal expansion at t days (1/°C), t = equivalent age (days), t_{fs}= final setting time (days), coefficients a_1 and b_1= material constans and $b_1 = 7.0 \times 10^{-6}$ in this study.

Figure 15 shows separations of the actual strains of OPC27 under semi-adiabatic curing into thermal strains and autogenous shrinkage strains, with the coefficient of thermal expansion being assumed in one case to be constant at the measurement at an age of 3 months and in another case to be increasing according to Figure 14. A nearly exponential curve of autogenous shrinkage strain was obtained when the increasing coefficient of thermal expansion was applied, whereas a wavy and unreasonable strain curve was obtained when the constant coefficient was applied. The development of the exponential strain curve became about 64% of that of 20°C-curing. Figure 16 shows the autogenous shrinkage strains of other concretes with OPC or BPC, also suiting to exponential curves when the increasing coefficient was applied. The exponential strain curves

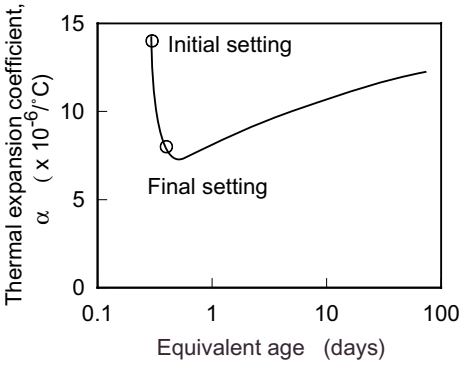

Fig.12 - Model of coefficient of thermal expansion at early age.

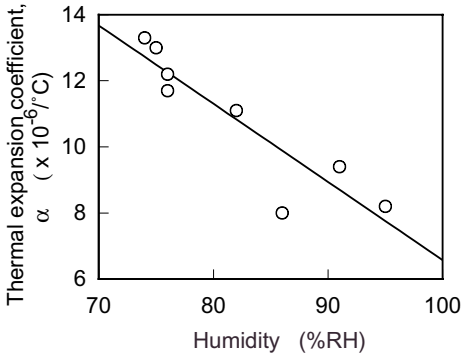

Figure13 - Pore humidity versus coefficient of thermal expansion.

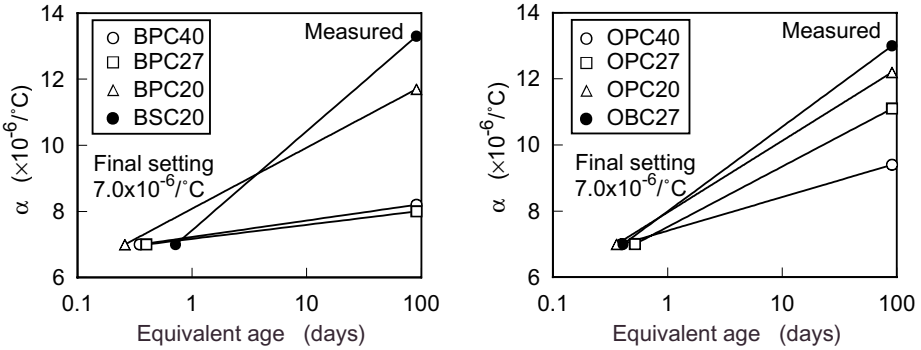

Figure 14 - Assumed coefficients of thermal expansion, α, as a case study.

were about 49-93% of that of 20˚C-curing in all cases. In other words, autogenous shrinkage strain remains lower when subjected to a high temperature history at early ages than when maintained at 20˚C, similarly to strength development. These results in the case study suggest that by taking account of the increase in the coefficient of thermal expansion, reasonable autogenous shrinkage curves suiting to exponential functions are obtained.

Figure 17 shows the autogenous shrinkage strains of OBC27 and BSC20, also suiting to exponential curves but having some complexity even when the increasing coefficient was applied. Figure 18 shows the relationship between the maximum temperature in the history and the ratio of the development of autogenous shrinkage in the history to that of 20˚C-curing ($\varepsilon_{as}/\varepsilon_{as20}$). Though the amount of data is limited, the figure clearly reveals that the autogenous shrinkage of high-strength concrete with usual Portland cements is highly dependent on the temperature conditions regardless of the cement type. Therefore $\varepsilon_{as}/\varepsilon_{as20}$ of such concrete may be roughly expressed by equation (4).

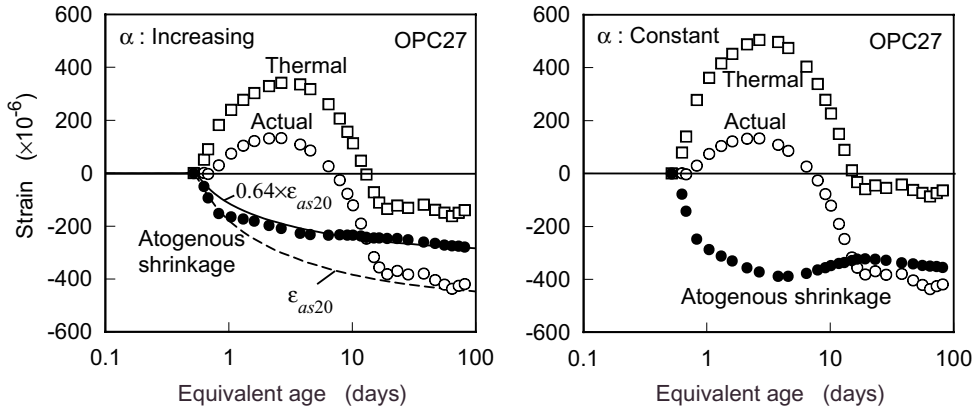

Figure 15 - Separations of actual strain of OPC27 under semi-adiabatic curing into thermal strain and autogenous shrinkage strain.

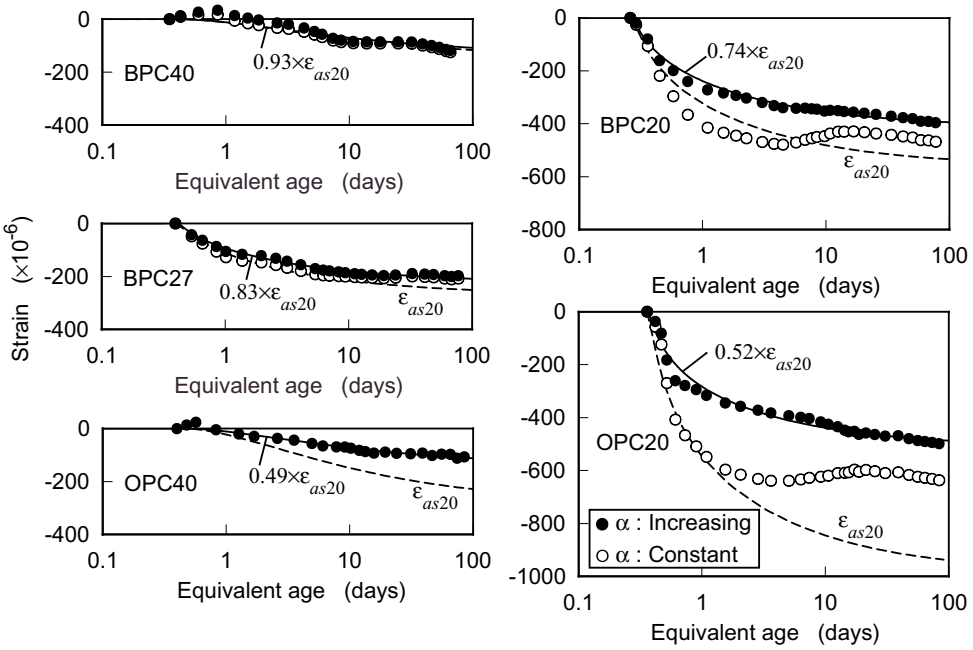

Figure 16 - Estimated autogenous shrinkage strains of BPC and OPC specimens under semi-adiabatic curing.

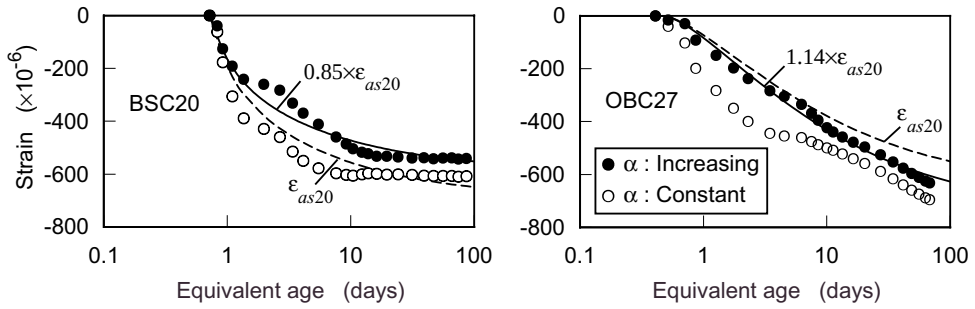

Figure 17 - Estimated autogenous shrinkage strains of BSC20 and OBC27 under semi-adiabatic curing.

$$\varepsilon_{as} / \varepsilon_{as20} = -0.0095 \cdot T_{\max} + 1.36 \quad (T_{\max} \geq 40^{\circ}\mathrm{C}) \tag{4}$$

where $T_{\max}$= maximum temperature of concrete during curing (˚C).

It should be noted, however, that OBC27 and BSC20 show higher developments, especially OBC27 is higher than 1.0, presumably due to the fact that temperature has a great influence on the hydrating activity and hydrated microstructure of admixtures such as blast furnace slag and silica

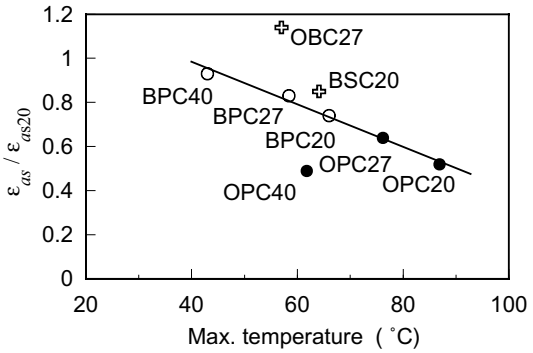

Figure 18 - Effect of maximum temperature on autogenous shrinkage.

fume. The singularly low development of OPC40 cannot easily be evaluated and requires further investigation.

4.2 Estimation of actual strain and stress in the columns

Figure 19 shows the autogenous shrinkage strains of OPC-Rm and BPC-Rm at 20˚C measured in the same manner as the laboratory test. The lines in the figure are the strain curves approximated by equation (1). The strain curves at 20˚C and the temperature changes measured were the basic data to estimate the actual strain and stress in the model columns. For the actual strain in the U-column, we roughly estimated the temperature change at the boundary (CB in Figure 20) where the internally restricted thermal stress is assumed to hardly occur. Then the coupled strain from autogenous shrinkage and thermal expansion at the boundary, which meant the actual strain in the U-column, was estimated through the process as described above. For the actual strain and the average stress of concrete in the R-column, we applied the step-by-step method based on the principle of superimposition of creep and on the self-equilibrium between concrete and reinforcing bars. The stresses of concrete at the center (C1) and at the corner (C3) were estimated based on the difference between the actual strain and the coupled strain at each point. The principle of the estimating process is shown in Figure 20.

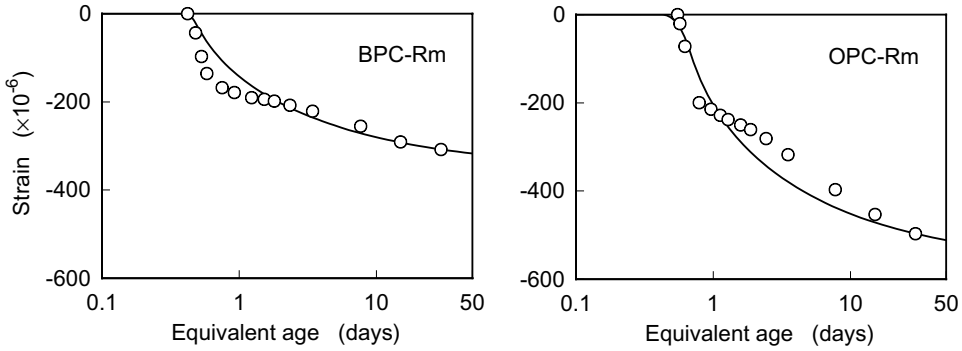

Figure 19 - Autogenous shrinkage strains of OPC-Rm and BPC-Rm at 20˚C.

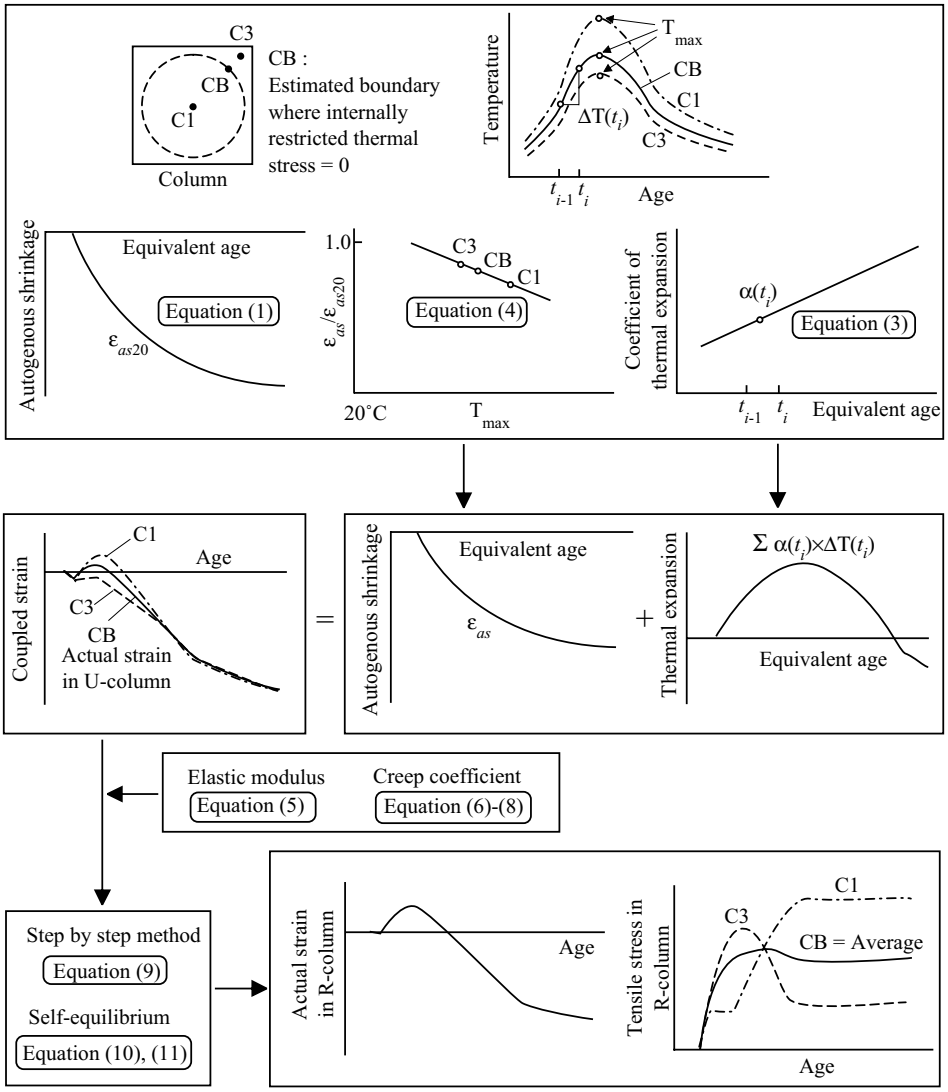

Figure 20 - Flow chart, in principle, for the estimation.

Elastic modulus and creep coefficient required for the estimation were determined with the following equations, referring to previous papers [1, 8]:

$$E_c(t) = E_{cs} \cdot \exp\left\{ s_E \left[1 - \left(\frac{28 - t_{fs}}{t - t_{fs}} \right)^{0.5} \right] \right\} \tag{5}$$

Table 5 - Coefficients and measurements of BPC-Rm, OPC-Rm used for the estimation.

Coefficient/ Mesurement	Eq. (1)			Eq. (3)		Eq. (4) : at CB		Eq. (5)		Eq. (7)	
	ε_{ass} ($\times 10^{-6}$)	s_ε	t_{fs} (day)	a_1 ($\times 10^{-6}$)	b_1 ($\times 10^{-6}$)	T_{max} (°C)	$\varepsilon_{as}/\varepsilon_{as20}$	E_{cs} (kN/mm^2)	s_E	a_2	b_2
BPC-Rm	307	0.13	0.40	0.37	7.0	50	0.89	36.8	0.115	4.0	4.9
OPC-Rm	495	0.13	0.51	0.77	7.0	64	0.75	39.2	0.075	4.9	5.8

where $E_c(t)$= elastic modulus at t days, t = equivalent age (days), E_{cs}= 28-day elastic modulus of standard-cured specimen, s_E= factor for rate of elastic modulus development and t_{fs}= final setting time (days).

$$\phi(t,t_0) = \phi_0 \frac{(t-t_0)^{0.6}}{\beta + (t-t_0)^{0.6}} \tag{6}$$

where $\phi(t,t_0)$= creep coefficient at t days of specimen loaded at t_0 days, t and t_0= equivalent age (days), ϕ_0= apparent ultimate creep coefficient determined by equation (7) and β= factor for rate of creep progress determined by equation (8).

$$\phi_0 = b_2 - a_2 \frac{E_c(t_0)}{E_{cs}} \tag{7}$$

$$\beta = 0.05 \exp\left[5.0 \frac{E_c(t_0)}{E_{cs}}\right] \tag{8}$$

where coefficients a_2 and b_2 = material constans. As seen from the equations above, the creep coefficient was determined as a function of elastic modulus. The coefficients, factors and measurements of BPC-Rm and OPC-Rm inputted in the equations are listed in Table 5. The estimation of the actual strain and the stress of concrete in the R-column was done with the following equations:

Step-by-step method;

$$\sigma_c(t_{i+1/2}) = \frac{1}{J(t_{i+1/2},t_i)}\left[\varepsilon_c(t_{i+1/2}) - \varepsilon_{ce}(t_{i-1/2}) - \varepsilon_{co}(t_{i+1/2})\right] \tag{9}$$

where,

$$J(t_{i+1/2},t_i) = \frac{1}{E_c(t_i)} + \frac{\phi(t_{i+1/2},t_i)}{E_{cs}} ,$$

$$\varepsilon_{ce}(t_{i-1/2}) = \sum_{j=1}^{i-1} \Delta\sigma_c(t_j) \cdot J(t_{i+1/2},t_j) - \sigma_c(t_{i-1/2}) \cdot J(t_{i+1/2},t_i) ,$$

$$\Delta\sigma_c(t_i) = \sigma_c(t_{i+1/2}) - \sigma_c(t_{i-1/2}) ,$$

$t_{i-1/2}$, t_i and $t_{i+1/2}$= at the beginning, the middle and the end of i th time interval, $\sigma_c(t_{i+1/2})$= stress of concrete at time $t_{i+1/2}$, $\varepsilon_c(t_{i+1/2})$= actual strain of concrete at time $t_{i+1/2}$ and $\varepsilon_{co}(t_{i+1/2})$= coupled strain at time $t_{i+1/2}$.

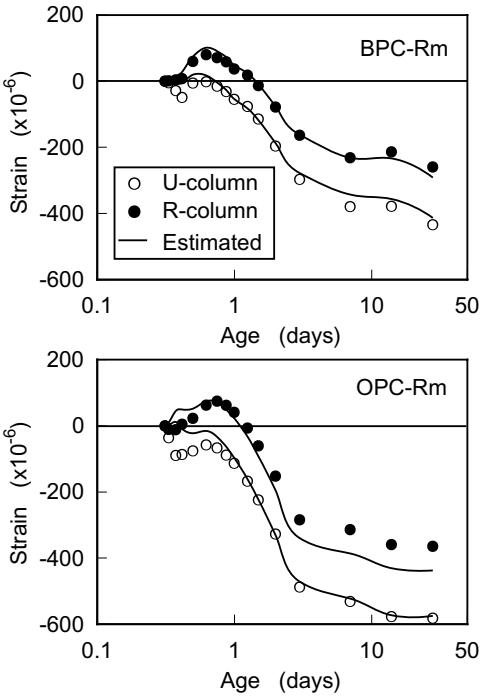

Figure 21 - Measured and estimated actual strains in columns.

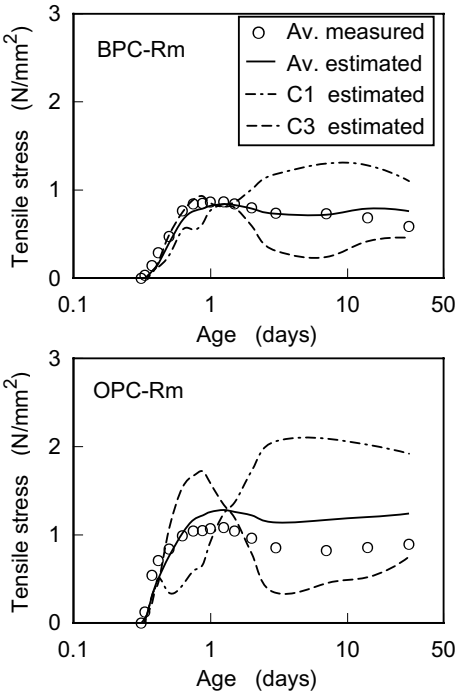

Figure 22- Measured and estimated stresses in R-columns.

Self-equilibrium condition;

$$A_c \cdot \sigma_c(t_{i+1/2}) + A_s \cdot E_s\left[\varepsilon_s(t_{i+1/2}) - \varepsilon_{sT}(t_{i+1/2})\right] = 0 \tag{10}$$

$$\varepsilon_c(t_{i+1/2}) = \varepsilon_s(t_{i+1/2}) \tag{11}$$

where A_c = sectional area of concrete, A_s = total sectional area of main bars, E_s = elastic modulus of main bar, $\varepsilon_s(t_{i+1/2})$ = actual strain of main bar at time $t_{i+1/2}$ and $\varepsilon_{sT}(t_{i+1/2})$ = thermal strain of main bar at time $t_{i+1/2}$.

Figure 21shows the measured and the estimated actual strains in U-columns and R-columns. Each measured value was the average of three measurements, C1-C3 or R1-R3. The measured and the estimated values agree enough except OPC-Rm after the age of 2 days in R-column, probably due to cracking. Figure 22 shows the measured average stress, converted from the strain of reinforcing bar, and the estimated stress in R-columns. While the average stress estimated of BPC-Rm agrees well with the measured one, that of OPC-Rm overestimates the measured one, corresponding with cracking. It was considered that the stress at the corner (C3) of OPC-Rm up to the age of 1 day was too high to protect against the crack.

These results make clear that the estimating approach including the concept of strain

composed of autogenous shrinkage and thermal expansion are very useful for the analysis of actual strain and stress of high-strength concrete structural members.

5. Conclusions

Autogenous shrinkage strain and coupled strain resulting from autogenous shrinkage and thermal expansion of high-strength concrete specimens were experimentally investigated. Then the actual strain and stress in full-scale model columns of high-strength concrete were experimentally and analytically investigated. Though the amount of data is limited, the following were found:

1) Autogenous shrinkage strain beginning at final setting was obtained, and its practical development model was proposed.
2) By taking account of the increase of thermal expansion coefficient with age, it was possible to estimate coupled deformation due to autogenous shrinkage and thermal expansion of high-strength concrete subjected to a high temperature history at early ages, such as structural members.
3) While autogenous shrinkage of concrete with usual Portland cement subjected to a high temperature history was considered to be smaller than that of 20˚C-curing, autogenous shrinkage of concrete with mineral admixtures, such as silica fume and blast furnace slag, was considered to be larger when the admixture content was high.
4) The actual strain and stress in the reinforced concrete columns could be estimated based on the concept of coupled deformation.

References

[1] Tomosawa, F., Noguchi, T., Park, Q.B., Sano, H., Yamazaki, N., Hashida, H. & Kuroda, Y., Experimental determination and analysis of stress and strain distribution of reinforced high-strength concrete column caused by self-desiccation and heat of hydration, Self-desiccation and its importance in concrete technology, Rep. TVBM-3075, Lund Inst. of Technology, Lund, (1997) 174-192.

[2] Technical committee on autogenous shrinkage of concrete (TCASC), Japan Concrete Institute, Committee rep. Proc, Intern. Workshop on Autogenous Shrinkage of Concrete, Hiroshima, 1998 (Ed. by Tazawa, E., 1999) 1-62.

[3] Bjøntegaard, Ø. & Sellevold, E.J., Thermal Dilation-Autogenous shrinkage: How to separate? Proc, Intern. Workshop on Autogenous Shrinkage of Concrete, Hiroshima, 1998 (Ed. by Tazawa, E., 1999) 245-256.

[4] Hedlund, H. & Westman, G.: Autogenous deformations and stress development in hardening concrete, Proc, Intern. Workshop on Autogenous Shrinkage of Concrete, Hiroshima, 1998 (Ed. by Tazawa, E., 1999) 339-350.

[5] CEB-FIP Model Code 1990.

[6] Wittmann, F. & Lukas, J., Experimental study of thermal expansion of hardened cement paste. Materials and Structure 7(40), (1974) 247-252.

[7] Neville, A.M., Properties of Concrete, 3rd Edition. Longman Scientific & Technical, (1986) 493 pp.

[8] Hashida, H. & Yamazaki, N., A calculation method of autogenous shrinkage stress in high-strength concrete structures subjected to elevated temperature at early age, J. Struct. Constr. Eng., AIJ, No.537, (2000) 7-12 (In Japanese).

AUTOGENOUS SHRINKAGE OF CEMENT PASTES HYDRATED AT DIFFERENT TEMPERATURES: INFLUENCE OF MICROSTRUCTURE AND RELATIVE HUMIDITY CHANGE

Ki-Bong Park
Delft University of Technology, The Netherlands
Takafumi Noguchi
The University of Tokyo, Japan

Abstract

This paper presents the results of an experimental study on the influence of temperature, relative humidity and microstructure development on the autogenous shrinkage in hardening cement pastes. The cements used were ordinary Portland cement (OPC) and belite rich Portland cement (BPC). Two different water/cement ratios were used, viz. 0.28 and 0.33 and the temperatures were 20, 40 and 60 ъ. The results of tests indicate clearly that, increasing curing temperature resulted in increased porosity, particularly for pores between 5 to 50 nm as measured by MIP, and increased autogenous shrinkage, as a consequence of a reduction of relative humidity at early ages.

1. Introduction

When cement is mixed with water, the pressure of the part which is occupied by air is 1 atmospheric pressure. However, with progress of the hydration process the total volume of hydration product is smaller than the initial volume of cement and water, the reduced volume is called pore volume and it will be filled with air. Due to the increase of the pore volume the gas pressure in the pore decreases. Under such circumstance, the pore water will be partly consumed in the hydration process and therefore the relative humidity in the vapor filled pores gradually decreases. This phenomenon is called self-desiccation and it is the mechanism for autogenous shrinkage in cement paste [1].

There are quite two categories of factors influencing the speed and the amount of autogenous shrinkage, namely the material and environmental factors. The former includes the type of cement, addition of mineral filler and water/cement ratio; the latter includes the size of specimens and curing temperature [2]. It is worthwhile to point out that among these factors, the curing temperature is directly related to the progress of hydration and consequently directly influence the development of autogenous shrinkage.

Several investigations of autogenous shrinkage of hardening cement paste have demonstrated that at higher curing temperatures, while the early autogenous shrinkage is accelerated, autogenous shrinkage might level off or even decrease at later stage [3,4,5]. The adverse effect of high temperature on autogenous shrinkage is not yet fully understood, however, and further research is needed to provide information to increase the knowledge of this field.

In this paper, we examine the microstructure, relative humidity and autogenous shrinkage changes in cement pastes with water-cement ratio 0.28 and 0.33 cured at constant temperatures of 20, 40, 60 ъ , and discuss the importance of these changes. Temperature effects on the autogenous shrinkage, relative humidity and microstructure development are discussed. We also discuss the relationship between autogenous shrinkage and microstructural changes of cement pastes at higher curing temperatures. This study is intended to provide a better understanding of the factors influencing autogenous deformation of concrete subject to practical curing conditions and to facilitate the prediction of autogenous shrinkage development.

2. Experimental

Two types of cement were used in this study, namely ordinary Portland cement (OPC) and belite-rich Portland cement (BPC). The mineral composition and physical properties of the cements are shown in Table 1. Cement paste was proportioned to have a water-cement ratio of 0.28 and 0.33.

The size of the specimens for the autogenous shrinkage and relative humidity measurement was 40x40x160 mm. The specimens were kept in a temperature and RH controlled chamber during the 5-day for autogenous shrinkage and relative humidity measurement. For porosity measurement, cylindrical specimens with a radius of 50 mm and height 100 mm were prepared. The ages of the specimens for the porosity measurement were 8, 12, 24, 72 and 120 hours after initial setting time. In addition, all the specimens were seal-cured under 20, 40 and 60 ъ .

We used two types of sensors for the autogenous shrinkage measurement, Figure 1. An ammeter (EX-502, Keyence) sensor was used for the measurement at 60 ъ . Laser transducer sensor (AY-22, Keyence) was used for the measurements at 20 ъ and 40 ъ . For relative humidity measurements, the measuring position was in the center of the sealed 40x40x160 specimen and the measurements were done using the relative humidity sensor (AY-22, Yamato) and the working range of RH-sensor is within 0-100 ъ , 15-97 % RH. The RH-sensor was calibrated by saturated salt solutions and it has a resolution of ± 1 ъ and ± 3 % RH. The experimental setup is shown in Figure 2.

In order to prepare the samples for total pore volume, the cement paste specimens were cut into approximately 5 mm cubes using a diamond saw. Specimen fragments were immediately immersed in acetone to prevent further hydration. The 5 mm cubes for MIP measurements were D-dried for about 2 weeks before testing. The porosity and pore distribution were determined using mercury intrusion porosimetry (Micromeritics Auto Pore 9420). The pressure applied was from zero to 200 MPa.

Table 1-Bogue composition of cements used in cement pastes

Cement	Blaine	Density	Mineralogical properties (%)			
	(cm^2/g)	(g/cm^3)	C_3S	C_2S	C_3A	C_4AF
OPC	3310	3.16	52	24	9	9
BPC	3150	3.21	29	54	3	8

OPC: ordinary Portland cement, BPC: belite-rich Portland cement

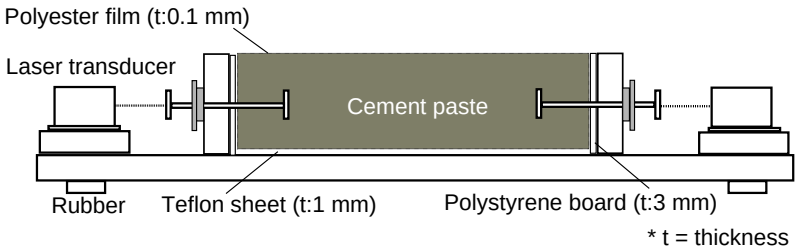

Figure 1-Experimental setup of autogenous shrinkage measurement

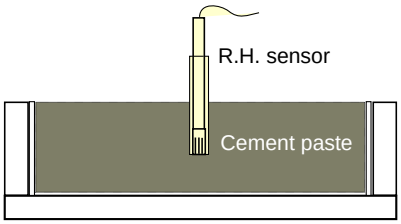

Figure 2-Experimental setup of relative humidity measurement

3. Results

3.1 Autogenous shrinkage

Figure 3 shows the development of autogenous shrinkage in the specimens made with OPC and BPC. As expected, the autogenous shrinkage was accelerated with the increase of curing temperatures at early age. For OPC cured at 20 ъ , the autogenous shrinkage slowly increases with age. However, at higher temperatures both the amount of autogenous shrinkage and the speed of autogenous shrinkage development at early age increased more rapidly than that at 20 ъ . At later stage, the absolute value of autogenous shrinkage at 60 ъ is smaller than that at 20 ъ and it levels off in 24 hours after initial setting time.

In the case of BPC, the autogenous shrinkage increases with higher curing temperatures. The tendency holds in the first 5 days in our experiment. From the experimental data, we found that autogenous shrinkage is significantly affected by temperature and the type of cement used. However, water/cement ratio showed minor influence to the autogenous shrinkage development in this test.

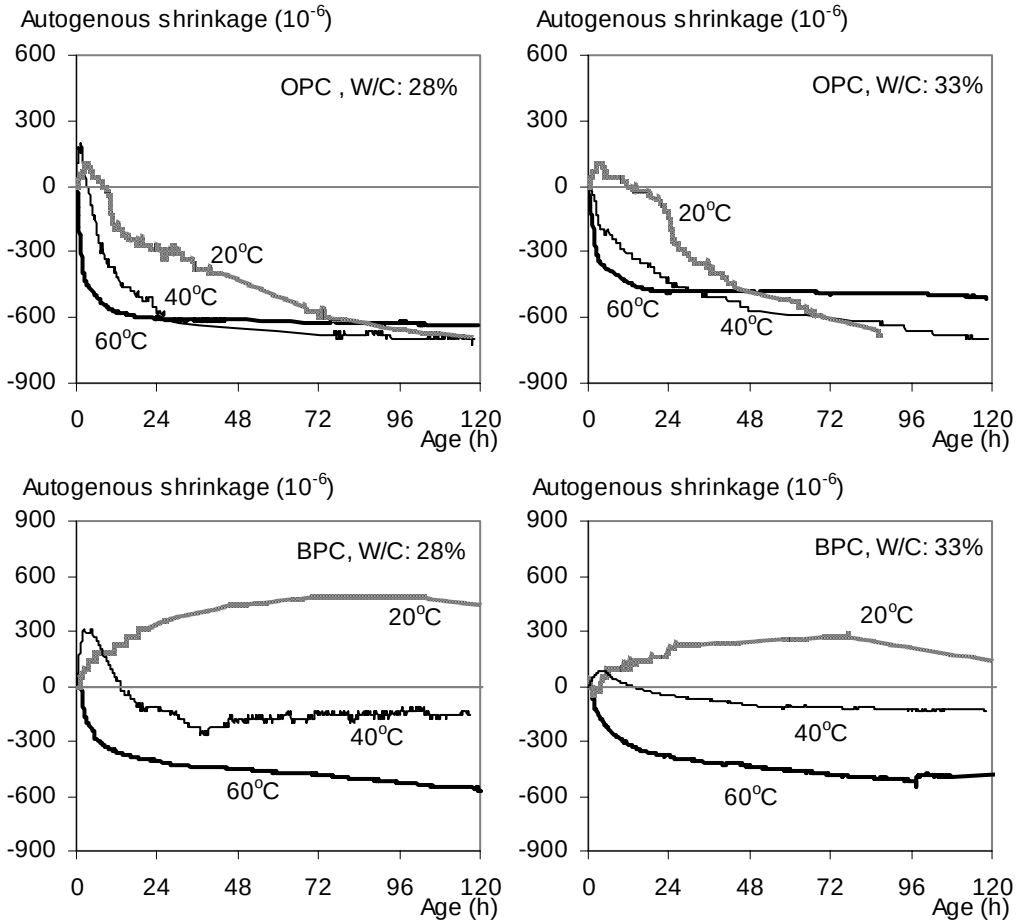

Figure 3-Autogenous shrinkage vs. time curves of cement pastes under various temperatures

3.2 Relative humidity

Figure 4 shows the evolution of the relative humidity of OPC and BPC. For OPC cured at 20 ъ and with lower water cement ratio, relative humidity decreases much faster. However, at 40 ъ and 60 ъ, relative humidity of specimens with higher water/cement ratio drops faster than the lower water/cement ratio case. In addition, when the curing temperature is 60 ъ, the relative humidity of the sample will level off after 24 hours. It can be noticed that the relative humidity in OPC changes very rapidly at early age and the higher curing temperature is, the earlier the decrease of relative humidity occurs.

For the BPC paste, the RH changes much insignificantly with the time. The influence of water/cement ratio is quite moderate and the RH values fall in the range of 90-100%. However, higher curing temperature still induces higher reduction of the relative humidity.

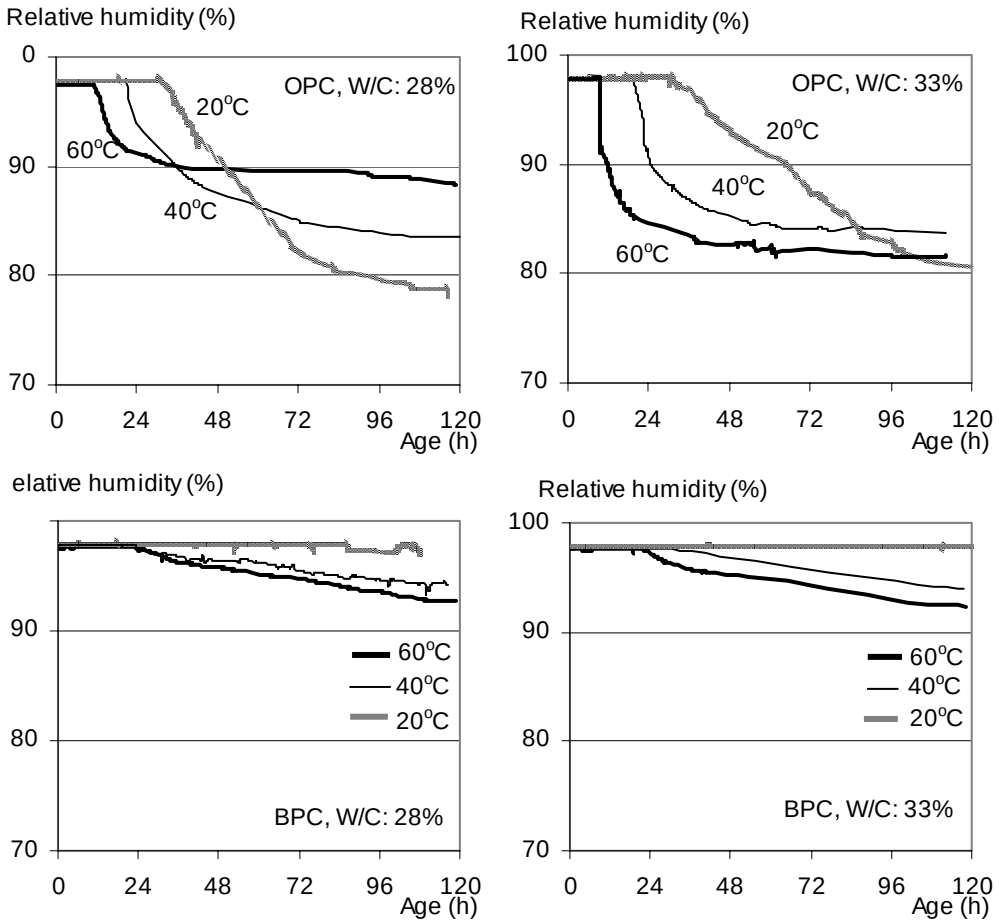

Figure 4-Relative humidity vs. time curves of cement pastes under various temperatures

3.3 Microstructure

Figure 5 shows the development of total pore volume of OPC and BPC. The total pore volume of OPC and BPC decreases with the progress of hydration in the observed period. At higher temperatures, the volume of pores between 5 to 50 nm (capillary pore) increases at early age. For OPC with water-cement ratio 0.33, the capillary porosity increases up to 72 hours at 40 ь curing and up to 24 hours at 60 ь curing after initial setting time.

For BPC, the capillary porosity increases slowly up to 24 hours for water-cement ratio 0.28 and up to 72 hours for water-cement ratio 0.33. The results in Figure 5 indicate that the capillary porosity of OPC is larger at early ages than that of BPC: this can be explained by the larger proposition of reactive cement clinker in OPC.

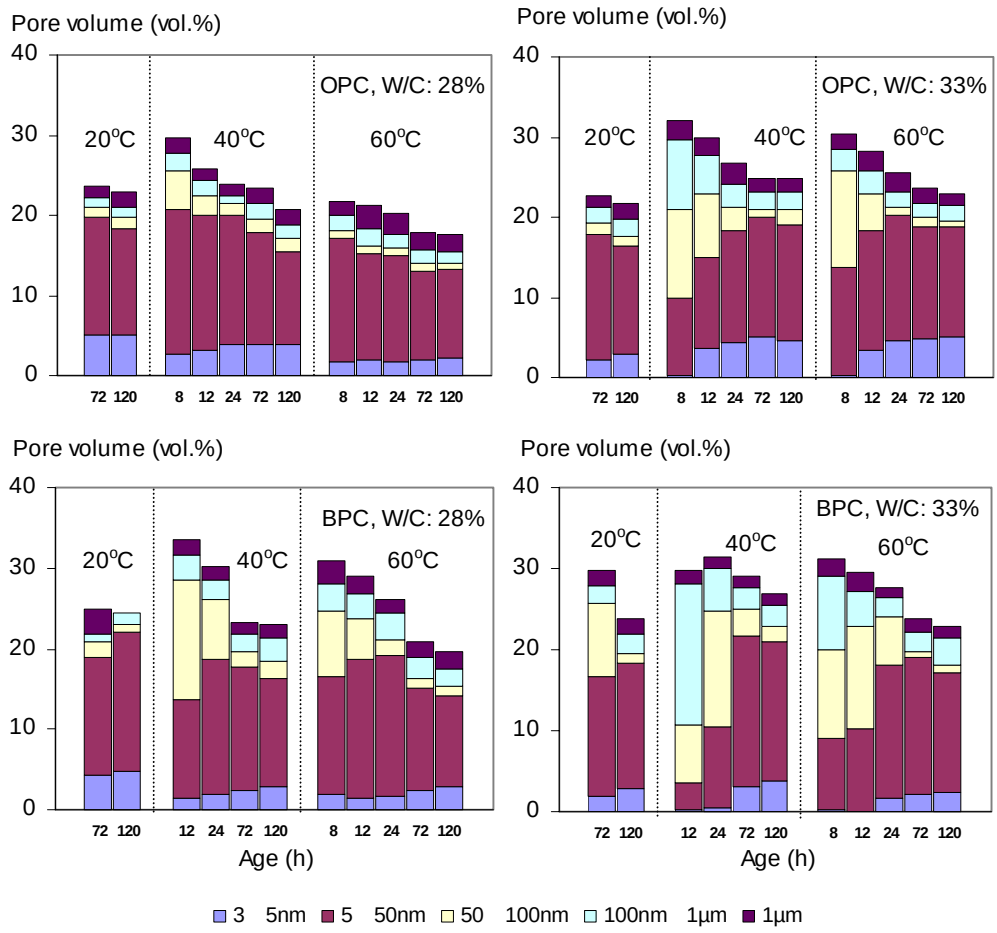

Figure 5-Total porosity vs. time for cement pastes under various temperatures

4. Discussion

4.1 Autogenous shrinkage vs. relative humidity

Based on the curves shown in Figure 3 and Figure 4, it is possible to explain the autogenous shrinkage as a function of the relative humidity. Figure 6 shows the relationship between the relative humidity change and autogenous shrinkage in OPC with W/C ratio 0.33. At 20 ׳C curing, the autogenous shrinkage occurring between 12 and 24 hours were not related to relative humidity change. However, after 24 hours the autogenous shrinkage varies linearly according to relative humidity, about 50µ/ %RH. At higher temperature the linear relationship between the relative humidity and autogenous shrinkage was also found, but about

20.5μ/ %RH at 40 ℃ and about 4.8μ/ %RH at 60 ℃. The autogenous shrinkage of cement pastes cured at higher temperature at early age increase greatly without the change in relative humidity because a substantial proportion had already increased due to chemical shrinkage [6].

In Figure 4, the relative humidity of cement paste cured at higher temperature drops faster than that at lower temperature. However, another literature [7,8] reported the internal temperature difference which causes an increase of about 0.3 %RH/ ℃ for the concrete with W/C 0.3. In Figure 4, the relative humidity in OPC paste ranges roughly between 80 and 100 %. It was shown that these results could be simulated by application of the Kelvin law [9]. In [9,10], it was proposed to calculate the autogenous shrinkage of hardening cement paste from the reduction of the pore pressure which is associated with the decreasing relative humidity in the gradually emptying pores. The relative humidity in the gradually emptying pore space is an unknown parameter which must be calculated from the actual moisture state of the hardening cement paste. The water content of a capillary system depends on the moisture content of the surrounding air and the capillary structure of the pore system [11].

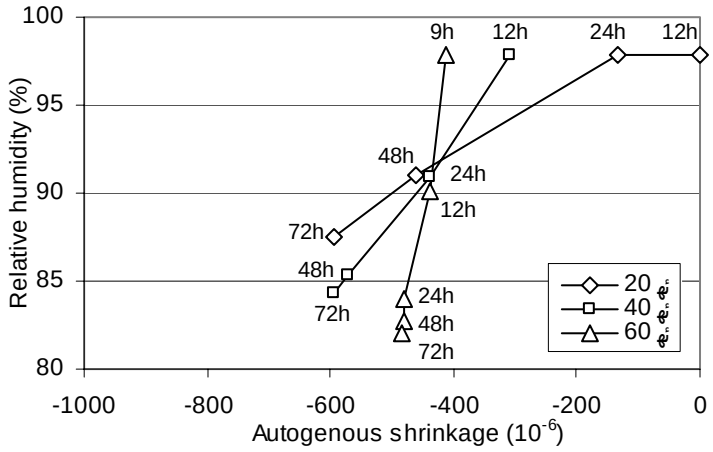

Figure 6-Relationship between autogenous shrinkage and relative humidity in OPC with W/C ratio 0.33 under various curing temperatures

4.2 Relative humidity vs. small porosity

As hydration proceeds, the capillary pores will be emptied, the relative humidity will decreased. For prediction of the relative humidity in the hardening cement paste, the pore structure of the space where RH changes must be investigated. The porosity emptied at relative humidity above 60 % arises from spaces between the original cement grains that have not become filled with cement hydrates and may be regards as capillary porosity [12]. In [9,13], it has estimated that the meniscus effects can be precisely evaluated from the Laplace law and the Kevin law for a meniscus radius greater than 5 nm. In this paper, it was assumed that the small porosity consists of pores in the range of 5 to 50 nm.

Normally the small porosity increases with hydration and thus is greater at early ages when curing at higher temperatures as shown in Figure 5. The smaller pores could induce higher capillary pressure which will be the driving force for the increase of the autogenous shrinkage. Figure 7 shows the relationship between the relative humidity change and small porosity in OPC with W/C ratio 0.33. It can be seen that the relative humidity decreases with the increasing of small porosity, particularly at 20 ъ curing. However, at higher temperature the reduction of relative humidity was not sensitive to the small porosity change like that on autogenous shrinkage.

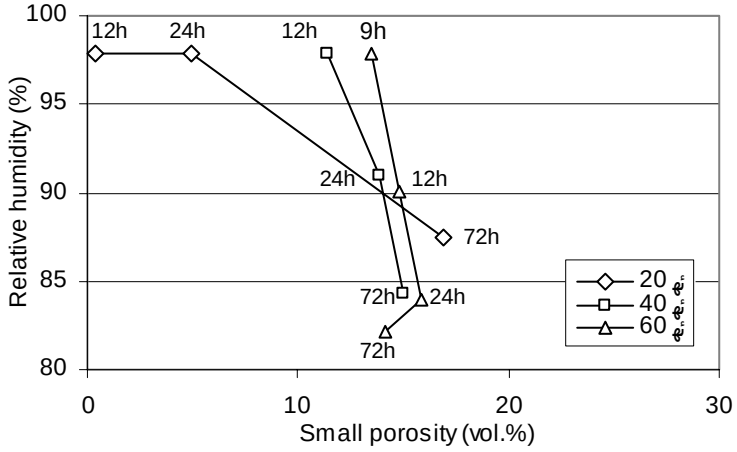

Figure 7-Relationship between relative humidity and small porosity (5nm-50nm) in OPC with W/C ratio 0.33 under various curing temperatures

5. Conclusions

From the investigation on the effect of temperature, relative humidity and microstructure development on the autogenous shrinkage in cement pastes, the following conclusions can be drawn.

1) The autogenous shrinkage is significantly affected by temperature. It is found that for both OPC paste and BPC paste, the autogenous shrinkage and the speed of autogenous shrinkage development are higher at early age when the temperature is higher. However for OPC paste, at later stage autogenous shrinkage at 60 ъ was found lower than that at 20 ъ .
2) The reduction of relative humidity is larger at early ages at higher temperature. RH of paste made with OPC falls in the range of 80-100 % while with BPC in the range of 90-100 %.
3) The total porosity decreases with the progress of hydration in the observed period. However, at higher temperatures the volume of pores between 5 to 50 nm increases at early age. The time for the increase of the pore volume is related to the age when the autogenous shrinkage levels off.

6. References

[1] Powers, T. C., Brownyard, T. L.; Studies of the physical properties of hardened Portland cement paste, Res. Lab. Portland Cem. Assoc., Bull. 22, Proc. Am. Concr. Inst., 43 (1947)

[2] Report of the research committee of the autogenous shrinkage, Japanese Concr. Inst. (1996)

[3] Tazawa, E., Matsuoka Y.,. Miyazawa, S., Okamoto, S.; Effect of autogenous shrinkage on self stress in hardening concrete, Proc. Int. Symp. Thermal Cracking in Concrete at Early Ages, RILEM Proc. 25, 221-228 (1995)

[4] Tomosawa, F., Noguchi, T, Park, K.B., Sano, H., Yamazaki, N., Hasida, H., Kuroda, Y.; Experimental determination and analysis of stress and strain distribution of reinforced hitgh-strength concrete column caused by self-desiccation and heat of hydration, Proc. Int. Sem. Self-desication and Its Importance in Concrete Technology, 99-115 (1997)

[5] Jansen, O. J., Hansen, P. F.; Influence of temperature on autogenous deformation and relative humidity change in hardening cement paste, Cem. Concr. Res. 29, 567-575 (1999)

[6] Baron, J., Buil, M.; Mechanical features of chemical shrinkage of cement paste, Cem. Concr. Res. 9, 545-547 (1979)

[7] Nisson, N. O.; Temperature effects in relative humidity measurements on concrete-some preliminary studies, The Moisture Group. Report 1987:1. BFR. 1987, 84

[8] Persson, B.; Self-desiccation and its importance in concrete technology, Mater. Struct. 30, 293-305 (1997)

[9] Hua, C., Acker, P., Ehrlacher, A.; Analyses and models of the autogenous shrinkage of hardening cement paste I. Modelling at macroscopic scale, Cem. Concr. Res. 25, No.7, 1458-1468 (1995)

[10] Koenders, E. A. B.; Simulation of volume changes in hardening cement-based materials, Doctoral Thesis, Delft University of Technology (1997)

[11] Kovler, K.; Why sealed concrete swells, Am. Concr. Inst. Mater. J., 93, No. 4, 334-340 (1996)

[12] Parrott, L. J.; Measurement and modeling of porosity in drying cement paste, Proc. MRS Sypo. on Microstructual Development during Hydration of Cement, 85, 91-104 (1987)

[13] Fisher, L. R.; Force due to capillary-condensed liquids: limits of calculation from thermodynamics, Advances in colloid and interface science, 16, 117-125 (1982)

A METHOD FOR SIMULTANEOUS MEASUREMENTS OF HEAT OF HYDRATION AND RELATIVE HUMIDITY

Lars Wadsö and Anders Anderberg

Building Materials, Lund University, Box 118, 221 00 Lund, Sweden

Abstract

Isothermal (conduction) calorimetry is a general method to study reaction processes by measuring the heat produced under isothermal conditions. The method is ideally suited for studies of cement hydration as the hydration reactions produce large amounts of heat. In the calorimeters we are using the sample is kept in a closed glass ampoule during the measurement. We have now further developed this technique by inserting a relative humidity probe in the glass vial. We can thus measure both thermal power (reaction rate) and relative humidity (self-desiccation) simultaneously. We have done test measurements on cement pastes with two types of cements and different w/c-ratios. At high w/c the measurements are good, but at low w/c the relative humidity measurements show large variations. We believe that this is caused by water vapour being lost through small leakages in the ampoules, and that this vapour cannot be replaced by vapour from the relatively dry and vapour tight low w/c cement pastes. It is thus essential to have very vapour tight ampoules for this type of measurement to work.

1. Introduction

The self-desiccation properties of concrete and other cementitious products are of large interest. The large amounts of water left after the hydration of ordinary high water/cement ratio (w/c) concrete is often a problem in the modern high tempo building process. In Sweden we have had many cases of floorings being degraded because they have been laid on concrete that was not dried enough. Two potential ways to overcome such problems is to use low w/c self-desiccating concrete or using a self-desiccating self-levelling flooring compound on top of an ordinary concrete.

The self-desiccation of a low w/c concrete is caused by the hydration reactions consuming water and thus lowering the relative humidity of the concrete. The self-desiccation of a cementitious material is best studied by measuring the relative humidity

of a gas phase in contact with the material in a closed container. Typically, a sample is cast in a jar that is closed by a vapour-tight lid. Inside the jar is placed a relative humidity probe. As the jar is vapour-tight, no vapour can escape and the relative humidity measured in the gas phase is the same as that of the material (or the pores inside the material). In whole constructions it is also possible to measure self-desiccation by measuring the relative humidity in a position inside a construction that has not been influenced by the external relative humidity.

Isothermal heat conduction calorimetry is the measurement of heat production rate (thermal power) at constant temperature conditions. As the thermal power is proportional to the rate of the hydration (reaction) isothermal calorimetry is an interesting technique to study different aspects of the hydration process. Some examples of studies that can be made:

- Determination of retardation by additives.
- Measurement of hydration rate as a function of temperature.
- Quality control of cement.

More examples can be found in [1] and [2]. In this paper we describe a method to simultaneously measure self-desiccation (relative humidity) and rate of hydration (thermal power). As far as we know only Penttala [3] has made measurements of relative humidity inside a calorimetric chamber before us.

2. Method

The isothermal calorimeters used (TAM Air, Thermometric AB, Järfälla, Sweden, www.thermometric.se) consists of eight isothermal heat conduction calorimeters in a thermostat (Figure 1). Each calorimeter holds a 20 ml glass or steel ampoule with the sample (Figure 2). The baseline stability of the TAM Air over a time period of a week is better than ∂5 σW.

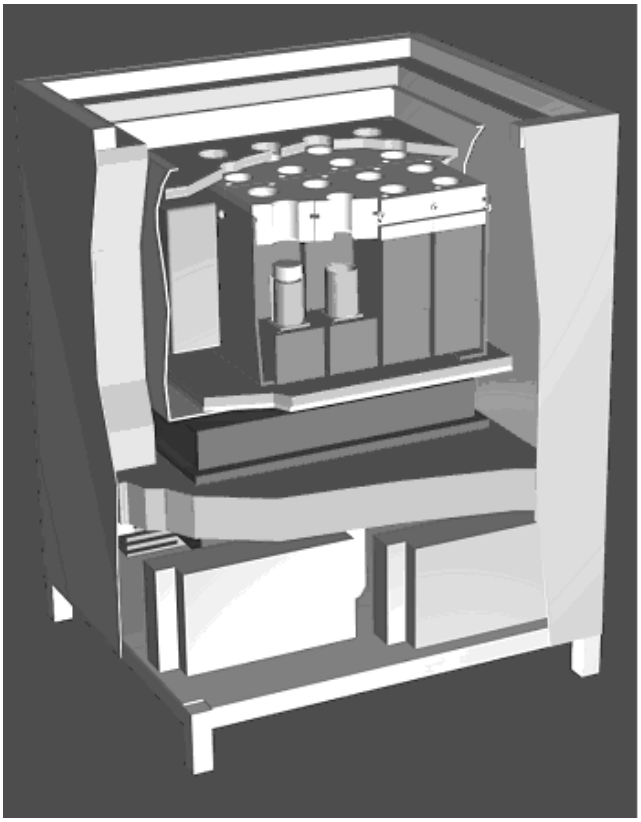

Figure 1 - A cut-away picture of the eight-channel TAM Air isothermal calorimeter used in this study. The samples are kept in the ampoules, two of which can be seen in the figure. Below the calorimeters is an air thermostat that together with the insulation provides a constant temperature environment for the calorimeters.

The samples of cement paste, cement mortar or concrete with small sized aggregate are placed in a 20 ml glass ampoule (Figure 2). As quite a lot of heat is produced during cement hydration only a small sample is needed; here we have used samples of about 10 g cement paste (about 4 ml) on the bottom of each ampoule. This leaves enough space for the relative humidity sensor above the sample.

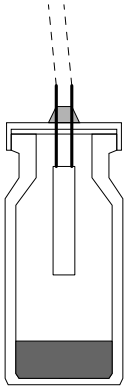

Figure 2 - A schematic drawing of the calorimetric glass ampoule with a cement paste sample and a relative humidity sensor inserted through the seal.

The relative humidity sensors were of type HumiGuard (Nordisk Industrifysik AB, Malmö, Sweden). This is a disposable sensor that does not need to be calibrated. It has been used quite a lot in Sweden on building sites. Calibration is not needed, but a sensor from the same batch of sensors is used as a reference and is kept above a calibration vial with 85% relative humidity. During each measurement the electrical conductivity and the temperature of each sensor (both measurement sensor and reference sensor) is measured. The relative humidity is then calculated with a computer program.

Normally, each HumiGuard sensor consists of a resistive RH-sensor and a temperature sensor (a thermistor). In the present set-up we only used the RH-sensor as the temperature of the calorimeter is very well known. During the present experiments the samples and the references were at approx. the same temperature of 20^{o}C.

3. Materials

The measurements were made with two cements from Cementa AB (Sweden):

- Portland cement EN 197-1 - CEM I 42,5 R "Standardcement"
- Portland-limestone cement EN 197-1 - CEM II/A-LL 42,5 R "Byggcement"

Each cement was mixed with tap water to the following water-cement ratios: 0.35, 0.40, 0.45 and 0.50. For the samples with water/cement-ration 0.45 and 0.50 some sand was added to prevent separation. Two samples from each mix were used in the combined measurements of thermal power and relative humidity.

4. Results

Figure 3 shows the result from the relative humidity measurements and Figures 4 and 5 show the results from the calorimetric measurements.

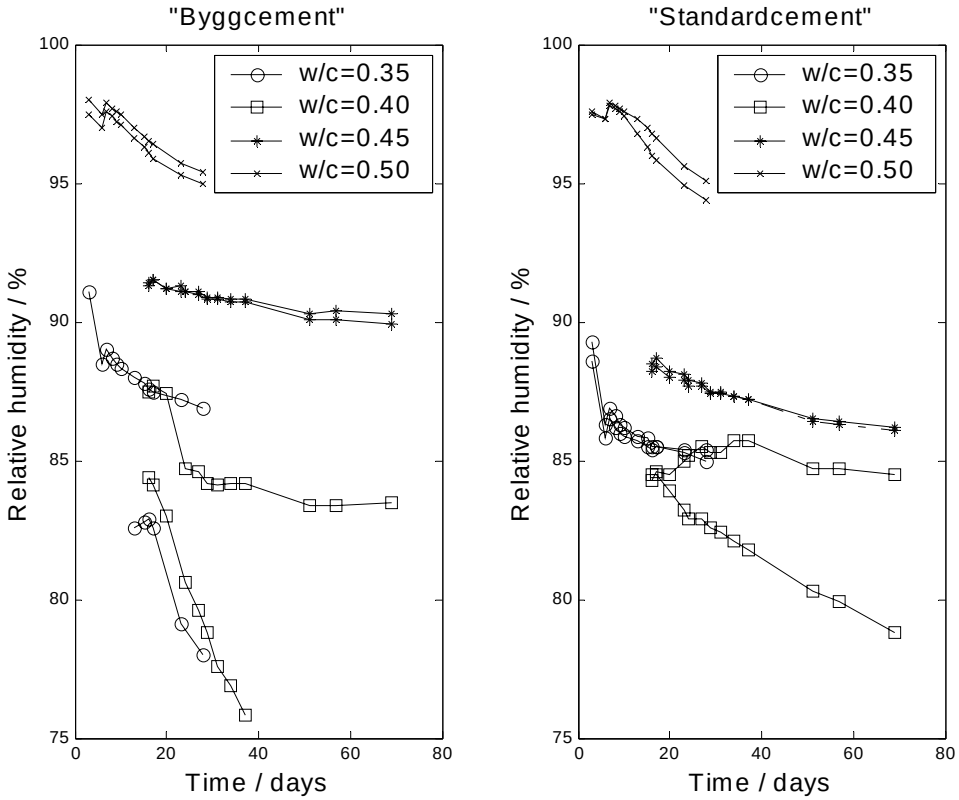

Figure 3 - Results from the measurements of relative humidity on a Portland limestone cement (left) and a Portland cement (right). Four water-cement ratios were used: 0.35 (circles), 0.40 (squares), 0.45 (stars), and 0.50 (crosses).

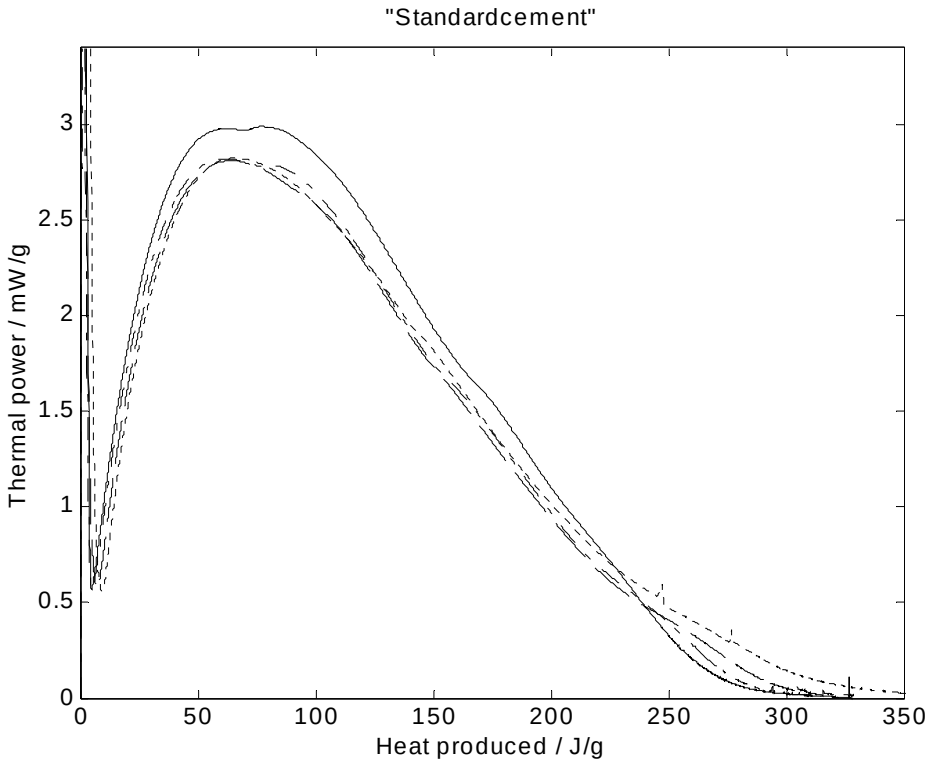

Figure 4 - Specific thermal power (watts per gram cement) as a function of produced heat (joules per gram cement) for the Portland cement. Each curve is a mean of two measurements on samples from the same mix. The differences between two curves were never more than 0.1 mW/g. W/c=0.35 (solid), w/c=0.40 (dash-dotted), w/c=0.45 (dashed) and w/c=0.50 (dotted).

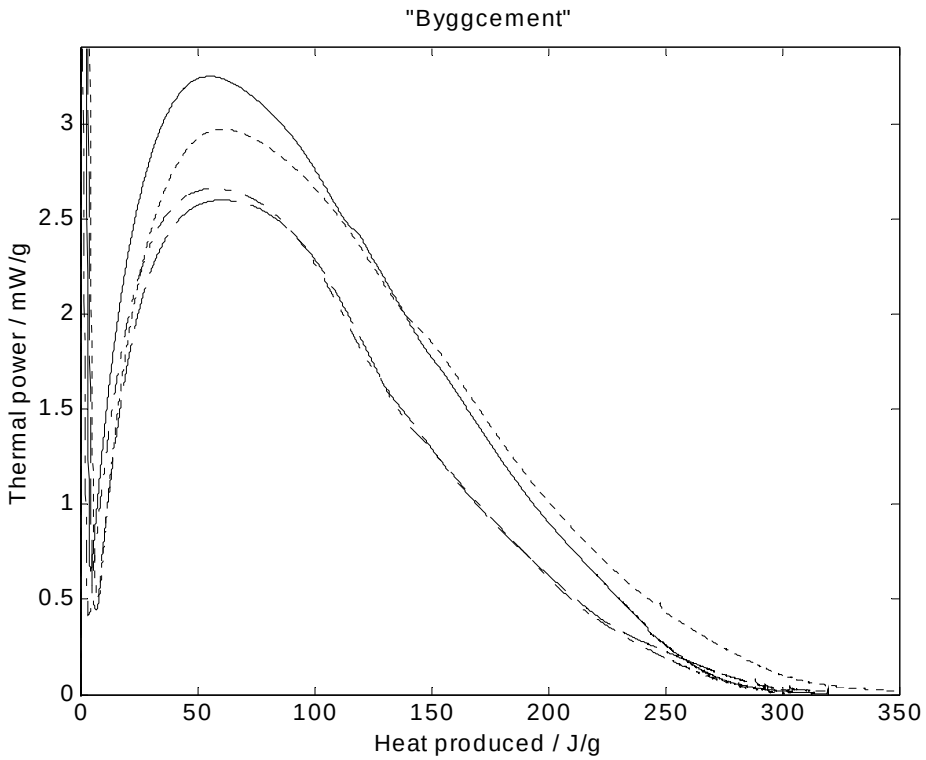

Figure 5 - Specific thermal power (watts per gram cement) as a function of produced heat (joules per gram cement) for the Portland limestone cement. Each curve is a mean of two measurements on samples from the same mix. The differences between two curves were never more than 0.1 mW/g. W/c=0.35 (solid), w/c=0.40 (dash-dotted), w/c=0.45 (dashed) and w/c=0.50 (dotted).

5. Discussion

The relative humidity measurements were successful at high w/c-ratios (0.45 and 0.50). At lower w/c (0.35 and 0.40) there were substantial differences between duplicate curves. We believe that this was caused by the fact that the low w/c samples were unable to supply enough moisture to the headspace of the ampoule; both because the low w/c

cement contains less water and because low w/c cement has much lower diffusivities than the high w/c-samples. The general idea of the method is that there should be water vapour equilibrium within the ampoule, i.e. there should be no relative humidity gradients in the ampoules. The differences between different samples are an indication that this has not been the case.

We have two possible explanations to the variation seen in the results from low w/c samples:

- Even very slight leakages remove enough vapour from the head-space to lower the relative humidity there. After the measurements we have tested the vapour tightness of the ampoules. With water in the ampoules and an external relative humidity of about 40% we found that some of the ampoules lost up to 5 mg of water during a 14 days period.
- It may also be that the relative humidity sensor itself has such high vapour absorption that the head-space is depleted of water vapour. To test this hypothesis we measured the sorption isotherm of a HumiGuard sensor and found that it quickly absorbed about 0.4 mg of water vapour in the range 0-85% RH and about 1 mg in the range 85-95% RH (slow absorption). We do not know in what RH-state the sensors were when we installed them, but it is possible that they need up to 0.5 mg to come into equilibrium with the relative humidity of the cement pastes.

It seems reasonable to assume that either of these hypotheses (or both) can explain the strange results with low w/c-samples. The headspace at high relative humidity at 20°C holds about 0.2 mg water vapour, so if the two factors discussed above are active the cement pastes have to supply several milligrams of water vapour to the headspace to keep up the relative humidity.

We conclude that the ampoules have to be very vapour tight for the method to work and that the relative humidity sensor should have as low moisture capacity as possible.

Figures 4 and 5 show the specific thermal power (watts per gram cement) as a function of produced heat (joules per gram cement). This is both a convenient and illustrative way to compare calorimetric cement hydration curves. The produced heat Q (J/g) on the x-axis can be seen as the extent of reaction • (g(reacted cement))/g(cement); more produced heat means that the hydration reaction has preceded further:

$$\bullet \mid \frac{Q}{\div h} \qquad (1)$$

Here, $\div h$ (J/g) is the specific reaction enthalpy. The specific thermal power P (W/g) on the y-axis is proportional to the rate of reaction τ (g/s):

$$\tau \mid \frac{P}{\div h} \tag{2}$$

A problem with the use of these equations is that the reaction enthalpy $\div h$ may have different values at different times of the hydration process. Apart from that, these relations are useful in modelling the cement hydration process as solid-state kinetic models usually have the form:

$$\tau \mid f(\bullet) \tag{3}$$

This can easily be rewritten using the calorimetrically measured parameters P and Q [1,2]:

$$Q \mid f_2(P) \tag{4}$$

Data from a calorimetric measurement can therefore be used to test different kinetic models.

All calorimetric measurements worked well. The duplicates were close to each other and it is seen in Figures 4 and 5 that the reaction rate is not very much influenced by the water/cement-ratio. For both cements the hydration reaction continues longer for the highest w/c-ratio of 0.50. After three weeks the thermal power from these samples is still in the order of 100 σW. For the other w/c-ratios the reaction rate is so low after two or three weeks that it is not measurable with the instruments used. The lower w/c-ratios seem to have a slightly higher rate of reaction at the maximal rate of reaction (main peak of curves).

We plan to continue the present type of measurements with the same calorimeter, but with another type of RH-sensors.

6. Conclusion

We conclude that the combination of isothermal calorimetry and relative humidity measurements is an interesting combination for the study of self-desiccating systems. However, great care must be taken to prevent leakages and sorption in sensors.

Acknowledgements

We thank Bo Johansson for the measurements.

References

[1] Bensted, J., Some applications of conduction calorimetry to cement hydration. Adv. Cement Res., **1**(1): 35-44 (1987).

[2] Thermometric, TAM Air Cement, Järfälla, Sweden. (2002).

[3] Penttala, V., Freesing-induced strains and pressures in wet porous materials and especially in concrete mortars. Advn Cem Bas Mat, **7**: 8-19 (1998).

[4] Willson, R. J., A. E. Beezer, et al., Solid state reactions studied by isothermal microcalorimetry; the solid state oxidation of ascorbic acid. Int. J. Pharmaceutics **132**: 45-51 (1996).

[5] Willson, R. J., A. E. Beezer, et al., Determination of thermodynamic and kinetic parameters from isothermal heat conduction microcalorimetry: applications to long-term-reaction studies. J Phys Chem **99** (7108-7113) (1995).

INFLUENCE OF CEMENT COMPOSITION ON ENDOGENOUS SHRINKAGE

Françoise Beltzung and Folker Wittmann
Institute for building materials, Swiss Federal Institute of Technology, Zurich

Abstract

Investigations into early endogenous shrinkage allow us to better understand the influence of cement fineness and composition on shrinkage. Ettringite formation before setting turns out to be of considerable significance; if the content of the aluminate and ferroaluminate phases is low, very little ettringite forms. However, the higher the amount of these components, the more water is consumed at an early stage and hence self-desiccation increases. Early shrinkage was measured on cement suspensions, cement pastes and concretes directly after mixing. The experimental set-up for concrete allowed to measure both horizontal and vertical displacements. The time at which a stable three-dimensional network of hydration products is being formed coincides with the end of anisotropic behaviour of young concrete. Endogenous shrinkage was evaluated from this time onwards. A water sorption experiment showed that self-desiccation damages the composite concrete structure. Damage could be ascertained by an increased permeability.

1. Introduction

Up to now, it was not possible to visually observe endogenous shrinkage cracks except with the replica technique proposed by Ollivier [1,2]. Microscopic investigations are not trivial. Difficulties arise through sample preparation methods and microscopic techniques which influence the crack pattern and may even modify it. We do not actually know if visible cracks are to be expected at all. By drying samples from 100% to 70% RH in an ESEM chamber Bisshop [3] could not find any microcracks. Despite this uncertainty, some indirect work on self-desiccation damage yields interesting informations. Sadouki [4] simulated microcracking on the basis of the fictitious crack concept. He showed that, in case of drying of the concrete matrix, microcracks should be oriented normal to the surface of the much stiffer aggregates. It is also stated that concrete with low w/c ought to be damaged by strain softening during the very first days when tensile strength and fracture energy

compete with shrinkage induced stresses. The age of 2 to 3 days is often admitted to be critical [4,5]. An important indirect way to evidence damage due to self-desiccation is related to permeability measurements. For that reason we performed a water sorption test which showed damage for low w/c but yields neither qualitative nor quantitative information on the underlying microstructural defect.

The influence of endogenous shrinkage on durability is far from being well understood. As, for concretes with low w/c, the imposed deformations are of the same order of magnitude as in the case of drying shrinkage, it seems to be reasonable to try to minimize endogenous shrinkage.

Shrinkage mechanisms are identical for both exogenous and endogenous drying. They can roughly be divided into two humidity regions: (1) at high RH, the hygral length change is controlled by the complex interaction between hydration products and pore solution, which can be characterised by the counteraction of capillary underpressure and disjoining pressure; (2) at RH < 45%, the variation of the surface tension of the C-S-H particles is the main reason for hygral length change (Bangham equation). Endogenous shrinkage is particularly sensitive to the rate of drying during the accelerated hydration period. The actual w/c at the time when a three dimensional network is reached should, therefore, be a major parameter, which strongly affects endogenous shrinkage. This w/c is somehow lower than the initial w/c, depending upon early hydration, i.e. early chemical shrinkage.

In the present work, it is shown that one possibility of influencing endogenous drying shrinkage may be provided by the selection of a specific cement. A relationship between alkali concentration and exogenous drying shrinkage has already been pointed out [6]. Early shrinkage of a series of cements is now compared in order to establish a relationship between cement composition and endogenous shrinkage.

2. Experimental

2.1 Cements

Several types of cements, from different European countries, were examined with respect to their early shrinkage behaviour. The mineralogical composition was determined by means of the Rietveld method. The oxide analysis was performed by X-Ray fluorescence. Cement pastes and concretes contain a polycarboxylate type superplasticizer. Its dosage is either held constant or adjusted to have a similar consistency. Times of initial and final setting of cement pastes are measured by means of a Vicat needle. Tables 1 and 2 are summarizing characteristic properties of the investigated cements.

2.2 Pycnometry of cement dispersions

This kind of volumetric measurements are performed with a very simple set-up. An Erlenmeyer flask is instrumented with a scaled burette, a thermocouple and a magnetic stirrer. The thermocouple is fixed on the wall of the flask. The container is almost filled with water, cement is added and, as soon as the remaining empty volume is topped up with some more water, it is plugged. Thereafter the volume variation can be followed by means of the

burette. This set-up is only adapted for cement slurries, i.e. w/c higher than 1.

Table 1 - Mineralogical composition according to Rietveld analysis in % by weight.

Cement	C_3S ±1	C_2S ±1	C_3A ±0,5	C_4AF ±1	C*S* ±0,3	C*S*H_2 ±1
AL	80	8	7,8	traces	0,4	1,2
LT	68	17	2,3	8	1,0	0,8
EC	59	8	1,9	23	0	4,9
SG	67	6	2,1	15	1,3	3,0
TA	54	18	11,4	9	0,4	3,6
UV	57	19	5,2	10	1,3	3,2
WE	59	16	3,7	12	traces	3,5
LE	58	16	traces	21	1,5	1,8
BL	62	12	5,9	14	2,3	2,3

Table 2 - Cement type, Blaine fineness in m^2/kg and oxides in % by weight.

Cement	CEM I type	Blaine	SO_3	Na_2O	K_2O
AL	52,5	500	2,3	0,1	0,1
LT		350	2,3	0,2	0,2
EC	42,5	400	2,6	0,4	0,9
SG		330	3,0	0,1	1,1
TA		340	2,8	0,1	0,6
UV		350	3,1	0,2	1,0
WE		280	3,1	traces	1,1
LE		350	2,8	0,2	0,7
BL		300	3,0	traces	0,5

The volumetric change of cement slurries as a function of time has been reported in a preliminary study [7]. It has been shown that chemical shrinkage should be subdivided into dissolution shrinkage and hydration shrinkage. The main contribution to hydration shrinkage during the first hour can be attributed to ettringite formation:

$$C_3A + 3\ CSH_2 + 26\ H \rightarrow C_3A{\cdot}3CS{\cdot}32H$$

The reasons for it are that the involved ions are known to react instantaneously and the corresponding water consumption is considerable (26 mole water per 1 mole ettringite). A typical shrinkage curve measured by pycnometry is shown in Figure 1.

Several pycnometric measurements with different w/c have been carried out in order to identify specific behaviours. During the preliminary study [7] it has been assumed that a linear relationship prevails between dissolution shrinkage and w/c. Later it turned out that linearity fails to describe the behaviour for small w/c. It is likely that shrinkage is affected

by different equilibrium solubility products of the dissolved ions since new phases form through solution.

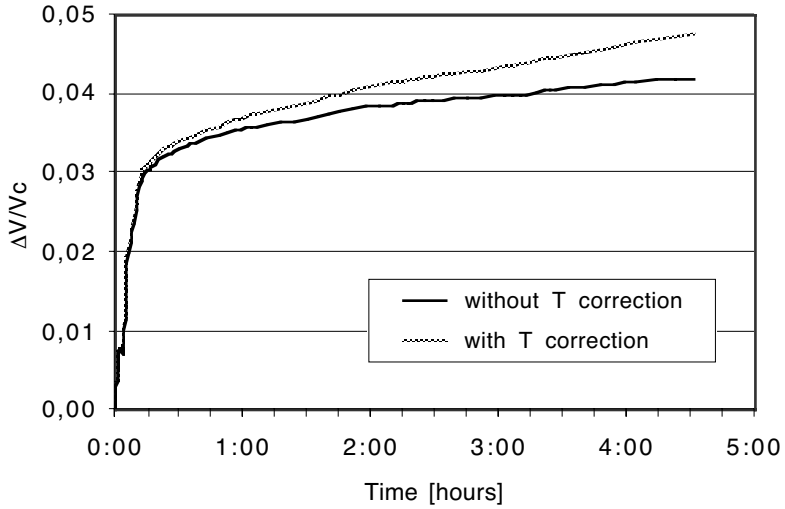

Figure 1 - Chemical shrinkage of cement LT as volume decrease per unit volume of cement; w/c = 1. Measurements started as soon as 30 seconds after mixing cement and water. Readings were corrected for change of temperature T due to heat of hydration.

Ma et al. [8], for instance, determined the saturation concentration of gypsum as a function of alkali concentration. Figure 2 shows that the higher the alkali concentration of the pore solution, the higher the saturation concentration of gypsum.

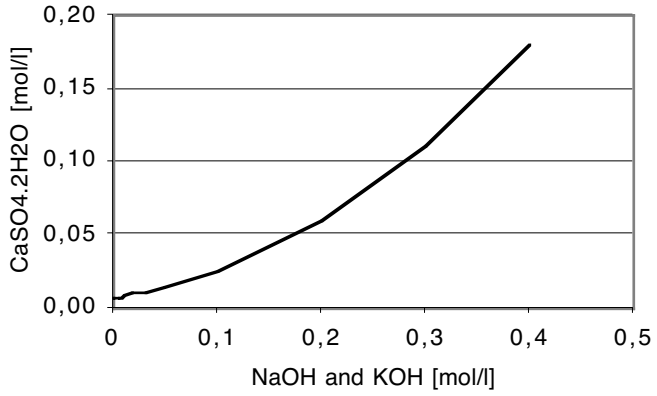

Figure 2 - The solubility of gypsum in presence of alkalies (after [8]).

By analysing the extracted pore solution Longuet [9] showed that low alkali cements (~0.5 total wt.%) give rise to combined alkali concentration of the order of 0.2 M, whereas common cements, with more than 1 wt.% alkalies, develop pore solutions of the order of 0.6 M. As a result of such a significant difference, the rate of ettringite formation, according to the gypsum solubility curve, may be related to the alkali concentration of the pore solution. This effect is pointed out in two different ways in Figure 3: (1) the shrinkage of cement EC, containing 1.3 wt.% alkalies, drops as cement dilution is increased up to w/c = 4 and (2) the low alkali cement LT is less sensitive to the phenomenon described above. On the other hand, for high dilutions, differences in alkali concentrations become negligible and shrinkage increases with increasing w/c.

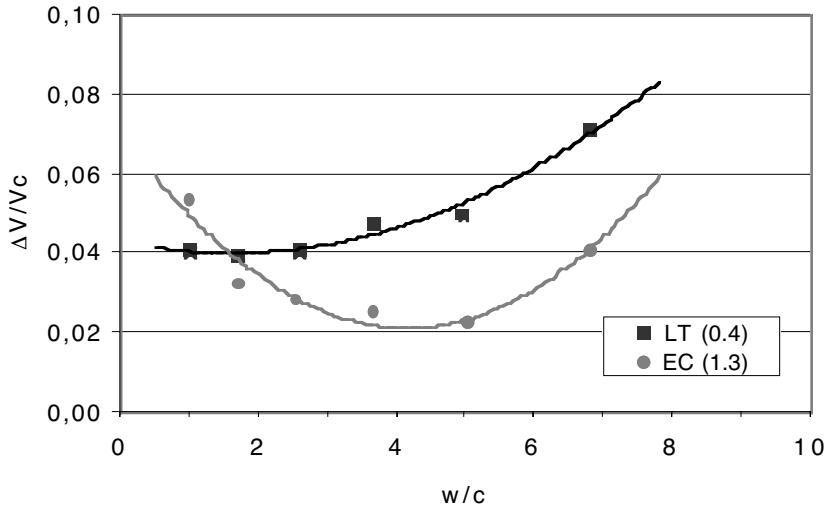

Figure 3 - Volume decrease per unit volume of cement at the age of two hours versus w/c. Cement LT and EC contain 0.4 and 1.3 wt.% alkalies respectively.

2.3 Gravimetry experiments on cement paste

The experimental set-up is based on the principle of Archimedes, i.e. on the buoyancy force which acts on an immersed solid.

The sum of the forces,

$$m_{above} \cdot g - m_{water} \cdot g - m_{immersed} \cdot g = 0$$

since $m = \rho \cdot V$ and assuming $\rho_{water} = 1$, leads to the very simple relationship between the mass variation as indicated by the balance and the volume reduction of the immersed body:

$$\Delta m_{immersed} = -\Delta V_{water} = -\Delta V_{body}$$

The cement pastes were poured into previously water soaked latex bags. A tight knot in the latex membrane was considered to be a waterproof sealing. In fact some water diffused

through the latex membrane into the sample by osmosis. A 0.02% to 0.05% mass increase of the samples was noticed at the end of the immersion period.

A w/c = 0.29 was chosen for this experiment. In order to attain similar consistencies for all the cement pastes, superplasticizer was added and its dosage was adjusted accordingly. With the same superplasticizer dosage setting times according to Vicat were evaluated in parallel. The results are given in Table 3.

The sample preparation and installation was performed within 10 to 15 minutes. Figure 4 shows a typical example for the evolution of shrinkage as a function of time with cement UV. Each cement was measured twice on identical weighing devices and only experiments with a satisfactory reproducibility were considered as valuable. On the basis of these curves the endogenous shrinkage of the cement pastes were determined from final setting according to Vicat up to seven days.

Table 3 - Initial and final setting time for w/c = 0.29 and different dosages of superplasticizer (SP).

Cement	SP [wt.% of C]	Initial setting [h]	Final setting [h]
AL	0,30	3:00	6:10
LT	0,07	4:00	5:15
EC	0,11	6:40	8:30
SG	0,08	4:00	6:00
TA	0,25	3:10	5:30
UV	0,08	3:40	5:30
WE	0,10	4:00	6:00
LE	0,13	5:15	6:15
BL	0,06	3:40	5:30

2.4 Determination of the endogenous length change of concrete

Linear deformations were measured on 300x300x300 mm^3 concrete cubes. The experimental set-up is an instrumented box with 3 pairs of horizontal displacement gauges and one vertical. Temperature was recorded in the centre and at the surface of the cube. The set-up is depicted in [7].

In order to choose the time at which a three dimensional network of hydration products and a porous microstructure appear, the deformations along the different measurement axes were analysed. It was assumed that the beginning of endogenous shrinkage can be fixed at the time when the three horizontal deformation rates become identical. Derivation of the deformation curves versus time yields this peculiar age with an accuracy of ± 30 minutes. An alternative might be to select the time when horizontal and vertical deformation rates become equal. The basic idea is to find a characteristic time which indicates the beginning of isotropic behaviour of the young concrete. Starting from this age the dead weight does no longer contribute to the observed volume change.

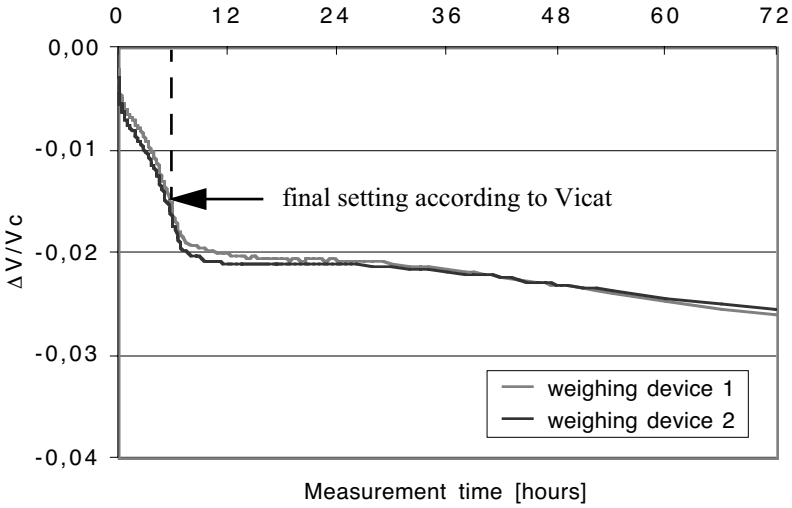

Figure 4 - Endogenous volume decrease of UV cement paste as measured by gravimetry; w/c = 0.29.

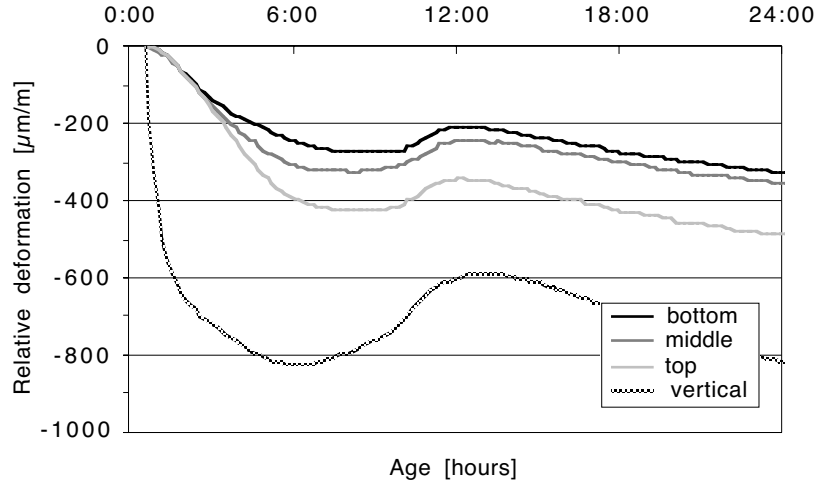

Figure 5 - Linear relative deformation of UV concrete with w/c = 0.32. The edge of the cubic sample is 300 mm. The horizontal measurements at 3 different heights are referred to as bottom, middle and top. The displacement of the upper surface is referred to as vertical.

The mean linear deformation ε of the concrete cube was defined as $\varepsilon = (2 \cdot \varepsilon_h + \varepsilon_v)/3$, where $\varepsilon_h = (\varepsilon_b + \varepsilon_m + \varepsilon_t)/3$. The subscripts h, v, b, m and t refer to horizontal, vertical, bottom, middle and top respectively. For each cement, endogenous shrinkage was determined from the time of first appearance of the isotropic deformation behaviour up to 20 days.

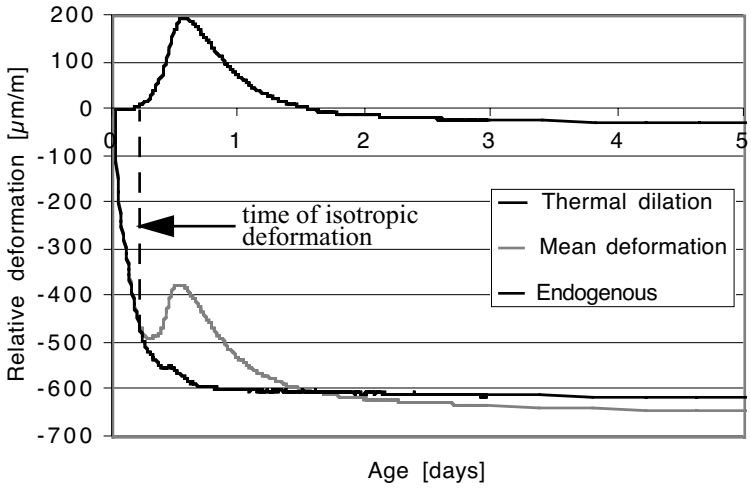

Figure 6 - Shrinkage and thermal dilation of UV concrete; w/c = 0.32.

2.5 Damage due to self-desiccation

According to the numerical simulation work carried out by Sadouki [4], damage due to self-desiccation is expected to appear at the interfaces between the stiff coarse aggregates and the fine cement mortar, hereafter referred to as the matrix. In order to check the validity of this macroscopic concrete model a water absorption test on a similar material was undertaken. Mortars with water-to-cement ratios equal to 0.28 and 0.35 were mixed with cement TA, 0/1 sand and superplasticizer. Concretes were then made out of the mortars by adding 50 vol.% of 8/16 gravels. Four 100x100x100 samples for each of the four batches were cast in wooden moulds which in turn were immediately sealed with plastic foils during the first 24 hours. The cubes were then demoulded, quickly wrapped into aluminium foils and stored at 20 °C for the following 3 weeks. Before water absorption measurements were carried out, 4 vertical surfaces were coated with a resin and the cubes were sawn in two halves.

3. Results

3.1 Pycnometry

Figure 7 shows the two hour chemical shrinkage of each cement brand for two distinct

dilutions. Data for w/c = 1 are given as measured. Data for w/c ≈ 0.3, on the other hand, were extrapolated from the $\Delta V/V_c$= f(w/c) functions shown in Figure 3 and have, therefore, the disadvantage of being partly subjective. The abscissa value C3A·alkali denotes the capacity of each cement to form ettringite.

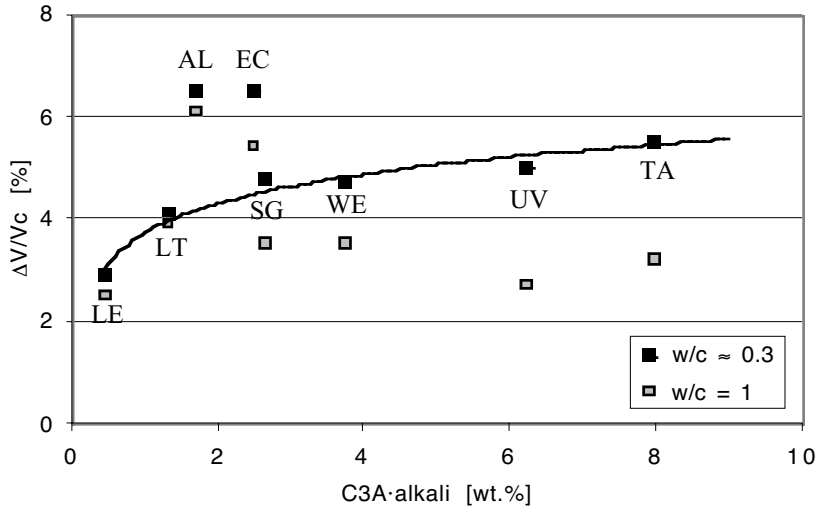

Figure 7 - Volume decrease per unit volume of cement at the age of two hours versus the concentration product of aluminate and combined alkali oxides. The values for w/c ≈ 0.3 were extrapolated from the data shown in Figure 3.

The C_3A content stands for the available aluminate surface. In order to allow for the solubility variation of gypsum as a function of the alkali concentration, C_3A content is weighed by the total alkali content, even if only soluble alkalies should actually be considered. It is to be noted that fineness was not considered and cements EC and AL exhibit, therefore, a somehow different behaviour.

3.2 Gravimetry

Figure 8 shows clearly the relationship between the aluminate and ferroaluminate contents and the volumetric endogenous shrinkage as measured by gravimetry.

The results from pycnometry were compared with those from gravimetry. For both measuring devices data between 15 minutes and 2 hours were retained only. They agree fairly well, although a tendency of higher chemical shrinkage measured by pycnometry can be observed.

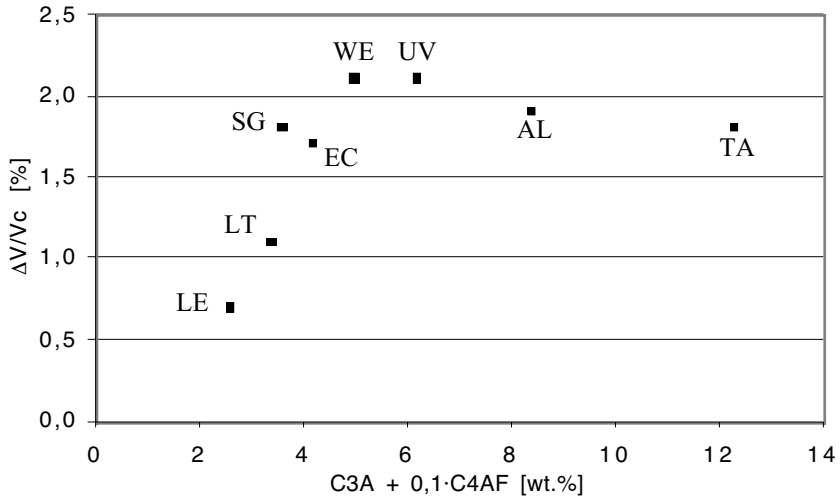

Figure 8 - The volumetric endogenous shrinkage of cement pastes from time of final setting up to 7 days; w/c = 0.29. The measurements began 15 minutes after the mixing.

3.3 Endogenous shrinkage of concrete

Figure 9 shows the endogenous length change of concrete as a function of the sum of C_3A and one tenth of C_4AF. The w/c was held constant at 0.32 for all the batches. The data were taken from the beginning of isotropic length change up to 20 days.

3.4 Water absorption test

The water absorption ability for mortar and concrete at different w/c after 3 weeks aging under sealed conditions is shown in Figure 10. The sample weighing was carried on for 30 days. The results are in accordance with the expected permeability increase from w/c = 0.28 to w/c = 0.35. The experiment was carried out in a 75% RH climate. The samples were then allowed to dry through the upper surface. This parallel water loss was found to be negligible.

During a first stage, when capillary suction is the driving force for water absorption, it can be described by means of a linear relationship between the mass increase per unit surface of matrix Δw and the square root of time,

$$\Delta w = A\sqrt{t}$$

where the slope A is proportional to an effective capillary radius r_{eff}. The characteristic r_{eff} of a microstructure increases in case of cracking or loosening.

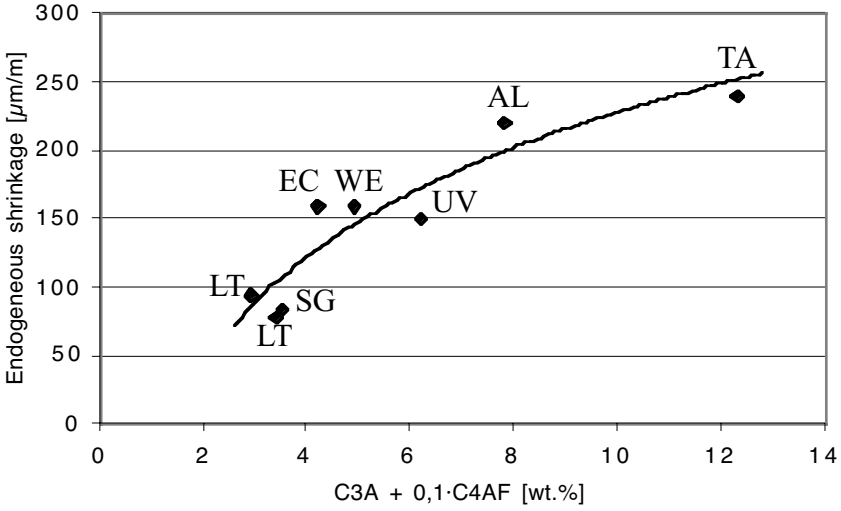

Figure 9 - Endogenous shrinkage of concrete versus the sum of aluminate and one tenth of ferroaluminate content; w/c = 0.32.

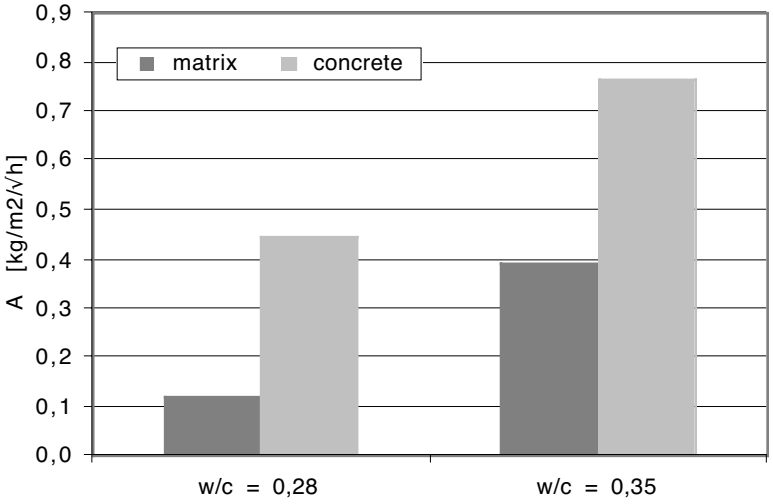

Figure 10 - Water absorption coefficient A versus w/c after 3 weeks of sealed aging. Matrix samples were made of fine mortar. Concrete samples were made of 50 vol.% mortar and 50 vol.% gravel.

4. Discussion

Endogenous shrinkage measurements were carried out on different cementitious materials, each of it being studied by means of a proper experimental device. All the cement compounds involved in the ettringite formation have a great influence on the early self-desiccation process as well as on the following endogenous shrinkage.

The self-desiccation begins with chemical shrinkage, as soon as water and cement are mixed and form a suspension. Rapidly water becomes saturated with respect to gypsum. Its saturation concentration is variable and depends on how much soluble alkalies are already dissolved (Figure 2). Supposing aluminate and ferroaluminate surfaces are not limited, the rate of ettringite formation would only be determined by the actual SO_4^{2-} concentration, whereas the maximum ettringite content would be determined by the initial amount of sulphate phases (gypsum, bassanite, anhydrite). In reality, available aluminate and ferroaluminate surfaces are not unlimited. Furthermore, aluminate is supposed to dissolve more rapidly than ferroaluminate and should, therefore, play the major role at the very early ages. Thus, the chemical shrinkage, after 2 hours of hydration, depends widely on the alkali and aluminate concentrations of the cement as it is shown in Figure 7 for w/c = 0.3. The product C3A·alkali was introduced in order to allow for these two elements. The higher C3A·alkali, the higher the early chemical shrinkage that can be expected. In addition, the available aluminate surface is not only related to the content but also to the fineness. The Blaine fineness of the cements EC and AL are 400 and 500 m^2/kg respectively and actually these cements shrink more than it is expected from their C3A·alkali value. For the higher dilution at w/c = 1, aluminate and alkali contents no longer influence the shrinkage. Cement composition seams to become indifferent, while the dissolution component of chemical shrinkage gains in importance.

For higher degrees of hydration (7 and 20 days), alkali concentration has little influence on the relation between endogenous shrinkage and cement composition. The C_3A and C_4AF contents alone are enough to predict whether endogenous shrinkage will be rather high or low (Figures 8 and 9). In fact, only a tenth fraction of C_4AF was considered in order to allow for its lower reactivity. According to Figure 8, up to C3A + 0.1·C4AF = 6, endogenous shrinkage is increasing. For higher values shrinkage shows a slight decrease. This observable maximum for cement pastes is not seen if concrete is considered (Figure 9). The phenomenon could be explained through late ettringite formation, at a time when hardened material puts up with one-directional crystal growth by swelling.

According to the water absorption results as depicted in Figure 10, self-desiccation does damage concretes. At w/c of 0.35 and 0.28, it is likely to have endogenous strains. The matrix shrinks and, in the vicinity of aggregates, undergoes tensile stresses. The microstructural damage caused by these stresses should in turn increase the permeability. That is what is displayed in Figure 10. For w/c = 0.35, concrete absorbs almost twice as much water than does the homogenous matrix material. The same fact is emphasized for w/c = 0.28, for which three time as much water is taken up by the concrete. These results illustrate that, while the absolute permeability decreases by lowering w/c, the damage increases. Thus,

the expected benefits of low w/c ought to be kept in perspective.

5. Conclusions

- Endogenous shrinkage damages the microstructure of concrete. It can be observed as increased water permeability.
- Endogenous shrinkage of a cement can be related to its potential to form ettringite.
- A limiting parameter seems to be the available aluminate and ferroaluminate surface, rather than the amount of sulphate phases.
- It is possible to minimize endogenous shrinkage by selecting a cement with low aluminate and low ferroaluminate content.

References

[1] J-P. Ollivier, A non destructive procedure to observe the microcracks of concrete by SEM, Cement and Concrete Research, Vol.15, 1055-1060 (1985).

[2] M-P. Yssorche-Cubaynes, J-P. Ollivier, La microfissuration d'autodessiccation et la durabilité des BHP et BTHP, Materials and Structures, Vol.32, 14-21 (1999).

[3] J. Bisshop, J.G.M. van Mier, How to study drying shrinkage microcracking in cement-based materials using optical and scanning electron microscopy?, Cement and Concrete Research, Vol.32, 279-287 (2002).

[4] H. Sadouki, F.H. Wittmann, Shrinkage and internal damage induced by drying and endogenous drying, Rilem Proceedings 17 on Shrinkage of Concrete, Paris, (2000).

[5] R. Sato, M. Xu, Y. Yang, Stresses due to autogenous shrinkage in high strength concrete and its prediction, Proceedings of JCI Workshop on Autogenous Shrinkage of Concrete, Hiroshima, Japan, 351-362 (1999).

[6] F. Beltzung, F.H. Wittmann, L. Holzer, Influence of composition of pore solution on drying shrinkage, Proceedings of Concreep-6, Cambridge (MA), USA, (2001).

[7] F. Beltzung, F.H. Wittmann, Early chemical shrinkage due to dissolution and hydration of cement, Materials and Structures, Vol.34, 279-283 (2001).

[8] W. Ma, P. Brown, D. Shi, Solubility of Ca(OH)2 and CaSO4·2H2O in the liquid phase from hardened cement paste, Cement and Concrete Research, Vol.22, 531-540 (1992).

[9] P. Longuet, L. Burglen, A. Zelwer, La phase liquide du ciment hydraté, Revue des matériaux; ciments et bétons, Vol. 1/1973, N° 676, page 35 (1973).

AUTOGENOUS DEFORMATION AND RH CHANGE IN PORTLAND AND BLAST FURNACE SLAG CEMENT PASTES

Pietro Lura
Delft University of Technology, THE NETHERLANDS
Ole Mejlhede Jensen
Aalborg University, DENMARK
Klaas van Breugel
Delft University of Technology, THE NETHERLANDS

Abstract

In this paper, the autogenous deformations and relative humidity (RH) change of cement pastes are investigated. Two cement pastes with water/cement ratio 0.37 and 5% silica fume addition were tested. The two cement pastes differed in the kind of cement: Portland cement or Blast-Furnace Slag (BFS) cement. The autogenous deformations, the autogenous RH change, and the rate of heat evolution in the first week after casting were measured at 20°C. For both pastes, the internal RH change followed closely the kinetics of hydration. The BFS cement paste showed increased autogenous RH change and self-desiccation shrinkage when compared to the Portland cement paste. This is principally due to higher chemical shrinkage and finer pore structure of the BFS paste. An additional reason might be that the reaction of slag with calcium hydroxide is less sensitive to a RH drop than hydration of Portland cement.

1. Introduction

In High Performance Concrete, a low water/binder ratio and addition of silica fume cause a significant RH drop in the cement paste during sealed hydration [1]. Closely related to this autogenous RH change, the cement paste undergoes autogenous shrinkage. In concrete autogenous shrinkage results in tensile stresses in the cement paste due to restraint from the aggregates [2]. Furthermore, it leads to bulk deformation of the concrete itself. Autogenous shrinkage should be limited since it may induce micro- or macro-cracking and impair the concrete quality [3].
Most of the reported experimental research on autogenous shrinkage has been performed on Portland cement mixtures. On the other hand, in some European countries as The Netherlands BFS cements have widely and successfully been applied [4]. These cements are considered to be more environmental-friendly than Portland cement, due to the reuse of an industrial waste material. A further advantage of BFS cement is a fine pore

structure, which improves water tightness in marine structures and reduces the chloride penetration. Finally, it develops a lower heat evolution during hydration than Portland cement concrete, reducing temperature gradients in massive concrete structures at early-age. On the other hand, a high chemical shrinkage has been reported for BFS cements [5]. Since autogenous RH change and autogenous shrinkage depend on the chemical shrinkage of the cement and on the pore size distribution of the cement paste, it may be expected that BFS cement mixtures will show an increased autogenous shrinkage and RH drop when compared to Portland cement mixtures.

2. Experimental Procedure

2.1 Materials

In the present study a Portland cement (CEM I 52.5 R) and a BFS cement (CEM III/B 42.5 LH HS) were used. The Portland cement had Blaine fineness 530 m^2/kg and calculated Bogue composition of C_3S 53.6%, C_2S 20.1%, C_3A 8.2%, and C_4AF 9.1%. The BFS cement contained 76% slag and had Blaine fineness 390 m^2/kg.
Two cement pastes were studied, one with Portland cement and one with BFS cement. In both cases, the w/c ratio of the pastes was 0.37. Silica fume with a BET surface area of 19 m^2/g was added in slurry form, 5.2% by cement weight. A lignosulphonate-based plasticizer (0.2%) and a naphthalene-sulphonate-based superplasticizer (1.7%) were also added to the mix.
One-point-five l of cement paste was mixed in a 5 l epicyclic Hobart mixer. Demineralized water was previously mixed with the admixtures and added in two steps to ensure homogeneity. Total mixing time from first water addition was 5 minutes.
To avoid bleeding, the BFS cement paste was slowly rotated (4 rev./min) with a Rotator drive STR4 by Stuart Scientific. Rotation was stopped a few hours after casting, when no further bleeding was observed.

2.2 Internal RH measurements

The fresh cement paste (about 10 grams) was cast into the measuring chamber of two Rotronic hygroscopic DT stations equipped with WA-14TH and WA-40TH measuring cells. The RH stations were placed in a thermostatically controlled room at 20±0.1°C. The development of the RH in the samples and the temperature were measured every 15 minutes for a period of about one week after water addition. Before and after the measurements, calibration of the stations was carried out with four saturated salt solutions in the range of 75-100% RH. This procedure results into a measuring accuracy of about ±1% RH.

2.3 Autogenous deformation measurements

The cement paste was cast under vibration into tight plastic moulds, which were corrugated to minimize restraint on the paste. The length of the samples was approximately 300 mm and the diameter 25 mm. The specimens were placed in a dilatometer, immersed into a temperature controlled glycol bath at 20±0.1°C. Two

samples were tested simultaneously in the dilatometer, with a measuring accuracy of ±5 μstrain. Linear measurements every 15 minutes were started directly after casting. A detailed description of the dilatometer can be found in [6].

2.4 Measurement of isothermal heat development

The rate of heat evolution of the two cement pastes was measured with isothermal calorimetry at 20°C (3114/3236 TAM Air Isothermal Calorimeter by Thermometric AB). The specimens of cement paste weighted 10 grams. The test was performed in twofold.

3. Results and Discussion

3.1 Internal RH and reaction kinetics

RH changes of the cement pastes were measured in twofold for a period of at least 6 days. After casting and before starting the RH measurements, the BFS paste was rotated in order to avoid bleeding. Rotation started about 50 min after water addition and lasted for 4 hours. The development of internal RH with hydration time (obtained after calibration) is provided in Figure 1. After an initial equilibrium of the sensors was achieved, the RH decreased with hydration time.

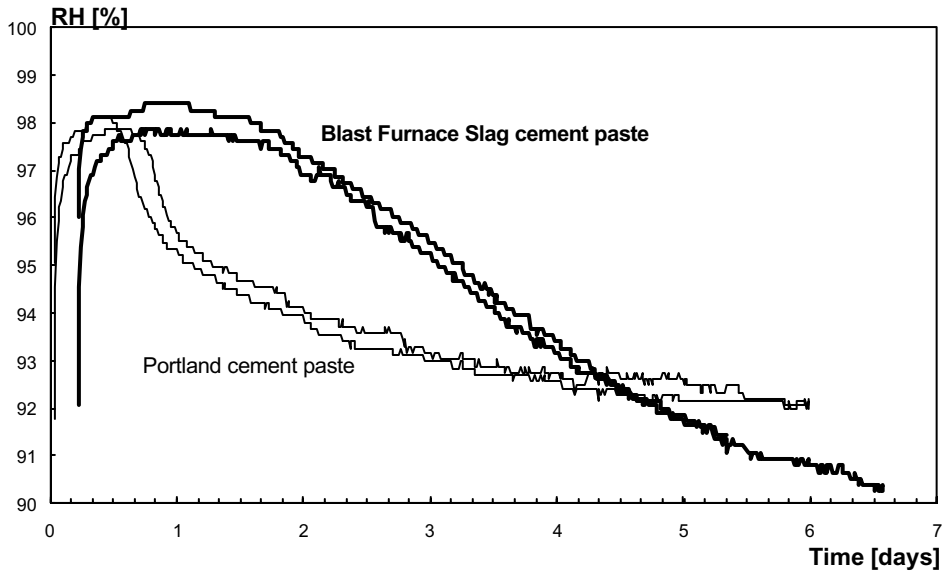

Figure 1 - Internal relative humidity vs. time for the two cement pastes.

Besides the initial transition to equilibrium (Fig.1), a lack of thermal equilibrium between the sensor and the sample may occur during the test, due to insufficient

thermostatic control or to development of heat of hydration in the paste. This may lead to a significant measuring error: for example, it has been calculated that near saturation at 20ºC a temperature difference of 1ºC may lead to an error of about 6% RH [7]. Other researchers have measured a dependence of the RH on the curing temperature [8]. The BFS cement paste develops less and slower heat of hydration than the Portland cement paste; therefore the temperature, also due to the small dimensions of the sample, is closer to isothermal and the measured RH should be more reliable. In fact, the temperature measured inside the Rotronic stations was always less than 21ºC in the case of the Portland cement paste, while for the BFS cement paste the temperature remained practically constant.

As a consequence of hydration, a solid skeleton forms in the cement paste. Right from the formation of the solid skeleton, the chemical shrinkage results in creation of internal pores. If the water supply is restricted, the pores empty and air-water menisci form. The RH due to menisci formation in a circular cylindrical pore can be calculated according to Kelvin's equation, which assuming perfect wetting reads:

$$RH_K = \exp\left(\frac{-2\gamma V_m}{rRT}\right) \quad (1)$$

where ã [N/m] is the surface tension of the pore solution, V_m [m^3/mol] its molar volume, r [m] the radius of the largest water-filled pore, R [8.314 J/mol· K] the universal gas constant, and T [K] the temperature.

However, according to Fig.1, in both cement pastes the internal RH was about 98% before setting, when the pastes were still fluid and the pore system saturated. Dissolved salts in the pore fluid can account for this initial RH drop [9]. The RH due to dissolved salts in the pore fluid can be estimated with Raoult's law [9]:

$$RH_S = X_l \quad (2)$$

where X_l is the molar fraction of water in the pore fluid.

While the dissolved salts are the principal cause of the RH change before setting, their effect on the RH development in the following of the hydration is superimposed to the effect of self-desiccation (eq.1). A possible strategy to estimate the value of RH_S is to determine the pore fluid composition at different hydration times, and to calculate the resulting RH value using eq.2.

Separation of the contribution of the effect of dissolved salts and the effect of the menisci formation in the measured RH is essential if one wants to proceed to numerical modeling of the self-desiccation phenomenon in general and of self-desiccation shrinkage in particular. This issue has been discussed in another paper [10].

Figure 1 shows that the initial RH level is similar in the two pastes, about 98%. Therefore, one might suppose that the initial RH drop due to dissolved salts is roughly the same in the two pastes. In fact, initial RH values around 97-98% were measured on a number of Portland cement pastes [1,11].

Only after setting, formation of pores and of air-water menisci in the cement pastes takes place. Therefore, a drop in the internal RH might be used to estimate the setting time.

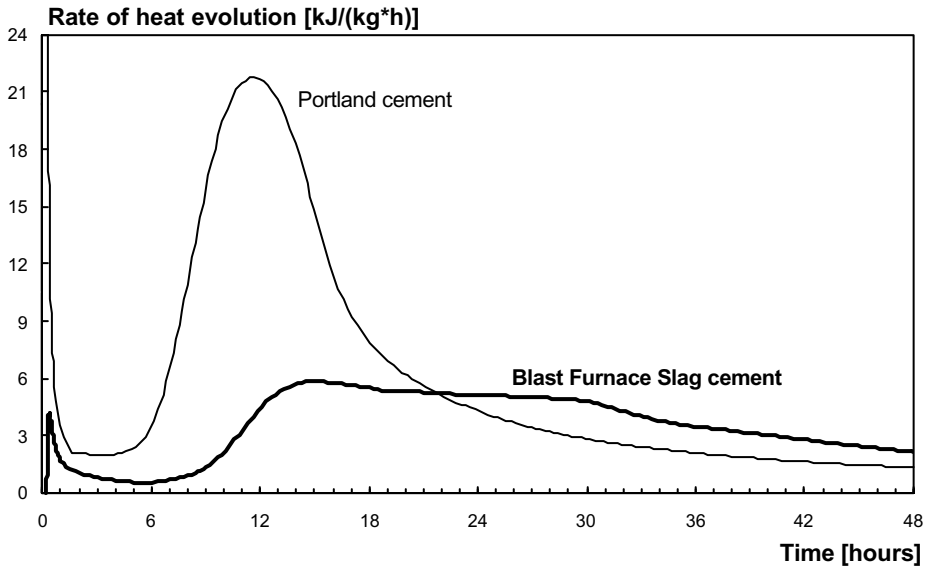

Figure 2 - Rate of heat evolution of the cement pastes in the first 48 hours after water addition, measured with isothermal calorimetry at 20°C.

The development of the internal RH in time follows the hydration kinetics. In Figure 2 the rate of heat liberation at 20°C of the two cement pastes in the first two days of hydration is shown. The cement pastes were placed into the calorimeter after mixing; therefore, only a part of the first reaction peak, happening immediately after water addition, was recorded. Hydration of the Portland cement paste took place in the first hours at a very fast rate, also due to its very high fineness, 530 m^2/kg. A reaction peak occurred at 12 hours and it coincided with the start of self-desiccation (Fig. 1); then the reaction proceeded at a slower rate. In the case of the BFS cement paste, hydration of the Portland cement fraction, 24% by weight, was postponed; this was possibly due to a higher w/c ratio, if only the clinker is considered. The peak was correspondingly lower than in the Portland cement paste, about 1/4. Just after the first peak, the pozzolanic reaction of the slag with calcium hydroxide, formed by the Portland cement hydration, started [12]. This reaction peaked at about 30 hours after water addition. Also in this case, a decrease in the rate of the reaction coincided with the beginning of the RH drop. A possible explanation of this fact is that in both pastes hydration decelerated because of a water shortage. The consequences of this water shortage are evident in the RH measurements. Furthermore, it is noticed that in the Portland cement paste the RH dropped rapidly in the first hours (3% RH drop at 1 day hydration) and then the RH change decelerated. The same tendency was found in the rate of heat evolution. On the other hand, in the BFS cement paste both the RH change and the rate of heat evolution evolved more gradually.

The internal RH in the Portland cement paste remained almost constant after four days of hydration, at a value around 92% RH. The BFS cement paste, on the other hand, reached an internal RH of 90% at 6.5 days of hydration, and the RH was still decreasing by that time (Fig. 1). Also in [13] BFS cement pastes reached lower internal RH than Portland cement pastes.
A number of different causes might contribute to the higher RH drop in BFS cement pastes:
1) A higher chemical shrinkage of the BFS cement if compared to Portland cement might lead to greater self-desiccation. In fact, a chemical shrinkage of 0.26 ml/g slag reacted vs. about 0.06 ml/g cement reacted was measured [5]. The chemical shrinkage of slag is quite similar to the one of silica fume, 0.22 ml/g silica fume reacted [9].
2) BFS cement pastes have a finer pore structure than Portland cement pastes. Researchers measured lower permeability [12] and also MIP tests confirmed this fact [13]. This finer pore structure should be the product of the dissolution of the calcium hydroxide crystals and the precipitation of CSH produced by the pozzolanic reaction. Finer pores result in a lower RH according to eq.1.
3) The reaction of BFS might also be less affected by a RH-drop than Portland cement hydration. Some evidence was found for the case of the pozzolanic reaction of silica fume. NMR measurements [9] on a cement paste with w/c 0.25 and 10% silica fume addition showed that the degree of reaction of silica fume increased after the hydration of C_3S and C_2S had stopped, at RH lower than 80%. If the BFS had the same behavior, the ongoing pozzolanic reaction would result in a progressive RH decrease.
4) Finally, a different composition of the pore water in Portland cement paste and in BFS cement paste could influence the RH depression due to dissolved salts. This may explain, however, only a minor part of the differences in the RH levels.

3.2 Autogenous deformation

The measured autogenous deformations for the two mixtures are provided in Figure 3. Deformations were recorded for about 6 days in the case of the Portland cement paste and 9.5 days in the case of the BFS cement paste. The deformations have been zeroed at the moment of setting, which occurred at 7 hours from mixing for the Portland cement paste and at15 hours for the BFS cement paste. The initial deformation of the two pastes in Figure 3, until the moment of setting, was due to chemical shrinkage. After setting, a self-supporting skeleton formed and chemical shrinkage resulted mostly in internal voids. Setting was identified by a change in the slope of the deformations, in the case of the Portland cement paste, or by the occurrence of expansion, in the case of the BFS cement paste. Vicat measurements performed previously on the same cement pastes gave a setting time of 6 hours for the Portland cement paste and 11 hours for the BFS cement paste. The large difference in setting of the BFS cement paste was presumably due to a change of both fineness and slag content between two different batches of BFS cement (CEM III/B 42.5 LH HS). In fact, the previous batch had a slag content of 70% (vs. 76%) and a Blaine fineness of 490 m^2/kg (390 m^2/kg).
Expansion in the BFS cement paste was very different in the two samples, while both the initial deformations due to chemical shrinkage and the shrinkage after 36 hours of

hydration were the same (Fig. 3). Since the pastes were rotated for 4 hours after casting, the expansion did not come from reabsorption of bleeding water and must be considered as an autogenous phenomenon, perhaps caused by formation of ettringite. According to [12] ettringite is in fact also formed in BFS cement pastes. Since this reaction occurs with a chemical shrinkage [9], expansion can only take place if the reaction products form inside a solid skeleton.
The very large scatter in the expansion of the BFS cement pastes could have different explanations:
1) It can be supposed that the forces producing expansion (i.e. crystallization pressure of ettringite or other hydrates), acting in a still very weak paste, are influenced by very small differences in the samples, for example due to differences in the temperature regime or inhomogeneities within the sample.
2) Alternatively, the expansion could be a localized phenomenon in the paste and lead to an irregular and unpredictable overall response. In fact it has been often reported in literature that the expansion caused by expansive cements, used for example to compensate autogenous shrinkage, is difficult to control. These expansive reactions are often based on ettringite formation.
3) Since the paste was bleeding right from mixing, the single samples might have had a slightly different w/c ratio, depending on the way of pouring them into the moulds. However, inhomogeneities between the samples do not explain why they experienced the same shrinkage after the expansion phase ended.

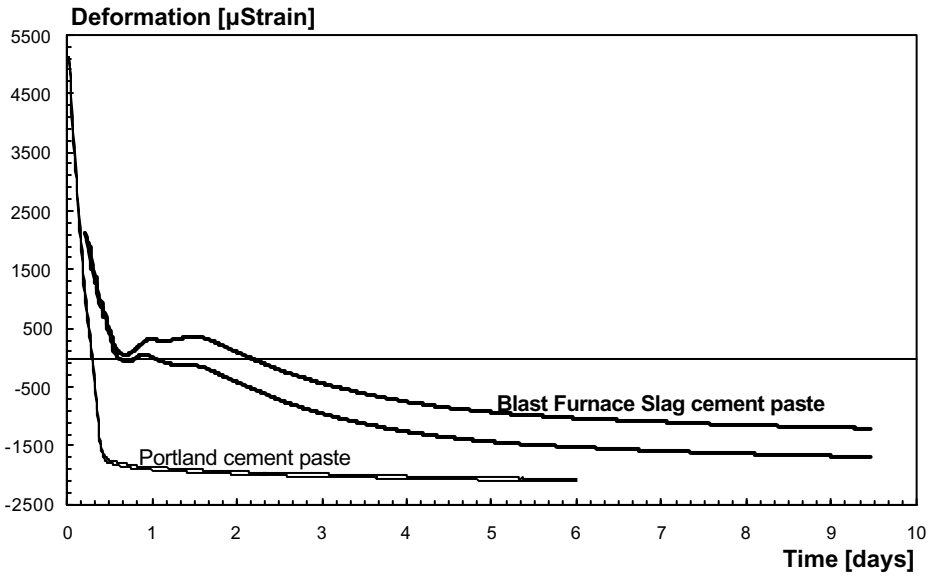

Figure 3 - Autogenous deformation vs. time for the two cement pastes.

In Figure 4 the autogenous deformation of the Portland cement paste is plotted vs. the RH change starting from about 11 hours after mixing with water. The RH drop is a measure of the tension state in the pore water, due to increasing capillary depression and changes in the disjoining pressure [10]. In the first 24 hours the steepness of the curve decreased, corresponding to an increase of the elastic modulus of the cement paste [10]. Afterwards, the RH drop decelerated (Fig. 1) and the deformation per % RH increased. This fact could be due to the onset of the pozzolanic reaction of silica fume that consumed the calcium hydroxide crystals. Internal restraints in the paste were removed and a further shrinkage took place [1]. Creep of the cement paste could be an additional reason. In fact, the effect of creep becomes evident because in the second part of the curve the deformations were occurring during a longer time (as seen from the marks in Fig. 4). Creep in the first hours occurred probably at a higher rate and was measured as a quasi-instantaneous deformation. This behavior can be modeled with a reduction of the elastic modulus of the paste [9] that takes the effect of creep indirectly into account. It is noticed that the measured increased slope of the shrinkage-RH curve after one-day hydration cannot be related to temperature changes due to heat of hydration, which occurred only in the first hours after mixing with water. After the reaction peak (see Fig.2), the temperature of the sample remained almost constant.

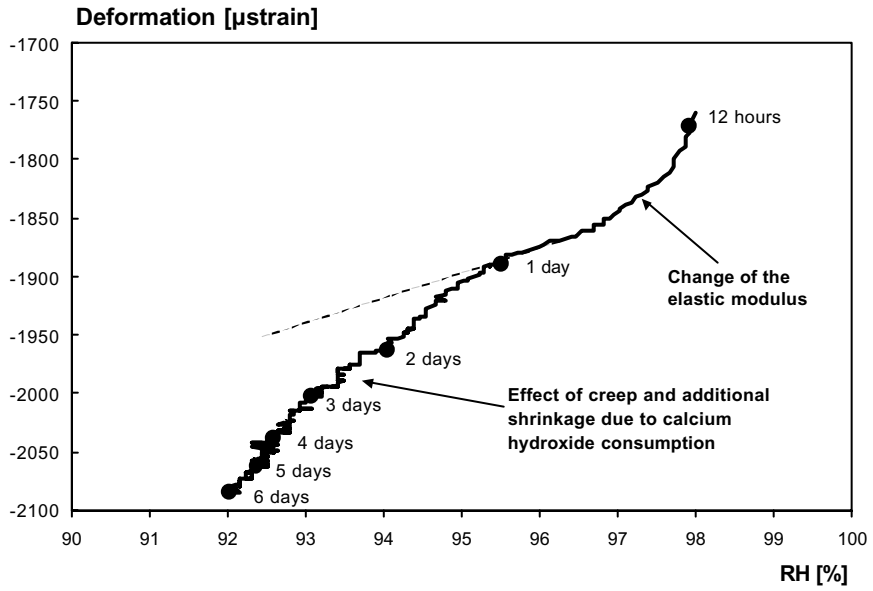

Figure 4 - Autogenous deformation of the Portland cement paste plotted as a function of autogenous RH.

In Figure 5 the autogenous deformation of the BFS cement paste is plotted vs. the RH starting from 36 hours after mixing with water, coinciding with the end of the expansion period. The deformations were zeroed at 36 hours. As for the Portland cement paste (Fig. 4), the decreasing slope of the shrinkage-RH curve in the first hours was probably due to the increase of the elastic modulus of the cement paste. It is noticed that in the case of drying shrinkage measurements on hardened Portland cement pastes, where the elastic modulus is constant during the test, the measured slope of the shrinkage-RH curve was almost constant in the RH range 90-40% [14]. However, some dependence of the elastic modulus on the RH cannot be excluded.
From the third day after casting, the speed of the RH-drop in the BFS cement paste decreased and the deformation showed an almost constant slope, about 105 µstrain/%RH. For a comparison, Jensen [9] found a value of 80 µstrain/%RH for a Portland cement paste with w/c=0.4 and 10% silica fume addition. In the case of the BFS cement paste no increase in the slope of the deformation at a later time was found, as was the case for the Portland cement paste (Fig. 4). One possible reason is that the RH was still decreasing after one week, when the measurements were stopped. This continuous increase of the shrinkage-inducing internal stress possibly masked the effect of creep. Another possible explanation is that creep in BFS cement paste could be less pronounced than in Portland cement pastes, as was already measured [15]. This lower creep of BFS cement pastes could be possibly related to their finer pore structure [12,13]

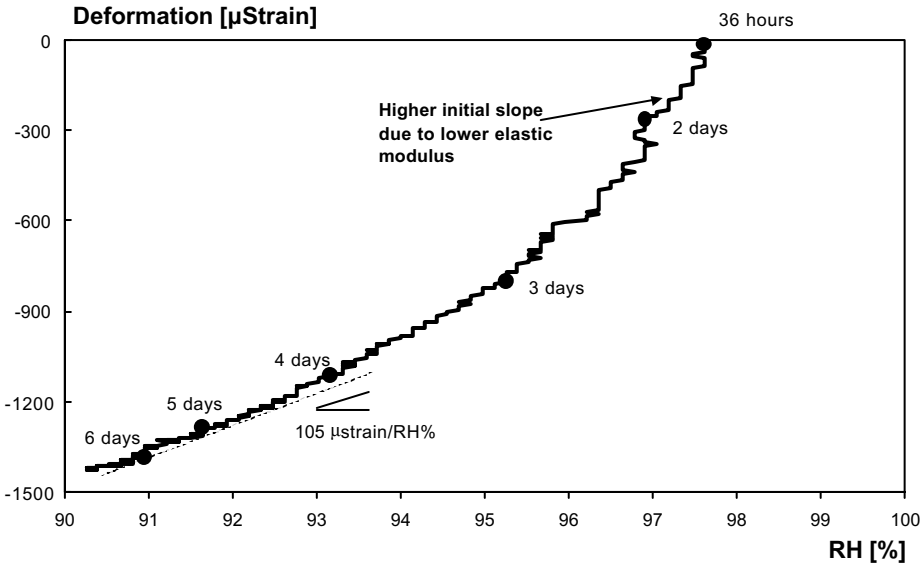

Figure 5 - Autogenous deformation of the Blast Furnace Slag cement paste plotted as a function of autogenous RH.

4. Conclusions

From the analysis of the experimental results regarding cement pastes with Portland or BFS cement and 5% silica fume addition, the following conclusions can be drawn:
1) Self-desiccation occurred earlier for the Portland cement paste than for BFS cement paste, due to a faster hydration. In time, the internal RH of the BFS paste decreased at a higher rate and eventually became lower than in the Portland cement paste.
2) Most of the autogenous deformation of the Portland cement paste occurred before and around setting and did not correspond to a RH drop, but was due to chemical shrinkage. On the other hand, the BFS cement paste expanded after setting. A substantial shrinkage followed, accompanied by a drop of the RH.
3) Plots of RH vs. shrinkage for the Portland cement mix showed a decreasing slope in the first days, corresponding to a stiffness gain of the paste. A further increase in the deformation rate followed. In the case of the BFS cement paste, only the decreasing slope in the first days was observed. Globally, the BFS cement paste showed higher shrinkage per unit RH decrease and greater self-desiccation shrinkage than Portland cement pastes.

3. References

[1] Jensen, O.M. and Hansen, P.F., 'Autogenous Deformation and Change of the Relative Humidity in Silica Fume-Modified Cement Paste', ACI Mater. J. **93**(6) (1996) 539-543.

[2] Dela, B.F., 'Eigenstresses in hardening concrete', Ph.D. Thesis, Department of Structural Engineering and Materials, Report No 64,The Technical University of Denmark, Lyngby, Denmark, 2000, pp. 147.

[3] Paillere, A.M., Buil, M., and Serrano, J.J., 'Effect of Fiber Addition on the Autogenous Shrinkage of Silica Fume Concrete', ACI Mater. J. **86**(2) (1989) 139-144.

[4] Bijen, J., Blast furnace slag cement for durable marine structures, CIP Royal Library Den Haag, 1996.

[5] Bentz, D.P, unpublished results, 2002.

[6] Jensen, O.M., and Hansen, P.F., 'A Dilatometer for Measuring Autogenous Deformation in Hardening Portland Cement Paste,' Mater. Struct. **28** (1995) 406-409.

[7] Jensen, O. M., and Hansen, P. F., Influence of temperature on autogenous deformation and relative humidity change in hardening cement paste, Cem. Concr. Res. **29**(4) (1999) 567-575.

[8] Nilsson, L.O., Temperature Effects in Relative Humidity Measurements on Concrete – Some Preliminary Studies. The Moisture Group. Report 1987:1. BFR. 1987, 84.

[9] Jensen, O.M., 'Autogenous deformation and RH-change – self-desiccation and self-desiccation shrinkage' (in Danish), Ph.D. thesis, Building Materials

Laboratory, The Technical University of Denmark, Lyngby, Denmark, 1993, TR 284/93.

[10] Lura, P., Jensen, O.M., and Breugel, K. van, 'Autogenous shrinkage in high-performance cement paste: An evaluation of basic mechanisms', submitted to Cem. Concr. Res., 2002.

[11] Bentz, D.P., Jensen, O.M., Hansen, K.K., Olesen, J.F., Stang, H., and Haecker, C.J., 'Influence of Cement Particle Size Distribution on Early Age Autogenous Strains and Stresses in Cement-Based Materials,' J. Amer. Ceram. Soc. **84**(1) (2001) 129-135.

[12] Roy, D.M., and Idorn, G.M., 'Hydration, Structure and properties of Blast Furnace Slag Cements, Mortars, and Concrete', ACI Journal **79**(6) (1982), 444-457.

[13] Hanehara, S., Hirao, H., and Uchikawa, H., 'Relationship between autogenous shrinkage and the microstructure and humidity changes at inner part of hardened cement pastes at early ages', Proc. Autoshrink'98, Int. Workshop on Autogenous Shrinkage of Concrete, Hiroshima, 1998, E & FN Spon, London, UK, pp. 89-100.

[14] Baroghel-Bouny, V., Mainguy, M., Lassabatere, T., and Coussy, O., 'Characterization and identification of equilibrium and transfer moisture properties for ordinary and high-performance cementitious materials', Cem. Concr. Res. **29**(8) (1999) 1225-1238.

[15] Cornelissen, H.A.W., 'Creep of concrete A stochastic quantity' (in Dutch), PhD Thesis, Eindhoven University of Technology, 1979, pp. 149.

EFFECT OF SELF-DESICCATION ON FROST RESISTANCE OF CONCRETE

Osamu Senbu
Division of Building Materials
Graduate School of Engineering
Hokkaido University, Sapporo Japan

Yukio Hama
Fuculty of Engineering
Muroran Institute of Technology, Muroran, Japan

Fumiori Tomosawa
Division of Building Materials
Graduate School of Engineering
Hokkaido University, Sapporo Japan

Abstract

Self-desiccation of concrete reduces its water content and can induce autogenous shrinkage, causing fine cracks. However, its effect on the frost resistance of concrete has not been made clear. Concrete specimens having different water-cement ratios and types and contents of coarse aggregate were subjected to initial curing and drying to induce autogenous shrinkage and drying shrinkage. Freezing and thawing tests were then conducted on the specimens in accordance with ASTM C 666 and RILEM CIF. This paper reports on the total plan of this study and the part for self-desiccation. The results revealed that self-desiccation can reduce the frost resistance of concrete.

1. Introduction

The effect of autogenous shrinkage on the frost resistance of concrete has not been elucidated yet. Self-desiccation is both advantageous and disadvantageous to frost resistance of concrete. The advantage is that it reduces the water content of concrete; the disadvantage is that it may cause fine cracks within concrete. The effect of such fine cracks on the frost damage of concrete is also unknown.

Concrete with a low water-cement ratio (W/C) is said to be highly resistant to frost damage even without entrained air. However, it is reported that low W/C concrete with no entrained air subjected to weather for 10 years may exhibit low frost resistance by freezing and thawing testing in accordance with ASTM C 666[1]. This may be because repeated drying and wetting during exposure to weather caused fine cracks in concrete.
This study intends to elucidate the effect of autogenous shrinkage and drying shrinkage, which presumably cause fine cracks in concrete, on the frost resistance of concrete. This paper reports on the outline of the study and the part related to autogenous shrinkage.

2. Experiment plan

Table 1 gives the total plan of this study, in which concretes cured and dried in various ways are subjected to freezing and thawing tests in accordance with Procedure A of ASTM C 666 and RILEM CIF. Initial curing conditions up to 2 weeks after placing included general water curing and seal curing to induce autogenous shrinkage. Various types of drying and outdoor exposure are carried out after initial curing to induce drying shrinkage. Different water-cement ratios, as well as types and contents of coarse aggregate, are adopted to vary the autogenous and drying shrinkage values. The target air contents are 1% and 4%.

The measurement items include those specified in the ASTM and CIF tests, bottom water absorption under the absorption conditions of the CIF tests, as well as autogenous shrinkage and compressive strength. The drying shrinkage rate is also determined from the length changes of specimens for freezing and thawing tests in accordance with ASTM after exposure to weather. Measurement of fine cracking is under study, but not determined in detail. The symbols for specimens represent the type of mixture and type of initial curing/drying (e.g., 2NPW). This paper reports on the items expressed by solid black marks.

Figure 1 shows the flow of freezing and thawing tests. Specimens to be water-cured were demolded at an age of 1 day and subjected to initial water curing up to an age of 2 weeks. Specimens to be seal-cured were left in the molds and seal-cured until testing. After initial curing, specimens were directly tested or subjected to various types of drying or exposure before testing.

Table 1-Test program

Variety of concrete					Curing condition (Initial/Dry)										Other test methods
W/C (%)	Air (%)	Coarse aggregate		Sign** of concrete	In water for 2W (Initial)					Sealed for 2W (Initial)					
		Type	Vol. (l/m^3)		none [W]*	Dry [WD]*	20 Dry [WD]*	40 Dry [WD2]*	Exposure [WE]*	none [S]*	Dry [SD]*	20 Dry [SD]*	40 Dry [SD2]*	Exposure [SE]*	
25		T	360	2NP											
			300	2NQ											
		O	360	2NO											
	4	T	360	2AP											
			300	2AQ											
		O	360	2AO											
50		T	360	5NP											
	4			5AP											

(Note : ASTM method
: CIF method
( ) : Compressive strength test for concrete (mortar) at the age of 2weeks
( ) : Self-desiccation of concrete (mortar)
Black mark means fulfillment at present(2002.4)
* : Sign of curing condition
W, S : without artificial drying process
WD,SD : Exposed Indoors (+40 Dry)
WD ,SD : 20 for 2 weeks
WD2,SD2 : 40 for week + 20 for week
WE, SE : Exposed Outdoors
**:Element of "Sign of concrete"
2: W/C=25%
5: W/C=50%
N: Target air content= %, A: Target air content=4%
P: Type & volume of coase aggregate = T & 360l/m^3
Q: Type & volume of coase aggregate = T & 300l/m^3
O: Type & volume of coase aggregate = O & 360l/m^3
Name of Specimen = (Sign of Concrete) + (Curing Condition) ex. 2NPW

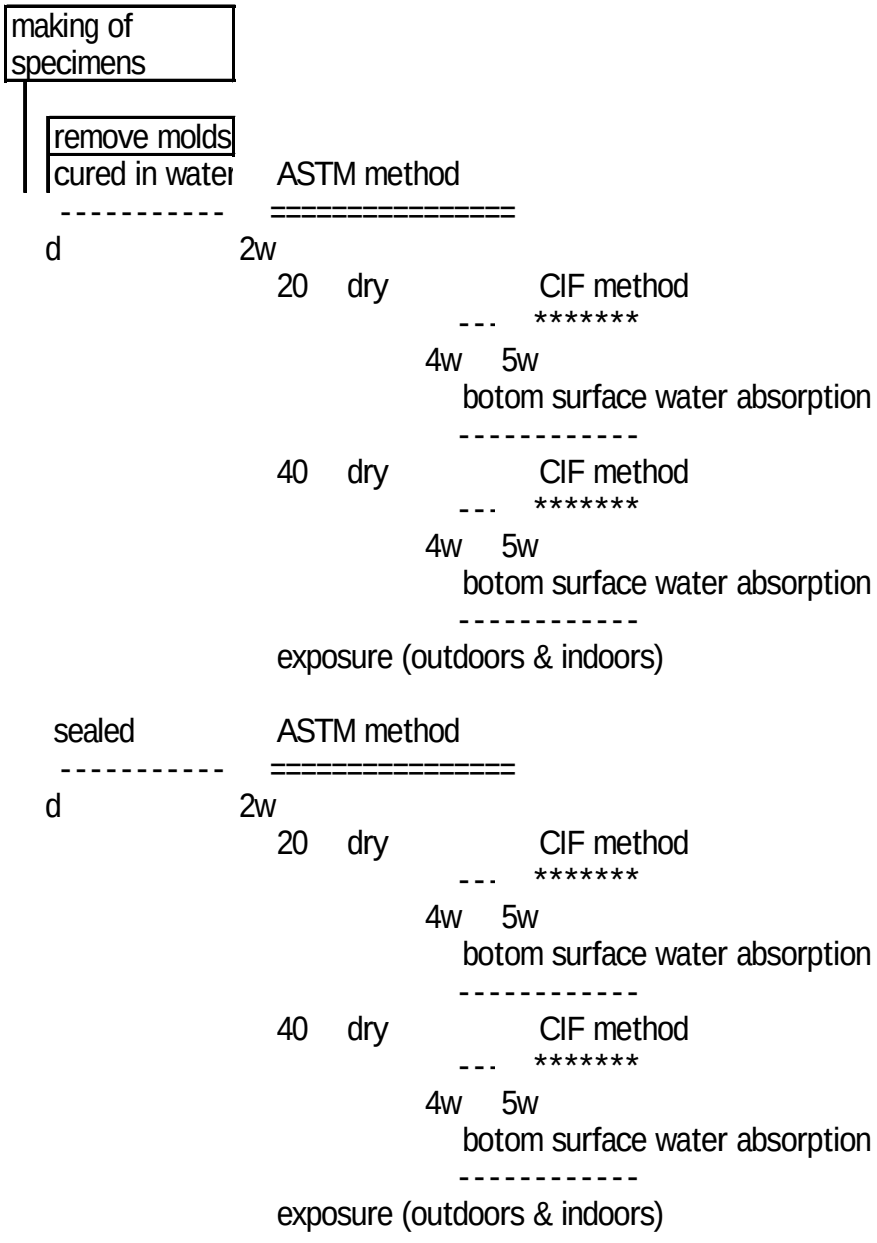

Figure 1-Flowchart of Freezing and Thawing Test

3. Test procedures

3.1 Proportioning, specimen fabrication, and curing

The mixture proportions are given in Table 2. The unit water content is fixed at 175 kg/m^3. Two levels of W/C were prepared: 25% selected to induce large autogenous shrinkage and 50%. The corresponding cement content thus was 700 and 350 kg/m^3.Coarse aggregate in concrete restrains shrinkage, presumably causing fine cracks in cement paste. For this reason, two levels of volume content of coarse aggregate were prepared: 360 l/m^3 and 300 l/m^3. Since the restraining effect of coarse aggregate depends on its rigidity as well, two types of coarse aggregate (T and O) were prepared.

The air content, slump, slump flow, density, and temperature of concrete were measured after its mixing in a forced mixing-type biaxial mixer. Concrete was then placed in molds suitable for each test method and cured as specified. Since the air content of some of the air-entrained concretes showed significant changes over time, the air content 30 min after mixing was also measured in addition to the as-mixed measurement. The molds and specimens for each test method are described below.

a) Specimens for ASTM method: each mould measures was 7.5 by 7.5 by 40 cm. Concrete was placed in the moulds with a gauge plug attached to each end to mea sure length changes, as shown in Figure 2. Prior to placing, PTFE sheeting was applied to all sides and ends except the placing side of the mold to prevent bond between the mold and concrete from restraining autogenous shrinkage of concrete. The bolts for setting gauge plugs were removed 3 hours after placing so that the gauge plugs would not restrain autogenous shrinkage.

b) Specimens for CIF method and bottom water absorption method: concrete was placed in moulds 10 cm in diameter and 20 cm in length and cut and polished after demolding. The size of the cut specimens was 10 cm in diameter and approximately 9 cm in length. Cut and polished surfaces were used for absorption in the CIF tests and bottom absorption tests.

c) Specimens for compression testing: concrete and mortar were placed in moulds 10 cm in diameter and 20 cm in length and 5 cm in diameter and 10 cm in length, respectively. Mortar was taken from freshly mixed concrete by wet screening.

d) Specimens for autogenous shrinkage testing: moulds for concrete and mortar having the same sizes as those for compression testing were used. Referring to Nawa's method [2], concrete and mortar were placed in easy molds with PTFE sheeting on the inside to minimize restraint by the molds, while embedding a gauge for measuring autogenous shrinkage and thermocouple for measuring temperatures in each mould. Figure 3 shows the specimen and gauge for autogenous shrinkage.

Table 2- Mix proportions of concrete

Sign of concrete	W/C (%)	Air (%)	S/A (%)	W (kg/m^3)	Absolute vol.(l/m^3)			SP (C*%)	AE (C*0.0 %)	Type of coarse aggregate
					C	S	G			
2NP	25		39.3	75	222	233	360	.30		T
2NQ			49.5			293	300			
2NO			39.3			233	360			O
2AP		4	36.			203		. 0	5.6	T
2AQ			46.8			263	300		4.2	
2AO			36.			203			5.6	O
5NP	50		48.9			344	360	0.60		T
5AP		4	46.6			3 4		0.45	.225	

Note) Air : Air content
S/A : Sand-aggregates ratio
W : Unit water content
C : Cement(=3. 6)
S : Fine aggregate(s=2.67)
G : Coarse aggregate
(T: s=2.69, Qs=2.24, FM=6.75 / O: s=2.66, Qs=0.66, FM=6.72)
s: Surface-dry specific gravity
Qs:Percentage of water absorption
FM:Finess modulus
SP : Superprasticizer
AE : Air-Entraining Agents

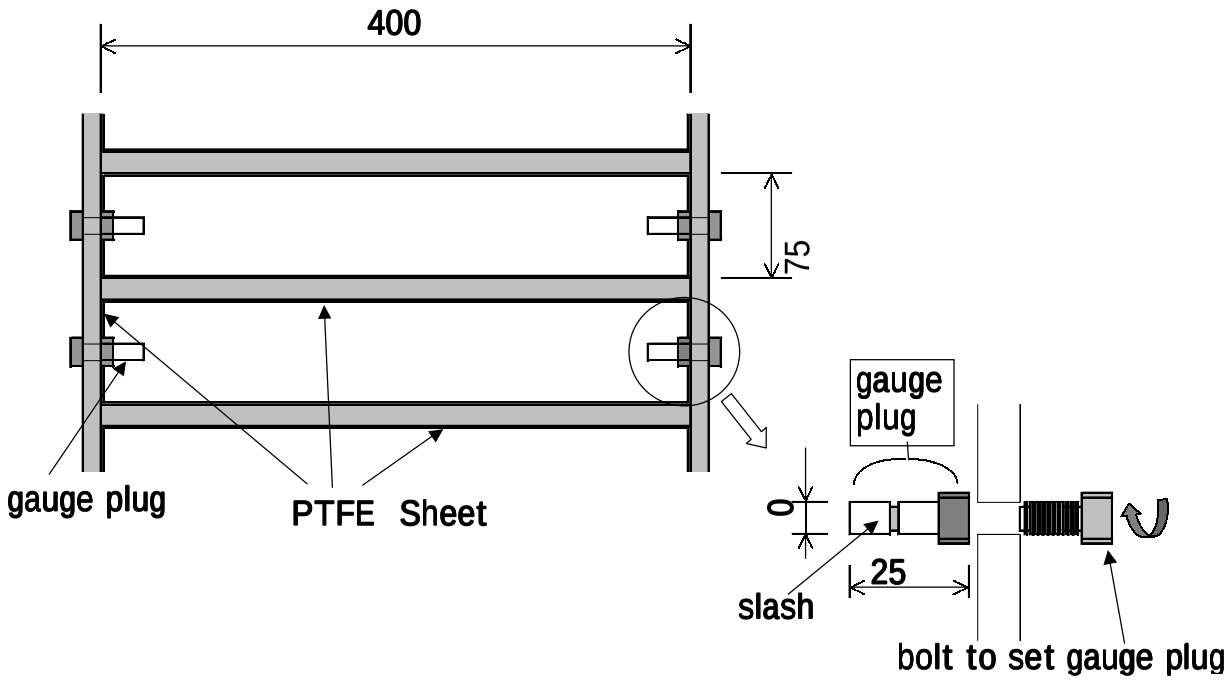

Figure 2-Mold for ASTM method

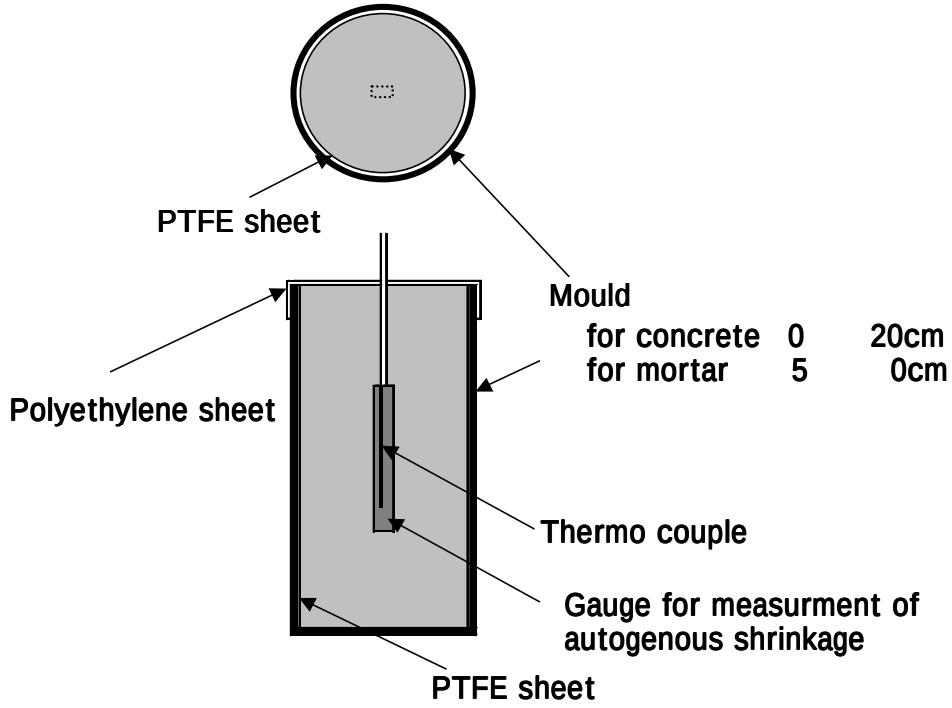

Figure 3-Measurement method of autogenous shrinkage

e) Specimens for exposure to weather: beams 7.5 by 7.5 by 40 cm and cylinders 10 cm in diameter and 20 cm in length were prepared for testing by the ASTM and CIF methods, respectively, after exposure to weather.

After initial curing for 2 weeks, the drying process or exposure testing were carried out as shown in Figure 1. The drying/exposure conditions are as follows:

"20°C dry" : drying in a thermo-hygrostatic room at 20°C and 60% RH
"Dry" : drying in a laboratory without air conditioning
"40°C dry" : drying in a thermostatic chamber at 40°C
"Exposure" : outdoor exposure on a stand 70 cm in height in Sapporo, Japan
"None" : no drying or exposure process

3.2 Freezing and thawing testing in accordance with Procedure A of ASTM C 666

ASTM C 666 is described as "Standard test method for resistance of concrete to rapid freezing and thawing." Procedure A refers to testing comprising freezing in water and thawing in water. This is the most commonly practiced test method in which freezing and thawing are repeated at a rate of 6 cycles a day in the range of specimen temperature between -18°C and +5°C. Dynamic modulus of elasticity, mass, and length change are measured.

3.3 RILEM's CIF testing and bottom water absorption testing

RILEM's CIF testing refers to testing in which freezing and thawing are carried out while the specimen absorbs water from the bottom surface as shown in Figure 4. Water absorption from the bottom is measured under these conditions in the bottom water absorption testing. CIF testing is conducted by allowing specimens cured and dried as specified to absorb water from the bottom for 1 week and then applying cyclic freezing and thawing. The measurement items for CIF testing include the dynamic modulus by longitudinal vibration, ultrasonic wave velocity, mass, and amount of scaling.

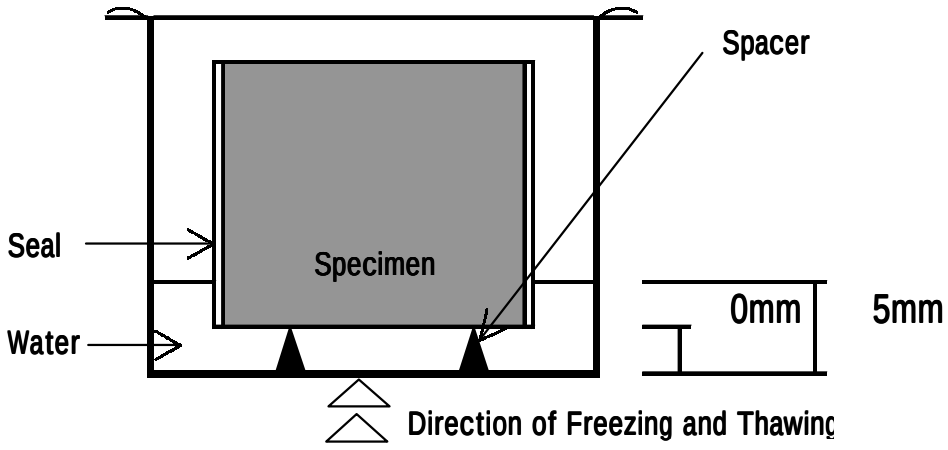

Figure 4-Water absorption of CIF testing

3.4 Compressive strength

Compression tests on concrete and mortar were conduced in accordance with JIS A 1108 (Method of test for compressive strength of concrete). Specimens were water-cured and tested at an age of 2 weeks.

3.5 Autogenous shrinkage strain

Autogenous shrinkage strain was measured using data loggers from immediately after placing. Autogenous shrinkage strain was determined by subtracting the thermal strain from the strain measured by the gauges. The linear expansion coefficient was assumed to be $10 \times 10^{-6}/^{o}C$.

4. Results and discussion

4.1 Basic properties of concrete

Basic properties of concrete used in these tests are summarized in Table 3.

4.2 Autogenous shrinkage of concrete

Figure 5 shows typical autogenous shrinkage measurements. The reason for the large scatter for mortar without entrained air is unknown. The average for each set of proportions is therefore taken here as the autogenous shrinkage strain for each type of mixture.

Table 3-Pperties of concrete

Sign of concrete	Properties after Mixing				Compressive strength(Mpa	
	Air (%)	Temp. ( )	Slump (cm)	Slump flow (cm)	Concrete Fc2w	Mortar Fm2w
2NP	.	20	24.2	56.3*57.9	86.	9 .6
2NQ	.6	9	24.2	49.6*47.5	83.4	92.4
2NO	0.9	7	>26	79.0*57.9	84.4	89.8
2AP	5.5(4.2)*	9	22.5	40. *36.7	73.4	67.5
2AQ	6.8(4.6)*	9	2 .3	47.5*3 .6	69.3	74.6
2AO	7.6(4.8)*	6	25	50.0*36.7	66.4	7 .5
5NP	.7	7	2.		4 .8	42.7
5AP	5. (4.6)*	7	9.2		29.2	30.0

Note) Air : Air content
*bracked value means air content mixing after 30min.
Fc2W : Strength of concrete at the age of 2weeks
Fm2W : Strenght of concrete at the age of 2weeks
**:Element of "Sign of concrete"
2: W/C=25%
5: W/C=50%
N: Target air content= %, A: Target air content=4%
P: Type & volume of coase aggregate = T & 360l/m^3
Q: Type & volume of coase aggregate = T & 300l/m^3
O: Type & volume of coase aggregate = O & 360l/m^3

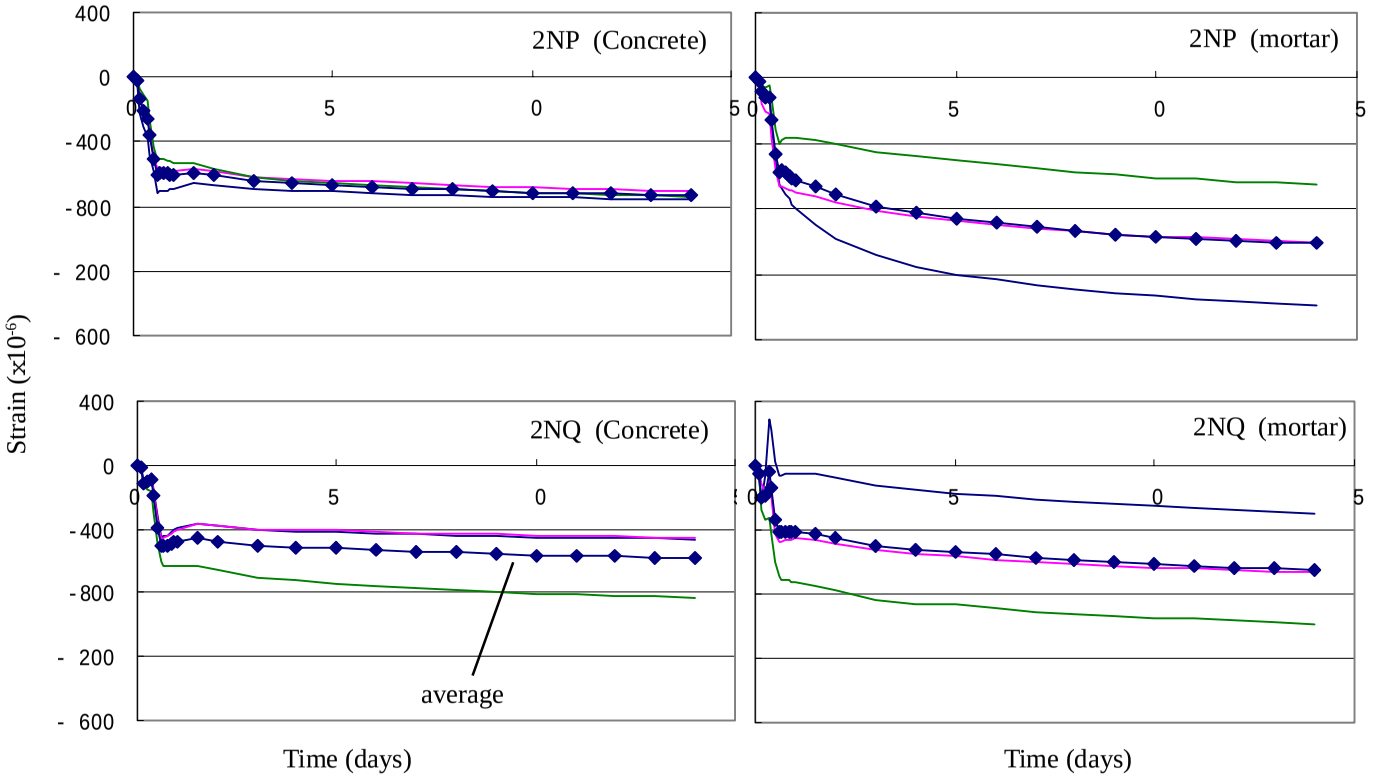

Figure 5(1)-Test results of measurement of autogenous strain
(data of each specimen and average)

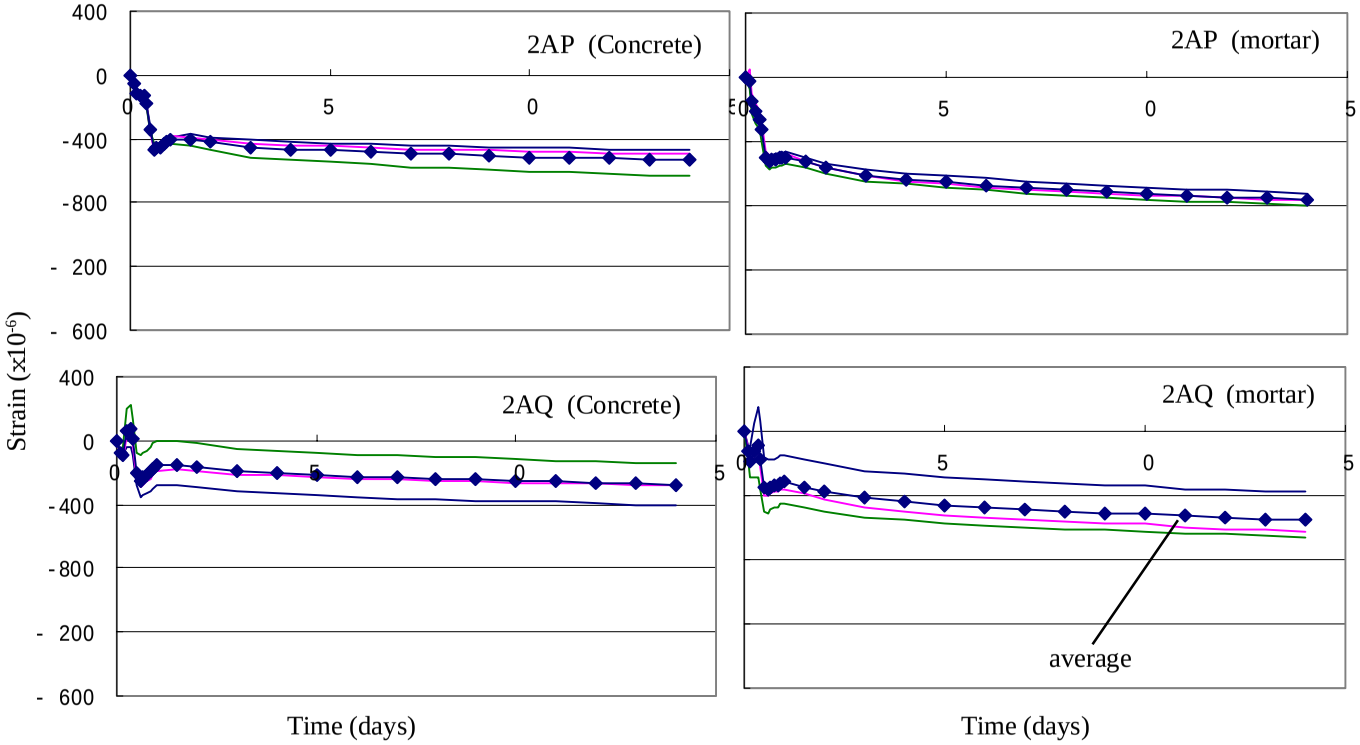

Figure 5(2)-Test results of measurement of autogenous strain
(data of each specimen and average)

Figure 6 shows the average autogenous shrinkages of concrete and wet-screened mortar of each type of mixture. When the W/C is 50%, the autogenous shrinkage is small and greater in mortar than in concrete. The autogenous shrinkage values of concrete/mortar vary with a W/C of 25%, among which those of specimens having entrained air tend to be smaller. The autogenous shrinkage values for an age of 14 days are summarized in Table 4. This table also includes the autogenous shrinkage values of concrete minus autogenous shrinkage values of mortar (SFc - SFm), as it was considered that the wider the difference, the higher the probability of fine cracks occurring within concrete due to restraint by coarse aggregate.

Table 4 Results of autogenous shrinkage at the age of 14days

Sign* of concrete	Self-desiccation strain ( )		
	Concrete [SFc]	Mortar [SFm]	SFc-SFm
2NP	-736	- 0 3	277
2NQ	-584	-648	64
2NO	-663	- 046	383
2AP	-535	-76	226
2AQ	-274	-553	279
2AO	-5 6	-706	90
5NP	-4	- 4	0
5AP	- 27	- 04	-23

(Note) SFc : Self-desiccation strain of concrete at the age of 4days
SFm : Self-desiccation strain of mortar at the age of 4days
*:Element of "Sign of concrete"
2: W/C=25%
5: W/C=50%
N: Target air content= %, A: Target air content=4%
P: Type & volume of coase aggregate = T & 360l/m^3
Q: Type & volume of coase aggregate = T & 300l/m^3
O: Type & volume of coase aggregate = O & 360l/m^3

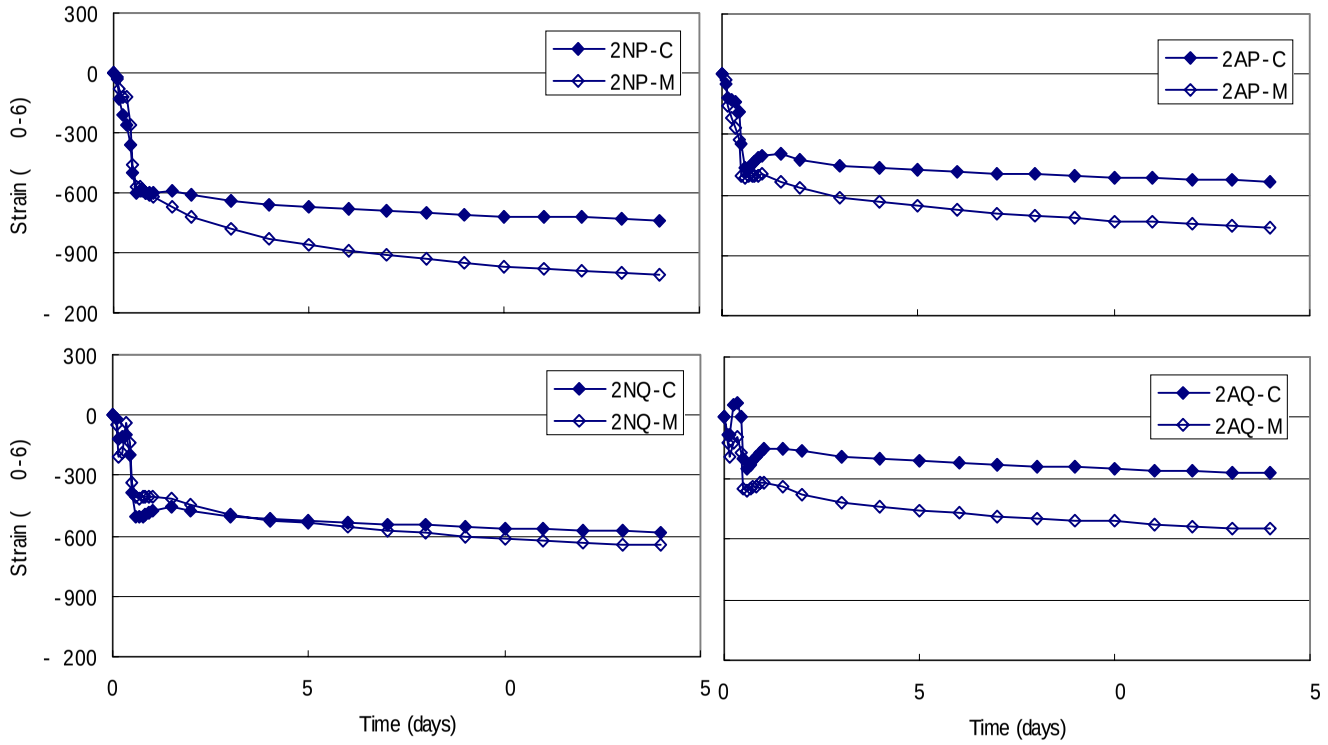

Figure 6(1)- Test results of measurement of self-desiccation strain
(average value, C: concrete, M: mortar)

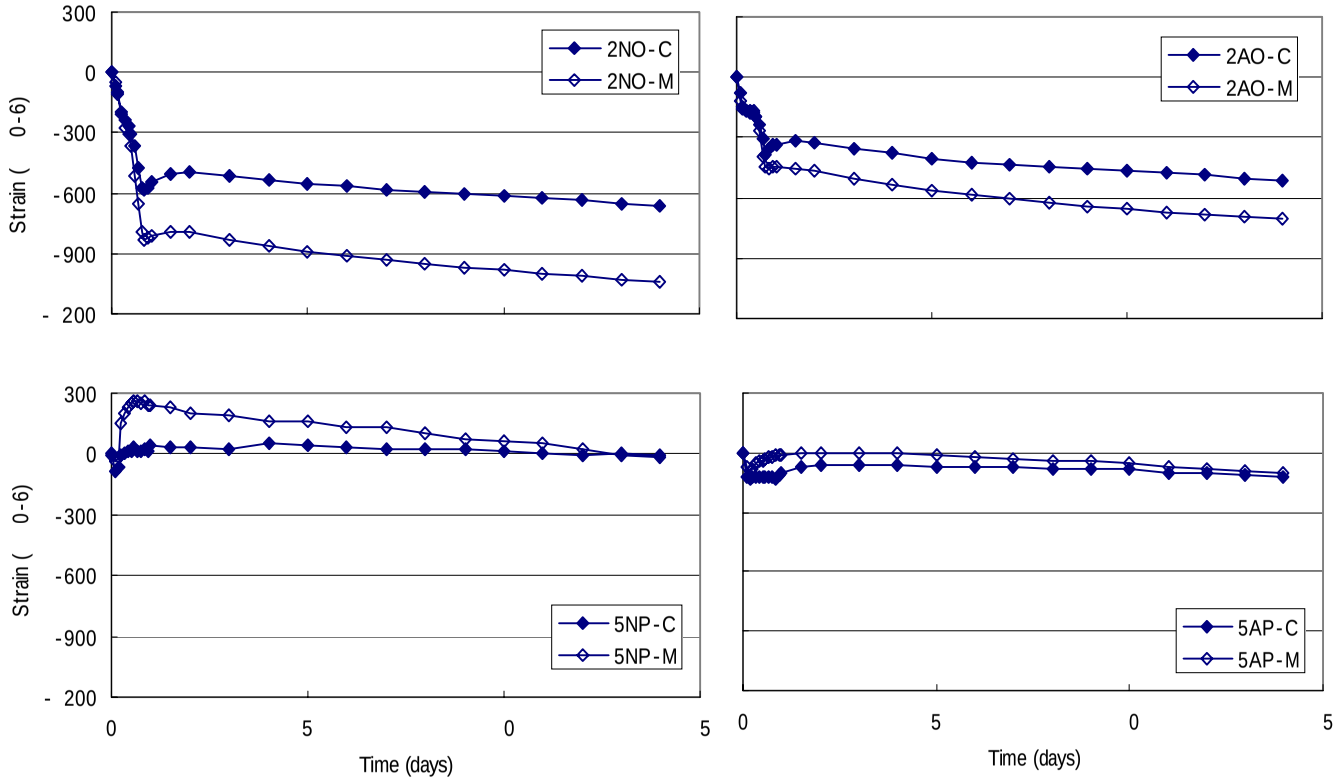

Figure 6(2)-Test results of measurement of self-desiccation strain
(average value, C: concrete, M: mortar)

4.3 Deterioration measured by ASTM C 666

Figure 7 shows the changes in the relative dynamic modulus of concrete water-cured or seal-cured for 2 weeks after placing measured by the ASTM method. With a W/C of 50%, the values for 5NP with no entrained air rapidly decrease, whereas the values for the type with entrained air scarcely decrease over time, indicating the frost resistance-improving effect of entrained air. When the W/C is 25%, no abrupt losses in the relative dynamic modulus are observed even without entrained air. The values rather increase over time in some cases. The value for seal-cured 2NQ (2NQS) significantly decreases over time. This may be because autogenous shrinkage induces fine cracks in the concrete, causing deterioration. Similar losses in the relative dynamic modulus appear to begin in seal-cured 2NP (2NPS).

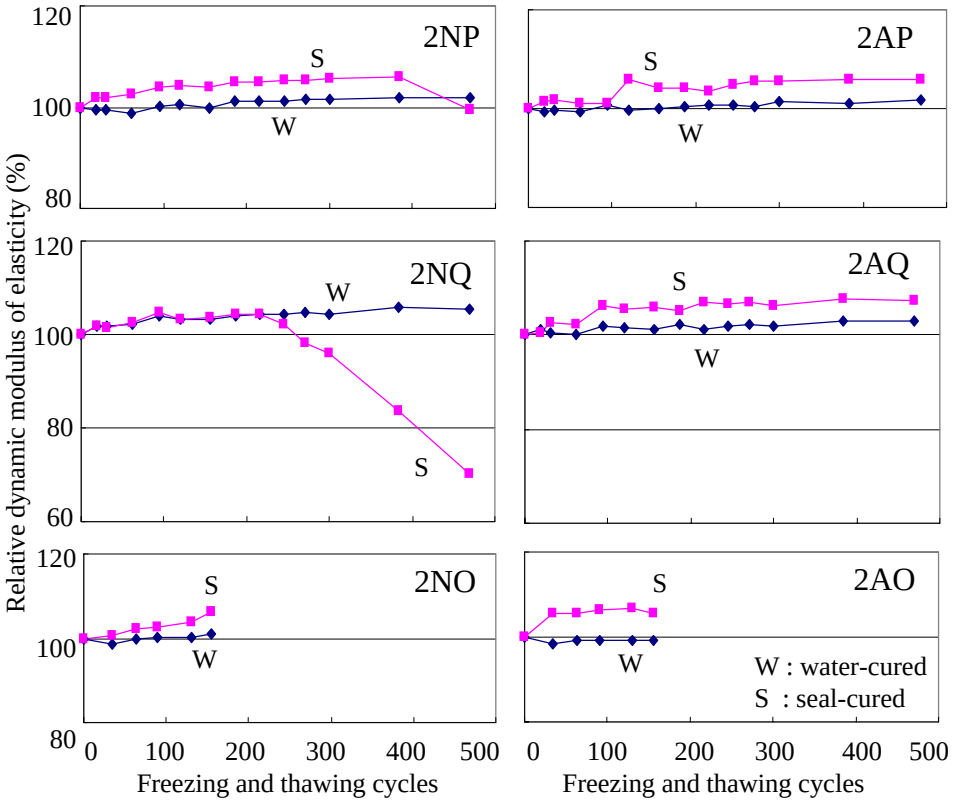

Figure 7(1)-Test results of ASTM method
(change of relative dynamic modulus of elasticity)

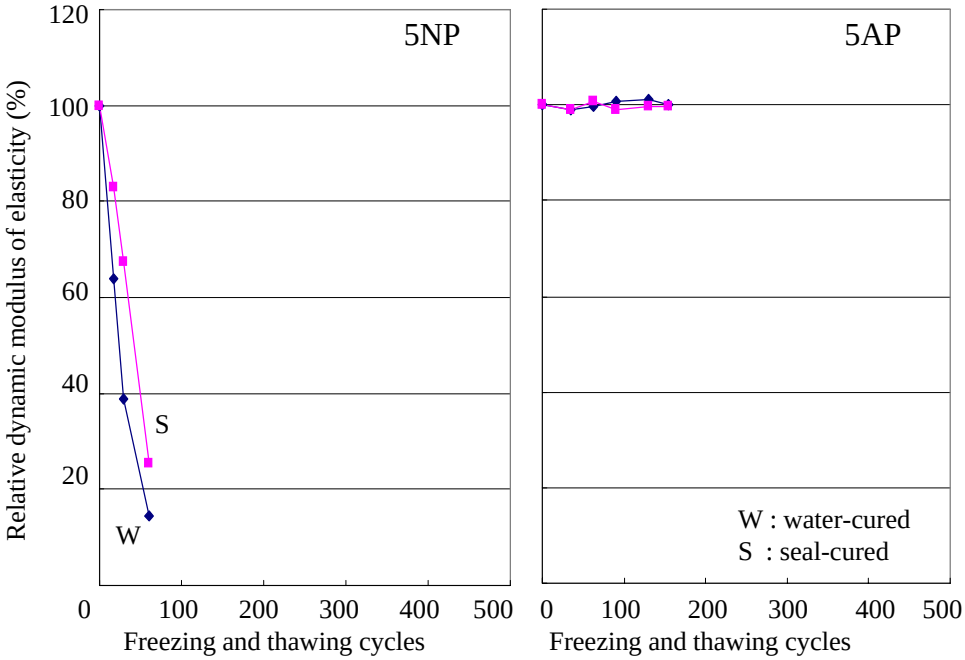

Figure 7 (1)-Test results of ASTM method
(change of relative dynamic modulus of elasticity)

Figure 8 shows the relative dynamic modulus, mass change rate, and length change rate related to the number of freezing and thawing cycles of 2NQ and 5NP, which are evidently found to be deteriorated by the ASTM method. 5NP with a W/C of 50% exhibits increases in the relative dynamic modulus and length change rate, suggesting loosening of its microstructures. The mass of 5NP also decreases, suggesting scaling of concrete. No differences by curing conditions are observed in 5NP. In the case of 2NQ with a W/C of 25%, water-cured 2NQW shows no losses in the mass or length, proving to be sound. However, seal-cured 2NQS shows losses in the relative dynamic modulus and increases in the length change rate, which suggest loosening of microstructures, while the mass increases, which suggests absence of scaling. Accordingly, deterioration without scaling, which is characteristic of concrete with a low W/C, is observed.

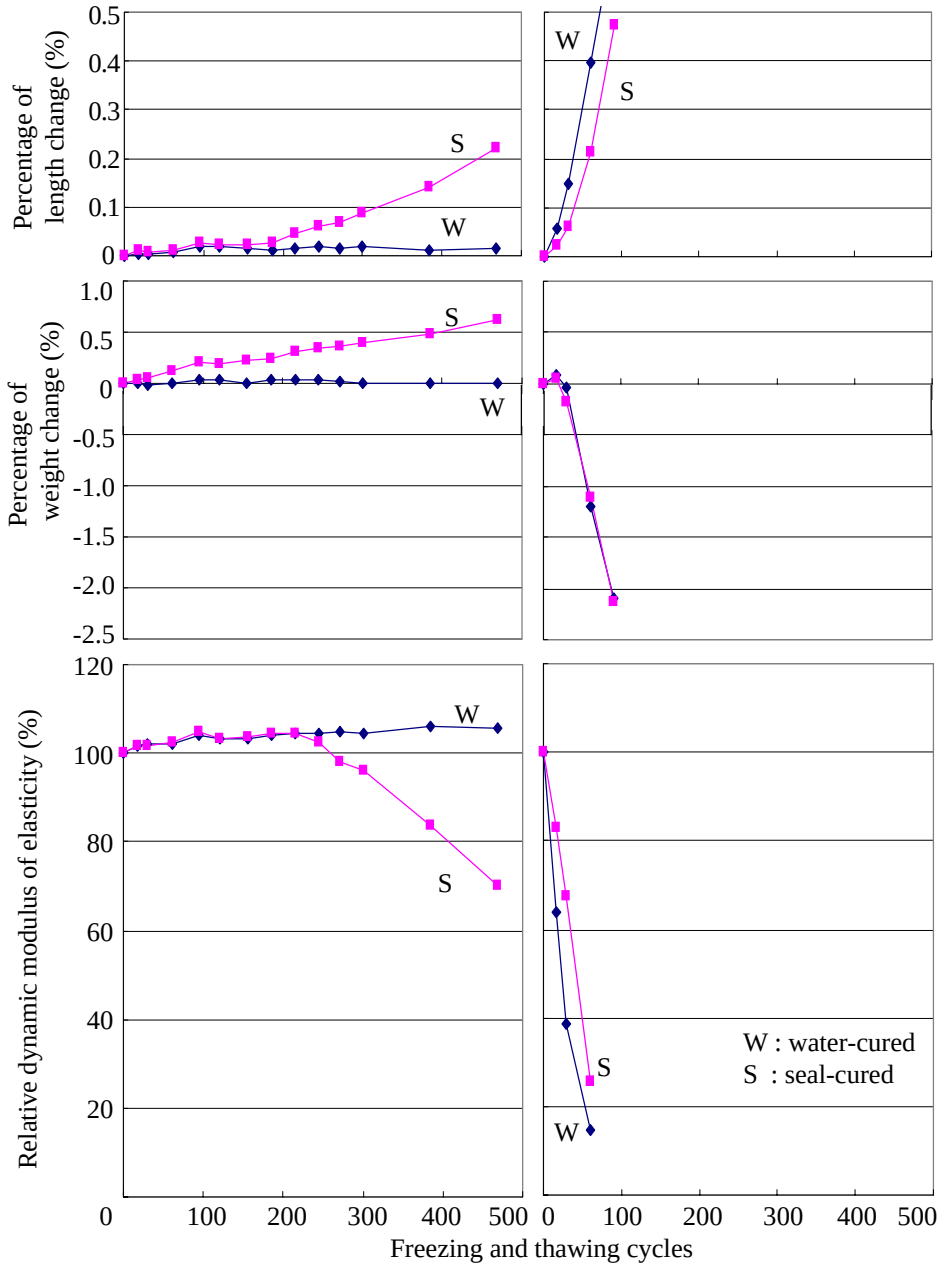

(a) 2NQ (b) 5NP

Figure 8-Test results of ASTM method

4.4 CIF testing and bottom absorption testing

Figure 9 shows the changes in the relative dynamic modulus by longitudinal vibration resonance testing in accordance with the CIF method. Though CIF testing also includes measurement of ultrasonic wave velocity, it was not adopted in the present study due to the wide scatter. Since freezing and thawing from one side specified in the CIF testing are mild conditions when compared with the ASTM method, these cause little deterioration, except that specimens with a W/C of 50% appear to begin to deteriorate.

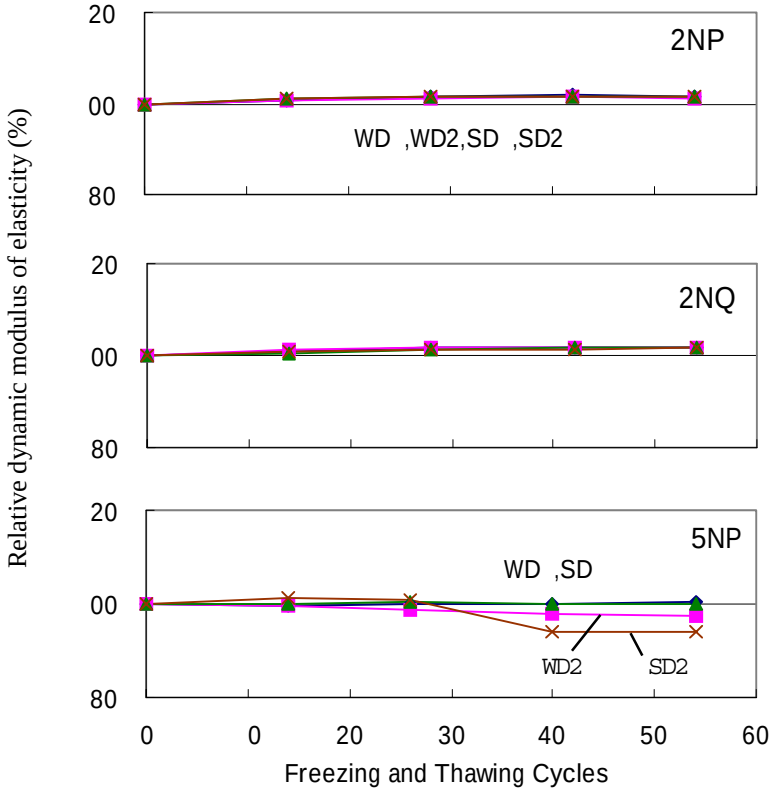

Figure 9-Test results of CIF method

Figure 10 shows the water absorption curves determined in the CIF tests and bottom absorption tests. It should be noted that the zero point on the horizontal axis represents the beginning of water absorption from the bottom. Bottom water absorption tests are conducted for the first 7 days in the CIF tests as well. The curves for 25% W/C are discontinuous at the 7th day, because the specimens were stored frozen due to the insufficient capacity of the CIF test apparatus.

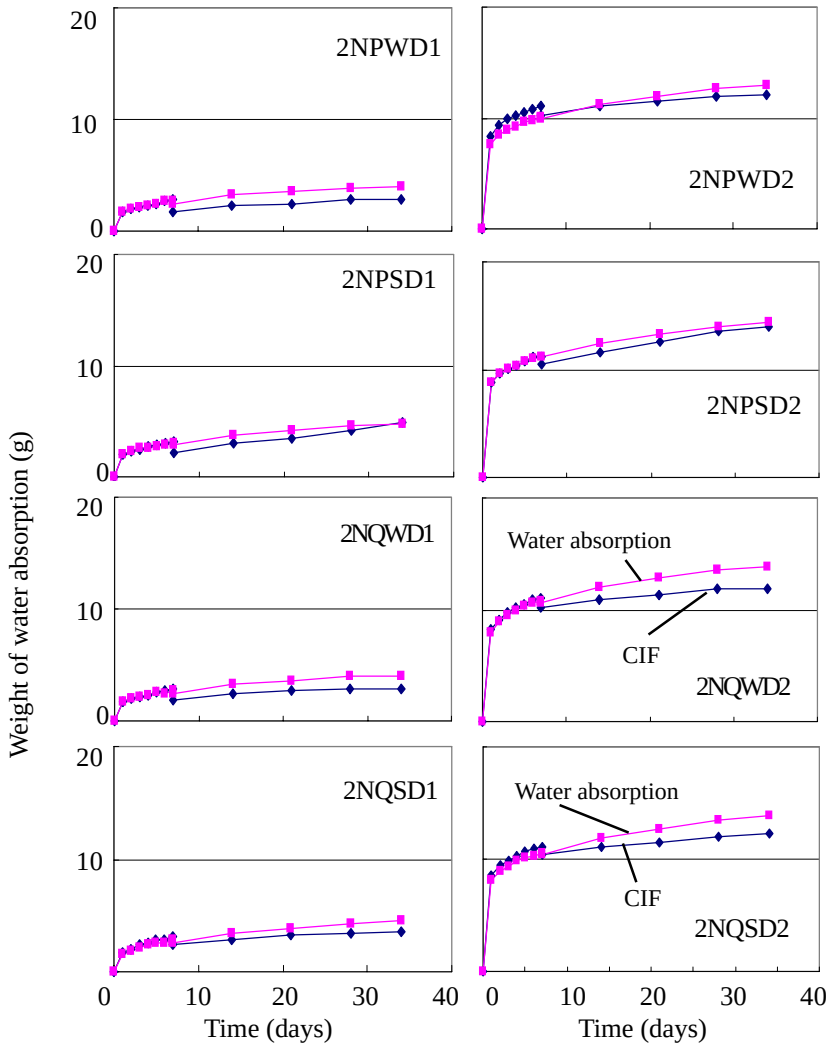

Figure 10(1)-Water absorption curve of CIF method

When the W/C is 50%, the water absorption becomes high after freezing and thawing begin, suggesting that freezing and thawing action has the effect of increasing water absorption. When the W/C is 25%, the water absorption is low, exhibiting no particular tendencies, partly because of the changes in the water absorption during the freezing storage.

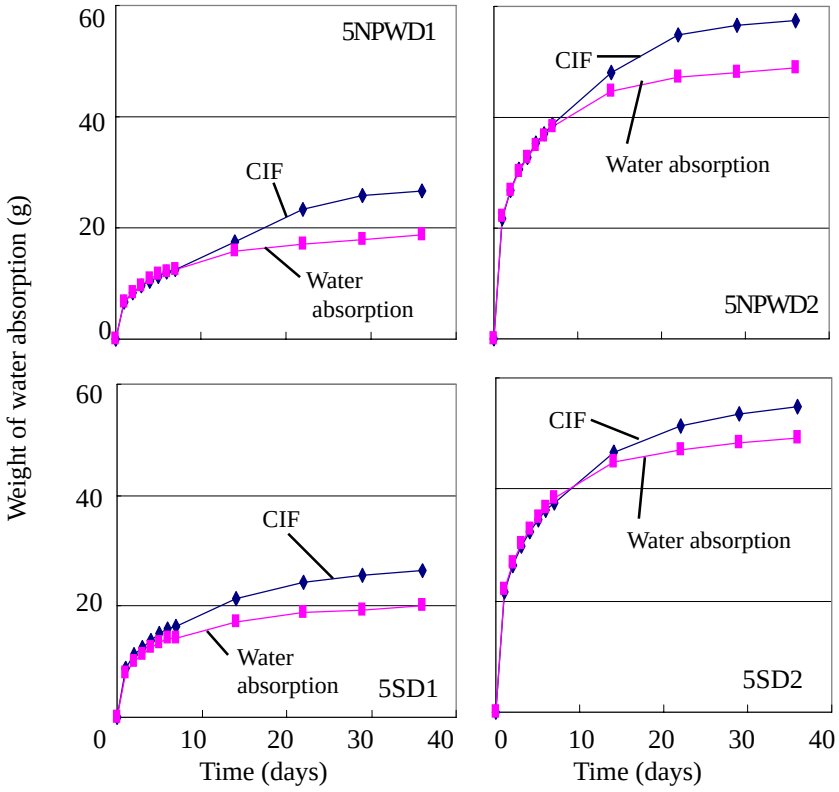

Figure 10(2)-Water absorption curve of CIF method

5. Conclusions

Autogenous shrinkage measurement and freezing and thawing testing by the ASTM and CIF methods were conducted on mortar and concrete specimens made with different initial curing conditions. The results are as follows:

(1) In the autogenous shrinkage measurement using gauges, the results of certain mixtures varied from one specimen to another. The reason for this scatter should be elucidated.
(2) In regard to average autogenous shrinkage, the values of mortar tended to be greater than those of concrete, and the values of specimens with a W/C of 50% tended to be small.
(3) Autogenous shrinkage of specimens with a W/C of 25% varied depending on the mixture proportions. The values of those containing an air-entraining admixture tended to be low. The type and quantity of coarse aggregate are also considered to have produced strong effects on the shrinkage.
(4) Concrete with a low W/C exhibited excellent resistance to frost deterioration even without entrained air, provided it is initially water-cured.
(5) Deterioration was found during testing by the ASTM method in some of low W/C concrete specimens with no entrained air when they were initially seal-cured. Autogenous shrinkage may have degraded the frost resistance of the concrete.
(6) Unlike normal concrete, deterioration of concrete with a low W/C was characterized by an increase in the mass when tested by the ASTM method.
(7) By the CIF method, no deterioration was observed in concrete with a low W/C. Concrete with a W/C of 50% subjected to drying at 40°C exhibited a tendency towards deterioration.
(8) In the CIF testing, the moisture content of specimens increased during repeated freezing and thawing, suggesting that freezing and thawing action has the effect of increasing the moisture content.

6. References

[1] Hama, Y., Senbu, O., Tomosawa, F., Effect of Curing Condition before Freezing and Thawing Test to Frost Resistance of High Performance Concrete, 6th International Symposium on Utilization of High Strength/High Performance Concrete, Leipziger (2002).
[2] Horita, T., Nawa, T., A study on autogenous shrinkage of cement mixes, Journal of Structural and Construction Engineering, No.542 9-15, Architectural Institute of Japan (2001). (in Japanese)

AUTOGENOUS CURING OF HIGH-STRENGTH CONCRETE USING PRE-SOAKED PUMICE AND PERLITE SAND

S. Zhutovsky, K. Kovler and A. Bentur
National Building Research Institute - Faculty of Civil Engineering
Technion - Israel Institute of Technology

Abstract

High Strength Concretes with extremely low water to binder (w/b) ratios are characterized by high cracking sensitivity as a consequence of increased autogenous shrinkage. Self desiccation which is the driving force for autogenous shrinkage can not be eliminated by traditional curing methods. The novel approach, that has been recently proposed, is autogenous (internal) curing. It suggests incorporating pre-soaked lightweight aggregate into the mix, which will act as internal water reservoir, preventing reduction in relative humidity. This method is frequently named "autogenous curing". Previous experimental work demonstrated that autogenous curing can be successfully applied to obtain improved high strength concrete with reduced sensitivity to cracking. However, the lightweight aggregate content required to eliminate autogenous shrinkage was high, which resulted in reduced compressive strength and increase in the price of the concrete.

Optimization of lightweight aggregate usage as internal curing agent is hampered by excessive number of factors influencing the process of internal curing. Since the internal curing of HPC is quite complex phenomena, the role of each factor in controlling the effectiveness of autogenous curing is not always clear. Most of the developments so far were based on replacement of a large portion of the coarse aggregate by lightweight aggregate of similar size, in order to effectively eliminate autogenous shrinkage. The approach presented in this paper is intended to optimize the structure and properties of the lightweight aggregate so that it could be added in small amounts which will be sufficient for eliminating autogenous shrinkage. From a practical point of view this approach will eventually lead to the concept of "internal curing agent", namely adding small amounts of fine lightweight aggregates that would effectively eliminate autogenous shrinkage, and would be thus viewed as additives rather than replacements of conventional aggregates.

1. Introduction

In recent years, use of High-Strength Concrete (HSC) / High-Performance Concrete (HPC) received general acceptance. This type of concrete is characterized by extremely low water to binder (w/b) ratio. Mixes with w/b ratio below 0.4 are now easy to produce due to modern high range water reducing admixtures development. However, the use of concrete with extremely low w/b ratio is accompanied with a variety of problems, one of which is high sensitivity to cracking [1 - 4].

The primary source of the elevated cracking sensitivity is autogenous shrinkage resulting from self-desiccation, which, in its turn, is a consequence of chemical shrinkage. Normally, proper curing provides a means for keeping concrete in a wet state. However, conventional curing methods fail in the case of HSC and HPC, since water cannot penetrate quickly into the dense structure, which develops. Thus, with the consumption of internal pore water and reduction of relative humidity, capillary stresses are generated causing external volume changes which are not accompanied by exchange of water with the surrounding; this shrinkage is called autogenous shrinkage [5, 6].

Thus, concretes having very low w/b ratio exhibit substantial autogenous shrinkage, which can lead to early-age cracking if deformations are restrained. Moreover, self-desiccation affects hydration kinetics, resulting in lower degree of hydration than the one, which can be achieved under saturated conditions [5].

The strategy to counteract self-desiccation by use of pre-soaked lightweight aggregate as internal water reservoir was suggested by Weber et al [7, 8]. It was named "autogenous curing" and examined practically in [7, 8] for its influence on strength development, to facilitate hydration. Afterwards, several researchers evaluated this strategy experimentally from the point of view of reducing autogenous shrinkage [9 - 17]. In these studies the lightweight aggregate content required to eliminate autogenous shrinkage was quite high, from 200 to 600 kg/m^3, which resulted in reduced compressive strength and increased the price of the concrete. This is a practical limitation on the use of this concept of internal curing.

Analysis of these studies [18] revealed that the content of water entrained in the lightweight aggregates was considerably higher than the theoretical amount required to eliminate self desiccation. This led to the notion that if the aggregate size and internal structure are optimized, effective elimination of the self-desiccation and autogenous shrinkage might be achieved with small quantities of specially formulated aggregates. In such a case, due to the small content, the aggregates might be viewed as "curing additives" rather than replacement of aggregates. To develop this concept there was a need to resolve the factors which control the effectiveness of the aggregates. The concept pursued was that highest effectiveness would be achieved if the aggregates are to be very small (sand size range) and highly porous, so that when they are uniformly dispersed in the concrete, each

site in the concrete mass will be at a small distance from an aggregate and water could be easily transported to the site as it dries out. This is similar to the concept of entrained air, where the small bubbles are uniformly distributed and the paste volume is effectively protected, since the spacing between the air sites is sufficiently small. Bentz and Snyder [19] carried out numerical simulation of this concept, and with the assumption that the "sphere of influence" of the lightweight aggregate is about 0.2 mm; they concluded that there is a need for replacement of a great portion of the sand to achieve full elimination of self-desiccation. Zhutovsky et al. [18] evaluated this concept experimentally, and found that the "sphere of influence" of sand size lightweight aggregate was in the range of few millimeters, which indicated the feasibility of using very small contents of fine lightweight aggregates to eliminate autogenous shrinkage.

The present paper presents additional studies into the efficiency of small lightweight aggregates, attempting to demonstrate the feasibility of the concept of using extremely small amounts of lightweight aggregates as "internal curing agents". The concept is based on evaluation of some of the parameters which control the efficiency of lightweight aggregate, to demonstrate their applicability when using extremely porous lightweight aggregates.

2. Efficiency of Lightweight Aggregates for Internal Curing

2.1 General approach

The water content in the lightweight aggregate required to eliminate self desiccation can be calculated from chemical shrinkage (Equation (1) [19]):

$$W_{ic}\,(kg \text{ water}/\ m^3 \text{ concrete }) = C \cdot CS \cdot \alpha_{\max} \tag{1}$$

where C is the cement content, CS is the chemical shrinkage in kg of water per kg of cement hydrated and α_{max} is the maximum degree of hydration. Accordingly, the lightweight aggregate content required for effective internal curing can be calculated by Equation (2):

$$W_{LWA} = \frac{W_{ic}}{S \cdot \phi} \tag{2}$$

In this equation ϕ denotes the water absorption capacity of the lightweight aggregate. Consequently, the content of normal weight aggregate should be reduced by a volume equal to the volume of the lightweight aggregate introduced to the mix. In the current study it was decided to use only fully saturated lightweight aggregates, i.e. with degree of saturation equal to one (S = 1).

In practice, greater contents of aggregates are required, than the values calculated from Equation 2. This implies that not all of the internal water can become effectively available for internal curing. From an engineering point of view, one may address this effect by assigning an efficiency coefficient to the system (aggregates and matrix) which ranges between 0 and 1. This coefficient may be determined experimentally by actual observations of the autogenous shrinkage of a reference system without the lightweight aggregates, and the reduction in the autogenous shrinkage when they are present. Taking into account these considerations, the efficiency of lightweight aggregates can be calculated here by Equation (3):

$$\eta = \frac{W_{ic}}{S \cdot \phi \cdot W_{LWA}} \cdot SR \tag{3}$$

where SR is percentage of shrinkage reduction and W_{LWA} is the LWA content actually used.

In previous work the authors demonstrated that in certain conditions the efficiency can be quite high, about 80% [18].

The efficiency is dependent on several processes and parameters which are not yet clearly resolved. Some of them are outline below.

2.2 Lightweight aggregate grain size

Effectiveness of internal curing depends not only on whether there is sufficient water in the lightweight aggregate, but on whether it is readily available to the surrounding cement paste as well. Hence, if the distance from a certain site in the cement paste matrix to the nearest lightweight aggregate surface will be too long, water will not permeate over such a distance within acceptable time interval. This distance can be called paste-aggregate proximity. Additionally, aggregate distribution can be described by means of aggregate-aggregate proximity, which is the distance between two nearest lightweight aggregate surfaces; it is often called spacing. Consequently, if the amount of aggregate is prescribed by the required curing water in it, the paste-aggregate proximity can be adjusted by the size of the aggregate. The finer is the aggregate size the closer will be the paste-aggregate proximity, or, in other words, the smaller will be the spacing.

In the previous work the authors [18] studied three different sizes of pumice aggregate:

- "Pumice0" with particles in the range of 0.15 to 1.18 mm;
- "Pumice1" with particles in the range of 1.18 to 2.36 mm;
- "Pumice2" with particles in the range of 2.36 to 4.75 mm.

It was shown that the best effect was observed with the coarser aggregate (Pumice2). In this aggregate, although the spacing was the largest (about 4 mm), an efficiency of 80%

was achieved. This was probably the result of the pore structure of the aggregate, as discussed below, for the influence of aggregate pore structure.

2.3 Lightweight aggregate pore structure

Previous experimental works, for the most part, dealt with coarse lightweight aggregates of expansive clay type. This type of artificial aggregate usually has a layered structure, which hinders water exchange between the aggregate and the surrounding matrix. Since the main purpose of the lightweight aggregate in autogenous curing is water supply, a lightweight aggregate with more homogenous structure would be advantageous. Additionally, it can be concluded from the previous experimental works that lightweight aggregate with higher absorption capacity is beneficial for internal curing, as higher porosity is associated perhaps with a more open pore structure.

3. Experimental

3.1 Aggregates for internal curing

In order to prove the feasibility of the concept of "internal curing agent", aggregates of high porosity and high efficiency were evaluated and compared. The two aggregates chosen were markedly different in their pore structure: pumice and perlite. The pumice is a natural aggregate and the perlite is an artificial one. In preliminary studies several size fractions of these aggregates were evaluated.

In the case of the pumice aggregate, the highest efficiency was achieved with the size fraction 2.36-4.75mm (Pumice2), due to its higher porosity (Table 1). Therefore, the performance of this aggregate was compared with that of Perlite2, which was the one closer to the size of the Pumice2. The properties of both Pumice2 and Perlite2 aggregates are presented in Table 1.

Table 1 - Properties of lightweight aggregates

Aggregate	Specific Gravity, kg/m^3	Grain size, mm	Water absorption capacity	
			% by weight	% by volume
Pumice2	1210	2.36 – 4.75	26.7	32.3
Perlite2	160	1.18 – 2.36	450	72.0

The data of absorption in Table 1 were based on absorption in boiling water, which gave higher values than absorption obtained in "simple" immersion. The aggregates used in the concrete were also pre-soaked in boiling water, to obtain the highest possible internal water content.

3.2 Testing procedures

Shrinkage tests were conducted using the testing apparatus described in [20]. This system is characterized by complete automation and high accuracy of measurement. It allows deformation measurement immediately after the casting. The specimens had size of 40×40×1000 mm.

Since research was limited in time and the testing system has accepted reproducibility, generally the shrinkage tests were not repeated. For this reason, the curves presented are product of a typical test, and not average of several tests, even when the tests were repeated. The duration of the shrinkage tests was 168 hours, i.e. one week.

The numerical value of autogenous shrinkage, for the comparison purposes and calculations, is taken as deformation from the peak of initial swelling to the point at the end of the experiment, i.e. at 168 hours.

Cube specimens of 50 mm size were used to determine compressive strength. The compressive strength tests were carried out at the age of 1, 3, 7 and 28 days. For all mixtures, 5 specimens were tested for every age and the calculated compressive strength is the average value.

For the mixes with pumice and for reference mixes, a pan mixer with 10-liter capacity was used. Mixing time was 5 min for these mixtures.

Use of pan mixer for mixes containing perlite caused excessive increase in the workability of the concrete accompanied by significant bleeding. This was the result of the collapse of almost all of the saturated perlite grains, starting suddenly and releasing the absorbed water into the fresh mix, during the mixing process. For this reason, two additional mixing methods were evaluated for the perlite mixes. The first one was hand mixing for a period of 10 min. This period was determined as the time to obtain concrete, which is sufficiently homogenous with only partial collapse of perlite. The second method was mixing in a free fall tilting drum mixer for 3 min. This mixing time was determined as a maximum time during which the workability of concrete was within acceptable limits, i.e. slump of S1 – S2, as in the reference mix.

Specimens for measuring the free autogenous shrinkage and strength were cast immediately after the slump test. The shrinkage molds were filled with concrete in one layer and compacted by tamping. Molds for strength specimens were filled with concrete in one layer and compacted by means of vibrating table.

All the specimens were cured in sealed conditions in a room at a constant temperature of 30±1°C. The sealing was provided by polyethylene sheets, which covered the concrete by at least five layers. The cubes were demolded and sealed after 24 hours.

3.3 Materials and mix composition

3.3.1 Aggregates

The fine aggregate was natural quartz sea sand with grain size below 0.6 mm. Effective water absorption according to ASTM C-128 1994 was 0.4% by weight, with specific gravity of 2630 kg/m^3.

The coarse aggregate was crushed dolomite of 2.36 mm<d <9.5 mm. The effective water absorption, according to ASTM C-127 1994, was 1.5% by weight, with specific gravity of 2700 kg/m^3.

The properties of the lightweight fine aggregates are presented in Table 1. The pumice was a crushed natural aggregate produced in Greece. The perlite fine aggregate was produced by Agrical, Israel.

3.3.2 Cement

Commercially available ordinary Portland cement manufactured by Nesher – Israel Cement Factories Ltd. was used. The chemical composition of the Portland cement is given in Table 2. The loss on ignition was 4.2 % by weight.

Table 2 - Chemical composition of Portland cement

Oxide	CaO	SiO_2	Al_2O_3	Fe_2O_3	MgO	TiO_2	K_2O	Na_2O	SO_3
% by weight	64.8	19.38	4.3	1.95	1.09	0.38	0.25	0.19	1.92

The specific surface area of the Portland cement, tested according to ASTM C204, was 323 m^2/kg.

3.3.3 Concrete composition

The effect of saturated pumice sand on the autogenous shrinkage and the strength of high strength concretes was investigated on the mixes with w/b ratio 0.33. The superplastisizer used was of the naphthalene formaldehyde sulfonate type at content of 1.5% by weight of cement. In the mixes with lightweight aggregates, sand was replaced with equal volume of lightweight aggregate.

The mix proportions are given in Table 3, including the corresponding replacement percentages of normal weight fine aggregate by lightweight one.

In order to study the effect of the type of lightweight aggregate, two types of lightweight fine aggregates were studied: Pumice2 and Perlite2. The same water content, corresponding to 100% of water required to counteract self-desiccation (calculated as 20 kg/m^3 according to Equation (1)), was introduced with all the fractions of the aggregate. This means that the content of the pumice and perlite lightweight aggregates in Table 3 are such that each contains 20 kg/m^3 of water required to eliminate self-desiccation; the

aggregate content was adjusted in accordance with its water absorption capacity. Thus, the total water content, free and entrained, in both mixes, was the same.

Table 3 - Mix proportions (kg/m^3)

Mix notation	Cement	Mix water	Sand	Gravel	Pumice	Replacement of sand, % by volume	Replacement of sand % by weight
Reference "REF"	506	167	574*	1162*	0	0	0
Pumice2+20kg water "Pumice2"	506	167	410*	1162*	75**	28.6	23.2%
Perlite2+20kg water "Perlite2"	506	167	508*	1162*	9***	11.5	5.7%

* Saturated surface dry (SSD)

** Dry weight; the soaked SSD aggregate contains 20 kg/m^3 of water

*** Dry weight; part of the soaked aggregate collapses, releasing 20 kg/m^3 of water, which is included in the mix water, and 20 kg/m^3 of water remaining entrained

4. Results and Discussion

4.1 Autogenous shrinkage

Autogenous shrinkage curves for the reference mixes and the ones with Pumice2 and Perlite2 are presented in Figures 1 and 2. In all cases initial expansion can be observed within the first 24 hours, and shrinkage starts thereafter. Values of autogenous shrinkage were calculated relative to the peak expansion point.

The autogenous shrinkage of the reference concrete (Figure 1) was 100.5 microstrains and the presence of the Pumice2 resulted in its reduction to 19.7 microstrains. This reflects an efficiency factor of 80.4%, calculated according to Equation 3.

In the case of the perlite the results were affected by the type of mixing (Figure 2). The very high early expansion and the high autogenous shrinkage later on (87.3 microstrain, similar to the reference) in the concrete produced by pan mixer reflects the collapse of the particles during the mixing, resulting in a greater amount of free water, leading to high early expansion. As a consequence less entrained water is present, which would have reduced the autogenous shrinkage later on. This greater amount of free water was also reflected in the slump, as will be shown later on. The curves obtained in concretes produced by drum mixing and by manual mixing are very similar. Their expansion is similar to that of the reference mix, and the autogenous shrinkage later on is almost completely eliminated. This is consistent with the observation that no collapse of the

particles occurred in these mixing procedures. The efficiency coefficients of the manual and drum mixed concretes are 100% and 80%, respectively, calculated according to Equation 3.

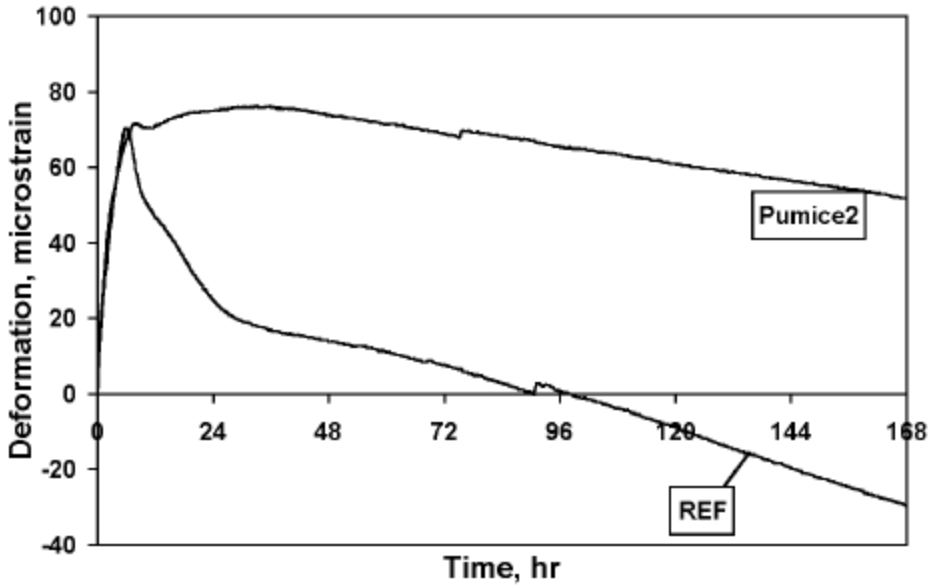

Figure 1: Effect of autogenous curing using Pumice2 aggregate on free deformation of mixes with w/b ratio 0.33

Comparison of the autogenous shrinkage curves of the pumice and manually mixed perlite concrete are shown in Figure 3. Both are similar, reflecting the very high efficiency coefficient in both, being 80.4% for the pumice and 100% for the perlite. It should be noted that although both have similar efficiency, the content of perlite required to achieve this performance was 9 kg/m^3 (dry) and 29 kg/m^3 (wet), whereas the quantities of pumice were much greater, by factors of 3 to 8 (75 kg/m^3 (dry) and 95 kg/m^3 (wet)). The quantity of the perlite is sufficiently small to be considered as an additive rather than aggregate replacement.

The spacing factors calculated for the perlite and the pumice were around 4 mm for both, suggesting that in both cases water can be easily extracted from the paste and transported over the 4 mm distance. Different trends may be obtained for lower w/b ratios, where the matrix is less permeable.

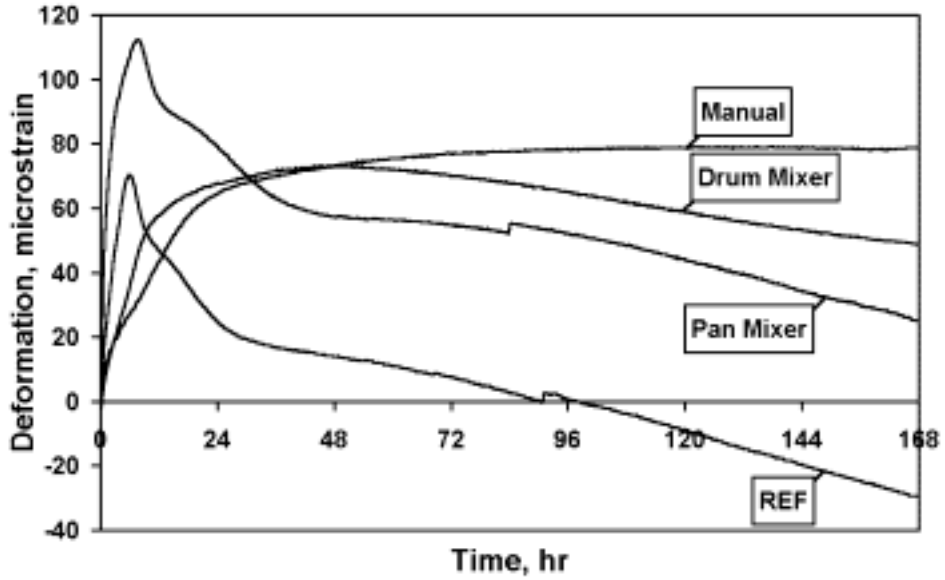

Figure 2: Effect of mixing on free shrinkage of mixes with w/b ratio 0.33 containing Perlite2

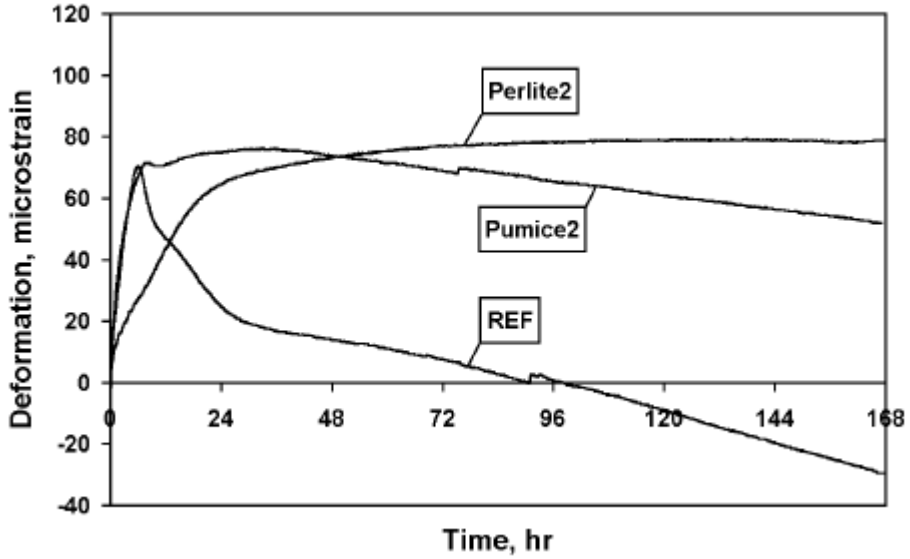

Figure 3: Effect of lightweight aggregate type used as curing agent on free shrinkage

4.2 Workability and compressive strength

Slump, specific weight and compressive strength are presented in Tables 4 and 5.

Table 4 - Slump, specific weight and compressive strength for reference concrete of w/b ratio 0.33 and concrete containing pumice sand

	Slump, mm	Specific weight, kg/m^3	Strength, MPa			
			1	3	7	28
REF	62	2443	34.3	53.6	60.0	72.0
Pumice2*	45	2378	28.8	46.1	55.8	64.7

*Using normal weight aggregates in air dry state

Table 5 - Strength, specific weight and slump for mixes containing perlite

	Mixing method	Slump, mm	Specific weight, kg/m^3	Strength, MPa			
				1	3	7	28
Perlite2	Manual	30	2362	14.2	33.6	44.5	55.8
	Pan mixer	205	2413	22.8	42.9	51.6	61.4
	Drum mixer	35	2402	21.6	41.4	51.7	67.1

It can be seen that except for the pan mixed perlite mix, all the concretes had a similar range of slump values, reflecting a similar content of free mixing water. The strength development of the perlite concretes was somewhat slower than that of the reference and pumice concrete, but by 28 days it reached a similar strength. The slow beginning may reflect a somewhat adverse effect of the highly porous perlite aggregate. Yet, the fact that this was overcome by 28 days suggests that this effect is easily compensated by the matrix, when it develops its full microstructure at 28 days.

5. Conclusions

The results of the present study indicate that by controlling the size and the porosity of lightweight aggregates, highly efficient systems of internal curing can be obtained. In these systems the presence of the saturated lightweight aggregates can eliminate almost all of the autogenous shrinkage, without any need for external water curing. In the optimized systems the content of the aggregates is sufficiently low to have only a small effect on reduction in strength.

In the extremely high porosity-fine aggregate the optimization is such that the content of aggregate required is about 10 kg/m^3 in the dry state (30 kg/m^3 in the wet state), which is sufficiently small for it to be considered as a curing additive. Addition of small amount of sand-size porous aggregates was effective in eliminating almost all of the autogenous shrinkage.

References

1. A. Bentur, S. Igarashi and K. Kovler, “Control of Autogenous Shrinkage Stresses and Cracking in High Strength Concretes”, Proceeding of International Conference, Norway, pp. 1017-1026.

2. E. Sellevold, Ø. Bjøntegaard, H. Justnes and P.A. Dahl, “High Performance concrete: Early Volume Change And Cracking Tendency”, Proceedings of International RILEM Symposium “Thermal Cracking in Concrete at Early Ages”, Edited by R. Springenschmidt, Munich, Germany, October 1994, pp. 229-236.

3. I. Schrage and T. Summer, “Factors Influencing Early Cracking of High Strength Concrete”, Proceedings of International RILEM Symposium “Thermal Cracking in Concrete at Early Ages”, Edited by R. Springenschmidt, Munich, Germany, October 1994, pp. 237-244.

4. E. Tazawa, Y. Matsuoka, S. Miyazawa and S. Okamoto, “Effect of Autogenous Shrinkage on Self Stress in Hardening Concrete”, Proceedings of International RILEM Symposium “Thermal Cracking in Concrete at Early Ages”, Edited by R. Springenschmidt, Munich, Germany, October 1994, pp. 220-228.

5. D.P. Bentz, K.A. Snyder and P.E. Stutzman, “Microstructural Modeling of Self-Desiccation During Hydration”, Proceeding of an International Research Seminar in Lund “Self-Desiccation and Its Importance in Concrete Technology”, Editors B. Persson and G. Fagerlund, Sweden, 1997, pp. 132-140.

6. E.A.B. Koenders and K. van Breugel, “Modeling Dimensional Changes in Low Water/Cement Ratio Pastes”, Proceedings of an International Research Seminar in Lund, “Self-Desiccation and Its Importance in Concrete Technology”, Editors B. Persson and G. Fagerlund, 1997, pp. 158-173.

7. S. Weber and H.W. Reinhardt, “A Blend of Aggregates to Support Curing of Concrete”, Proceedings of International Symposium on Structural Lightweight Concrete, Edited by I. Holand, T.A. Hammer and F. Fluge, Sandefjord, Norway, 1996, pp. 662-671.

8. S. Weber and H.W. Reinhardt, “A New Generation of High Performance Concrete: Concrete with Autogenous Curing”, Advanced Cement Based Materials 6(1997), 59-68.

9. K. Takada, K. van Breugel, E.A.B. Koenders and N. Kaptijn, “Experimental Evaluation of Autogenous Shrinkage of Lightweight Aggregate Concrete”, Proceedings of International Workshop on Autogenous Shrinkage of Concrete, JCI, Edited by E.Tazawa, June 13-14, 1998, Hiroshima, Japan, pp. 221-230.

10. A. Bentur, S. Igarashi and K. Kovler, “Prevention of Autogenous Shrinkage in High-Strength Concrete by Internal Curing Using Wet Lightweight Aggregates”, Cement and Concrete Research, 31, 2001, pp.1587-1591.

11. F. Collins and J.G. Sanjayan, “Strength and Shrinkage Properties of Alkali-Activated Slag Concrete Containing Porous Coarse Aggregate”, Cement and Concrete Research, 29, 1999, pp. 607-610.

12. K. Kohno, T. Okamoto, Y. Isikawa, T. Sibata and H. Mori, “Effects of Artificial Lightweight Aggregate on Autogenous Shrinkage of Concrete”, Cement and Concrete Research, 29, 1999, pp. 611-614.

13. P. Schwesinger and G. Sickert, “Reducing Shrinkage in HPC by Internal Curing by Using Pre-soaked LWA”, Proceedings of International Workshop on Control of Cracking in Early-Age Concrete, Tohoku University, Japan (2000), pp. 313-318.

14. K. van Breugel, H. Outwerk and J. de Vries, “Effect of Mixture Composition and Size Effect on Shrinkage of High Strength Concrete”, Proceedings of International RILEM Workshop on Shrinkage of Concrete, Paris (2000).

15. P. Lura and K. van Breugel, “Moisture Exchange as a Basic Phenomenon to Understand Volume Changes of Lightweight Aggregate Concrete At early Age”, Proceedings of International RILEM Workshop on Shrinkage of Concrete, Paris (2000).

16. Y. Kitsutaka, M. Tamura, A. Iihoshi and K. Goto, “Early-Age Shrinkage Properties of High-Strength Lightweight Aerated Concrete”, Proceedings of International Workshop on Control of Cracking in Early-Age Concrete, Tohoku University, Japan (2000), pp. 199-204.

17. P. Lura, K. van Breugel and I. Maruyama, “Autogenous and Drying Shrinkage of High-Strength Lightweight Aggregate Concrete at Early Ages – The Effect of Specimen Size”, RILEM Proceedings PRO 23 “Early Age Cracking in Cementitious Systems – EAC’01”, Proc. Intern. RILEM Conf., Haifa, Israel, March 12-14, 2001, Ed. K. Kovler and A. Bentur, RILEM Publications S.A.R.L., 2002, pp. 335-342.

18. S. Zhutovsky, K. Kovler and A. Bentur, “Influence of Wet Lightweight Aggregate on Mechanical Properties of Concrete at Early Ages”, Materials & Structures, 35, 2002, pp. 97-101.

19. D.P. Bentz and K.A. Snyder, “Protected Paste Volume in Concrete. Extension to Internal Curing Using Saturated Lightweight Fine Aggregate”, Cement and Concrete Research, V. 29 (1999), pp. 1863-1867.

20. K. Kovler, “Testing System for Determining the Mechanical Behavior of Early Age Concrete under Restrained and Free Uniaxial Shrinkage”, Materials and Structures, 27, 1994, pp. 324-330.

SELF-DESICCATION AND CHLORIDE MIGRATION

Bertil Persson
Division Building Materials, Lund University, Lund, Sweden

Abstract

In this article 13-year development of the relative humidity, RH, at self-desiccation is dealt with experimentally and analytically. The effect of self-desiccation is related to chloride ingress in view of the requirement for water for the chloride ions to be transported at all. RH is studied for concrete with water-binder ratio, w/b, varying between 0.20 and 0.60, half of the concrete with 10% silica fume. The concrete specimen, 1 m in diameter and 0.1 m long, is either sealed (RH at self-desiccation), air- or water-cured for 13 years. Chloride ingress is studied by migration tests based on a NORDTEST method developed by Tang on concrete with w/b varying between 0.30 and 0.50. Specimens in the chloride study were much smaller, cylinders 0.1 m in diameter and 0.05 m in length. The results show some importance of self-desiccation for the ingress of chlorides in concrete, mainly related to the presence of silica fume. In turn the temperature of the concrete affects RH. However, the cement content plays a more vital role to limit chloride ingress in concrete than self-desiccation or temperature do.

1. Introduction and objective

Self-desiccation has been observed and analysed for concrete for at least 60 years [1]. The consequences of self-desiccation became obvious after the development of superplasticiser, which in turn made it possible to cast concrete with w/b less than 0.40. For concrete with w/b less than 0.40 autogenous shrinkage causes cracking even in submerged concrete [2-10]. However, self-desiccation has also been widely used in Sweden in order to avoid moisture-related problems when applying plastic or rubber flooring with adhesives on concrete with or without plaster [11-29]. High-moisture related reactions between concrete, adhesive and the plastic or rubber flooring in many cases cause high amount of volatile organic compounds, which in turn may cause allergic health injuries to human beings [30]. In cases of a relative humidity, RH < 0.85, moisture-related additional volatile organic compounds are more or less avoided. A NORDTEST method has been introduced in order to verify self-desiccation in concrete [31]. It became quite clear that the chemical shrinkage of water when attached to cement, about 25% by volume, causes an under-pressure in the pore water and subsequently compression in the aggregate of concrete with volumetric external shrinkage as an obvious technical disadvantage [32]. Through time, long-term explorations became available, correlating the affects of self-desiccation such as autogenous shrinkage mainly to w/b and content of silica fume in the concrete [33]. Self-desiccation became an important topic of many international workshops, congresses and conferences connected to the use of High Performance Concrete, HPC [34-45]. Models for shrinkage of normal concrete have been adjusted, more or less successfully, for HPC with low w/b [46-50]. The objective was to present self-desiccation and its effect on chloride migration.

2. Self-desiccation

2.1 General

Normal concrete is regarded as a porous material affected by the ambient climate. Self-desiccation hardly affects the moisture state of normal concrete with w/c > 0.40. In HPC, with w/c $\leq$ 0.40, the rate of hydration is decreased substantially due to self-desiccation. The pore volume created in the concrete due to the chemical shrinkage that takes place when the water is chemically bound to the cement [1] decreases RH as low as 0.70 at low w/c. This low RH may affect several characteristics, primarily hydration and curing. The corrosion of reinforcement and the freeze-thaw resistance are factors affected entirely by the lower moisture content in the concrete. The chloride diffusion is dependent on RH in the concrete as well as the diffusion of gas [51]. Above a certain degree of pore saturation a substantial amount of surface concrete will spall due to ice lenses created in freeze-thaw periods [52,53]. A freeze-thaw resistant concrete must be either air-entrained or contain a sufficient air-filled pore volume developed due to the chemical shrinkage that takes place during the hydration. In this case knowledge of the state of moisture in the concrete is of the utmost importance, too.

2.2 Moisture-related problems

The maximum ambient RH in dwelling houses is normally restricted to RH < 0.70. For houses made of concrete it was considered essential to estimate the time required for the drying of the concrete to achieve this level of RH. When wood is placed directly on the concrete, RH of the concrete must not exceed 0.75 [54] or else the moisture of the concrete can cause mould fungus between the concrete and the wood. These organisms will have secondary effects such as bad smell in the house, allergic reactions etc. When RH > 0.80 the wood starts to rot [54]. At RH > 0.85 funguses may also occur between the plastic carpet and the concrete [54]. Finally, when RH > 0.90 glued carpets may loosen from the concrete due to saturation of the pores (no space for the glue resin to enter or penetrate concrete pores) [54]. The self-desiccating effect of concrete has been used in practice in Sweden since 1990 to avoid these problems in dwelling houses [11,34]. Until today more than three million m^2 of concrete sub-flooring has been made using concrete with w/b < 0.38 for the purpose of obtaining fast desiccation. This method has also been used in Finland [6].

2.3 Theory

Concrete, which is regarded as a fine porous material, has great ability to bind moisture. The higher RH, the more water can be bound. The ability to bind moisture, hygroscopic, depends on either adsorption, at RH < 0.45, or capillary condensation, at RH > 0.45. The water that evaporates during desiccation at 105 °C is denoted evaporable water, w_e. HPC possesses less mixing water than necessary to reach maximum degree of hydration, α = 1. This can only be obtained at a w/c $\geq$ 0.39. The maximum degree of hydration, α, of curing of HPC with a w/c < 0.39 is linearly dependent on w/c [1,7-9,14,55]:

$$\alpha_{max} = w/(0.39 \cdot c) \quad (1)$$

α_{max} denotes the maximum degree of hydration
w denotes the mixing water of the concrete (kg/m³)
c denotes the cement content of the concrete (kg/m^3)

The degree of hydration, α, can also be expressed as:

$$\alpha_{max} = w_n/(0.25 \cdot c) \quad (2)$$

w_n denotes the non-evaporable water content of the concrete (kg/m^3)

Dividing equation (2) by equation (1) gives the maximum value of the relative hydration defined as (the symbols are given above):

$$(W_n/w)_{max} = 0.64 \quad \{0 < w/c < 0.39\} \quad (3)$$

$$(W_n/w)_{max} = 0.25 \cdot c/w \quad \{w/c > 0.39\} \quad (4)$$

2.4 Models

Models for self-desiccation of Portland cement or silica fume concrete are normally based on w/c and time. Few well-known relationships related to self-desiccation exist [29,48]:

$$RH(t,w/c) = 1.09 \cdot (w/c)^{0.17 \cdot (1+0.0451 \cdot t)} \quad \{R^2 = 0.54\} \quad (5)$$

$$RH(t,w/c)_s = 1.13\,[1-0.065 \cdot \ln(t)] \cdot (w/c)^{0.24 \cdot [1-0.1 \cdot \ln(t)]} \quad \{R^2 = 0.76\} \quad (6)$$

t denotes the age of the concrete {1<t <15 months}
w/c denotes the water-cement ratio {0.22<w/c <0.58 }
s denotes 10% silica fume

RH(t,w/c) denotes RH in sealed-cured Portland cement concrete
$RH(t,w/c)_s$ denotes RH in sealed-cured concrete with 10% silica fume

$$RH(wbr_{eff}, t) = 0.38 \cdot [w/(c+2 \cdot s) + 2.4 - 0.1 \cdot \ln t] + \Delta RH_{sl} \quad \{R^2 = 0.83\} \quad (7)$$

c denotes the cement content in the concrete (CEM I, kg/m^3)
s denotes the content of silica fume in the concrete (kg/m^3)
t denotes the age of the concrete {1<t<1000 days}

w denotes the water content in the concrete (kg/m^3)
ΔRH_{sl} = - 0.035 for 5-10% silica fume slurry at age, t≤ 28 days

$RH=0.965\cdot t^{\,0.0188}\cdot(w/c)^{0.0331\cdot\ln(t)+0.0505}$ {1<t<1000 days; 0.25<w/c<0.38; R^2 = 0.53} (8)

In Figures 1-4 typical examples of self-desiccation are given for concretes with w/c varying between 0.25 and 0.57 and (in the case of 10% silica fume) with w/b varying between 0.22 and 0.51, i.e. silica fume only applies for the notations RHs and RHwb. Blended cement with 10% silica fume had a substantial effect on the self-desiccation of concrete, Figures 1-4.

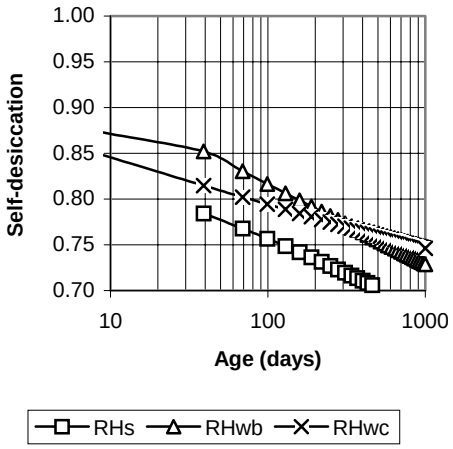

Figure 1 – Self-desiccation with c = 500 kg/m³(s = 50 kg/m³) and w = 125 kg/m³.

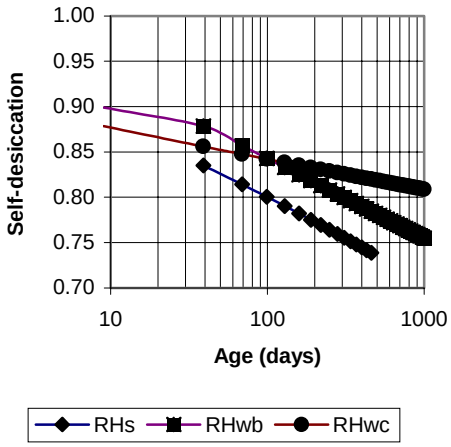

Figure 1 – Self-desiccation with c = 450 kg/m³(s = 45 kg/m³) and w = 150 kg/m³.

The chemical composition of the cement had a substantial influence on the measured self-desiccation mainly due to the so-called alkali-effect. Recently it was shown that a significant relationship exists between the C_3A and C_4F content and autogenous shrinkage [29]. The influence of these components was ten times as large as that of C_2S and C_3S. Based on estimations of ΔRH and the degree of hydration shown in Table 1, the following equation was obtained [29,56]:

$$-\Delta RH = 6\cdot\Delta(C_3A)\cdot\alpha_{C3A} + 8.6\cdot\Delta(C_4AF)\cdot\alpha_{C4AF} - k\cdot\Delta(K_2O). \quad (9)$$

k constant given in Table 1
Δ denotes difference in a property between low-alkali and normal-alkali cement
α denotes degree of hydration
RH denotes the internal relative humidity

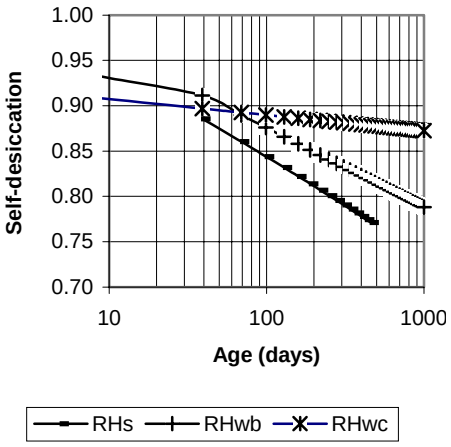

Figure 3 – Self-desiccation with c = 400 kg/m³(s = 40 kg/m³) and w = 175 kg/m³.

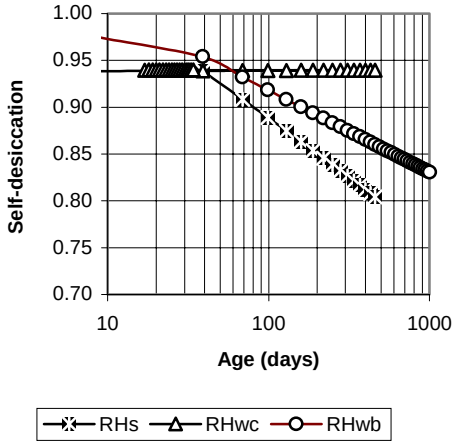

Figure 4 – Self-desiccation with c = 350 kg/m³(s = 35 kg/m³) and w = 200 kg/m³.

Table 1 - Adopted 28-day degree of hydration in estimation of equation (9) [29,56].

+w/c	α_{C3A}	α_{C4AF}	k
0.32	0.67	0.45	-5
0.38	0.74	0.53	-4.7
0.50	0.83	0.62	-6.6
0.65	0.93	0.74	-9.9

2.5 Test methods

The following procedure applies [21-23]:

1. Fragments from a specimen, minimum 75 mm in diameter, which is drilled out of the concrete, are used for the self-desiccation measurements.
2. The use of fragments eliminates possible faults, which may result from differences in the development of self-desiccation within the specimen, Figure 5 [10,46].
3. Fragments are put in a glass tube with minimum length 10 times the diameter of the sensor, Figure 6 [10,46].
4. The diameter of the glass tube is slightly bigger than the diameter of the sensor.
5. Each glass tube is quickly filled each with fragments obtained from different depths from the surface of the concrete specimen.
6. After the glass tube is filled a rubber plug is placed directly, Figure 6.
7. The temperature of all the material and the equipment is held at 20 ± 0.1 °C.
8. One day in advance of the measurement the fragments are to be held at 20 ± 0.1 °C.
9. When a capacity sensor is used the measurement time of RH is 1 day, Figure 7.
10. When a dew point meter is used the measurement time of RH is 2 days

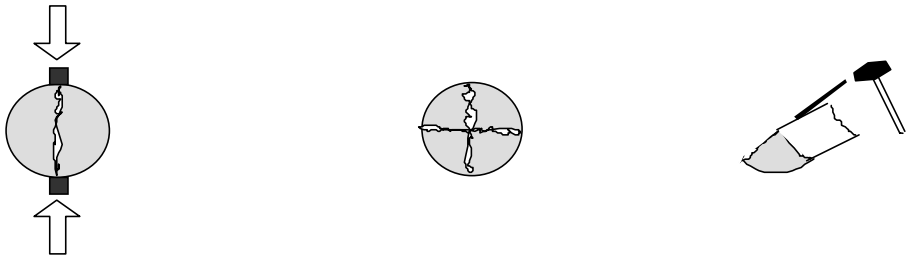

Figure 5 - Concrete pieces collected from the specimen and placed in glass tubes that in turn were sealed by rubber plugs [10,46].

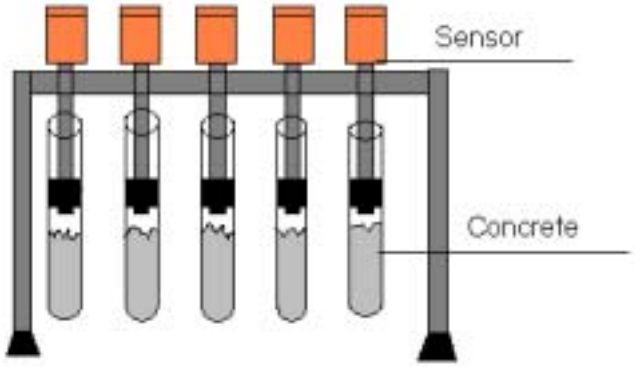

Figure 7 - RH measurements in tubes sealed the glass by an expanding rubber ring. Measurement: 1 day with capacity sensors or 2 days with dew point meters [10,46].

2.6 Calibration of RH-sensor

The accuracy of measurement of RH depends mainly on the calibration of the sensors, and (in the field) also greatly on possible ambient temperature differences (1 °C difference between temperature of sensor and concrete results in an error of about 6% RH). Therefore field measurements are neither accurate nor recommended for scientific purposes. They can serve only as an indication. Final RH must be measured in a temperature-stable laboratory climate of ± 0.1 °C. Moisture measurement sensors are calibrated according to the following procedure [10,46], Figure 8:

1. With salt solutions at 20 °C and at:
   RH = 0.331 (Magnesium Chloride),
   RH = 0.755 (Sodium Chloride),

RH = 0.851 (Potassium Chloride),
RH = 0.946 (Potassium Nitrate) and
RH = 0.976 (Potassium Sulphate)

2. A saturated solution of the salts mentioned above is used
3. Calibration takes place within 1 month of the time of measurement [10,46]
4. The temperature of the material and the equipment is held constant at 20 ± 0.1 °C
5. The calibration time is to be ample for RH to stabilise at each level, normally 1 day
6. The accuracy of the sensors is to be within ± 0.015 RH
7. No drift of the sensors is to be observed or systematic errors may occur
8. Mechanical humidity generators must be calibrated by salt solutions once a year

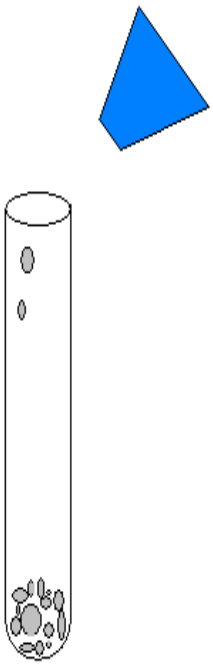

Figure 6 –Pipe is to be filled to 2/3 with fragments of concrete and then tightened at once [10,46].

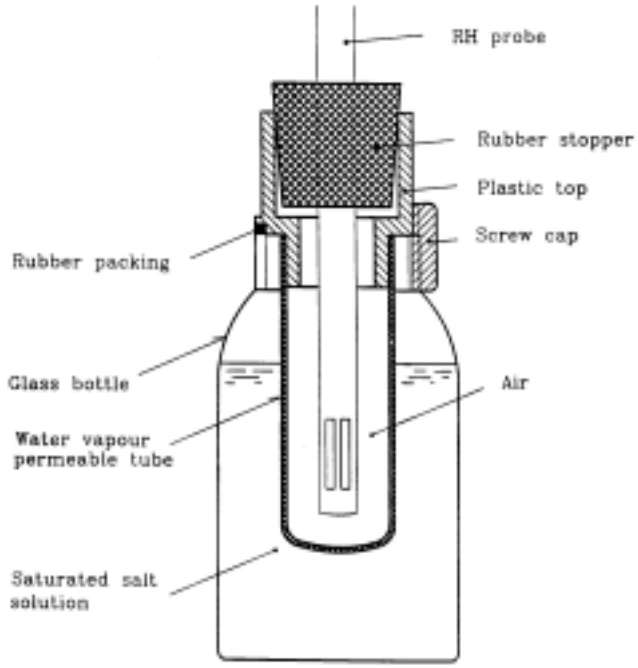

Figure 8 – Set-up for salt container and sensor during calibration [10,46].

2.7 Effect of temperature on RH

An external increase of temperature by 1 °C in the air decreases RH by about 6%. An internal increase of temperature works in the opposite direction, i.e. increases RH. Since

water increases more than the concrete matrix, RH in concrete will also increase with the temperature, at any rate between 0 °C and 100 °C. The most extreme example of this phenomenon is the formation of water in concrete during fire exposure [57]. Even in dry concrete free water is formed during accidental fire. When temperature increases RH also increases and the water moves from the concrete surface towards the inner part of the concrete. Once RH = 1 the water vapour is transformed into water and the pressure increases in the concrete pores above the external. The pressure may increase until the tensile strength is reached in the concrete, Figure 9 [57].

RH-increase with temperature may also affect other concrete properties such as shrinkage, chloride migration, thermal dilatation coefficient and so forth. RH due to chemical shrinkage and autogenous shrinkage certainly are temperature-dependent properties [16,58]. At 20 °C the influence of temperature on RH is given in Figure 10 and 11, varying between 0.1%RH/°C (w/c = 0.70) and 0.3%RH/°C (w/c = 0.40). In Figure 11 the average of 5 tests of concrete with w/c = 0.37, 0.48 and 0.76 are shown [59]. At low w/c, when self-desiccation occurs in concrete, the influence of temperature may be even larger than 0.3%RH/°C.

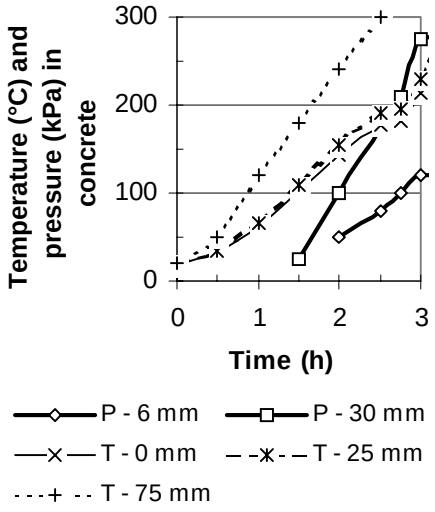

Figure 9 - The pressure increases until the tensile strength is reached in the concrete.

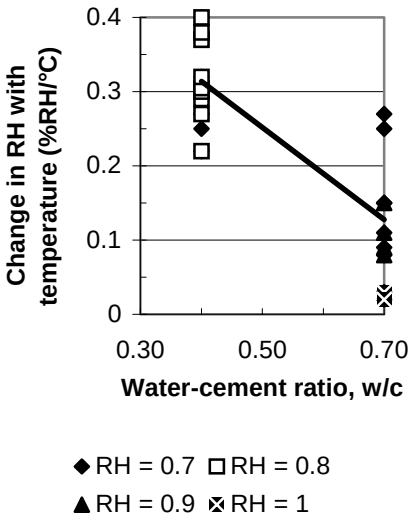

Figure 10 – Change of RH versus w/c at 20 °C (%RH/°C) [16,58].

Based on Figures 10 and 11, the following relationship was evaluated [16,58,59]:

$$\delta RH/\delta T = 0.6\ (1- w/c) \qquad \{R^2= 0.64\} \qquad (10)$$

w/c denotes water-cement ratio {0.35 < w/c < .075}
δRH/δT denotes change in RH with temperature (%RH/°C) {15 < T < 25 °C}

However, the tests shown in Figures 10 and 11 only cover a limited temperature field. The influence of temperature on RH may be different for other temperatures. Knowledge in this field is lacking but required in order to fully understand in turn the effect of self-desiccation on autogenous shrinkage. The influence on RH due to the curing conditions for different kinds of studies is also quite different, as shown in Table 2.

Table 2 - The influence on RH due to the curing conditions for different kinds of studies.

Influence	Laboratory	Cast on site	Prefabricated element
Temperature (max, °C)	25	40	55
Long-term temperature (°C)	20	10	15
Difference from curing (°C)	-5	-30	-40
Influence on RH (%)	-1.5	-9	-12
Final RH (%)	75	75	75
Effect on RH (%)	20	11	8

Since the RH-influence is quite different in the field and in the laboratory due to the temperature conditions, this ought to be taken into account when dimensioning structures for autogenous shrinkage (in practice the influence of autogenous shrinkage after demoulding is much less than observed in the laboratory). The higher the temperature during curing, the less the influence on RH and autogenous shrinkage will be, Figure 12.

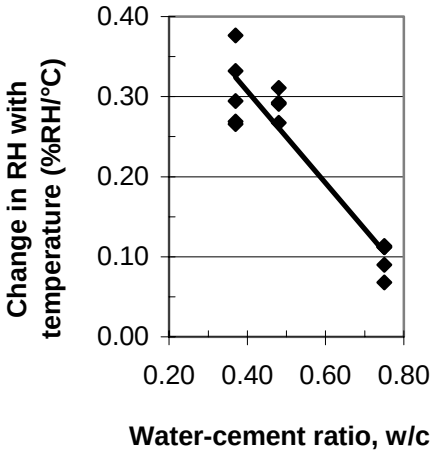

Figure 11 – Change of RH versus w/c at 15-20 °C (%RH/°C) [59]. Fifteen tests.

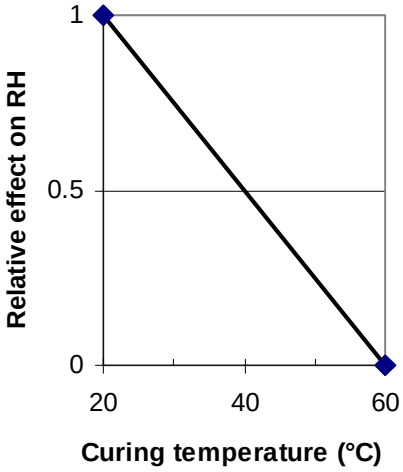

Figure 12 – Effect on RH (autogenous shrinkage) of curing temperature.

2.8 Long-term self-desiccation

A 7-year study of the effect of ageing on self-desiccation 50 mm from the surface of simulated concrete columns 1 m diameter is shown in Figure 13 [15,17,22,28]. The shortage of space in concrete with low w/c will actually stop both hydration and chloride ingress hand in hand with the effect of self-desiccation in the cover layer of the reinforcement. The cover layer of reinforcement exceeds 50 mm in severe conditions. Figure 14 shows the 13-year development of RH at self-desiccation of the same type of columns (9 drilled cores of each concrete, 250 mm from the surface of the 1-m simulated column). Figure 15 shows RH at the same location of drilled cores taken 250 mm from the surface of the 1-m simulated column as a function of w/c. After 13 years of curing the following relationships for RH were obtained, 250 mm from the surface of concrete columns, 1 m in diameter at self-desiccation (S), air (A) or water (W) curing versus w/c:

$$RH_A = 0.905 \cdot (w/c)^{0.232} \quad \{R^2 = 0.93\} \quad (11)$$

$$RH_S = 0.956 \cdot (w/c)^{0.199} \quad \{R^2 = 0.82\} \quad (12)$$

$$RH_W = 0.844 \cdot (w/c)^{-0.0152} \quad \{R^2 = 0.53\} \quad (13)$$

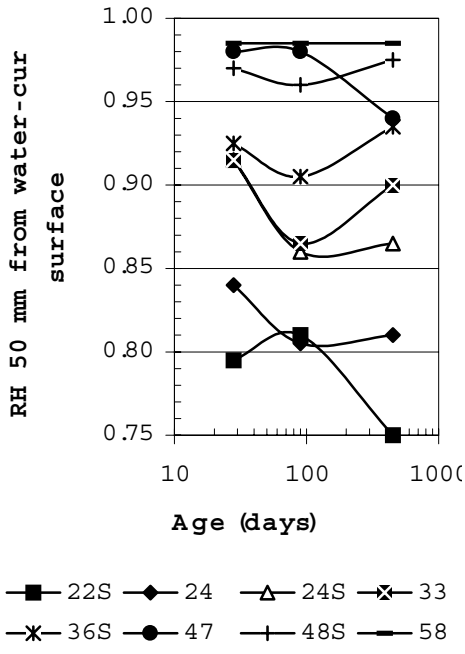

Figure 13 - RH 50 mm from water of 1-m simulated columns vs age [15,17,22,28].

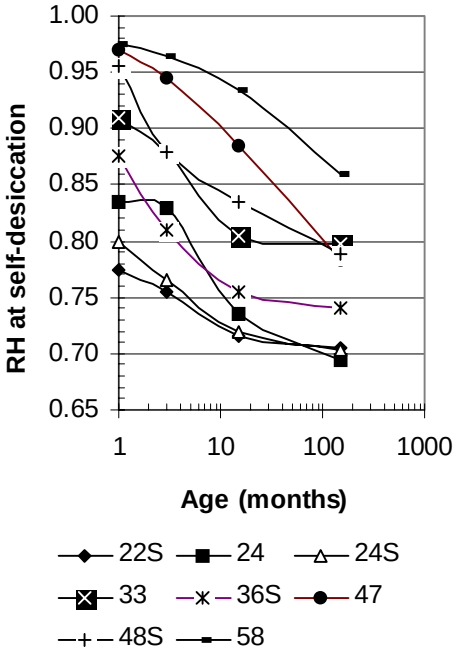

Figure 14 – RH at self-desiccation after 13 years. S = 10% silica fume; 20 = w/c (%).

3. Chloride migration coefficient, D

3.1 General

Buenfeld called attention to the detail that chlorides could not be transported in air [60]. During self-desiccation in concrete with low w/c, chlorides may be transported from the surface of the concrete to the depth of liquid water front but no further, since the pores at self-desiccation are disconnected by air-filled voids. For concrete presently being used in severe environments, i.e. with low w/c $\leq$ 0.40, the depth of water ingress varies from 20 up to 50 mm even after 2 years of exposure, Figure 16 [61]. As close as 10 mm from the exposed surface there seemed to be a substantial self-desiccation even after 2 years. The question was whether the self-desiccation would be only temporary and the pores finally saturated by water and then also by chlorides. After 13 years of water exposure the concrete is not saturated 250 mm from the exposed surface, anyhow, Figure 15. RH did not exceed 90% even at high w/c. No significant difference was obtained between concrete with silica fume or without, i.e. no effect of silica fume on RH after 13 years was not observed at all. In marine environments the temperature is about 10 °C lower than in the laboratory that decreases RH with 3%.

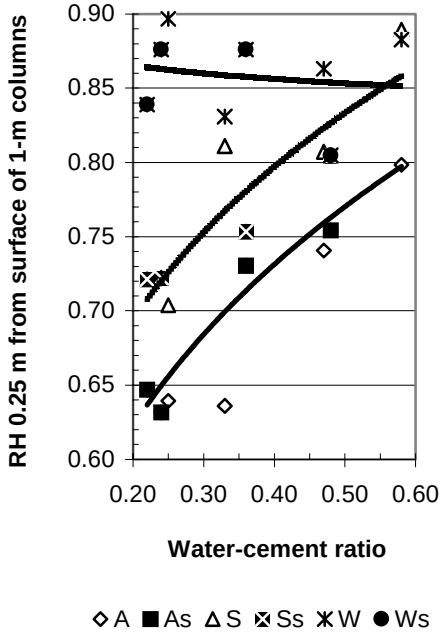

Figure 15 – Thirteen-year RH at self-desiccation (S), air (A) or water (W) curing versus w/c. s = 10% silica fume.

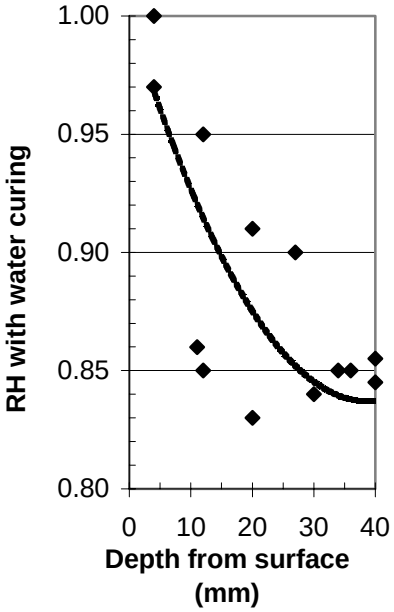

Figure 16 - RH measured after 2 years vs depth from water-cured surface (w/b=0.4, 5% SF) [61].

3.2 Long-term chloride ingress

In another extreme long-term study the 17-year effect of ageing on the chloride diffusion coefficient was shown on the Farø Bridge, Denmark, Figure 17 [62]. The concrete with 12% fly ash but no silica fume had w/b = 0.42 (1:1). According to measurements on drilled cores by grinding D remained at 0.7 x 10^{-12} m²/s even after 17 years. The chloride ingress was then 40 mm at 0.1% chloride content (the cover layer of the concrete being 50 mm). The surface chloride content was not affected by ageing, about 1% chlorides in the concrete surface [62]. Reinforcement corrosion owing to chloride ingress will normally be slowed down by use of concrete with sufficiently low w/b < 0.40, an adequate concrete cover provided that the surface is free from cracks [63]. Self-desiccation probably played an important role in delaying the chloride ingress. Formulas in general use for estimating the chloride ingress were introduced some 30 years ago for water-saturated structural concrete in use at that time, i.e. with w/c > 0.40. These formulas do not account for self-desiccation since concrete with sufficiently low w/c was not in use at the time [64]. A great step in the understanding D in concrete with w/c > 0.40 was taken when the binding capacity related to the cement content was clarified [51]. Rapid tools for examining concrete were a great advantage when optimising concrete in use under severe conditions [65]. Different models for estimating chloride ingress were put forward but still the relation to self-desiccation was not considered nor understood [66,67].

3.3 Test method

Between drilling and testing the specimens were stored in water saturated with limestone powder. The determination of D was performed in an apparatus developed by Tang [67]. After sawing, brushing and washing away any burrs from the surface of the specimen, excess of water was wiped off the surface of the specimen. When the specimens were surface-dry, they were placed in a vacuum container to a pressure in the range of 1-5 kPa within a few minutes [67]. The vacuum was maintained for 3 h, and then, with the vacuum pump still running, the container was filled with water saturated with $Ca(OH)_2$ in order to immerse the specimen. The vacuum was maintained another hour before air was allowed to enter the container. Part of the effect of self-desiccation was probably eliminated by the vacuum treatment. However, studies on HPC with 25 mm thickness show that water penetrated the specimen rapidly [11]. However, water did not penetrate 50 mm thick HPC with low w/c, not even after 450 days [11]. The situation may be the same for the specimen used for studies of D, which also is 50 mm in thickness [67]. After vacuum treatment the specimen was kept in the water saturated with $Ca(OH)_2$ solution for 18 h. The catholyte solution was 10% NaCl (100 g NaCl in 900 g water, about 2 N) and the anolyte solution 0.3M NaOH in distilled water (about 12 g NaOH in 1 l water). The catholyte solution, 10% NaCl, was poured to fill the 12-l container. A rubber sleeve was assembled to the specimen. The specimens was placed on the plastic support in the catholyte reservoir (10% NaCl). The sleeve was filled with 300 ml anolyte (0.3 M NaOH). An anode was immersed into the anolyte solution. The chloride penetration depth was determined by measuring three cut specimens, Figure 18-19 [67].

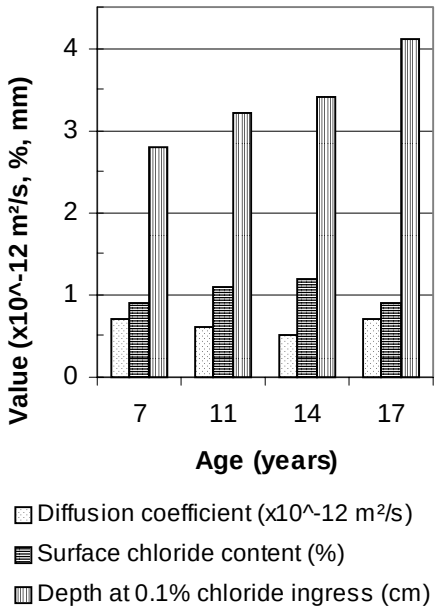

Figure 17 – Seventeen-year chloride diffusion coefficient on Farø Bridge [62].

Figure 18 - A rubber sleeve assembled to the specimen that was cut afterwards.

3.4 Modelling

The following equation was used to calculate the chloride migration coefficient, D [67]:

$$D = 0.0239 \cdot (273+T) \cdot L \cdot / [(U-2) \cdot t] \cdot \{x_d - 0.0238 \cdot [(273+T) \cdot L \cdot x_d)/(U-2)]^{1/2}\} \quad (14)$$

t denotes the test duration (h)
x_d denotes the average chloride penetration depth (mm)
D denotes the non-steady-state migration coefficient, x10 $^{-12}$ m²/s
L denotes the thickness of the specimen (mm)
T denotes the average initial and final temperatures in the anolyte solution (°C)

After broad studies a relationship was found between D, cement content and w/b [68]:

$$D = \{[(0.0055 \cdot \ln(t) - 0.2122) \cdot c - 3.5 \cdot \ln(t) + 104] \cdot (4 \cdot w/b - 1.2)/0.4\} \cdot (10^{-12}) \ \{R^2 = 0.88\} \quad (15)$$

c denotes the cement content ($375 < c < 450$ kg/m³)
ln(t) denotes the natural logarithm of concrete age ($1 < t < 36$ months)
w/b denotes the water-binder ratio, 1:1 ($0.35 < w/b < 0.50$)

4. Discussion

As shown above, chlorides cannot be transported in the air or in voids of vacuum that were obtained due to self-desiccation. However, it is not feasible to measured RH in concrete during chloride transport since water is required for this transport to take place. Therefore D from several tests [68-72] was related to RH with self-desiccation, equation (7). Factors of the efficiency factor (effect of 1 kg additive to the effect of 1 kg cement on the chloride migration coefficient, D) shown in equation (16) were used in order to estimate RH with self-desiccation in equation (6) [69,70]:

$$c_{eq.} = c + 0{,}21 \cdot fl + 1{,}6 \cdot sf + 1{,}03 \cdot sl \qquad \{R^2 = 0{,}81\} \qquad (16)$$

$c_{eq.}$ denotes the equivalent amount of cement to be used in equation (7)
c denotes amount of Portland cement
fl denotes the amount of fly ash
sf denotes the amount of silica fume
sl denotes the amount of slag

At water-binder ratios varying between 0.30 and 0.40 it seemed as if it was an advantage to add about 17% fly ash in concrete with 5% silica fume in order to further decrease the chloride migration coefficient [69,70]. At 10% addition of fly ash in the concrete the effect was more dubious [69,70].

In resource-saving concretes a lot of the cement was replaced by silica fume and fly ash. Even though the water-binder ratio (1:1) was larger in concrete with additives the chloride migration coefficient was substantially lower, less than one third of that of concrete based on pure Portland cement, one fourth with 40% fly ash and 5% silica fume. The dependence of the cement content on D was dominating besides the effect of RH, Figure 20. The following formula was calculated in order to describe the effect of self-desiccation on the chloride migration coefficient, D, taking into account the cement content ($x10^{12}$ m^2/s):

$$D = 3000 \cdot e^{-0{,}0118 \cdot c} \cdot (RH)^{0{,}04 \cdot c - 9{,}1} \qquad (17)$$

c denotes cement content ($375 < c < 450$ kg/m^3)
RH denotes the internal relative humidity with self-desiccation, equation (16)

The question was whether self-desiccation would be temporary and the pores finally saturated as well by chloride. Two different concrete mixes based on the different cements and pozzolans having the same active porosity can have very different shape of the pore system, therefore resulting in different tortuosity factors [73]. The relation between the binding capacity of chlorides and the cement content follows the same pattern as the relation between the tortuosity factor and porosity, i.e. for the same type of cement and Pozzolan-based concrete with different w/b ratios the binding capacity decreases with the cement content [73]. Figure 21 shows results with equation (17).

Figure 19 - The chloride penetration depth determined by measuring three cut specimens with silver nitrate [67].

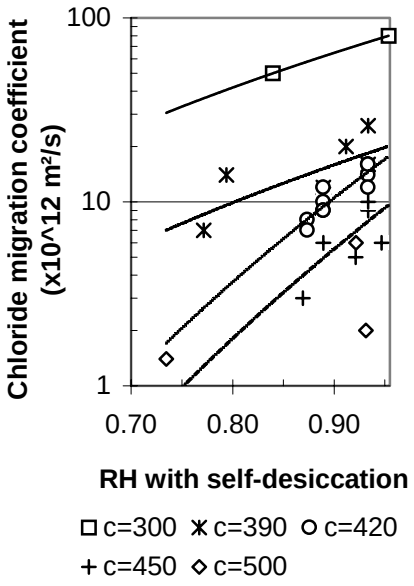

Figure 20 – Chloride migration coefficient, D, measured acc. to [5,10] and self-desiccation calculated acc. to equation (5).

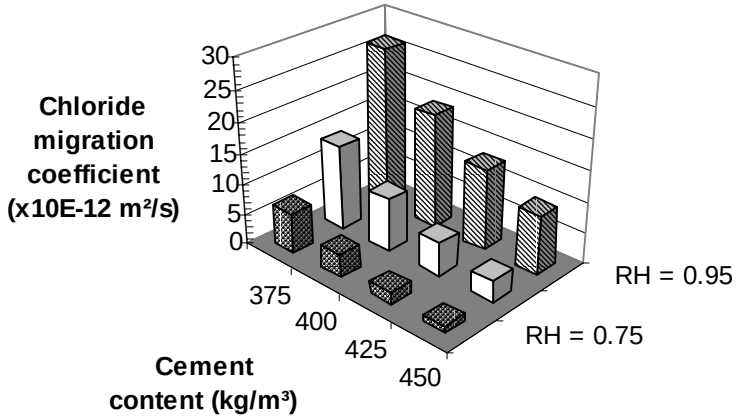

Figure 21 – Influence of RH and cement content on D with equation (17).

5. Summary and conclusions

Extensive studies of self-desiccation in concrete over 13 years were presented coupled to studies on chloride ingress. The following conclusions were drawn:

1. After 13 years' self-desiccation with RH = 0.70 at low w/c = 0.20 and RH = 0.90 at w/c = 0.60 was observed
2. Even after 13 years of water exposure a 1-m concrete column was not saturated by water, 0.25 m from the surface but RH = 0.90 was obtained even at w/c = 0.60
3. Correlations were observed between RH and chloride ingress in concrete
4. Since saturated conditions are a condition for chlorides to be transported the ingress of chlorides may be stopped more or less at low w/c where self-desiccation occurs
5. It seems as if the cement content of the concrete is much more important than the effect of self-desiccation since cement has its ability to bind chlorides
6. The effect of temperature on RH and then also on self-desiccation and autogenous shrinkage is often foreseen, and this effect may explain differences in measured chloride ingress in the field and at laboratory conditions since the curing temperature in the field is higher.

References

[1] Powers, T.C., Brownyard, T.L., Studies of Physical Properties of Hardened Portland Cement Paste, Research Laboratories, PCA **22,** 194, 473-488, 845-864 (1946-1948).

[2] Tazawa, E., Miyazawa, S., Effect of Constituents and Curing Conditions on Autogenous Shrinkage of Concrete, Proc. Int. Workshop, Hiroshima, 269-280 (1998)

[3] Sellevold, E., Bager, D., Klitgaard-Jensen, E., Knudsen, T., Silica Fume-cement pastes: hydration and pore structure. Proceedings of a Nordic Seminar on Silica Fume in Concrete, Cement and Concrete Research Institute, The Norwegian Institute of Technology, Trondheim, Norway (1981).

[4] Nilsson, L.-O., Desorption Isotherms for Silica-Fume/Cement Mortars, Report IF 8431, Institute of Moisture Issues on Material & Building Technology, Trelleborg, Sweden, pp 2-11 (1984).

[5] Christoffersen, A. K., Sørensen, T. B., Nielsen, A., Self-Desiccation of Concrete, Danish Concrete Magazine Beton, No **4** (1988).

[6] Penttala, V., Merikallio, T., Wirtanen, L., Early Floor Covering of Concrete Slabs and Adhesion between Concrete and Floor Covers, Proc. 5th Nordic Concrete Research Meeting: Helsinki, Ed: Norsk Betongforening, Oslo, 107-108 (1996).

[7] Geiker, M. Studies of Portland Cement Hydration, Measurement of Chemical Shrinkage and a Systematic Evaluation of Hydration Curves by Means of Dispersion model, PhD Thesis, The Institute of Mineral Industry, The Technical University of Denmark, Lyngby, 107-117 (1983).

[8] Christoffersen, A.K.; Sørensen, T.B., Self-Desiccation and Chemical Shrinkage of Cement Mortar, Technical Report no 158/86, The Technical University of Denmark, Dep. Civil Eng. Building Materials Laboratory, Lyngby, 56-61 (1986).

[9] Hooton, D., Chemical Shrinkage of Cement Pastes with or without Silica Fume, 93rd Annual Meeting of the American Ceramic Society, Westerville (1991).
[10] Hansen, E. J., Hansen, K. K., Persson, B., Concrete, hardened: Self-desiccation. Nordtest Method NT Build 490, NORDTEST OY, Espoo, Finland, 8 pp. (1999).
[11] Persson, B., Hydration, Structure and Strength of High-Performance Concrete. Report TVBM-1009. Division of Building Materials. Lund Institute of Technology. Lund University. Lund. 400 pp. (1992).
[12] Persson, B., Quasi-instantaneous and Long-term Deformations of High-Performance Concrete with Some Related Properties. Report TVBM-1016. Division of Building Materials. Lund Institute of Technology. Lund University. Lund. 500 pp. (1998).
[13] Aevarsson, M., Rahim, A., High-Performance Concrete – Time of Desiccation as Compared to Normal Concrete, Report TVBM-5025, Division of Building Materials. Lund Institute of Technology, Lund University, Lund, 50 pp. (1993).
[14] Persson, B., Hydration and Strength of High-Performance Concrete. Advanced Cement Based Materials **3**, 107-123 (1996).
[15] Persson, B., Seven-year Study of the Effect of Silica Fume in Concrete. Advanced Cement Based Materials **7**, 139-155 (1998).
[16] Persson, B., Self-desiccation and Its Importance in Concrete Technology, Materials and Structures **30**, 293-305 (1997)
[17] Persson, B., Moisture in Concrete Subjected to Different Kinds of Curing, Materials and Structures **30**, 533-544 (1997).
[18] Persson, B., Long-term Effect of Silica Fume on the Principal Properties of Low-Temperature-Cured Ceramic, Cement and Concrete Research **27**, 1667-1680 (1997).
[19] Persson, B., Experimental Studies on Shrinkage in High-Performance Concrete. Cement and Concrete Research. **28**, 1023-1036, (1997).
[20] Persson, B., Chemical Shrinkage and Self-Desiccation in Portland Cement Based Mortars. Concrete Science and Engineering **1**, 228-237 (1999).
[21] Persson, B., Basic Deformations of High-Performance Concrete at Early Ages. Nordic Concrete Research **20**, 59-74 (1997).
[22] Persson, B., Self-desiccation and Its Importance in Concrete Technology. Nordic Concrete Research **20**, 1998 (120-129).
[23] Persson, B., Effect of Cement Type, Silica Fume, Water-cement Ratio, Age and Moderate Shift in Temperature on Self-desiccation in Concrete, Nordic Concrete Research. 21. 97-116. 1999,
[24] Persson, B., Pozzolanic Interaction between Portland Cement and Silica Fume in Concrete, Sixth CANMET/ACI International Conference on Fly Ash, Silica Fume, Slag and Natural Pozzolans in Concrete, 631-660 (1998).
[25] Persson, B., Shrinkage of High-Performance Concrete, Proceedings of an International Workshop on Autogenous Shrinkage of Concrete, Hiroshima, Ed: E Tazawa, 101-118 (1998).
[26] Persson, B., Long-term Shrinkage of High-Performance Concrete. Proceedings of the 10th International Congress on the Chemistry of Cement. Contribution 2ii073. Gothenburg, Ed. by H Justnes, 9 pp. (1997).

[27] Persson, B., Strength and Shrinkage of Self-compacting Concrete, Proceedings of an International RILEM Workshop on Shrinkage in Concrete, Paris, Ed. by V Baroghel-Bouny and P-C Aïtcin, 81-99 (2000).
[28] Persson, B., Shrinkage of High Performance Concrete. Proceedings of an International RILEM Conference on Early Age Cracking in Concrete. Haifa, Ed. by A Bentur, 301-311 (2001).
[29] Persson, B., Consequence of Cement Constituents, Mix Composition and Curing Conditions for Self-Desiccation in Concrete, Materials and Structures **33**, 352-362 (2000).
[30] Persson, B., Compatibility between Flooring Materials and Concrete. Materials and Structures **35**, 170-182 (2002).
[31] Persson, B., A NORDTEST Method for Verification of Self-desiccation in Concrete. Cement and Concrete Research. **31**, 199-203 (2001).
[32] Persson, B., On the Under-Pressure in the Pore Water of Sealed High Performance Concrete, Concrete Science and Engineering **2**, 213-221, (2000).
[33] Persson, B., Eight-Year Exploration of Shrinkage in High-Performance Concrete. Cement and Concrete Research, 12 pp. (Accepted for publication, 2002.)
[34] Persson, B., Self-Desiccation of High-Strength Concrete Slabs, Proceedings at the 3rd International Symposium of High-Strength Concrete in Lillehammer, Norway, The Norwegian Concrete Association, Oslo, Ed. by I Holand and E Sellevold, 882-889 (1993).
[35] Persson, B., Self-Shrinkage and Reversible Creep of High-Strength Concrete. Proceedings of the Nordic Research Meeting, Gothenburg, The Norwegian Concrete Association, Oslo, Ed. by L-O Nilsson, 59-61 (1993).
[36] Persson, B., Self-Desiccation of High-Strength Concrete Slabs, Proceedings of the Nordic Research Meeting, Gothenburg, The Norwegian Concrete Association, Oslo, Ed. by L-O Nilsson, 62-64 (1993).
[37] Persson, B., Shrinkage of Filler-Optimised High-Performance Concrete, Contribution at the 16th Symposium on Nordic Concrete Research, Helsinki, Finland, The Norwegian Concrete Association, Oslo, Ed. by K Söderlund, 85-87, (1996).
[38] Persson, B., Effect of Silica Fume on Self-Desiccation and Strength, Contribution at the 16th Symposium on Nordic Concrete Research, Helsinki, Finland, The Norwegian Concrete Association, Oslo, Ed. by K Söderlund, 128-130 (1996).
[39] Persson, B., Experimental Studies of the Effect of Silica Fume on Chemical Shrinkage and Self-Desiccation in Portland Cement Mortars, Proceedings of an International Research Seminar on Self-Desiccation and Its Importance in Concrete Technology, Division of Building Materials, Lund Institute of Technology, Lund University, Lund, Ed. by B Persson and G Fagerlund, 116-131, (1997).
[40] Persson, B., The Effect of Silica Fume on the Principal Properties of Concrete, Symposium on Advanced Design of Concrete Structures, Gothenburg, CIMNE. Barcelona, Spain, Ed. by K Gylltoft; B Engström; L-O Nilsson, N-E Wiberg and P Åhman, 161-168 (1997).

[41] Persson, B., Creep and Shrinkage in Young or Mature High Performance Concrete, Proceedings of the 5th International Symposium on Utilisation of High-strength/High-performance Concrete, Sandefjord, The Norwegian Concrete Association, Oslo, Ed. by I Holand and E Sellevold, 1272-1281 (1999).
[42] Persson, B., Influence of Mix Design on Self-desiccation in Concrete. Self-Desiccation and Its Importance in Concrete Technology, Co-editor. Report TVBM-3085. Division of Building Materials, Lund Institute of Technology. Lund University, Lund, 85-108 (1999).
[43] Persson, B., Specific Volume of Chemically Bound Water and Self-desiccation in Silica Fume and Portland Cement Based Mortars, Contribution at a Nordic Mini Seminar on Hydration of Cement, Skagen, 19 pp. (1999).
[44] Persson, B., Ninety-month Pozzolanic Interaction between Portland Cement and Silica Fume in Concrete, Contribution at a Nordic Mini Seminar on Hydration of Cement, Skagen, 25 pp. (1999).
[45] Persson, B., Shrinkage of High-Performance Concrete, Proceedings of an International Workshop on Autogenous Shrinkage of Concrete, Hiroshima, Ed: E Tazawa, 101-118 (1998).
[46] Persson, B., Chemical Shrinkage and RH Tests, Contribution to the RILEM Technical Committee EAC, Early Age Cementious Systems Ed.: Arnon Bentur 257-275 (2002).
[47] Persson, B., Shrinkage of Concrete, Contribution to the RILEM Technical Committee EAS, Early Age Cementious Systems, Ed.: Arnon Bentur, 102-114 (2002).
[48] Persson, B., Self-desiccation, Chapter 9.4, Contribution to the fib Technical Committee 8.2, Ed.: Harald Müller, 16 pp., (2001).
[49] Persson, B., Validation of Fédération International de Béton, fib, 2000 Model for Shrinkage in Normal and High-Performance Concrete, HPC, Proceedings of CONCREEP6, Boston, Ed. by F-J Ulm, Z Bazant and F.H. Whittmann, Elsevier, 741-746 (2001).
[50] Persson, B., Validation of Fédération International de Béton, fib, 2000 Model for Shrinkage in Normal and High-Performance Concrete, HPC, Report TVBM-7157, Division of Building Materials, Lund Institute of Technology. Lund University. Lund, 108 pp., (1999).
[51] Tuutti, K., Corrosion of Steel in Concrete, Report Fo 4:82, The Cement and Concrete Research Inst., Stockholm, 277-286, 302-303 (1982).
[52] Fagerlund, G., The Critical Degree of Saturation Method - A General Method of Estimating the Frost Resistance of Materials and Structures, Report Fo 12:76, The Cement and Concrete Research Inst., Stockholm (1976).
[53] Fagerlund, G., Influence of Environmental Factors on the Frost Resistance of Concrete, TVBM-3059, Lund Inst. of Technology, Lund, 19-22 (1994).
[54] Nilsson, L.-O., Moisture Problems at Concrete Floors, TVBM-3002, Lund Inst. of Technology, Div. of Building Materials: Lund, 36-51 (1980).
[55] Persson, B., Hydration, Structure and Strength of HPC, Laboratory Data, TVBM-7011, Lund Inst. of Technology, Div. of Building Materials, Lund, 37-58 (1992).

[56] Tazawa, E. and Miyazawa, S., Effect of Cement Composition on Autogenous Shrinkage in Concrete, Proceedings of the 10th International Congress on the Chemistry of Cement, Gothenburg, (Edited by Justnes, H).2ii072 (1997).
[57] Thelandersson, S., Mechanical Behaviour of Concrete under Torsional Loading at Transient, High-Temperature Conditions, Bulletin 46, Div. Structural Mechanics and Concrete Construction, 25-35 (1974).
[58] Nilsson, L.O., Temperature Effects in Relative Humidity Measurements on Concrete – Some Preliminary Studies, The Moisture Group, Report 1987:1. BFR, 84 (1987).
[59] Persson, B., Compatibility between flooring material on concrete and moisture, volatile organic compound and adhesion, Report 0202:01, Division of Building Materials, Lund Institute of Technology, Lund University, Lund, 46 pp. (2002).
[60] Buenfeld, N., Personal information, Imperial College, London, (2001).
[61] Nilsson, L.-O., Hedenblad, G., Norling-Mjörnell, K., Suction after Long Time, HPC Handbook, Svensk Byggtjänst, 209-226 (2000).
[62] Stoltzer, E., Buhr, B, Engelund, S., The Faroe Bridges – Chloride Penetration Rate Estimated on a Basis of Measurements from 1988 to 1997. Durability of Exposed Concrete Containing Secondary Cementitious Materials, Hirtshals, Ed.: D. Bager, 19 pp. (2001).
[63] Castel, R., Francois, G., Arliguie, A., Clarification of Corrosion of Reinforcement in Concrete Structures Exposed to Chloride Environment, Contribution at the fib Meeting and Nordic Mini Seminar, Gothenbourg, 10 pp. (2001).
[64] Collepardi, M., et al., The Kinetics of Chloride Ions Penetration in Concrete. Il Cemento. 67 157-164 (1970).
[65] Tang, L., Nilsson, L.-O., Rapid Determination of Chloride Diffusitivity of Concrete by Applying an Electric Field, ACI Material Journal 49/1, 49-53 (1992).
[66] Maage, M., Helland, S., Carlsen, J. E., Chloride Penetration in HPC Exposed to Marine Environment. RILEM Workshop on Durability, Ed.: H. Sommer, 194-207 (1994).
[67] CTH Rapid Test for Determination of the Chloride Migration Coefficient, D, in Concrete, NT BUILD 492 (2000).
[68] Tang, L., Nilsson, L.-O., Modelling of chloride penetration into concrete – Tracing five years' field exposure, Concrete Science Engineering **2** 170-175 (2000).
[69] Persson, B., Assessment of Chloride Migration Coefficient, Salt Frost Resistance, Internal Frost Resistance and Sulphate Resistance of Self-Compacting Concrete. Report TVBM-3100, Lund, 86 pp. (2001).
[70] Boubitsas, D., Paulou, K., Self Compacting Concrete for Marine Environment. TVBM-5048, Lund Institute of Technology, Lund University, Lund 55 pp. (2000).
[71] Persson, B., Chloride Migration Coefficient of Self-Compacting Concrete. Materials and Structures, 20 pp. (Submitted for publication, 2001).
[72] Persson, B., Chloride Migration Coefficient of Self-Compacting Concrete, Nordic Seminar on Durability of Exposed Concrete Containing Secondary Cementitious Materials, Hirtshals, Ed.: D. Bager, 20 pp. (2001).
[73] Johannesson, B., Transport and Sorption Phenomena in Concrete and Other Porous Media, TVBM-1019, LTH Building Materials, Lund 491 pp (2000).

ON THE MITIGATION OF EARLY AGE CRACKING

Dale P. Bentz
National Institute of Standards and Technology, USA
Mette Geiker
Technical University of Denmark, DENMARK
Ole Mejlhede Jensen
Aalborg University, DENMARK

Abstract

Potential means of limiting early age cracking of concrete structures have been investigated. Three different methods of mitigating autogenous strains and stresses in cement mortars (water-to-solid binder mass ratio = 0.35, 8 % silica fume) are compared: 1.) a reduction of the surface tension of the pore solution via addition of a shrinkage reducing chemical admixture, 2.) an increase of the internal water supply by replacement of a portion of the sand by saturated low-density fine aggregates or the addition of superabsorbent polymer particles, and 3.) the use of a slower reacting (coarser) silica fume. The effectiveness of each of these measures is presented, along with a basic physical explanation of self-desiccation and autogenous shrinkage.

1. Introduction

The recent trend in concrete technology towards so-called high-performance, or low water-to-solid binder mass ratio (w/s), concretes has not been without its problems. One of the major observed problems with these mixtures is their increased tendency to undergo early-age cracking. While this cracking may or may not compromise the (higher) compressive strengths of these concretes, it likely does compromise their long-term performance. The phenomenon of early-age cracking is complex and depends on thermal effects, autogenous strains and stresses, drying, stress relaxation, and structural detailing and execution [1,2]. In concretes with low w/s, a major contributor to early-age cracking can be the autogenous shrinkage induced by the self-desiccation that occurs during hydration under sealed or partially saturated conditions [3]. As the cementitious materials hydrate under sealed conditions, empty porosity is created within the 'set'

microstructure, because the hydration products occupy less volume than the starting materials. The water menisci created by these empty pores in turn induce autogenous shrinkage stresses on the three-dimensional microstructure. The magnitude of these stresses is influenced by both the surface tension of the pore solution and the meniscus radius of the largest water-filled pore within the microstructure [3]. In this paper, a variety of engineering methods for reducing autogenous stresses and strains that focus on these two factors are explored. These methods include using a shrinkage-reducing admixture (SRA) [4], increasing the internal water supply via the replacement of sand by saturated low-density fine aggregates (LWA) [5,6,7] or the addition of superabsorbent polymer particles (SAP) [8,9], and using a coarser silica fume.

2. Experimental procedure

Mortars were prepared using a low-alkali Portland cement with a water-to-solid binder (w/s – where solid binder is cement + silica fume) mass ratio of 0.35 and an 8 % by mass fraction replacement of cement by silica fume. The cement has a Blaine fineness of 368 m^2/kg and a Bogue phase composition of 58 % C_3S, 25 % C_2S, 4.0 % C_3A, and 7.3 % C_4AF, with a 3.4 % calcium sulfate content. The two silica fumes used had specific surface areas of 23.2 m^2/g (reference) and 15 m^2/g (coarse), respectively. The mortars were prepared with CEN standard sand EN 196-1. For two of the mortars, either 8 % or 20 % of the sand by mass was replaced by low-density aggregates of size less than 4 mm. A summary of the six mixtures tested is provided in Table 1. All mortars were prepared by mixing in a 5-liter epicyclic mixer. All mixtures were prepared using freshly boiled (then cooled), distilled water. The 'extra' water in Table 1 refers to the water contained in the low-density aggregates or absorbed by the polymer particles.

Table 1 - Differences in the mortar mixtures.

Mixture characteristic	FSF	CSF	SRA	LWA20	LWA08	SAP
Silica fume, 23.2 m^2/g	X		X	X	X	X
Silica fume, 15 m^2/g		X				
Shrinkage-reducing admixture (2 % by mass of cement)			X			
Low-density aggregate 0-4 mm				20 % of sand	8 % of sand	
Assumed absorption of LWA (by mass)				25 %	25 %	
Superabsorbent polymer						X
Extra water/solid binder				0.126	0.046	0.046

The following measurements were performed: compressive strength of cylinders (diameter 60 mm, height 120 mm) after 7 d and 28 (or 27, 29, or 50) d sealed curing, internal relative humidity (RH), and autogenous deformation using a custom-built

dilatometer immersed in a constant temperature oil bath [10,11]. All curing and measurements were conducted at a temperature of 30 ^{o}C ± 0.5 ^{o}C and under sealed conditions. Typical standard deviations measured on companion specimens were 5 MPa to 7 MPa, 0.17 % RH, and 5 microstrain to 17 microstrain, for compressive strength, internal RH, and autogenous deformation, respectively [4].

3. Results and discussion

The measured changes in internal RH with hydration time are provided in Figure 1. The measured internal RH is a function of temperature, and is projected to be about 3 % higher at 30 ^{o}C than at 20 ^{o}C [12,13]. After initial equilibrium of the sensors is achieved, the RH decreases with hydration time. This is a direct consequence of the creation of empty pores within the specimens hydrating under sealed conditions. The Kelvin equation describes the relationship between the size of these pores and the internal RH (assuming cylindrical pores and a contact angle of zero degrees between the pore solution and the pore walls) [14]:

$$\ln(RH) = \frac{-2\gamma V_m}{rRT} \quad (1)$$

$_m$ is its molar volume, r is the radius of the largest water-filled pore (or the smallest empty pore), R is the universal gas constant, and T is the absolute temperature. In the experiments presented in this paper, both ã and r are a function of the different mixture proportions. The addition of the shrinkage-
either LWA or SAP will alter the size of the pores being emptied due to self-desiccation (hydration) of the paste. In general, it is assumed that the largest water-filled pores empty first as the surrounding cement paste hydrates.

These effects can be observed in Figure 1. The RH in the system containing the SRA remains above that of the 'reference' (FSF) system, remaining about 3 % RH higher after the first 15 d of hydration. For the mixtures with an internal supply of water (either LWA or SAP), the RH remains even higher throughout the course of the hydration, only falling to about 95 % after 12 d or so of hydration. While not shown in Figure 1 (for visual clarity), the results for the mortar containing coarser silica fume particles (CSF) were virtually identical to those measured for the mortar (FSF) with the fine silica fume.

The water menisci created during self-desiccation will induce capillary stresses in the pore solution (and on the solid network containing the pore solution). Assuming a cylindrical pore geometry, the tensile stress in the pore solution, ó$_{cap}$, is given by [14]:

$$\sigma_{cap} = \frac{2\gamma}{r} = \frac{-\ln(RH)RT}{V_m} \quad (2)$$

where all other terms have been defined above.

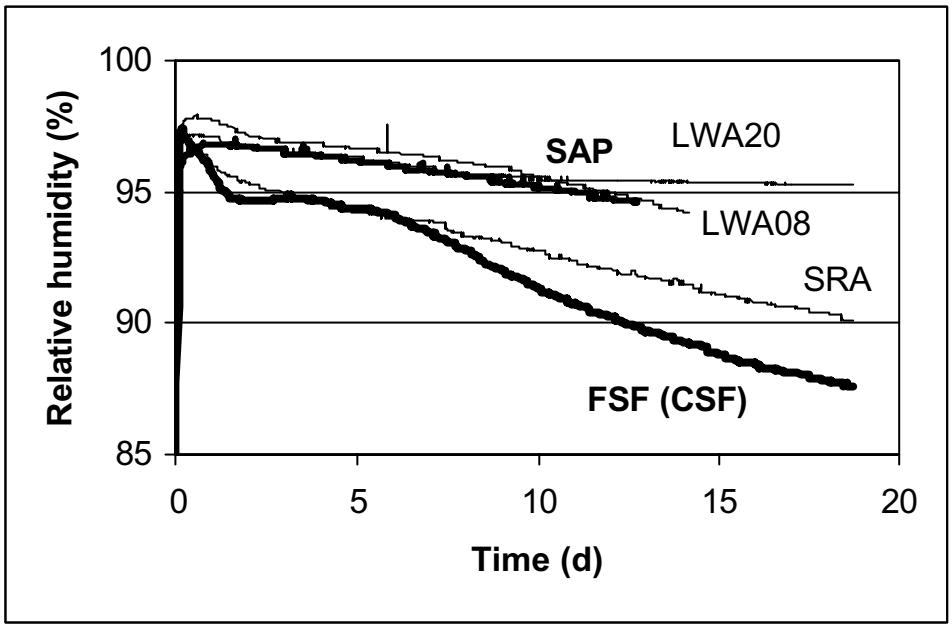

Figure 1 - Measured internal RH vs. time for the various mortars during sealed hydration at 30 ^{o}C.

The shrinkage strain of a partially saturated porous medium due to these capillary stresses in the water-filled pores can be estimated as [15]:

$$\varepsilon = \frac{S\sigma_{cap}}{3}\left(\frac{1}{K} - \frac{1}{K_s}\right) \quad (3)$$

where å is the shrinkage (negative strain), S is the degree of saturation (0 to 1) or fraction of water-filled pores, K is the bulk modulus of elasticity of the porous material, and K_s is the bulk modulus of the solid framework within the porous material. This equation is only approximate for a partially-saturated visco-elastic material such as hydrating cement paste, but still provides insight into the physical mechanism of autogenous shrinkage and the importance of various physical parameters.

The measured autogenous deformations for the various mixtures are provided in Figure 2. Once again, for clarity, the results for the CSF mortar are not shown but were basically identical to those shown for the reference FSF mortar. For the other mortars, however, major differences are observed. All of the other mixtures are somewhat effective in reducing/eliminating the autogenous shrinkage observed for the reference FSF mixture. The SRA reduces the autogenous shrinkage by a factor of two after 15 d of hydration. From the equations shown above, this reduction in measured shrinkage is consistent with the typical reduction in surface tension of the pore solution provided by

addition of the SRA. For example, at NIST, a reduction in pore solution surface tension from (0.0665 ± 0.0006) N/m (standard deviation of five measurements) to (0.0400 ± 0.0003) N/m has been measured for pore solutions filtered from a cement paste (with and without a 2 % addition by mass of cement of SRA, w/s=0.45) 1 h after mixing [16].

The use of internal curing (by providing a supply of free water) is also seen to be a highly effective means of mitigating autogenous shrinkage. Each of the three internal curing mixtures (LWA08, LWA20, and SAP) either significantly reduces or eliminates the measured autogenous shrinkage. Because it provides the most extra curing water, the LWA20 mixture totally eliminates autogenous shrinkage, resulting instead in a small autogenous expansion, perhaps due to ettringite formation and/or swelling of the cement hydration products due to water absorption. While the SAP and LWA08 mortars contain basically the same quantity of 'extra' water (Table 1), the SAP mortar is more efficient in reducing autogenous shrinkage at later ages, most likely due to a more homogenous distribution of the extra curing water within the three-dimensional mortar microstructure. A comparison of the water distribution in these different mortars, based on computer modeling [17] and direct observation of two-dimensional cross sections, will be the subject of a future paper.

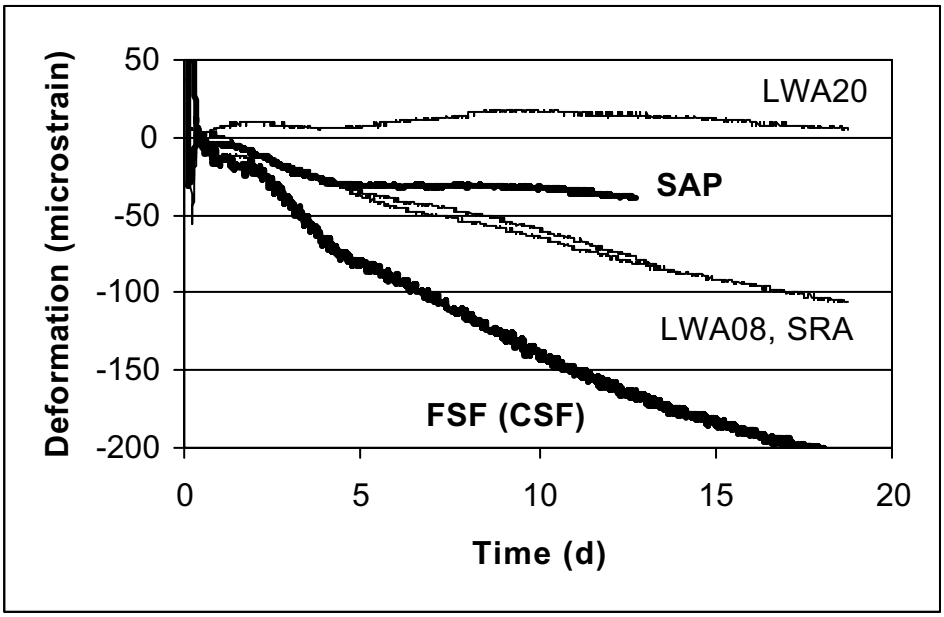

Figure 2 - Measured autogenous deformation vs. time for the various mortars during sealed hydration at 30 ^{o}C.

Figure 3 provides a plot of the autogenous deformation vs. the natural log of the internal RH for the different mixtures, during the first 12 d of hydration. According to equations (1) to (3), the local slope of this plot should be proportional to the ratio of the mixture saturation to its current elastic modulus (assuming that $K_s >> K$). Also, according to these equations, the relationship between autogenous shrinkage and relative humidity should be independent of the surface tension of the pore solution. Thus, any differences in slope between the mortars with and without the SRA are due instead to the fact that when lower RHs are finally achieved in the SRA mortar, the elastic modulus is higher and the system saturation is less (both due to its increased degree of hydration). This illustrates that if the development of autogenous stresses can be substantially delayed, the resulting shrinkage will be much less due to the increased stiffness developed by the hydrating cement paste.

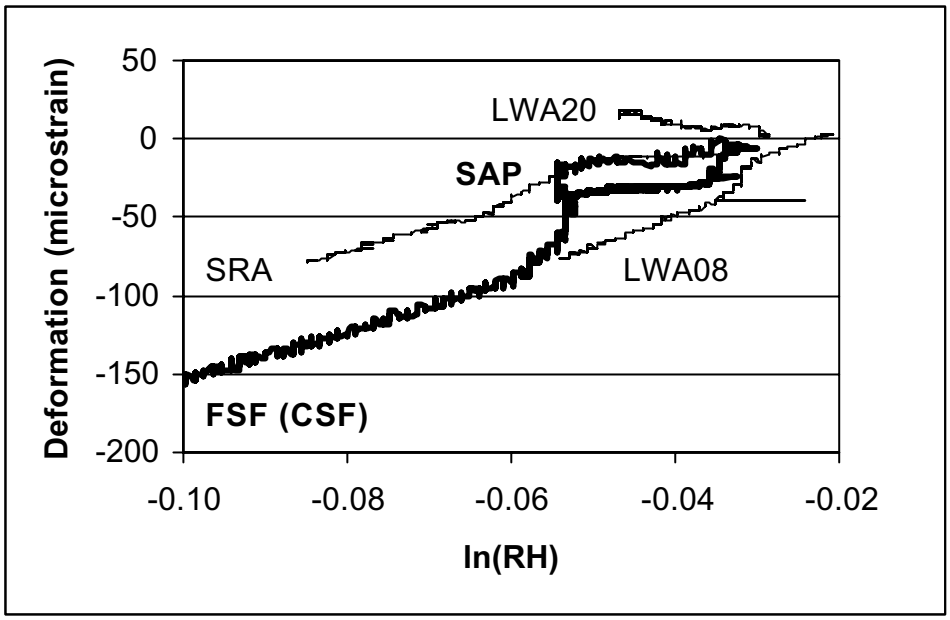

Figure 3 - Autogenous deformation vs. RH for the various mortars during sealed hydration at 30 ^{o}C.

Finally, the results of the compressive strength testing are provided in Figure 4. The measured proportional gains in compressive strength between 7 d and later ages (27 d to 56 d) can be linked to the internal RH data presented in Figure 1. It is consistently observed that for those specimens where a higher internal RH is maintained during this time period, a greater gain in compressive strength is found. This is a natural consequence of the linkages between moisture availability, hydration rates, and strength

development. It is well known that hydration proceeds at a reduced rate as the specimen internal RH is decreased [18,19,20]. This highlights a possible secondary benefit of internal curing in addition to the primary reduction in autogenous deformation, namely the achievement of an increased degree of hydration and a potentially higher compressive strength (and lower permeability/diffusivity) under sealed curing conditions. The increased degree of hydration may not always lead to an increase in compressive strength for the mortar or concrete specimens, as the increased strength of the cement paste binder may be offset by the increased porosity of the composite as a whole (due to the internal porosity of the low-density aggregates or the hollow voids introduced by the SAP particles). In practice, the influence of specimen RH on measured compressive strength presents an additional complication [9,21].

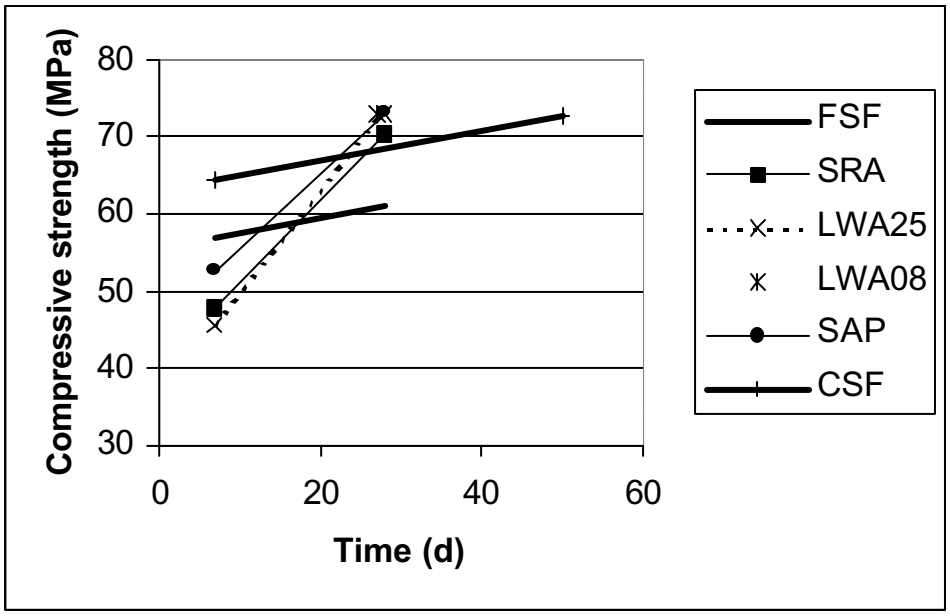

Figure 4 - Compressive strength development for the various mortars during sealed hydration at 30 ^{o}C.

4. Conclusions

The experimental results presented in this paper clearly demonstrate that autogenous shrinkage can be reduced by several different means. Shrinkage-reducing admixtures that reduce the surface tension of the pore solution reduce both the decrease in internal RH and the measured autogenous shrinkage. Internal curing, either by the use of

saturated low-density fine aggregates or the addition of superabsorbent polymer particles, provides the extra curing water needed for cement hydration under sealed conditions. In this case, autogenous shrinkage is reduced due to the fact that much larger pores (within the LWA or formed by the SAP particles themselves) are being emptied than those typically emptied in cement paste during sealed hydration. The use of a coarser silica fume had a negligible influence on both internal RH development and measured autogenous shrinkage. An additional benefit of the approaches that were successful in reducing autogenous shrinkage may be an increased degree of hydration and measured compressive strength at later ages, due to the increased and persistent availability of moisture.

References

[1] Lura, P., van Breugel, K., and Maruyama, L., Effect of Curing Temperature and Type of Cement on Early-age Shrinkage of High Performance Concrete, Cem. Concr. Res., **31** (12) (2001) 1867-1872.

[2] Shah, S.P., Weiss, W.J., and Yang, W., Shrinkage Cracking – Can It Be Prevented?, Concr. Inter. **20** (4) (1998) 51-55.

[3] Bentz, D.P., and Jensen, O.M., Mitigation Strategies for Autogenous Shrinkage Cracking, submitted to Concr. Inter., 2001.

[4] Bentz, D.P., Geiker, M.R., and Hansen, K.K., Shrinkage-reducing Admixtures and Early-age Desiccation in Cement Pastes and Mortars, Cem. Concr. Res. **31** (7) (2001) 1075-1085.

[5] Weber, S., and Reinhardt, H.W., A New Generation of High Performance Concrete: Concrete with Autogenous Curing, Adv. Cem.-Based Mater. **6** (1997) 59-68.

[6] van Breugel, K., and Lura, P., Effect of Initial Moisture Content and Particle Size Distribution of Lightweight Aggregates on Autogenous Deformation, in 'Proceedings of the Second International Symposium on Structural Lightweight Aggregate Concrete', Eds. S. Helland, I. Holand, and S. Smeplass (2000) 453-462.

[7] Bentur, A., Igarashi, S., and Kovler, K., Prevention of Autogenous Shrinkage in High Strength Concrete by Internal Curing Using Wet Lightweight Aggregates, Cem. Concr. Res. **31** (11) (2001) 1587-1591.

[8] Jensen, O.M., and Hansen, P.F., Water-entrained Cement-based Materials I. Principle and Theoretical Background, Cem. Concr. Res. **31** (2001) 647-654.

[9] Jensen, O.M., and Hansen, P.F., Water-entrained Cement-based Materials II. Experimental Observations, accepted by Cem. Concr. Res., 2002.

[10] Jensen, O.M., and Hansen, P.F., A Dilatometer for Measuring Autogeneous Deformation in Hardening Portland Cement Paste, Mater. Struct. **28** (1995) 406-409.

[11] Jensen, O.M., and Hansen, P.F., Autogeneous Deformation and Change of Relative Humidity in Silica Fume Modified Cement Paste, ACI Mater. J. **93** (6) (1996) 539-543.

[12] Nilsson, L.O., Temperature Effects in Relative Humidity Measurements on Concrete – Some Preliminary Studies. The Moisture Group. Report 1987:1. BFR. 1987, 84.

[13] Persson, B., Compatibility Between Flooring Material on Concrete and Moisture, Volatile Organic Compound, and Adhesion, Working Report 0202:01, Division of Building Materials, Lund Institute of Technology, Lund, 2001, 29 (in Swedish).

[14] Alberty, R.A., and Daniels, F., Physical Chemistry (John Wiley & Sons, New York, 1980).

[15] MacKenzie, J.K., The Elastic Constants of a Solid Containing Spherical Holes, Proc. Phys. Soc. A **224** (1950) 526-544.

[16] Bentz, D.P., unpublished results, 2001.

[17] Bentz, D.P., and Snyder, K.A., Protected Paste Volume in Concrete – Extension to Internal Curing Using Saturated Lightweight Fine Aggregate, Cem. Conc. Res. **29** (1999) 1863-1867.

[18] Powers, T.C., A Discussion of Cement Hydration in Relation to the Curing of Concrete, Proc. Highway Res. Board **27** (1947) 178-188.

[19] Parrott, L.J., Killoh, D.C., and Patel, R.G., Cement Hydration Under Partially Saturated Curing Conditions, in 'Proceedings of the 8th International Congress on the Chemistry of Cement', Rio de Janeiro, Vol. III (1986) 46-50.

[20] Snyder, K.A., and Bentz, D.P., Early Age Cement Paste Hydration at 90 % Relative Humidity and the Loss of Freezable Water, to be published as a NISTIR, U.S. Department of Commerce, 2002.

[21] Neville, A., Properties of Concrete, 4th edition (John Wiley & Sons, New York, 1996).

EFFECTIVENESS OF EXPANSIVE ADDITIVE ON REDUCTION OF AUTOGENOUS SHRINKAGE STRESS IN HIGH-STRENGTH CONCRETE

M. TANIMURA, H. HYODO, H. NAKAMURA
Research & Development Center, Taiheiyo Cement Corporation, Japan
R. SATO
Department of Social and Environmental Engineering, Graduate School of Engineering, Hiroshima University, Japan

Abstract:

The effectiveness of expansive additive, shrinkage reducing agent, as well as low heat Portland cement on the reduction of autogenous shrinkage stress in high-strength concrete was experimentally investigated. Experimental results showed that the use of expansive additive was effective in reducing autogenous shrinkage stress of high-strength concrete. Furthermore, the combination of expansive additive with shrinkage reducing agent was particularly effective. On the other hand, low heat Portland cement was found to be useful for controlling autogenous shrinkage stress in high-strength concrete.

1. Introduction

Utilization of high-strength and/or high-flowability concrete enables to increase the ultimate capacity of structural members, to decrease the dimensions of element and to enhance the durability. However, such low water/binder ratio concrete has already been known to shrink significantly at early ages, which facilitates cracking in structural members [1-3]. Control of cracking in reinforced concrete members is a matter of concern because durability of concrete structures often goes down by crack formation. High-strength concrete (HSC) is expected to achieve higher durability as well as mechanical properties of structural members, and, therefore, more severe control of cracking is essential for HSC than that for conventional concrete.

Recently, in order to control the shrinkage in high-strength concrete, experimental investigations on the reduction of autogenous shrinkage have been carried out [4-5].

These studies indicated that expansive additives (EX) and/or shrinkage reducing agent (SRA) and/or low heat Portland cement (LPC) were effective in controlling the autogenous shrinkage strain. However, few studies have been performed to evaluate the sole contribution of LPC, SRA, and EX on the reduction of shrinkage-induced stress except an authors' study [6], while authors had already showed that shrinkage-induced stress could considerably be reduced by the ternary combination of LPC, EX and SRA [7].

The present study, therefore, is particularly focusing to evaluate how much each EX, SRA and LPC contributes to reducing autogenous shrinkage-induced stress in HSC. Furthermore the effectiveness of EX combined with SRA on the stress reduction is also investigated.

2. Experimental program

2.1 Materials and mix proportions

The materials used in the present study are summarized in Table 1. The contents of C_3S, C_2S, C_3A and C_4AF of ordinary Portland cement (OPC), calculated using Bogue's equations, were 52%, 22%, 9%, and 9%, respectively. On the other hand, those of low heat Portland cement (LPC) were 29%, 54%, 3%, and 9%, respectively. Previous study [4] revealed that autogenous shrinkage decreases when the contents of C_3A, C_4AF, and C_3S decrease, which means that LPC-based concrete may show a low autogenous shrinkage stress.

Table 2 shows the mix proportions of concrete investigated. Four OPC-based high-strength concretes and two LPC-based high-strength concretes were prepared. NC represents the conventional high strength concrete using OPC. NE, NS, and NES, on the other hand, represent the high strength concrete using EX, SRA and both EX and SRA, respectively. LC and LE denote the high strength concrete using LPC and both LPC and EX, respectively.

The water/(C+EX) ratio is set at 0.3 for all mixtures. The unit water content including SRA and coarse aggregate content are systematically fixed at 175 kg/m^3 and 832 kg/m^3 for all mixtures, respectively. Replacement dosage of EX is fixed at 7.5 % (unit content; 44 kg/m^3) of cement, regardless of type of cement. The unit content of SRA is 6 kg/m^3, which is usually adopted for normal strength concrete having relatively high water/binder ratio. The dosage of SP was adjusted to achieve a concrete mixture with a slump flow of 600 ± 50mm. The air content of all investigated mixtures was lower than 2.0 %.

Table 1 - Materials

Material	Designation	Kind / Characteristics
Cement	OPC	Ordinary Portland / Density: 3.16 g/cm^3, Specific surface area: 3310 cm^2/g
	LPC	Low heat Portland / Density: 3.22 g/cm^3, Specific surface area: 3280 cm^2/g
Expansive additive	EX	Lime-based / Density: 3.14 g/cm^3, Specific surface area: 3310 cm^2/g
Shrinkage reducing agent	SRA	Lower alcohol alkyleneoxide adduct
Fine aggregate	S	Land sand / Density: 2.62 g/cm^3, Absorption: 1.66%, F.M.: 2.84
Coarse aggregate	G (20mm)	Crushed sand stone / Density: 2.64 g/cm^3, Absorption: 0.85%, F.M.: 6.61
High-range water-reducing agent	SP	Polycarboxylic acid based / Density: 1.07 g/cm^3

Table 2 - Mix proportions of concrete

Mix proportion	Designation					
	NC	NE	NS	NES	LC	LE
W/(C+EX)	0.3	0.3	0.3	0.3	0.3	0.3
Sand-coarse aggregate ratio (%)	49.2	49.2	49.2	49.2	49.5	49.5
W (kg/m^3)	175	175	169	169	175	175
C (kg/m^3)	583	539	583	539	583	539
EX (kg/m^3)	-	44	-	44	-	44
S (kg/m^3)	794	794	794	794	803	803
G (kg/m^3)	832	832	832	832	832	832
SRA (kg/m^3)	-	-	6	6	-	-
SP (kg/m^3)	7.87	8.45	8.16	8.16	4.84	4.72

2.2 Specimens and curing condition

Six prismatic specimens were made to measure the stress caused by restraining autogenous shrinkage/expansion of concrete. Each specimen has dimensions of 100 x 100 x 1500 mm. Deformed bar with nominal diameter of 25 mm was placed at the centroid of the cross section of the specimen. The rib of the reinforcing bar was lathed in the central zone of 100 mm to be round bar with a diameter of 22.5 ± 0.5 mm as shown in Figure 1. The reinforcement ratio at lathed portion was about 4.0 % for all specimens. In order to reduce the friction between concrete specimen and steel mould as much as possible, polytetrafluoro ethylene sheet (1 mm thickness) was placed on the

bottom plate of the mould and a foamed polystyrene sheet (3mm thickness) was placed inside each end plate of the mould in accordance with practices proposed by JCI [3]. Cylindrical Specimens 100 x 200 mm were prepared to measure the compressive strength of concrete.

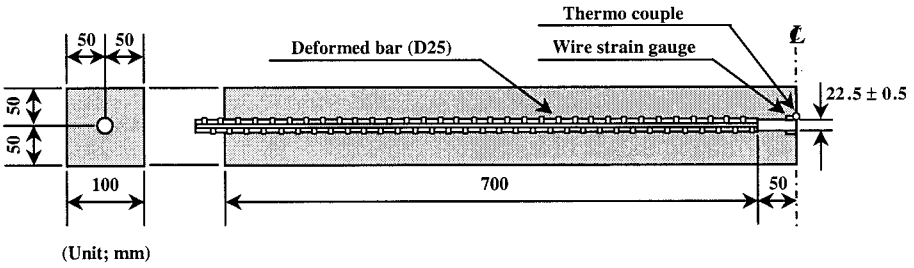

Figure 1 - Details of specimen for restrained stress

The specimens were covered with polyester film of 0.1 mm thickness and wet cloth to prevent the evaporation of water until they were demoulded. Then, the specimens were demoulded at 24 hours after casting and promptly sealed with aluminum adhesive tape of 0.05 mm thickness. All specimens were stored in room at temperature of 20 ± 2 °C.

2.3 Measurement

The self-temperature compensated wire strain gauges, as shown in Figure 1, were attached to the upper and lower surfaces of the reinforcing bar to measure the strain in the reinforcing bars. The temperature of concrete were also measured by thermo couple that are placed at the center of the specimens.

The stress caused by restraining autogenous shrinkage/expansion of concrete was calculated by the following equation (1), which derived based on the equilibrium force requirement:

$$\sigma_c = -A_s E_s \varepsilon_s / A_c \qquad (1)$$

σ_c denotes the autogenous shrinkage/expansion stress of concrete (N/mm^2)
ε_s denotes the measured strain in reinforcing bar
E_s denotes Young's modulus of reinforcing bar and is considered to be 200 kN/mm^2
A_s denotes the cross section area of reinforcing bar (mm^2)
A_c denotes the cross section area of concrete (mm^2)

Compressive strength of concrete and setting time of mortar extracted from concrete were measured in accordance with Japanese Industrial Standards, JIS A1108 and JIS A 1147, respectively.

3. Results and discussion

3.1 Compressive strength

Figure 2 shows the development of compressive strength of sealed concrete with age. There is little difference in strength between OPC-based concretes. It is considered, therefore, that the influence of addition of EX and/or SRA on strength development is not significant for the replacement dosage adopted in this study. Regardless of EX addition, the strength of LPC-based concrete is lower than that of OPC-based concrete over early ages before 7 days, whereas the rate of strength development of the former is more remarkably than that of the latter after 7days, which should be due to the relatively higher content of C_2S in LPC-based concrete. As a result, the compressive strength of LPC-based concretes is almost the same as that of OPC-based ones at the age of 91 days.

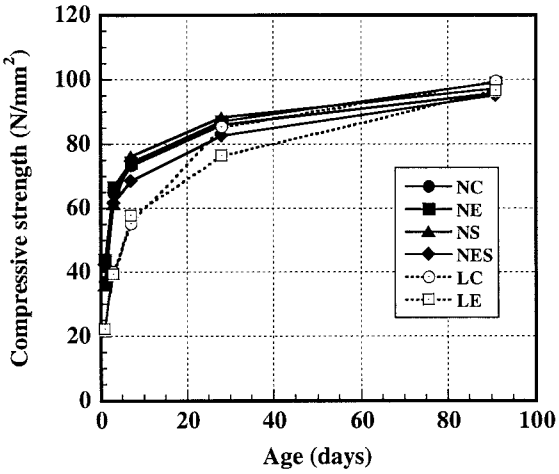

Figure 2 - Development of compressive strength of sealed concrete

3.2 Restrained stress

3.2.1 Effect of expansive additive

Figure 3 shows the comparison between NC and NE for restrained stress produced with age after the initial setting of concrete. The restrained stresses before 24 hours are represented in the left figure and that from 1 to 91 days in the right figure. The temperatures of concrete are also shown in the left figure. According to the left figure, the restrained stress begins obviously to be produced at final setting time of about 7 hours. Although the macroscopic volume change of unrestrained concrete begins by the initial setting time, the restrained stress is not generated, which is explained by the stress relaxation due to the lower Young's modulus and larger creep deformation of concrete at very early ages. Compared with NC concrete, the development rate of the restrained stress of NE is almost equal up to about 10 hours, and thereafter obviously low. The restrained stress observed in NE changed to the compression side at the age of about 12 hours. Thus the expansive additive contributes efficiently to reducing the restrained stress by restraining autogenous shrinkage, considering the fact that the autogenous shrinkage stress occurred rapidly in control specimen NC at the time from 10

to 14 hours is compensated by expansive additive. As a result, the restrained stress of NE, as shown in the right figure, was reduced to approximately 20 % of NC at the age of 91 days.

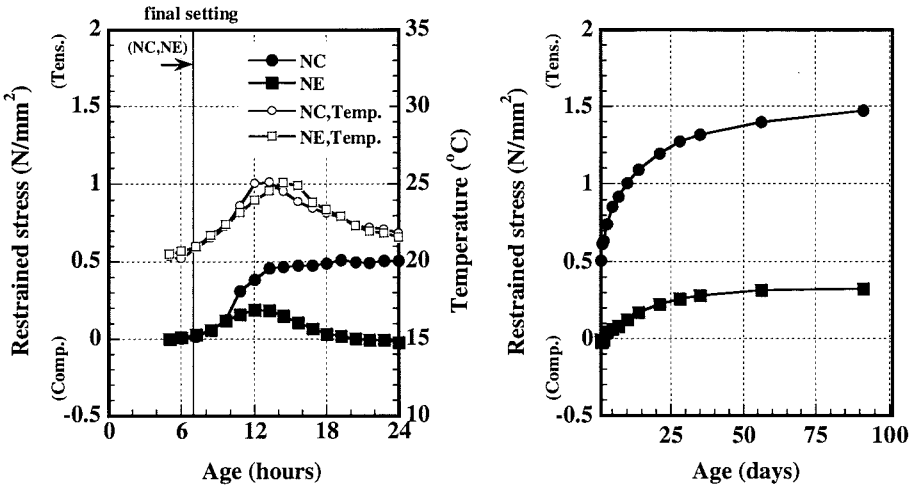

Figure 3 - Effectiveness of expansive additive on controlling restrained stresses

As for the NC concrete, the increase rate of the restrained stress has a close relation to that of concrete temperature as shown in the left figure. This stage should correspond to the acceleratory periods during hydration of C_3S [8].

3.2.2 Effect of shrinkage reducing agent

Figure 4 shows the effect of shrinkage reducing agent on reducing autogenous shrinkage stress. The restrained stress of NS also begins to develop from final setting time. The restrained stress observed in NS is maintained to be almost constant after the peak stress in tension at about 13 hours, while the shrinkage-induced stress in NC increases slightly. Thus, the mechanism for controlling restrained stress in concrete was quite different between expansive additive and shrinkage reducing agent. According to the right figure, the restrained stress of NS is reduced to approximately 85 % of that of NC, regardless of the age.

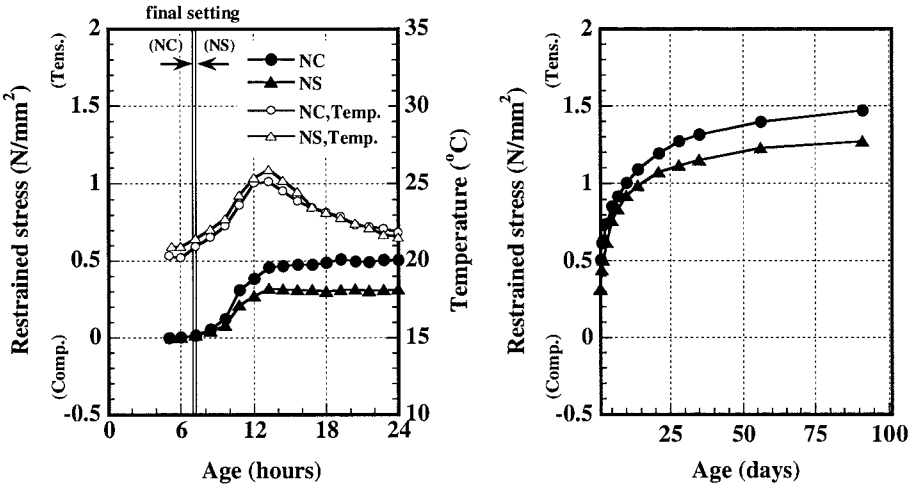

Figure 4 - Effectiveness of shrinkage reducing agent on controlling restrained stress

3.2.3 Effect of the combination of EX and SRA

Figure 5 shows the comparison between NC and NES specimens for the restrained stress. Compared with the restrained stress in NE, as shown in Figure 3, there exists

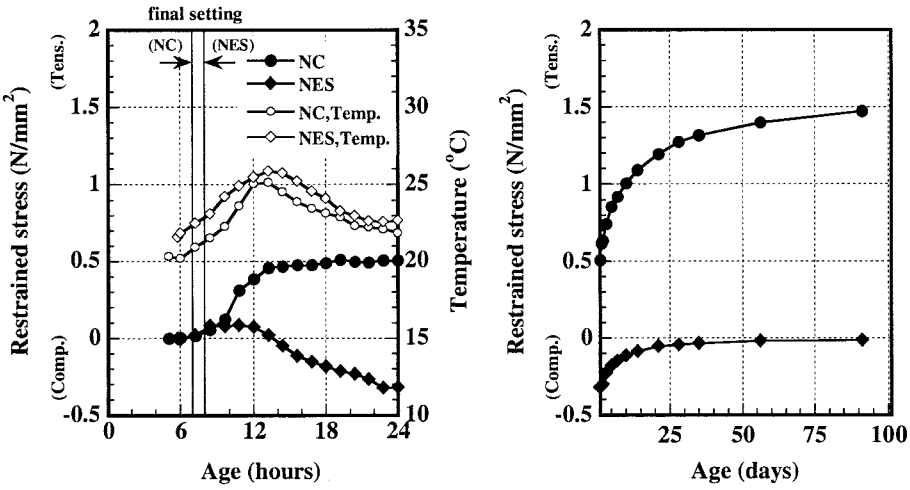

Figure 5 - Effectiveness of expansive additive combined with shrinkage reducing agent on controlling restrained stress

considerable difference between NE and NES for performance to reduce restrained stress, which is owing to the effect of SRA addition. As is shown in the right figure, the restrained stress of NES is almost zero even at the age of 91 days, while the tensile stress in NC reaches 1.5 N/mm^2. Thus the use of both EX and SRA was particularly effective in reducing the autogenous shrinkage stress.

Figure 6 shows the variation of restrained stress obtained by subtracting the restrained stress of NC from those of NE, NS, NES (hereafter referred as a compensated-restrained stress) with age. According to the figure, the compensated-restrained stress of NE and NES were approximately 6 and 7 times larger than that of NS at the age of 91 days, respectively.

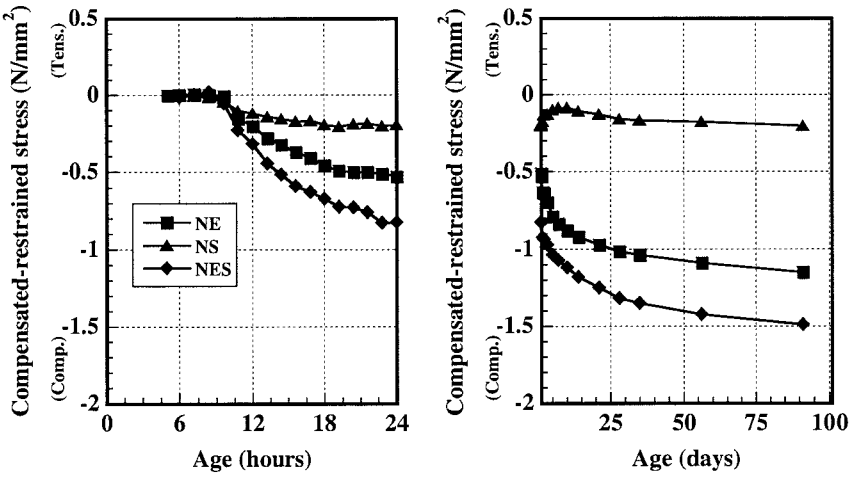

Figure 6 - Comparison between NE, NS and NES for compensated-restrained stress

Figure 7 shows the comparison of the compensated-restrained stress measured in NES and that obtained by superposing the compensated-restrained stress of NE to that of NS. Although the superposed values are in good agreement with measured ones at very young age, the difference of the stresses between measured and superposed is apparently observed and continues to be constant after the age of 1 day. It should be noted that there is synergistic effect in applying both EX and SRA.

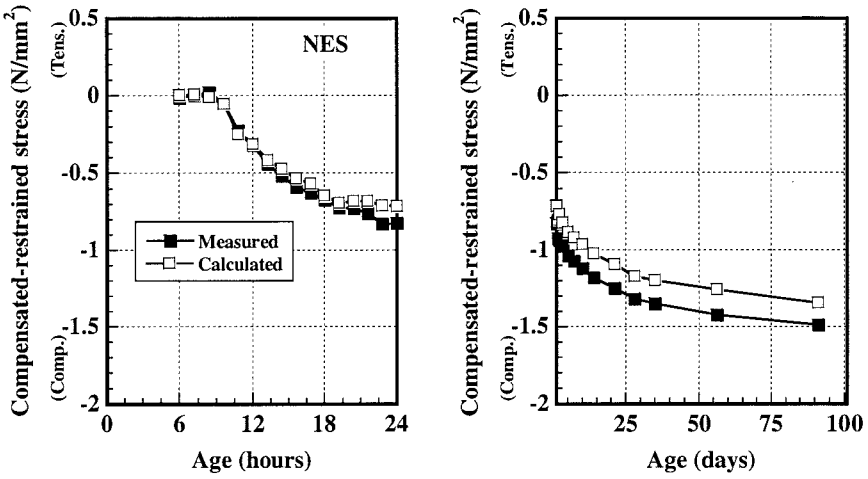

Figure 7 - Comparison between measured and superposed compensated-restrained stresses for NES

3.2.4 Effect of low heat Portland cement

Figure 8 shows the comparison between LC and LE for the restrained stress. The restrained stress observed in LC is remarkably small compared with that observed in NC using ordinary Portland cement, as shown in Figure 3. The restrained stress of LC was about 20 % of that of NC at the age of 91 days. The combination of LPC and EX resulted in the restrained stress in compression, known as chemical prestress, of about 1.0 N/mm^2 while the EX content of LE was the same as that of NE. Thus the LPC is effective in controlling autogenous shrinkage stress in high-strength concrete.

Figure 9 shows the comparison of the compensated-restrained stress between NE and LE. The compensated-restrained stress for LE is calculated by subtracting the restrained stress of LC from that of LE. According to the figure, the compensated-restrained stress of NE is higher than that of LE at early ages, but lower after the age of about 2 days. The rate and magnitude of expansion of concrete developing macroscopically should depend on the balance between formations of expansive hydrates and the development of strength and stiffness of the structure of cement hydrates to accommodate their growth [9]. Therefore, such a balance would be different between NE and LE. Further investigations are needed in order to explain this phenomenon.

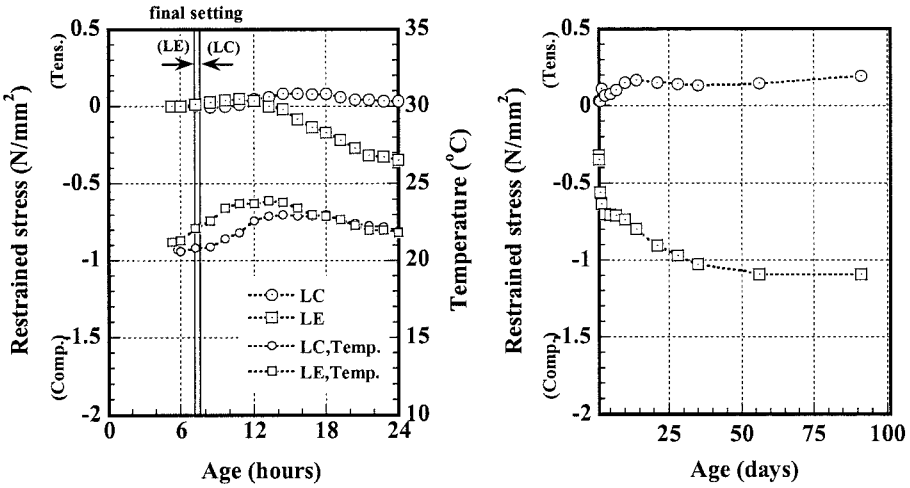

Figure 8 - Comparison between LE and LC on controlling restrained stress

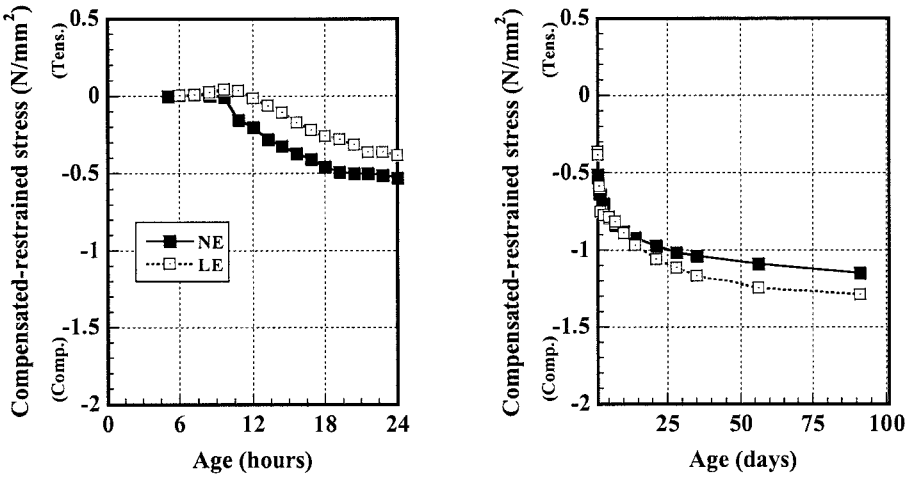

Figure 9 - Comparison between NE and LE for compensated-restrained stress

4. Conclusions

Based on results presented in this paper, the following conclusions can be drawn:

1. The restrained stress was obviously developed at final setting time, regardless of the addition of expansive additive (EX) and/or shrinkage reducing agent (SRA).
2. The restrained stress of high-strength concrete (HSC) using EX is reduced to approximately 20 % of that of HSC without EX at the age of 91 days.
3. The restrained stress of HSC containing SRA is about 85 % of that of HSC without SRA regardless of the age.
4. The restrained stress of HSC using both EX and SRA is almost zero even at the age of 91 days. There exists synergistic effect in applying both EX and SRA.
5. The use of EX is remarkably effective in reducing autogenous shrinkage stress in high-strength concrete and the combination of EX and SRA is particularly effective.
6. The restrained stress of HSC using low heat Portland cement is about 20 % of that of HSC using ordinary Portland cement at the age of 91 days. The combination of low heat Portland cement and EX resulted in the restrained stress in compression.
7. LPC cement is effective in controlling autogenous shrinkage stress in high-strength concrete.

5. Acknowledgement

The provision of expansive additive and shrinkage reducing agent from Taiheiyo Materials Corporation, Japan is gratefully acknowledged.

6. References

[1] Tazawa, E. and Miyazawa, S., Autogenous shrinkage caused by self desiccation in cementitious material, 9th International Congress on the Chemistry of Cement (1992), Vol.4, pp.712-718.

[2] Tazawa, E., Matsuoka, S., Miyazawa, S. and Okamoto, S., Effect of autogenous shrinkage on self stress in hardening concrete, Proceedings of the International Symposium on Thermal Cracking in Concrete at Early Ages (1994), pp.221-228.

[3] Technical committee on autogenous shrinkage of concrete, Japan Concrete Institute, Committee Report, edited by Tazawa, E., E & FN SPON (1998), pp.9-62.

[4] Tazawa, E. and Miyazawa, S., Influence of constituents and composition on autogenous shrinkage of cementitious materials, Magazine of Concrete Research (1997), 49, No.178, pp.15-22.

[5] Tanimura, M., Hyodo, H., Sato, T. and Sato, R., An investigation on reducing shrinkage of high strength concrete, Proceedings of the Japan Concrete Institute (2000), Vol.22, No.2, pp.991-996 (in Japanese).

[6] Tanimura, M., Hyodo, H., Omori, H. and Sato, R., Experimental study on reduction of shrinkage stress of high strength concrete, Proceedings of the Japan Concrete Institute (2001), Vol.23, No.2, pp.1075-1080 (in Japanese).

[7] Sato, R., Tanaka, S., Hayakawa, T. and Tanimura, M., Experimental studies on reduction of autogenous shrinkage and its induced stress in high strength concrete,

Proceedings of the 2nd International Research Seminar in Lund (1999), pp.163-171.
[8] Yano, M., Nawa, T., Ogiwara, J. and Horita, T., Experimental studies on autogenous shrinkage of self-compacting concrete, Cement Science and Concrete Technology, Japan Cement Association, No.54 (2000), pp.673-679 (in Japanese).
[9] Cohen, M.D. and Mobasher, B., Effects of sulfate and expansive clinker contents on expansion time of expansive-cement paste, Cement and Concrete Research, Vol.21 (1991), pp.147-157.

CHARACTERIZATION OF THE PORE SPACE IN HARDENING CEMENT PASTE TO PREDICT THE AUTOGENOUS SHRINKAGE

Christian Pignat, Parviz Navi and Karen Scrivener
Swiss Federal Institute of Technology, Institute of Material Sciences
Laboratory of Construction Materials
MX-G Ecublens, CH-1015 Lausanne, Switzerland

Abstract

It is widely accepted that the main driving force for autogenous shrinkage is the capillary forces caused by self desiccation of the cement paste due to the consumption of water by hydration. These capillary forces are inversely related to the radius of the capillary and become significant at radii below about 100 nm.

This presentation describes the development of an Integrated Particle Kinetics Model (IPKM) to simulate the evolution of cement microstructure during hydration. The capillary pore space is characterized by transformation into a network of cylindrical tubes. This transformation is analytical which allows a wide range of pore sizes to be described without a lower limit on resolution. This model therefore has the potential to model the effects of capillary depression on a microscopic scale.

1. Introduction

The evolution of the porous structure of hardened cement paste during hydration strongly influences the transport and mechanical properties of cement based materials. The dimensions of capillary pores in cement paste span several orders of magnitude varying from a few nanometers to several micrometers. These pores are mainly interconnected forming a highly complex network. Their shape and distribution are modified by parameters like water to cement ratio, the particle size distribution and shape and the chemical composition of the cement, temperature and additives. However, characterization of the pore space of hydrated cement at the nanometric level is complicated and there is no accurate method applicable to investigate the modification of pore space at early ages cement hydration. In practice, construction of the microstructure of porous medium is usually limited to two-dimensional SEM images.

An indirect, complementary approach to the characterisation of the pore structure of cement pastes during hydration is through simulation of the cement paste microstructure. The use computer models to represent the microstructure of cement paste provides an excellent possibility to investigate the modifications of pore space and to study the influence of these modifications on the early age properties of cement based materials.

Based on a continuum approach, we have implemented an Integrated Particle Kinetics Model, (IPKM) to simulate in three dimensions the evolution of the microstructure of tricalcium silicate (C_3S) during hydration. The model is based on a continuum approach, with the grains of C_3S represented by spheres, further details may be found in [1,2]. To determine properly the dimensions of the continuum pore space simulated during hydration, an analytical approach has been applied. This approach permits us to represent the different capillary pores of a continuum pore space spanning over several orders of magnitude. It is important to note that all techniques that employ pixel discretisation to characterize the pore distribution of a continuum pore space, eliminate the pores smaller than the pixel size and the result becomes size dependent. This problem is discussed also in [2,3]. To represent accurately the pore space, it is necessary to employ either very fine size of pixel (unwieldy for the larger pores and incompatible with the usual limitation of computing power) or use a technique without pixel discretisation.

In this paper the different kinetics of hydration employed in the simulation are discussed, the method to compute the network of cylindrical pores and mechanisms of autogenous shrinkage are presented, and finally, the pore size distributions computed for four different cement particle size distributions are demonstrated and discussed.

2. Hydration kinetics

The particle-size distribution of ordinary Portland cement particles is in the range of 0.5–50 μm and the particles are polymineralic, composed of four phases. Among these phases we have simulated the hydration of C_3S particles. After mixing with water, the anhydrous phase C_3S dissolves (hydrates) and new phases appear – calcium hydroxide (CH) and calcium silicate hydrate (C-S-H). In this simulation three different kinetic regimes are used to represent the rate of hydration of the tricalcium silicate (C_3S) grains, which represent the mechanisms of nucleation and growth, phase-boundary reaction, and diffusion. These three mechanisms are discussed in [4], and the corresponding kinetics are given by the following equations.

Nucleation and growth of products:

$$(-\ln(1-\alpha))^{1/3} = K_1 t \quad (1)$$

Phase-boundary reaction:

$$1-(1-\alpha)^{1/3} = \frac{K_2 t}{R_0} \quad (2)$$

Diffusion:

$$1-(1-\alpha)^{1/3} = \frac{\sqrt{K_3 t}}{R_0} \quad (3)$$

In these equations α is the hydration degree of the considered particle, R_0 its original radius, t the hydration time and K_1, K_2 and K_3 are parameters calculated from calorimetry curves for hydrating C_3S.

The rate of reaction (hydration) of each grain before interparticle contacts depends on the original radius of the anhydrous core, the thickness of C-S-H and time. The passage from one kinetic to another one occurs when two hydration rates become equal. Depending on grain size, hydration can process through the three mechanisms or only by the first and the third ones. A schematic representation of the three hydration kinetics for a single particle is shown in Figure 1. In this example the hydration of the grain considered is controlled by three mechanisms and the passage from the first mechanism to second one occurs in point A and from the second one to the third one in point B.

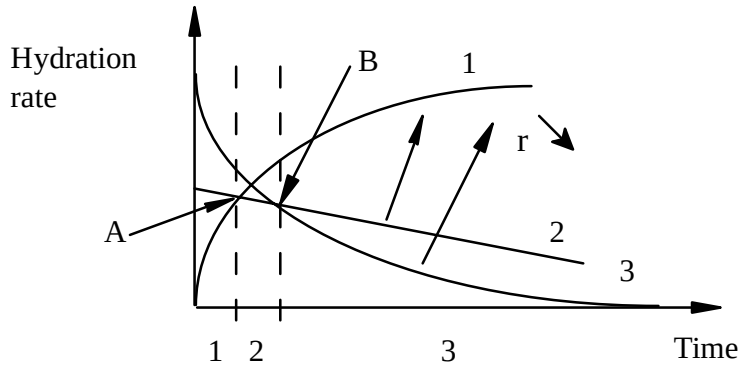

Figure 1 - Schematic representation of the variation of the three curves 1, 2, 3 with passage points from one mechanism to another one (points A and B).

After interparticle contacts occur during hydration, the rate of hydration of each cement particle is corrected (diminished), by taking into account the restrictive effect of the contacts with the other particles and the diminution of the available water in the system of capillary pores for continuing hydration.

3. Characterization of simulated pore space

In this approach, a pore center is defined as a local maximum of the distance to the grains and a neck center (boundary between two pores) is defined, as a local minimum of this distance. In a three dimensional structure, a pore center is defined by four neighboring grains and a neck by three grains. This analytical calculation of the pore centers was derived from algorithms developed in the field of molecular biology [5]. These algorithms, by analogy, allowed the pore centers to be defined as the places where a tangent sphere to four grains can be placed without overlapping other grains. The pore network can be represented as a network of tubes, where two neighboring pore centers are linked by a cylindrical tube whose effective radius is computed from the corresponding neck configuration.

In Figure 2, a 2D illustration of two pore centers and a relating cylinder is illustrated. At each step of hydration the program controls the existence of pore centers and necks throughout the pore system and constructs the network of cylindrical tubes.

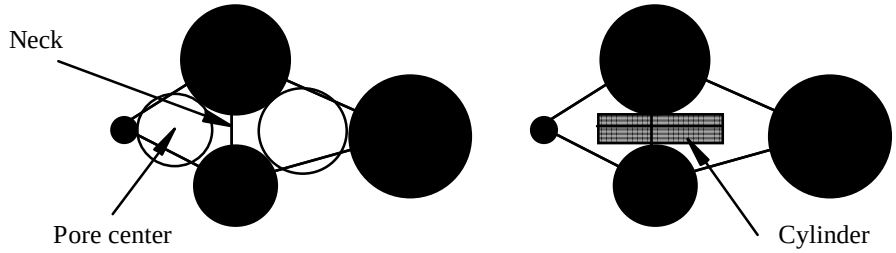

Figure 2 - 2D schematic representation of two pores and one cylinder. The black circles represent cement particles.

The effective radius of a cylinder is the hydraulic radius of the neck, this value is defined by the equation (4).

$$R = \frac{2 * area}{perimeter} \qquad (4)$$

This radius gives the circle radius when the neck is circular.

4. Autogenous shrinkage

Several mechanisms have been proposed to be the cause of autogenous shrinkage, including capillary depression, surface tension and disjoining pressure. During hydration, two types of pores are created in the material: the nano-pores associated with the C-S-H gel and capillary pores. According to [6], the nano-pores remain saturated during hydration and the internal relative humidity is higher than 80 % for normal cements under confined conditions. That means that, at relative humidities between 100 % and 80 % the surface tension mechanism cannot be active on the nano pore level and the disjoining pressure remains constant. Nevertheless, the capillary pores become partially saturated due to self-desiccation and capillary forces become significant at radii below about 100 nm.

So it seems reasonable to consider that the capillary forces are mainly responsible for the autogenous shrinkage. In this case one can relate the pressure gradient with the capillary radius and the relative humidity through equations (5) and (6), representing Laplace's law and Kelvin's law respectively.

$$p_C - p_V = -\frac{2\sigma}{r}\cos\theta \tag{5}$$

$$p_C - p_V = \frac{RT}{Mv}\ln(h) \tag{6}$$

Where, P_c is the pressure in water, P_v the pressure in water vapor, σ the surface tension of the water/water vapor interface, θ the wetting angle, r the capillary radius, R the ideal gas constant, T the temperature, M the water molar mass, ν the water specific volume and h the relative humidity.

Laplace's law contains the radius in the case of a circular tube, but this equation can be expressed as a function of the area and the perimeter for non-circular tubes. Indeed, the pressures are applied on the area and the surface tension on the perimeter. So, the hydraulic radius is a suitable choice, regardless the exact shape of the capillary.

Equation (7) is obtained by combination of equations (5) and (6) and setting P_v and θ equal to zero.

$$p_C = -\frac{2\sigma}{r} = \frac{RT}{Mv}\ln(h) \tag{7}$$

The aim of this work is to compute the pore distribution and the water content during hydration, which are a function of the water to cement ratio, the hydration degree and the volumetric coefficients in the hydration reaction. It is therefore possible to calculate the critical capillary radius r_c: pores bigger than this value are empty and those smaller are filled with water. By knowing all the cylinders and the connectivity, this should allow the critical capillary radius, the related pressure and corresponding relative humidity to be calculated in the future.

5. Effect of particle size distributions on the pore size distribution

The influence of cement particle size distributions on the pore size distribution of hydrated cement has been studied through numerical simulation. Table 1 presents the size characteristics of the five particle size distributions (PSDs) considered in this study. The cumulative weight distributions of the grains are also given in Figure 3. In this work the computational volume considered is 100μm*100μm*100μm and the water-to-cement ratio 0.42. In Table 1 the number of particles gives the number of spheres placed in the computational volume, which is function of the fineness of the cement, the Φ_{max}, Φ_{min} and specific surface are also given.

Table 1 - Characteristics of the four PSDs considered in the study and typical Portland cement.

	Number of particles	Specific surface (cm^2/g)	Φmax (μm)	Φmin (μm)
PSD1	191	1058	40.4	10.9
PSD2	932	1597	40.4	5
PSD3	2556	1976	40.4	2.95
PSD4	4182	2085	40.4	2
Typical Portland cement	110000	3585	40.4	0.5

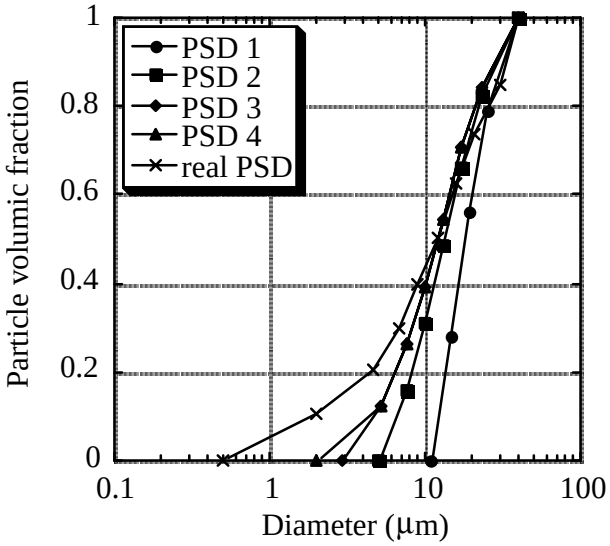

Figure 3 - Size distributions of the four PSDs considered in the simulation in comparison with a typical real cement

The hydration of the four PSDs was simulated and their pore distribution computed. The computed pore distributions corresponding to each PSD before and after hydration are given in Table 2. The number of particles, cylinders, the minimum and maximum pore radii for the four PSDs are presented. The degree of hydration reached was around 0.95 with a porosity corresponding porosity of around 7 % for the four PSDs.

Table 2 - Characteristics of computed cylinders; the number of grains and cylinders, the maximum and minimum cylinders radii for the four cements and cement pastes, before and after hydration.

	Number of grains	Number of cylinders	R_{max} (μm)	R_{min} (μm)
PSD1 before hydration	191	2398	6.93	0.96
PSD2 before hydration	932	11275	5.18	0.44
PSD3 before hydration	2556	30662	4.01	0.24
PSD4 before hydration	4182	49321	3.82	0.18
PSD1 after hydration	229	1067	4.93	0.0039
PSD2 after hydration	1118	3728	3.60	0.0011
PSD3 after hydration	3067	11550	3.19	0.00045
PSD4 after hydration	5018	16572	2.79	0.00023

Tables 3 and 4 give the cumulated number of computed pores (cylinders) in simulated cements before and after hydration respectively in terms of pore size.

Table 3 - Number of cylinders smaller than the given size for the four cements before hydration

Radius in μm	PSD1 before hydration	PSD2 before hydration	PSD3 before hydration	PSD4 before hydration
10	2398	11275	30662	49321
5	2119	11275	30662	49321
2	125	4277	22350	42257
1	1	299	3158	8483
0.5		3	141	532
0.2				2

Table 4 - Number of cylinders smaller than the given size for the four cement pastes after hydration

Radius in μm	PSD1 after hydration	PSD2 after hydration	PSD3 after hydration	PSD4 after hydration
5	1067	3728	11550	16572
2	693	3200	11216	16382
1	316	1667	6847	11178
0.5	135	631	2903	4711
0.2	45	213	861	1420
0.1	20	91	355	637
0.05	7	43	146	314
0.02	3	16	46	100
0.01	3	6	31	50
0.005	2	2	9	23
0.002		2	2	70
0.001			1	6
0.0005			1	6

6. Discussion and conclusion

As indicate in Table 1 the number of grains placed in a computational volume is function of the specific surface (fineness) of grains. This number becomes very large for normal Portland cement. The computing time and requirement for computer memory become extremely large for the simulation of the cement hydration with a realistic number of grains. Indeed, the calculation time is roughly proportional to the square of the number of grains. Consequently only coarser PSDs have been studied at this stage. This of course does not mean that the influence of fine particles can be ignored during the formation of paste structure. Fine particles have a highly significant influence on the microstructure and capillary pores of the paste. They are particularly important in determining the pore distribution and pore dimensions.

As it is not possible to completely simulate a typical PSD of real cement having about 110 000 grains in a computational volume, at this stage, coarser PSDs have been studied. From Table 2, it can be noted that the number of grains for all cases has increased about 20 % after hydration. This is due to calcium hydroxide grains that are created in the pore space during hydration. The number of cylinders (necks) is very high at the beginning of hydration and then decreases, this is due to the disappearance of the pores and necks at lower porosities.

For a hydration degree of 0.95, the number of necks reduces to about one third of the initial number of necks before hydration. R_{max} and R_{min} decrease with the increase of the number of grains in the computational volume.

Tables 3 and 4 show that the finer the cement is, the finer are the necks in cement before and after hydration. Also the number of small pores in finer cement is higher than in the coarser cements. Our preliminary results also confirm that, if we consider a larger number of the grains in a computational volume with a given water-to-cement ratio, the simulated cement will have more pores, but hydraulics radius will decrease.

Regarding cylinders sizes, Table 2 shows that, for all pores, the effective radius can be computed with this method. The minimum values after hydration are around a nanometer in size and the maximum value can be any value. So, the transformation of the pore space into a network of cylindrical tubes by an analytical approach, permits us to characterize pores over several orders of magnitude down the nanometer range. The problems of resolution of pixel based methods are avoided and the small pores pertinent for forces leading to shrinkage and cracking can be represented.

Although with current computer power it is not possible to simulate the cement with real grain size distribution, extrapolation from the results shown in Table 4 can give the approximate number of pores with the effective pore radius. For example, from the relation between the number of cement grains and the number of the pores smaller than 100 nanometers, the preliminary results indicate that this number will be around 20 000 for a cement with 110 000 particles in the computational volume.

Knowing all the tubes and the connectivity, the next step will be the calculation of the relative humidity and the internal capillary forces to predict autogenous shrinkage.

Acknowledgments
Financial support from Swiss National Science Foundation is gratefully acknowledged.

References

[1] Navi, P., Pignat, C., Advances in Cement Based Materials, **4** (1996) 58-67.

[2] Navi, P., Pignat, C., Cement and Concrete Research, **29** (1999) 507-514.

[3] Garboczi, E. J., Bentz, D. P., The effect of statistical fluctuation, finite size error, and digital resolution on the phase percolation of the NIST cement hydration model, Cement and Concrete Research, **31** (2001), 1501-1514.

[4] Bezjak, A., Jelenic, I., On the determination of rate constants for hydration processes in cement pastes, Cement and Concrete Research, **10** (1980) 553-563.

[5] Yeates, T. O., Algorithms for evaluating the long-range accessibility of protein surfaces, Journal of Molecular Biology, **249** (1995) 804-815.

[6] Hua, C., Acker, P., Ehrlacher A., Analyses and models of the autogenous shrinkage of hardening cement paste, Cement and Concrete Research, **25** (1995) 1457-1468.

TENSILE CREEP MODEL BASED ON CORROSIVE ATTACK OF WATER VAPOR ON C-S-H GEL AFFECTED BY SELF-DESICCATION AND APPLIED STRESS

Ippei Maruyama, Sun-gyu Park, Takafumi Noguchi
The University of Tokyo, Department of Architecture
7-3-1, Bunkyo-ku, Hongo, Tokyo, 113-8656 JAPAN

Abstract

With experimental result that the amount of chemically bound water of low water cement paste under restraint condition increase as against the same cement paste without restraint, hypothesis is presented that afford to explain this phenomena is proposed and the relation between tensile creep behavior and internal moisture content of cement paste. Based on this hypothesis, it is attempted to develop a tensile creep model.

1. Introduction

High-Performance Concrete, characterized by low water-binder ratio, are particularly sensitive to self-desiccation of the cement paste during the hydration process, which is a principal cause of autogenous shrinkage. If an external restraint is present, autogenous shrinkage, added to temperature-induced deformations, may lead to high self-induced stresses, possibly causing surface and even through cracks. In order to estimate the cracking risk, it is of vital importance to accurately calculate the self-induced stresses. In this calculation the early-age creep behavior of the concrete plays a prominent role, since the self-induced stresses will be substantially reduced due to relaxation.

A number of mechanisms of creep/relaxation, especially concerned with compressive creeping behavior, have been proposed and discussed over the years [1-5]. Concerning the cracking problem, it is the tensile creep that plays important and main role. The tensile creep mechanism is not discussed as much. In this contribution, chemically bound water of cement paste under 2 different conditions, i.e. restraint condition and non restraint condition, was measured. Hypothesis that afford to explain the phenomena of

this experiment is proposed and based on this hypothesis the simple tensile creep model is developed.

2. Experiment

Amount of chemically bound water of cement paste under different restraint condition, i.e. non-restraint condition and restraint condition by embedded screw bar, was measured. The cement used in this simple experiment is Ordinary Portland Cement, which chemical and physical property is shown in detail in Table 1. And the water-to-cement ratio of cement paste is 30% in weight. In addition, for smooth stirring and uniformity of cement paste, chemical admixture (salt of polycarboxylic acid) is used by 0.3% of cement in weight.

Table 1 - Properties of cement paste

Specific mass (g/cm^3)				Specific surface area (cm^2/g)				
3.16				3260				
SiO_2 (%)	Al_2O_3 (%)	Fe_2O_3 (%)	CaO (%)	MgO (%)	SO_3 (%)	Na. O (%)	K_2O (%)	Cl^- (%)
20.5	5.31	2.73	64.3	0.93	2	0.23	0.37	0.011

Specimen size is 40mm x 40 mm x 160 mm and curing conditions are sealed with polyester film or 100% RH after 1 day sealed condition. Both specimens are placed in 20 °C constant chamber. Screw bar of 8 mm in diameter and 140mm in length is embedded in the center of paste specimen as restraint on deformation of paste. (see Figure 1)

On 1, 3, 7 day after placing, chemically bound water of cement paste are measured. Specimens are crushed and immersed in acetone for 1 day, and then D-dried 2weeks in each. After D-drying the specimens were grinded and sieved. The grinded powder of cement paste, under 88 μm in diameter, is oven-heated up to 1000 °C. And the loss of weight is measured.

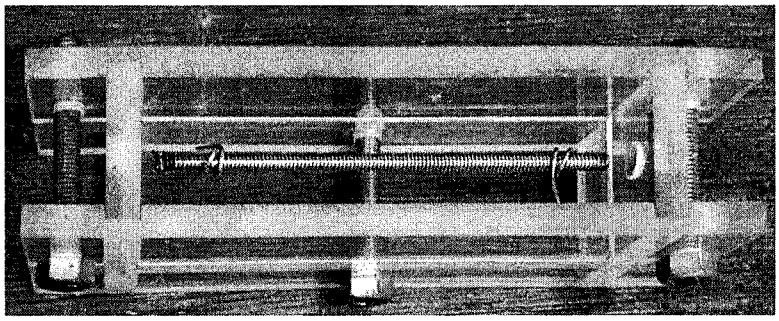

Figure 1 - Mold and screw bar placed at the center

3. Experimental Result

In Figure 2, the result of experiments is shown. The notation "w" and "s" represent the curing condition of 100% RH and sealed respectively. And "non" and "screw" stand for the restraint condition of free and screw bar restraint respectively.

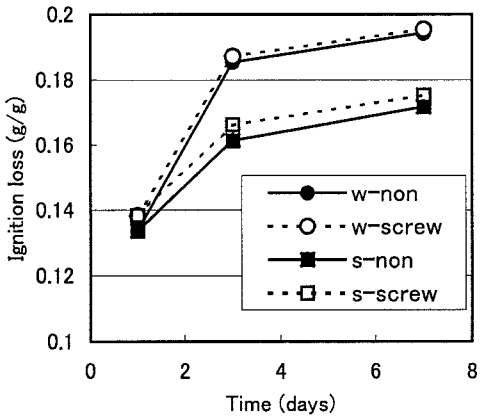

Figure 2 - Difference of chemically bound water of cement paste under free and screw-bar restraint with sealed and 100% RH curing.

As is shown in Figure 2, the amount of the chemically bound water under restraint condition is slightly increased compared with the one under non-restrained condition. The increase can be seen in both sealed and 100% RH curing. The difference is rather big in the cement paste with sealed curing than that of 100% RH curing.

4. Discussion

Amount of chemically bound water should be differentiated by the difference of condition in the cement paste specimen, i.e. different stress condition. With the restraint of autogenous shrinkage stress must be induced in the cement paste specimen especially around the screw bar. Thus the most likely explanation is that the stress induced by the autogenous shrinkage yields the increase of chemically bound water.

Kumano [6] investigated a relationship between the pore structure and the creep phenomena and he found that the amount of small pores of which diameter is around 1 μm in cement paste increase with tensile stress (see Fig. 3). According to his conclusion, micro-cracks are responsible for this increase of porosity [6].

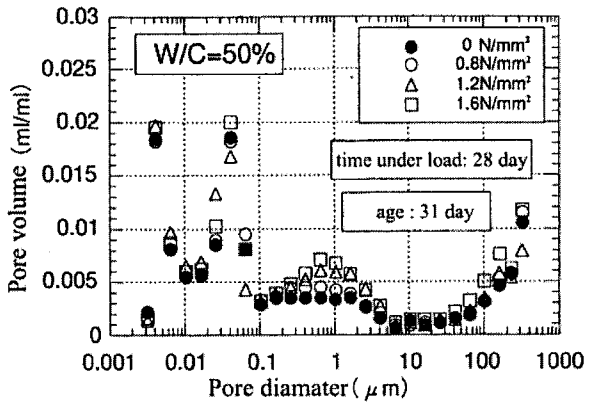

Figure 3 - Pore size distribution under different tensile stress [6]

Experimental results by Wiederhorn [7] may account for fundamental doubt about the feasibility of micro-crack under such a low stress/strength ratio. The double cantilever cleavage specimen made by soda-lime glass was used for crack propagation test. This test

was conducted with different constant force applied to the ends of specimen and different environmental condition of relative humidity. It is shown that even in a low strength/stress ratio the crack of soda-lime glass propagated slowly, especially in the condition of high relative humidity. In Figure 4 the crack velocity depending on the relative humidity is presented.

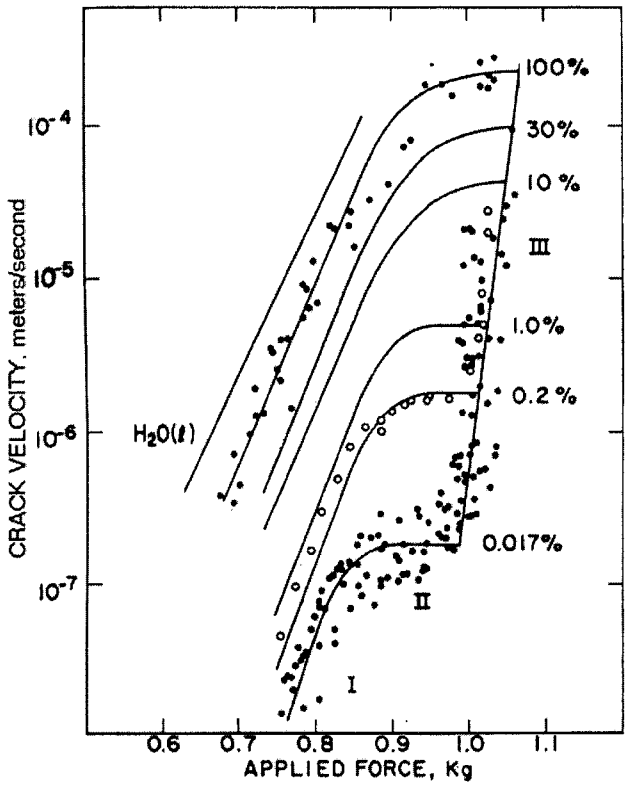

Figure 4 - Dependence of crack velocity on applied force. The percent relative humidity for each set of runs is given on the right-hand side of the diagram. [7]

Mould [8] proposed a mechanism of this slow crack propagation under low stress/strength ratio. According to his hypothesis, water is the most effective agent for

this process and the rate of crack growth is governed primarily by the localized stress at the crack tip and by the concentration of water or water vapor at that point. And the reaction generally appears to involve only water and the silica network of the glass and may be thought of as a simple hydrolysis of the surfaces formed during crack growth. The schematic of Si-O-Si and H_2O reaction is shown in Figure 5.

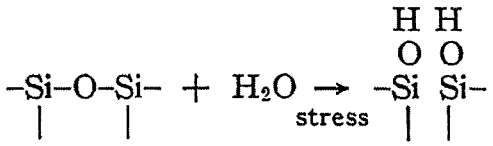

Figure 5 - Schematic of hydration under stress between Si-O bonds and water at the crap tip [8]

It follows from the hypothesis and the experimental results introduced above that the Si-O bonds, which exist in C-S-H gel as well, are activated with stress and become easy to hydrate. And based on this assumption, the increase of chemically bounds water can be explained.

5. Summary

To sum up the argument above, under stress condition, Si-O bonds are activated and easy to hydrate. And at low stress/strength ratio micro-crack propagation is mainly governed by this chemical reaction of Si-O hydration and its speed is very slow.

Many Si-O bonds can be found in C-S-H gel. The C-S-H gel of cement paste at ordinary temperature has many crystal defects and it is highly possible that stress is localized around these crystal defects and Si-O bonds hydrate with water at these points if the cement paste is restrained from autogenous shrinkage. Thereby chemically bound water increase.

6. Modeling of tensile creep phenomena

As is discussed above, the tensile creep-relaxation phenomenon can be explained by

the microcrack that is dominated by the chemical reaction between Si-O bond and H_2O. Based on this assumption, model of tensile creep phenomena is developed.

6.1 Nucleation of crack

The theory of crack nucleation in amorphous material under stressed condition is suggested by Fisher [9]. Reversible formation of the two surfaces of a semicircular crack requires work equal to $\pi r^2\gamma$ where γ is the solid surface tension and r is the radius of the crack. The work required for the reversible relaxation of strain energy in the neighborhood of the crack is $-4(1-\nu^2)r^3\sigma^2/3E$ where σ (in tension) is the stress in the direction normal to the plane of the crack, ν is the Poisson's ratio and E is the Young's modulus of material. The net work associated with the reversible formation of a circular crack of radius *r* is,

$$W = \pi r^2\gamma - 4(1-\nu^2)r^3\sigma^2/3E \tag{1}$$

The curve of *W* versus *r* has a maximum.

$$W_{max} = \pi^3\gamma^3E^2/12(1-\nu^2)^2\sigma^4 \quad \text{at} \quad r_{ini} = \pi\gamma E/2(1-\nu^2)\sigma^2 \tag{2}$$

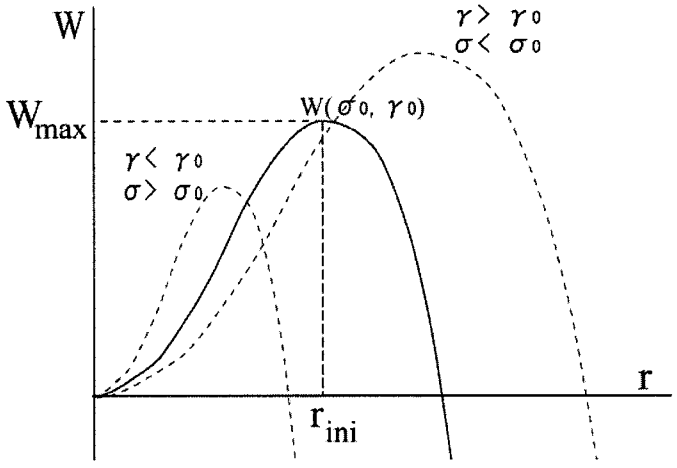

Figure 6 - Work required for reversible formation of a crack of radius r in a amorphous under tensile stress [9]

This maximum of reversible work depends on the surface tension of newly created surface and applied stress. Assuming that body of cement paste is composed of a uniform C-S-H gel and it has capillary pores filled with water vapor, many molecules of water are adsorbed on the internal surface of cement paste and it decreases the energy of surface tension of cement paste [10]. In respect that the surface energy of internal pore is low, it is highly possible that the nucleation of crack appear on the surface of capillary pore and the possibility of nucleation of crack depends on relative humidity in the capillary pore through the surface energy of C-S-H gel.

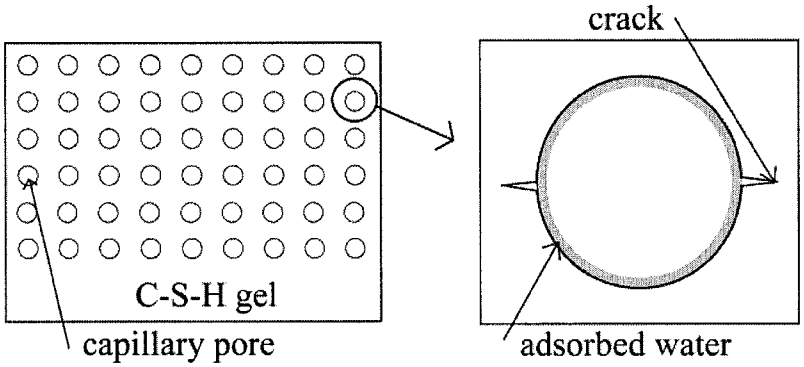

Fig. 7 Schematic structure of cement paste and capillary pore

Using the equation of the theory of nucleation [11], which is based on the theory of absolute reaction rates, the equation (3) shows the rate of nucleation of circular crack under stressed condition is derived.

$$\frac{dn}{dt} = \frac{NS_f kT}{h} \exp[-(E_s + W_{max})/kT] \qquad (3)$$

where Es denotes the free energy of activation for separating a pair of atoms

N denotes the number of bonds on capillary pores in stressed material

T denotes the absolute temperature

k denotes the Boltzmann constant

h denotes the Planck constant

S_f denotes the shape factor determined from pore structure of cement paste

n denotes the number of crack nucleation

According to the equation (3) and using the assumption that the total number of molecules that are able to fracture is constant, the following equation that shows the number of nucleation at time *t* is obtained.

$$C_{nucleate}(t) = N_0 e^{-\alpha t} \quad (4)$$

where $C_{culeation}$ denotes the number of nucleated crack per unit time at time *t*

N_0 denotes the number of bonds on the surface of capillary pore which is able to crack under stressed condition.

α denotes the $\frac{S_f kT}{h} \exp[-(E_s + W_{max})/kT]$

6.2 Crack propagation

Once a crack is nucleated, the crack propagates according to the rate of chemical reaction. Charles and Hillig [12] suggested following equation for the velocity of a moving crack under the influence of a corrosive environment and a crack tip stress σ` :

$$v = v_0 \exp[-(E^* - V^*\sigma' + c\sigma'^2 + \Gamma V_m / 2\rho)/RT] \quad (5)$$

where E^* denotes the activation energy for surface corrosion at a stress-free surface.

V^* denotes the activation volume for the process

$c\sigma`^2$ denotes the combined effect of the disappearance of strain energy due to corrosion and a second order term in the expansion of the activation energy

$\Gamma V_m/2\rho$ denotes the effect of curvature of the reaction surface

Γ denotes the surface free energy of the Si-O bonds of surface corrosion product interface

V_m denotes the molar volume of the C-S-H

ρ denotes the radius of curvature of the crack tip

σ` denotes the crack tip stress

Using this equation (4), the σ^2 term is small compared to the other terms in the exponential of equation (5) and can be neglected to a good approximation [7] and the surface energy term is assumed to be constant, the following equation is obtained:

$$v = v_0 \exp[-(E^* + \mu_s - \beta'\sigma')/RT] \quad (6)$$

where β` denotes the constant

μ_s denotes the energy required for new surface

E* denotes the activation energy for surface corrosion at a stress-free surface and surface energy required for new surface

Equation (6) describes the crack propagation velocity according to rate of chemical reaction.

Based on 1 mole of reacting Si-O-Si bonds, the equation for chemical reaction at a free surface is

$$H_2O + B \rightarrow B^* \quad (7)$$

E^* should be expressed as the difference in chemical potential between the reactants and product.

$$E^* = \mu_{B^*} - \mu_B - \mu_{H_2O} \quad (8)$$

where μ_{B^*} denotes the chemical potential of activated bond

μ_B denotes the chemical potential of bond

μ_{H2O} denotes the chemical potential of water

$$\mu_{H_2O} = RT \ln[(\frac{2\pi m_{H_2O} kT}{h^2})^{-3/2} \cdot \frac{P_{H_2O}}{kT}] \quad (9)$$

where P_{H2O} denotes the partial pressure of H_2O

m_{H2O} denotes mass of H_2O molecule

Assuming that μ_{B^*} and μ_B are independent of environment, μ_s is constant under constant relative humidity atmosphere and the crack tip stress σ is proportional to the applied stress σ` the following equation is obtained:

$$v = c \exp[-(RT \ln[(\frac{2\pi m_{H_2O} kT}{h^2})^{-3/2} \cdot \frac{P_{H_2O}}{kT}] - \beta\sigma)/RT] \quad (10)$$

where c denotes material parameter effected by RH and C-S-H gel properties

β denotes material parameter effected by pore structure

If it is now assumed that the crack velocity is proportional to the rate of chemical reaction at the crack tip, the following equation (10) is obtained:

$$N_{propergation} = \beta_1 \exp[\beta_2 \sigma / RT] \tag{11}$$

where β_1 denotes $\text{const.} \times (\frac{2\pi m_{H_2O} kT}{h^2})^{-3/2} \cdot \frac{P_{H_2O}}{kT}$:constant parameters affected by temperature and C-S-H gel properties

β_2 denotes constant parameter effected by pore structure

$N_{propagation}$ denotes the number of moles of bonds reacting at crack tip per unit area per unit time.

In former section the crack is assumed as circular crack. The increase ratio of radius of crack is obtained as follows.

$$r(t) = \sqrt{2A_B N_{propagation} (t + \frac{r^2_{ini}}{2A_B N_{propagation}})} \tag{12}$$

where $N_{propagation}$ denotes the number of moles of bonds reacting at crack tip per unit per unit time (see equation (11))

A_B denotes Area per bonds

t denotes span under load

r_{ini} denotes the radius r with W_{max} (see equation (2))

6.3 Time dependent deformation based on the linear elastic fracture mechanics

In this section time dependent deformation under constant tensile stress is discussed with crack nucleation concept and crack propagation concept. The creep tensile creep phenomena can be expressed by the rate of crack nucleation and the rate of crack propagation with the linear elastic fracture mechanics. For expression of creep phenomena with linear elastic fracture mechanics, several assumptions that are taken into account are detailed below:

- C-S-H gel is elastic even after cracks are nucleated.
- Nucleated crack has semicircular shape.
- Crack propagation keeps its shape.
- Stress intensity factor is the same in each crack and expressed in equation (13).

$$K_I = \sigma p\sqrt{\pi r} \tag{13}$$

where p denotes the shape parameter

- Strain energy release rate is expressed in equation (14)

$$G_I = \frac{1}{E'}K_I^2 \tag{14}$$

- Each crack does not affect applied stress of the others.
- On this tentative formulation, cylindrical specimen is assumed.
- The specimen has base in A[m^2] and height in L[m]

Released work of nucleated cracks:

The release energy of each nucleation of crack is given in the form:

$$\begin{aligned}\int_0^{A_{ini}} \frac{(\sigma p\sqrt{\pi r})^2}{E'}dA &= \int_0^{r_{ini}} \frac{\pi r p^2\sigma^2}{E'}(\pi r)dr = \frac{\pi^2 p^2\sigma^2}{E'}\int_0^{r_{ini}} r^2 dr \\ &= \frac{\pi^2 p^2\sigma^2}{3E'} r_{ini}^{\ 3}\end{aligned} \tag{15}$$

And the number of nucleated crack at time t is derived from equation (4):

$$N_{crack} = \frac{N_0}{\alpha}[1 - Exp(-\alpha t)] \tag{16}$$

Then the total strain energy release owing to the nucleation of cracks W_n at time t is given by:

$$W_n = \frac{\pi^2\sigma^2}{3E'} r_{ini}^{\ 3} \times \frac{N_0}{\alpha}[1 - Exp(-\alpha t)] \tag{17}$$

Released work by crack propagation:

The radius of crack at time t with the time of nucleation t_i is $r(t-t_i)$. Therefore released work $W_i(t-t_i)$ by crack propagation of each crack is:

$$W_i(t-t_i)=\int_{r(t_i)}^{r(t-t_i)}\frac{K_i^2}{E'}dr=\frac{\sigma\pi}{E'}\frac{r^2(t)}{2}=\frac{\sigma\pi}{E'}A_B N(t-t_i) \tag{18}$$

And the released work per unit time is determined:

$$\frac{dW_i}{dt}=\frac{\sigma\pi}{E'}A_B N \tag{19}$$

The rate of release work by crack propagation of each crack is constant. This means that that the rate of energy for crack propagation is independent of time of load and span under load. Therefore the total energy for crack propagation, W_p, per unit time is expressed as:

$$\frac{dW_p}{dt}=\frac{N_0}{\alpha}[1-\mathrm{Exp}(-\alpha t)]\times\frac{\sigma\pi}{E'}A_B N \tag{20}$$

Then accumulated total release work by crack propagation is:

$$\begin{aligned}W_p&=\int_0^t\frac{N_0}{\alpha}[1-\mathrm{Exp}(-\alpha t)]\times\frac{\sigma\pi}{E'}A_B N dt\\&=\left[\frac{\sigma\pi}{E'}A_B N\cdot\frac{N_0}{\alpha}t+\frac{\sigma\pi}{E'}A_B N\cdot\frac{N_0}{\alpha^2}\mathrm{Exp}(-\alpha t)\right]_0^t\\&=\frac{\sigma\pi}{E'}A_B N\cdot\frac{N_0}{\alpha}\left(t+\frac{1}{\alpha}\mathrm{Exp}(-\alpha t)-\frac{1}{\alpha}\right)\end{aligned} \tag{21}$$

Time dependent deformation:

The total released work by crack nucleation and crack propagation is:

$$W_{total}=W_n+W_p \tag{22}$$

The time dependent strain is determined by using W_{total} shown above:

$$\begin{aligned}\varepsilon&=\frac{1}{A\sigma\cdot L}W_{total}\\&=\frac{1}{A\sigma\cdot L}\left(\frac{\pi^2\sigma^2}{3E'}r_{ini}{}^3\times\frac{N_0}{\alpha}[1-\mathrm{Exp}(-\alpha t)]\right.\\&\quad\left.+\frac{\sigma\pi}{E'}A_B N\cdot\frac{N_0}{\alpha}\left(t+\frac{1}{\alpha}\mathrm{Exp}(-\alpha t)-\frac{1}{\alpha}\right)\right)\end{aligned} \tag{23}$$

In engineering expression, assuming that the α is less than 1, the term $\frac{1}{\alpha}\mathrm{Exp}(-\alpha t)-\frac{1}{\alpha}$ can be ignored compared to time span.

Therefore, the convenient expression of tensile creep stress is:

$$\varepsilon = A[1-\mathrm{Exp}(-Bt)]+Ct \qquad (24)$$

where A denotes the parameter for nucleation of crack

B denotes the parameter representing the magnitude of cracking tendency

C denotes the parameter for crack propagation

Validation of model:

Using the formulated engineering model of creep phenomena, comparison with experimental data is attempted. The result of this comparison is shown in figure 8. Experimental results that are represented as dots in fig.8 are shown in the reference of Illston [13]. Normal Portland cement is used, the water to cement ratio is 40% and aggregate/cement ratio is 1.5. Age of applied stress is 7 day after casting and the specimens are stored in the average condition of 18.3°C and 63% R.H.

Results of fitted parameters are listed in Table 2. The parameter A is concerning with the crack nucleation phenomenon. According to equation (17), as the applied stress increase or the surface tension in capillary pores decrease, this parameter A increase. Regarding parameter B, which represents the rate of crack nucleation, become smaller as the applied stress increase of the surface tension decrease (see equation (2) and (4)). The parameter C, which is the parameter of crack propagation, is affected by the applied stress and the surface tension as in the previous parameters (see equation (6)). These tendencies of parameters agree with the results of fitted parameters shown in Table 2.

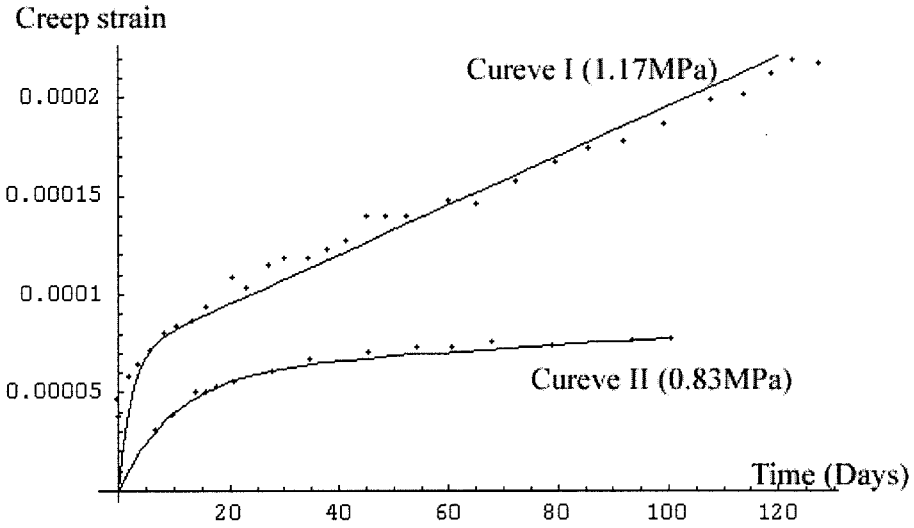

Figure 8 - Validation of engineering tensile creep model (doted data is the result of Illston [15]

Table 2 - Result of curve fitted parameters

Parameter	A	B	C
Curve I	0.00007	0.45	1.26-6
Curve II	0.00006	0.1	1.8-8

7. Conclusion

The chemically bound water under stressed condition increases. This phenomenon can be evidence of microcrack under low tensile stress by corrosive attack of water vapor. Based on this hypothesis with using absolute reaction rate theory and linear elastic fracture mechanics the tensile creep phenomena is formulated as the process of cracking and engineering model is suggested. The results of fitted curve parameters show correspondence with theories that are used in formulating.

References

1) Powers, T. C., Mechanisms of shrinkage and reversible creep of hardened cement paste, Proc. Int. Conf. On the Structure of Concrete, Cement and Concrete Association, London, U.K., pp.319-344, Sep. 1965

2) Neville, A. M., "Creep of concrete: plain, reinforced, and prestressed", North-Holland Publishing Company, pp. 258-309, 1970

3) Feldman, R. F., Mechanism of Hydrated Portland Cement Paste, Cement and Concrete Research, Vol.2, pp.521-540, 1972

4) Coutinho, A. Sousa, A contribution to the mechanism of concrete creep, Vol.10, N.55, Materiaux et Construction, pp.3-16, 1977

5) Bazant, Z. P., Anders Boe Hauggaard, Sandeep Baweja, Franz-Josef Ulm, Microprestress-Solidification Theory for Concrete Creep. I, II, Journal of Engineering Mechanics, pp.1188-1201, 1997

6) Kumano, T., et al., A study on the prediction model of tensile creep strain of concrete based on micro pore behavior, Journal of Material, Concrete Structure and Pavements, V-42, No.613, pp.121-135, 1999.2 (In Japanese)

7) Wiederhorn, S. M., Influence of Water Vapor on Crack Propagation in Soda-Lime Glass, J. Am. Cer. Soc. Vol.50, No.8, 1967, pp.407-413

8) Mould, R. E., Strength and Static Fatigue of Abraded Glass Under Controlled Ambient Conditions: IV, Effect of Surrounding Medium, J. Am. Cer. Soc., 1961, Vol.44, No.10, pp.481-491

9) Fisher, J. C., The Fracture of Liquids, J. App. Phys., 19, pp1062-1067, 1948

10) Hauggaard-Nielsen, A. B. Mathematical Modelling and Experimental Analysis of Early Age Concrete, DTU Report, p.59, 1997

11) Fisher, J. C., et al., Nucleation, J. App. Phys. 19, p775, 1948

12) Hillig , W. B., Charles, R. J., pp.682-705 in High-Strength Materials, Edited by V. F. Zackey, John Wiley & Sons Inc., 1965

13) Illston, J. M., The creep of concrete under uniaxial tension, Magazine of Concrete Research, Vol.17, No.51, June 1965, pp.77-84

INVESTIGATION OF SHRINKAGE STRESSES DEVELOPED AT SETTING OF THE CONCRETE BEARING POLYMER FILM COATINGS

D.Beilin[1] , V.Karchevsky[1], O.Figovsky[2]
[1] Corpem Ltd,
Migdal HaEmek , Israel
[2] Polymate Ltd,
Migdal HaEmek , Israel

Abstract

Experimental and theoretical investigations were carried out on the polymer coating influence on both shrinkage stresses and a concrete crack resistance at hardening. Shrinkage stresses develop in a polymer coating during the process of a concrete article moulding. These stresses produce a compression of the concrete contact layer, and are analogous to prestressed reinforced concrete structures. As the result, the crack forming bending moment increases. The set of concrete beams with the coating, based on a chlorine-sulfonated-polyethilene (CSPE) water suspension, and hardened by a water solution of Mannich alkalis (MA) was tested. It was experimentally found out that the crack forming bending moment had increased by 15-20% due to the coating shrinkage as the function of thickness and mechanical characteristics of the coating. The definition model of a shrinkage stresses was proposed, which fairly agrees with our test results.

1. Introduction

At moulding of concrete and reinforced concrete structures film coatings are widely applied for the purpose of acceleration of concrete hardening and reduction crack appearance at it setting. The film prevents evaporation of the water contained in concrete, promoting hydratation of cement and, thus providing reliable contact of a cement stone and a filler. It promotes increase of concrete strength up to 30 %, reduction of destruction and time of processing and restriction of moisture absorption. Within the framework of the research plan we have made attempt to apply the developed composition of high-adhesion coatings for moulding of concrete articles and to examinate the influence on process setting and hardening of concrete, and as well as the strength and deformation characteristics under loading .

2. Coating composition

For the first time we have prepared a vulcanized waterborne protective crack resistant coatings based on CSPE for concrete and other materials that possess a better corrosion-, crack-, gas- and water resistance than many commonly used coatings [1]. These properties have been achieved owing to the application of a waterborne vulcanizing agent, which had never been used before. It has been empirically revealed, that it is possible to induce cross-linking in water dispersion of CSPE by addition of tris-[dimethylaminoalkyl]-phenol or so-called Mannich base in the presence of epoxydimethylhydantoin resin. Compounds like Mannich alkalis ,cause formation of quaternary ammonium bonds in a vulcanized net of the saturated elastomer, which possesses reactive functional groups.

It has been established, that when all three components are combined the cross-linking reaction initiates and results in CSPE-based coating having very good mechanical properties and chemical resistance.

Application of MA as a structure-forming component of CSPE makes it possible to manufacture ecologically safe vulcanized coatings of any substrates. These coatings can be used in aircraft-, automotive-, shipbuilding, paint and varnish industries, civil engineering, etc. as crack- and corrosion resistant materials.

Application of polymeric film coatings for reinforced concrete structures allows not only to isolate concrete and reinforcement reliably from aggressive environment attack, but permits to affect positively on the stress-strain properties of a construction as well. As it follows from the analysis of the published works [2,3] elastomeric hardening coatings increase crack-resistance, capability and durability of the reinforced concrete structures.

Thus, the new composition material on the CSPE base having the formula

$$\{\ldots(-CH_2-CH_2-CH_2-\underset{\displaystyle Cl}{\underset{|}{CH}}-CH_2-CH_2-CH_2-)_{12}-\underset{\displaystyle SO_2Cl}{\underset{|}{CH}}-CH_2-\ldots\}_{17}$$

vulcanized by water solution of MA provides the formation of a saturated polymer vulcanized net, and makes it possible to obtain impenetrable crack resistant coatings for metal, concrete, plastic and other substrates protecting them from injurious effects of the environment.

Table 1 provides the optimal composition of waterborne CSPE coatings.

Table 1.Optimal composition of waterborne CSPE coatings

Component	Trade mark	Kind of coating	
		Anticorrosive (KM)	Crack-resistant (KB)
Water dispersion of CSPE	CSM-450N®	100	
Epoxydimethylhydantoin	CSM-200®		100
resin	EG-10®	15	10.5
Mannich alkalis			
Filler	DMP-30®	10	10
	$Mg(OH)_2$,MgO	5	5
	ZnO	5	5
Pigment	$BaSO_4$,	10	10
	Cr_2O_3	3	4

The composition is prepared as follows:

- Water dispersions of two main components, i.e. CSPE and epoxydimethylhydantoin resin are thoroughly mixed in a ball mill for 30-35 minutes at room temperature and normal pressure.
- The third main component, i.e. water solution of Mannich alkalis is added to the mixture immediate before applying the coating on the substrate surface.
- After all components have been mixed for 5-10 minutes the composition is ready for use as a coating.

3. Materials and methods

Developed waterborne compositions of CSPE coating cured by water solution of MA can be applied as a covering at concrete articles moulding. According to V. Solomatov and V.Seljaev theory [2] there are shrinkage stresses arise in a concrete coating, which create the compressive stresses σ_{con} in contact layer of a concrete substratum. Therefore value of the moment M_{crack} carried by section before crack formation in a substratum is increased and it is possible to determinate by formula offered for prestressed reinforced concrete.

$$M_{crack}= R_{con}W_{crack} + M_{cor} \quad (1)$$

As the forces arising from shrinkage strains are transmitted on the concrete in a plane of contact coating-substratum for element with rectangular cross section (Figure1) :

$$M_{cor}= N_{shr}(e_o + r_{core}) ; e_o= 0.5h_{con};\ r_{cor}= h_{con}/6;\ M_{cor}=2/3(N_{shr}h_{con})$$

Taking in account that $N_{shr}=\sigma_{shr}\,\delta_c b$ and $W_{crack}=(0.292+n\mu)bh^2_{con}$ we have:

$$M_{crack}= R_{con}W_{crack}[1+2\sigma_{shr}\delta_c/3R_{con}h_{con}(0.292+n\mu)] , \qquad (2)$$

where $n= 2E_{rf}/E_{con}$

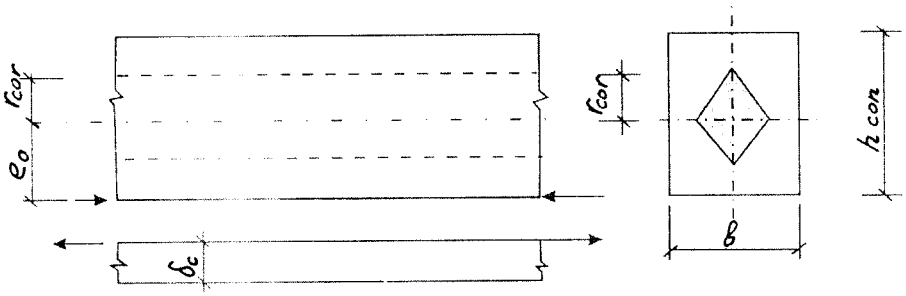

Figure 1 - To calculation of polymer coating shrinkage strains

From the formula (2) follows, that with increase of shrinkage stresses and thickness of a polymeric coating the moment of crack formation for reinforced concrete beams raises.

For check of analytical dependence conformity to experimental results the series of reinforced -concrete beams in the size 160x40x40 mm , reinforced by one bar Ø 6 mm was prepared. After vibrating the coating is put on a surface of a ready concrete mixture, following which curing takes place in natural conditions (Figure 2).

For the third day after moulding a beam had a curve f due to coating shrinkage. On value of this curve the shrinkage stress σ_{shr} which deformed the beam was determined:

$$\sigma_{shr} = 4\,E_{con}\,h^2_{con}\,f / 3\delta_c L^2 \qquad (3)$$

and further, under the formula (2) the crack formation moment was found.

4. Results

The samples were tested for a bend by the concentrated force in middle span of the beam with a polymeric coating in a tension zone. During the experiment the bending moment appropriate to appearance of the first visible crack was registered. From the analysis of experimental results submitted in Table 2, follows that owing to the shrinkage of polymeric coatings bending moment crack formation of the concrete substratum is increased on 12-19 %.

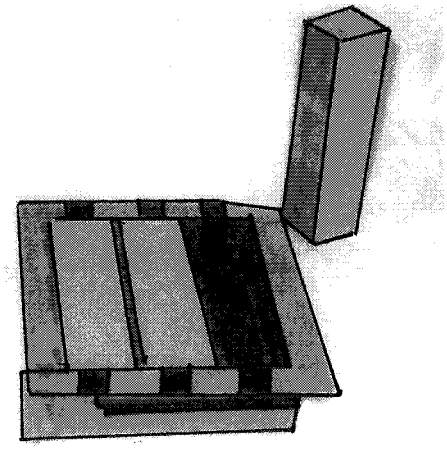

Figure 2- Samples of concrete with a coating during natural hardening

Table 2- Experimental results

N° beam	δ_c / h_{con}	f (μm)	σ_{sh} (MPa)	M_{crack} (%)
Beam 0 (without coating)	0	0	0	100
Beam 1	0.125	2	6.7	112
Beam 2	0.150	3	8.3	115
Beam 3	0.175	3.5	8.3	117
Beam 4	0.200	4	8.3	119

List of notations:

R_{con}- ultimate tensile strength of concrete:

σ_{shr} – shrinkage stress averaged on height of polymer coating;

μ – coefficient of reinforcement;

E_{rf} - modulus of elasticity of reinforcement;

E_{con} - modulus of elasticity of concrete;

L- span of the beam sample.

5. Conclusion

.It was experimentally found out that the crack forming bending moment had increased by 15-20% due to the CSPE based coating shrinkage as the function of thickness and mechanical characteristics of the coating. The definition model of a shrinkage stresses was proposed, which fairly agrees with our test results.

6. References

[1] Figovsky, O., Karchevsky, V., Beilin, D. Protective Crack-Resistant Waterborne Coatings Based on Vulcanized Chlorine-Sulpho-Polyethylene, Scientific Israel-Technological Advantages, vol3, No 1-2, 121-125 (2001)

[2] Solomatov, V., Seljaev, V., Chemical Strength of Composite Building Materials, Moscow, Stroiizdat (1987 , in Russia,)

[3] Weiss, W., Yang, W., Shah, S., Shrinkage Cracking of Restrained Concrete Slabs, J. of Engnr. Mechanics Div.. ASCE 124(7), 765-774 (1998)